CORROSION PERFORMANCE OF MIGRATORY INHIBITORS UNDER COMBINED CHLORIDE AND CARBONATION INGRESS

A Thesis

Submitted in fulfilment of the requirements for the award of the degree of

DOCTOR OF PHILOSOPHY

by

Ashish Kumar Tiwari

(Roll No. 901502001)

Under the Guidance of

Dr. Shweta Goyal
Professor
Department of Civil Engineering

Department of Civil Engineering

Thapar Institute of Engineering and Technology, Patiala-147004

Punjab, India

CERTIFICATE

Certified that the thesis "**Corrosion Performance of Migratory Inhibitors Under Combined Chloride and Carbonation Ingress**" which is submitted by Mr. **Ashish Kumar Tiwari**, in fulfilment of the requirement for the award of the degree of **Doctor of Philosophy** in the Department of Civil Engineering, Thapar Institute of Engineering & Technology, Patiala, is a record of the candidate's own independent and original research work carried out by him under my supervision and guidance. The matter embodied in this thesis has not been submitted in part or full to any other University or Institute for the award of any degree.

23/8/2023

Dr. Shweta Goyal
Professor
Department of Civil Engineering
Thapar Institute of Engineering & Technology

DECLARATION

I hereby declare that the work presented in the thesis entitled "**Corrosion Performance of Migratory Inhibitors Under Combined Chloride and Carbonation Ingress**" in the fulfilment of the requirement for the award of the Degree of **Doctor of Philosophy** in the Department of Civil Engineering, Thapar Institute of Engineering & Technology, Patiala, is an authentic record of my own work during the period January 2016 to January 2023, under the supervision of **Dr. Shweta Goyal**, Professor, Department of Civil Engineering, Thapar Institute of Engineering & Technology, Patiala. The material embodied in this thesis has not been submitted in parts or full in any other university or institute for the award of any degree in India or Abroad.

Place: Patiala
Date: 23/08/23

Ashish Kumar Tiwari
Department of Civil Engineering
Thapar Institute of Engineering
& Technology

ACKNOWLEDGEMENT

This thesis is the end of my journey in obtaining my PhD, probably the most stimulating activity of my life. It was a long and challenging yet very fulfilling journey that I completed. In pursuit of this academic endeavor, I have been exceptionally fortunate because inspiration, guidance, direction, cooperation, love, and care came my way in abundance. I feel nostalgic when I look back on my journey and find it difficult to put into words the never-ending support and encouragement of everyone throughout these years.

First and foremost, I would like to bow to Almighty for blessing me so abundantly, far beyond what I deserve. With a deep gratitude, I acknowledge my PhD Supervisor, Professor Shweta Goyal, Department of Civil Engineering, TIET, Patiala for giving me this wonderful opportunity to be a part of her research team. Her guidance, motivation, enthusiasm and dedication for research rendered to me during my work, without which the present endeavor would not have achieved the same status. Her support and faith in my ability made me strive for excellence and nothing less.

I am thankful to Dr. Vijay Luxami, Professor, School of Chemistry and Biochemistry, TIET, Patiala for her valuable guidance provided to me relating to selection of suitable corrosion inhibitors in my research work.

I am privileged to thank Prof. Prem Pal Bansal, Professor & Head, Department of Civil Engineering for providing excellent academic and lab facilities. I am thankful to doctoral committee members Dr. Rafat Siddique, Senior Professor & Dean of Research & Development Cell, Dr. Shruti Sharma, Professor and Dr. Raj Kumar Gupta, Professor, for their constant support and constructive criticism during my study.

I owe a special thanks to Ms. Purnima for continuously supporting me during my research work. She gave me support and help, discussed ideas and prevented several wrong turns. She helped me to stabilize myself during the weak days of my research and kept motivating me in different aspects of my work as well as life.

I thank my colleagues Mr. Kamal Anand, Mr. Sunil Garhwal, Mr. Upender Bishnoi, and Mr Anil Garhwal for their unconditional support throughout these years and for many fruitful and refreshing discussions. I would specially thank Dr. Kirti Vardhan for his continuous support.

I would also like to acknowledge my lab mates Himanshu, Shubham, Harvinder, Zinnia for stirring discussion and support. I owed a word of thanks to Mr. Gurjeet and Mr. Ram Simran.

I find it difficult to express in words, my sincere sense of indebtedness towards my parents. My unquestionable gratitude is for the never-ending love and support of my father Mr. Vishva Nath Tiwari and mother Mrs. Sunita Tiwari. My father is my backbone, and my mother is the pillar of my strength. I consider myself lucky to have such supportive and loving parents. I extend my respect to my other family members for their unconditional love and support.

Finally, I wish to acknowledge all those whose names have not been figured here but who helped me in any form during my research work.

(Ashish Kumar Tiwari)

Place: Patiala

Date: 23/08/23

ABSTRACT

Deterioration of reinforced concrete (RC) structures, due to exposure of rebar to aggressive environment, is a major cause of concern in terms of durability and overall structural integrity. The two main aggressive environments for rebar corrosion are the ingress of chloride ions and carbonation. While the former cause pitting corrosion and localized breakdown of passive film, the later results in a uniform corrosion of the rebar surface. In some typical environments where the rate of both chloride and carbonation penetration is high (due to simultaneous presence of pollution and de-icing or sea salts), a more severe damage to steel happens than the individual environments. The present study explores the severity level of combined action of carbonation and chloride on corrosion rate of RC.

Protection of RC against corrosion can be done by employing various techniques. Amongst all, application of corrosion inhibitors is found to be most effective in terms of cost, application, environment, and ease of handling. Corrosion inhibitors are chemicals that can effectively reduce the corrosion rate even when used in small quantities. The inhibition characteristics depend on their molecular structure, polarity, and presence of heteroatoms. Based on their mode of application, they are generally categorized as admixed inhibitor or migratory inhibitors. The major advantage of using migratory inhibitor is that they do not cause any negative affect on the concrete properties. Another advantage of migratory inhibitors is that they can be used both as preventive measure (i.e., can be applied before corrosion initiation) and as repair strategy (i.e., application after the steel has reached active corrosion state). Present study explores the potential of these inhibitors in migratory form to act as preventive as well as repair measure.

The study has been divided into three levels: pore solution test, migration ability test and ultimate application on reinforced concrete surface. The Level 1 of testing (i.e., pore solution test) was done to study the inhibition efficiency of some selected generic compounds with typical functional groups against combined (carbonated + chloride) exposure condition. Four different generic compounds, namely, triethyl phosphate (TEP), salicylaldehyde (SA), 2-Aminopyridine (AP) and 4-aminobenzoic acid (ABA) were selected on the basis of the presence of heteroatoms in their molecular structure and their solubility in high pH of pore solution. The potentiodynamic polarization curve behaviour and surface analysis test results (namely, Scanning Electron Microscopy, Energy Dispersive X-ray analysis and Fourier

Transform Infrared Spectroscopy) confirmed that the selected generic compounds effectively inhibit corrosion process in combined aggressive environment. From the test data, it was established that the inhibition efficiency of generic compounds depends upon the molecular structure, presence of functional group and number of heteroatoms. Based on pore solution testing, three generic compounds ABA, AP and SA that have the inhibitor effeciency of > 99% were finalized for the Level 2 of study i.e. percolation ability in concrete.

In Level 2 of testing, efficient compounds from Level 1 were applied on hardened concrete made by using either Portland cement (OPC) or fly-ash-blended cement (PPC) in order to study their percolation capacity in different concrete systems. The percolation ability was monitored at 15, 30, 45 and 60 days of inhibitor application by thin layer chromatography (TLC) and Ultraviolet visible spectroscopy (UV-Vis). Also, the effect of their application on the penetration of carbonation front and chloride ions was a accessed through carbonation depth and free chloride concentration. For percolation test, five different concentrations of generic compounds were applied (i.e., 0.1M, 0.3M, 0.5M, 0.8M and 1.0M) on 100 mm cubes. It was observed that at higher concentrations, all the compounds were able to penetrate within 15 days of their application. Further, the concentration reaching at different depths was observed to be dependent on the molecular weight, molecular structure of the compound, along with the type of cement. Among all the tested compounds, the concentration of ABA reaching at rebar level of 15 mm was highest, followed by AP and SA. Insignificant variation in carbonation depth and chloride profile of control and inhibitor applied specimens suggested that the tested generic compounds were not blocking the pores in concrete system. They were penetration upon application on concrete surface; and were also allowing the aggressive species to percolate through the concrete cover. Based on the migration studies conducted at this level, a concentration of 1M of the chosen generic compounds was finalized for application on RC specimens.

In Level 3 of the study, the selected generic compounds were applied on the surface of RC prism specimens that were prepared with one rebar at 15 mm cover depth. The inhibitors were applied in two formats: preventive and repair. The CoI is said to be applied in preventive format when the rebar in concrete was still in is its passive state (non-corroded); whereas in repair strategy, the inhibitor was introduced on the concrete surface when the rebar had reached the active state of corrosion. The specimens were subjected to a typical exposure cycle of seven days, which consisted of 2 days of chloride ponding (3.5% NaCl solution), followed by 2 days of air drying, 2 days of CO_2 exposure in a closed chamber (maintained at a concentration

of 5% by volume at 30 ± 2˚ C temperature and 60-70% relative humidity) and 1 day of air drying. The corrosion activity of specimens was monitored periodically after 10, 20, 30, 40 and 50 exposure cycles by electrochemical techniques namely, Half-cell potential (HCP), Linear Polarization resistance (LPR) and Electrochemical Impedance Spectroscopy (EIS). The test results confirmed the effectiveness of ABA in both the preventive and repair measure. AP was found to inhibit corrosion only in preventive measure, while SA could not perform in either of the two measures in both the concrete systems. Based on the test results, the inhibition mechanism of all the generic compounds was developed. Furthermore, pore solution testing was repeated with already corroded rebars to analyse the reason of performance/non-performance of any generic compound in repair measure. The results also indicated that the employment of inhibitors was highly effective in reducing the vulnerability of PPC concrete in the combined aggressive exposure.

LIST OF PUBLICATIONS

The following publications in peer reviewed journals are the outcome of the present research work:

1. **Tiwari Ashish,** Shweta Goyal, Vijay Luxami, Moloy K. Chakraborty, and G. Prabhakar (2021) "Assessment of corrosion inhibition efficiency of generic compounds having different functional groups in carbonated pore solution with chlorides and migration ability in concrete**." Construction and Building Materials, 290: 123275.** Impact factor = **7.58**
2. **Tiwari Ashish,** Shweta Goyal, Vijay Luxami, Moloy K. Chakraborty, and Prabhakar Gundlapalli (2021) "Evaluation of inhibition efficiency of generic compounds with additional heteroatom in simulated concrete pore solution and migration potential in concrete**." Journal of Building Engineering,** 43: 102490. Impact factor=**7.144**
3. **Tiwari A**, Dogra P, Goyal S, Luxami V, (2023) Influence of corrosion inhibitors on two different concrete system under combined chloride and carbonated environment. Structures, 48: 717-735. Impact Factor = **4.01**
4. **Tiwari A**, Dogra P, Goyal S, Luxami V (2023) Surface application of multifunctional compound to prevent and control combined chloride and carbonation corrosion in concrete. **European Journal of Environmental and Civil Engineering**. Impact factor: **2.187**

TABLE OF CONTENTS

LIST OF FIGURES

LIST OF TABLES

CHAPTER 1

INTRODUCTION

1.1 GENERAL

Reinforced concrete (RC) is the most widely used construction material all over the world from the mid-19th century. The popularity and use of this material gained momentum due to its various structural benefits. Concrete, which is good in compression, is complemented by steel that can take high tensile loads. Combination of both can provide adequate strength, stability, and durability to the RC structures. However, durability of this composite material was challenged by various factors like inadequate material selection, poor workmanship, inadequate design, and severe environmental conditions (*Heiyantuduwa et al., 2006*). The durability of RC structures is directly related to its service life which can be compromised either due to any individual factor or combination of above-mentioned factors.

Amongst various factors, environmental factors such as chloride and carbonation are the major cause of inadequate performance or decrease in service life of RC structures. Both chloride and carbonation attack directly on the embedded steel and cause corrosion of the rebar leading to its deterioration which not only challenges the structural integrity, but also causes huge economic loss all around the world. According to NACE report, global cost of distress related to corrosion in RC is estimated to be about 2.5 trillion US dollars, which is equivalent to 3.4% of the global GDP. India has a large coastal belt where the corrosion is extremely severe. The cost of corrosion in India is estimated to be around 1670 billion US dollar per year (*Bowman et al., 2016*).

The corrosion mechanism of RC is the combined function of the properties of both the materials i.e., steel and concrete. Firstly, the concrete microstructure provides the steel with physical barrier (cover concrete) against the various corrosive agents and secondly, steel embedded in the alkaline hydrated cement paste (pH = 12.5 to 13.5), rapidly forms a thin passive layer of oxides which strongly adheres to the underlying steel and gives it complete protection from reaction with oxygen and water, that leads to formation of rust and corrosion (*Ribeiro & Abrantes, 2016; Shen, 2017*). This state of steel is known as passivation. The passive layer becomes de-passivated due to ingress of aggressive ions from the outside environment. The two most common types of rebar corrosion are: chloride induced corrosion due to the action of chloride ions and carbonation induced corrosion due to ingress of atmospheric carbon dioxide (CO_2).

It is also worth mentioning that in comparison with individual attack, combination of both can cause more severe condition for the embedded steel in RC structures. Carbonation not only reduces the pH of the steel surrounding interstitial pore solution, it also affects the chloride binding capacity of concrete. Moreover, carbonation can reduce the critical chloride threshold value for corrosion initiation. All these factors can contribute to increasing the corrosion rate of embedded steel (*Aguirre-Guerrero et al., 2016; Byung Hwan Oh, Sang Hwa Jung, 2013; Geng et al., 2016; Ramezanianpour et al., 2014; Y. Wang et al., 2017; Ye et al., 2016; D. Zhang & Shao, 2016*).

1.2 SCOPE AND OBJECTIVE OF THE PRESENT RESEARCH WORK

Rebar embedded in concrete can be safeguarded from corrosion by using efficient protective measures such as using ultra high-performance concrete (*Zheng et al., 2022*), coated steel (*Hussain et al., 2020; Mei et al., 2022; Sharma et al., 2020; Tittarelli et al., 2018; Weishaar et al., 2018*), and corrosion inhibitors *(Guleria et al., 2021; Lapiro et al., 2022; Thuong et al., 2021; Zomorodian et al., 2021*). Among all the measures, application of corrosion inhibitors (CoI) is the cost-effective solution with additional benefit of its ease in application and handling (*J. Hu et al., 2018; J. Xu et al., 2020*). They protect steel by restricting the anodic and/or cathodic reactions on the rebar (*Lee et al., 2018*).

CoIs are classified as organic and inorganic inhibitors based on the type of functional group present in it, which further influences the mechanism of inhibition provided by them *(J. Z. Liu et al., 2016; Magdalena Osial, 2016*). The inorganic CoI's were initially used for chloride induced corrosion; but the use is now limited because of their toxicity and non-environment friendly properties. Thus, organic compounds are gaining attention due to their eco-friendly nature and their effectiveness in both chloride and carbonated environment *(J. Huang et al., 2022; Kaur et al., 2016; Q. Xu et al., 2022*). Organic inhibitors with additional heteroatoms (S, P, O and N) and heterocycle in their structures are reported to be more effective in combating against corrosion as the number of active sites for interaction with the metal increases; subsequently raising the chances for more complex and strong chemical interactions (*Bolzoni et al., 2022*). Different combinations of functional groups are helpful in obtaining more effective corrosion inhibition properties.

In RC, the role of organic compounds has been explored by taking chloride and carbonated environments separately. The performance of these chemicals in the combined corrosive environment (chloride + carbonation) has not been explored till now. Only a limited

work is available on their use in simulated concrete pore solution *(Cao et al., 2015; Monticelli et al., 2011a*), which cannot represent the actual concrete behavior with complex hydration process and a distinct steel-concrete interface. Moreover, different cement types are now-a-days available in the market with different constituents. The variation in the cement chemistry affects the efficiency of the CoI's; which cannot be represented by talking only simulated pore solution. Hence, there is a need to investigate the functional mechanism of organic compounds as CoIs in different types of concrete matrices subjected to aggressive corrosive environment.

CoI can be introduced in RC by two different methods i.e., either by directly adding into a freshly mixed concrete (admixed CoI) or by applying on hardened concrete surface (migratory CoI). Various negative effects on the fresh and hardened concrete properties have been observed when CoI is used in the admixed form (*Dharmaraj & Malathy, 2015; Kannan K, Rajkumar V, 2012*). These negative effects can be avoided when a CoI is employed on to the hardened concrete and is allowed to percolate through the concrete cover to reach the rebar level for protection (*Zheng et al., 2012*). Thus, it is more beneficial to use CoIs as migratory inhibitors that can be applied on the hardened concrete surface.

Based on the thorough understanding of the above related issues of corrosion on different cement type and challenges associated with the application of CoI in combined corrosive environment, the following objective were outlined:

1. To study the combined effect of chloride ions and carbonation on rebar corrosion.
2. To study the performance of two specific migratory type corrosion inhibitors in chloride and carbonated environment.
3. To investigate the performance of pozzolanic cement under combined exposure.

1.3 ORIENTATION OF THESIS

The thesis presentation has been divided into six chapters. In the first chapter, introduction about the topic along with the research objective has been outlined. In the second chapter, basic concepts of corrosion in different environments and extensive review on the application, type and efficiency of CoI's in different environments are presented.

To achieve the above-mentioned objectives, the study was divided into three levels: pore solution test, migration ability test and ultimate application on reinforced concrete surface. In the third chapter, outcomes of the Level 1 of study on bare steel specimens in concrete simulated pore solution containing various generic compounds as corrosion inhibitors are

presented in detail. The fourth chapter focuses on Level 2 of the study by highlighting the potential ability of generic compounds to percolate through concrete microstructure and its effect on the penetration of aggressive ions discussed in detail. In the fifth chapter, the results of Level 3 of the study are presented. In this part of the study, the selected generic compounds were employed on the surface of RC prisms to act as migratory inhibitors. The experimental outcomes of various electrochemical techniques, surface analysis of prism and rebar specimens and gravimetric analysis forms the basis of checking the potential of generic compounds as preventive and repair measures.

Sixth chapter deals with the relevant conclusions drawn from the present study and scope for future work. At the end, appendix and cited references used in the work are presented.

CHAPTER 2

LITERATURE REVIEW

2.1 INTRODUCTION

Corrosion is a natural process that occurs when processed or refined metals react with their environment, transforming into more stable oxide, carbonate, or sulfide forms. It is a major cause of metal degradation, leading to the loss of surface area through wastage. Therefore, it can be asserted that virtually all metals, apart from noble metals, are susceptible to the detrimental effects of corrosion. RC under certain environmental conditions undergo corrosion that effect the structural integrity, strength, durability, and service life of structure. According to NACE report the global cost of corrosion is estimated to be about 2.5 trillion US dollars, which is about 3-4% of global GDP (*Bowman et al., 2016*). This amount can be minimized by adopting a suitable corrosion control measure. The present chapter deals with the basics of reinforced steel corrosion and the literature review on the effectiveness of corrosion inhibitors for its mitigation.

2.2 REBAR CORROSION: BASIC MECHANISM

The corrosion of steel in concrete is considered as an electrochemical process with anodes and cathodes formed adjacently on the rebar and are surrounded by the concrete pore solution which acts as the electrolyte allowing the movement of ions between anodic and cathodic sites. This electrochemical process involves following reactions:

At anode, iron atoms losses its electron and move into a surrounding concrete as ferrous ions. This process is called half-cell oxidation reaction or anodic reaction (eq. 2.1). The electrons remain in the bar and flow to sites called cathodes, where they combine with water and oxygen in the concrete. The reaction at the cathode is called a reduction reaction (eq. 2.2).

$$2Fe \rightarrow 2Fe^{2+} + 4e^{-} \quad \ldots(2.1)$$

$$2H_2O + O_2 + 4e^{-} \rightarrow 4OH^{-} \quad \ldots(2.2)$$

The hydroxyl ions ($4OH^{-}$) are generated in cathodic reaction which increases the local alkalinity and therefore, strengthens the passivity around the steel surface. The anodic and cathodic reactions are only the first step in the process of creating rust. Several more stages must occur for rust to form. This must be expressed in several ways:

$$2Fe^{2+} + 4OH^{-} \rightarrow 2Fe(OH)_2 \quad \ldots(2.3)$$

$$4Fe(OH)_2 + 2H_2O + O_2 \rightarrow 4Fe(OH)_3 \quad \ldots(2.4)$$

$$2Fe(OH)_3 \rightarrow Fe_2O_3.H_2O + H_2O \quad \ldots(2.5)$$

Un-hydrated ferric oxide (Fe_2O_3) has a volume of about twice that of steel it. When it becomes hydrated, it swells even more and becomes porous. This results in increased volume at steel/concrete interface leading to cracking and spalling of concrete and becomes the cause of corrosion of steel in concrete (*Broomfield, 2006*).

2.3 CAUSES OF CORROSION

Concrete is an ideal material that protects steel rebar from corrosion. Environment within concrete is completely alkaline (with pH more than 12) due to which a thin oxide layer ($\gamma Fe_2O_3.H_2O$) is formed over the steel surface that protect steel rebar from corrosion (*Heiyantuduwa et al., 2006; Montemor et al., 2002, 2003*)**.** Yet, the two main reasons that can cause breakdown this passive layer are: ingress of chloride ions and carbonation. While the former causes pitting corrosion and localized breakdown of passive film, the later results in a uniform corrosion of the rebar surface. This section describes the mechanism of corrosion by the action of chloride and carbon-dioxide.

a) Chloride-induced corrosion

The ingress of chloride is the most important factor that is responsible for steel corrosion in RCC structure. It can destroy the passive layer surrounding steel and cause localized corrosion. The mechanism by which chlorides promote corrosion is still not entirely understood, but the most popular theory is that chloride ions penetrate the protective oxide layer easier than other ions, leaving the steel vulnerable to corrosion. **Neville** (*Neville, 1995*) stated that chloride ions activate the surface of steel to form an anode, the passivated surface being the cathode. The reactions involved are as follows:

$$Fe^{2+} + 2Cl^- \rightarrow FeCl_2 \quad \ldots(2.6)$$

$$FeCl_2 + 2H_2O \rightarrow Fe(OH)_2 + 2HCl \quad \ldots(2.7)$$

From equations 2.6 and 2.7, it is evident that chloride ions are regenerated during the corrosion process and persist to participate in further corrosion reactions. This continuous regeneration of chloride ions ensures their availability for sustaining the corrosion process. When chloride ions enter the concrete and reach steel/concrete interface, the normal passivity is disrupted. This disruption causes an active pitting corrosion initiation on steel surface. As corrosion occurs in a pit, the local pH becomes lower and a more active corrosion process

occurs in which more of the surface starts corroding, resulting in an increase in the corrosion rate (*Berke & Hicks, 2004*)**.**

The breakdown of the passive film occurs when the chloride concentration reaches or exceeds a critical value called critical chloride level or chloride threshold level (CTL) *(Andrade & Page, 1986; Goñi & Andrade, 1990; Ormellese et al., 2006)*. Thus, the number of chlorides in the concrete and in turn, the number of free chlorides in the aqueous phase (which is partly a function of cement content and partly, cement type) will influence the risk of corrosion.

b) Carbonation-induced corrosion

Carbonation is a process in which CO_2 from atmosphere penetrates within the concrete through pores and react with hydrated compounds' hydroxide like calcium hydroxide ($Ca(OH)_2$ and calcium silicate hydrate (C-S-H) (*Deng et al., 2023; Mi et al., 2023; Tian et al., 2023; X. Wang et al., 2023b; J. Zhang et al., 2023; Zhu et al., 2023*) gel to form calcium carbonates ($CaCO_3$). The basic chemical reactions involved during carbonation of concrete are:

$$CO_2 + H_2O \rightarrow H_2CO_3 \quad \ldots(2.8)$$

$$H_2CO_3 + Ca(OH)_2 \rightarrow CaCO_3 + 2H_2O \quad \ldots(2.9)$$

$$C\text{-}S\text{-}H + CO_2 + H_2O \rightarrow CaCO_3 + SiO_2 + H_2O \quad \ldots(2.10)$$

The formation of $CaCO_3$ (shown in eq. 2.9 and 2.10) is normally responsible for clogging of the microstructure and reducing the porosity of concrete; but the process also reduces the pH from ~13 to pH<9 at the steel-concrete interface (*SA HB 84:2018 Guide for concrete repair and protection*). Thus, causing de-passivation of surrounding passive layer (*Bertolini et al., 2008; B. Dong et al., 2014*). Also, decalcification of C-S-H gel (shown in eq. 2.10) may increase the porosity by increasing the number of capillary pores (*Ngala & Page, 1997*) within the concrete pore structure if the amount of un-reacted $Ca(OH)_2$ is less for CO_2 to react (*Hunt & Tomes, 1962; X. Wang et al., 2023a*). The actions of CO_2 take place even at a small concentration such as are present in rural air, where the CO_2 content is about 0.03 percent by volume. In an unventilated laboratory, the content may rise above 0.1 per cent. In large cities it varies from 0.3-1 per cent (*Pessu et al., 2020*). Carbonation occurs progressively from the outside of concrete exposed to CO_2 but does so at a decreasing rate because CO_2 must diffuse through the pore system, including the already carbonated surface zone of concrete. Rate of carbonation also depends upon the moisture content of concrete, which varies with the distance from its surface.

2.4 COMBINED ATTACK OF CHLORIDE AND CARBONATION

In some typical environments, where the rate of both chloride and carbonation penetration is high (due to simultaneous presence of pollution and de-icing or sea salts), a more severe damage to steel can occur than caused due to chloride or carbonated environment, individually. According to the literature, chloride induced corrosion and pH are closely related**.** A reduction in the value of critical threshold level (CTL) in corrosion initiation is observed in case of weathering carbonation (*Aguirre-Guerrero et al., 2016; Ramezanianpour et al., 2014; D. Zhang & Shao, 2016*). (*Cao et al., 2015*) found that CTL value changes with changing level of carbonation and during the testing authors observed CTL value of 0.08 mol/L for solution having pH 9.46. (*Monticelli et al., 2011a*) also prepared carbonated pore solution (pH 7) and contaminated it with 0.1 M NaCl to study the combined effect. Carbonation also accelerates the penetration of chloride salt which increases the total chloride content together with its penetration depth (*Geng et al., 2016*)**.** It is also reported that the ratio of free to bound chloride increases when carbonation is involved (*Kuosa et al., 2014a, 2014b*). Surprisingly, corrosion studies with concrete subjected to combined aggressive environment is scanty. A few studies that are available are only in concrete simulating pore solution or in mortar, but not in concrete; however, concrete matrix will play a significant role in deciding the corrosion kinetics.

2.5 FACTORS INFLUENCING THE CORROSION RATE DUE TO COMBINED EXPOSURE

The combined attack of chloride and carbon-dioxide causes more severe conditions for RC. However, there are two major factors i.e., binder type and sequence of exposure that can affect the corrosion rate and mechanism of degradation in combined environment which is explained in the subsections below.

2.5.1 Type of Binder

Sustainable development of construction industry can be achieved only by fully utilizing the cementitious and pozzolanic by-products like fly-ash, silica fume, slags which are known as the supplementary cementitious materials (SCM). The use of SCM has grown in the past three decades which contributes to energy conservation practices. The total CO_2 emissions from the cement industries which is nearly 8% can be reduced to a much lower value by the replacement of cement with SCMs (*Pacewska & Wilińska, 2020*)**.** Besides this, the inclusion of SCMs cause microstructural changes in concrete matrix by secondary pozzolanic reactions, which in turn influence its durability properties.

It is worth mentioning that incorporation of adequate amount of SCM has a significant impact on the permeability characteristics of concrete against diffusion of external agents. During hydration reaction of portland cement, water reacts with tricalcium silicate (eq. 2.11) and dicalcium silicate (eq. 2.12) producing calcium silicate hydrate (C-S-H) gel and soluble calcium hydroxide ($Ca(OH)_2$). Here, C-S-H gel is the major contributor for the strengthening of concrete, whereas $Ca(OH)_2$ remains unutilized during the entire hydration process.

$$2Ca_3SiO_5 + 7H_2O \rightarrow 3CaO.2SiO_2.4H_2O + 3Ca(OH)_2 + Heat \quad \ldots(2.11)$$

$$2Ca_2SiO_4 + 5H_2O \rightarrow 3CaO.2SiO_2.4H_2O + Ca(OH)_2 + Heat \quad \ldots(2.12)$$

Replacement of cement by SCM (containing active form of silica and alumina) consumes the soluble $Ca(OH)_2$ during secondary pozzolanic reaction to form additional amount of C-S-H and C-A-S-H (Calcium Aluminate Silicate Hydrate) which reduces the capillary pore size by acting as filler (eq. 2.13). As a result, this leads to a varied distribution of pore sizes within the microstructure of the concrete, which in turn limits the penetration and diffusion of chloride and sulfates through the material (*X. Hu & Poon, 2022; Jung et al., 2018*).

$$3Ca(OH)_2 + 2SiO_2 \rightarrow 3CaO.2SiO_2.3H_2O \quad \ldots(2.13)$$

In pozzolanic cement concrete, when chloride ions diffuse in, they chemically react with tricalcium aluminate or its hydrate to form calcium chloro-aluminate ($3CaO.Al_2O_3.CaCl_2.10H_2O$), commonly called Friedel's salt (eq. 2.14 and eq. 2.15) (*Florea & Brouwers, 2012; Thomas et al., 2012*). Thus, the increase in content of alumina due to incorporation of SCMs increases the chloride binding capacity of concrete at the hydration phase. Alongside, chloride also absorbs physically on surface of CSH gel *(X. Wang et al., 2023b*). Considering this, it can be said that SCM based concrete has high resistance against chloride-induced corrosion.

$$3Ca(OH)_2 + Cl^- \rightarrow CaCl_2 + 2OH^- \quad \ldots(2.14)$$

$$3CaO.Al_2O_3 + 10H_2O + CaCl_2 \rightarrow 3CaO.Al_2O_3.CaCl_2.10H_2O \quad \ldots(2.15)$$

On the other side, the influence of CO_2 ingress on SCM concrete is complicated to understand. Atmospheric CO_2 diffuses in concrete, from the empty pores of the surface, reacts with water and forms carbonic acid (H_2CO_3) (eq. 2.6). For portland cement, $Ca(OH)_2$ is the main buffering compound and H_2CO_3 reacts with it resulting in the formation of insoluble calcium carbonate ($CaCO_3$) (eq. 2.8 and 2.9). Formation of $CaCO_3$ has a positive effect on the concrete microstructure as it lines the concrete pores and reduces its porosity. Whereas, in SCM based concrete, the $Ca(OH)_2$ buffer is low due to reduced amount of clinker in it which further,

gets utilized in the secondary pozzolanic reactions; thus lowering the pH of the pore solution in the interstitial pores of concrete. As carbonation of concrete also consumes the $Ca(OH)_2$ present, the pH lowering effect is much more severe in SCM concrete than OPC concrete at certain favorable conditions (*Justnes et al., 2020; Lye et al., 2015; Stefanoni et al., 2018*). The embedded rebar in concrete is protected by the spontaneously formed passive layer over it which sustains only in alkaline media, however, due to lowering of pH, de-passivation of the protective layer takes place. This leads to uniform corrosion of rebar which is hazardous to the durability of concrete. Higher corrosion rates due to carbonation-induced corrosion are seen in SCM concrete *(Kaur, Goyal, Bhattacharjee, et al., 2017*).

2.5.2 Sequence of exposure

The mechanism of rebar corrosion in combined environment has still not been explored thoroughly. The major drawback is related to unavailability of any standard method to simulate combined exposure condition and knowledge of degradation mechanism under such conditions. Moreover, related studies also adopted different sequences of exposures to simulate combined environmental conditions. All the studies on corrosion performance under the combined exposure have tried to simulate the mixed environment by exposing the RC samples to individual environments, one at a time. It was noted that the whole of the carbonation exposure was done at once and the whole of the chloride exposure after/before carbonation. As already mentioned in the previous section, both the concrete systems (i.e., portland based or SCM based) behave differently in a chloride rich environment and CO_2 exposure. In chloride rich environment, SCM based concrete performs better due to its refined microstructure, whereas in CO_2 exposed conditions, portland cement concrete performs much better than SCM based concrete due to formation of insoluble calcite precipitates. Thus, exposure to individual environment one at a time will either cause corrosion of one concrete system or densification of other concrete system. All these studies were not subjecting the specimens to a cyclic or simultaneous kind of exposure. A few recent articles that adopted such a program are tabulated in Table 2.1.

Table 2.1 Tabulated literature review of various authors that have exposed the RC specimens to combined corrosive environments: one at a time

Authors	Mixed Environment Simulation	Type of study	Results
Hren et al. 2021	11 weeks carbonation followed by 52 weeks chloride exposure	Corrosion properties of multiple blended cements were assessed in carbonated and non-carbonated states. Also, alternate wetting-drying cycles was considered to introduce chloride in concrete.	Steel in blended cement experience high corrosion activity thus exhibits high corrosion rate initially, which later decreases as compared to OPC. Change in corrosion rate was due to beneficial changes in microstructure.
Y. Wang et al. 2017	1/2/3 months CO_2 followed by 1/2/3 months chloride and vice-versa	Effect of combined chloride and carbonation ingress regimes on ingress and redistribution of chlorides in concrete	Carbonation increases chloride transport within concrete, but the effect depends on the type of binder used. Carbonation also decreases chloride binding capacity and pushes chloride inwards
Guerrero et al. 2016	4 months carbonation followed by chloride exposure of 15 days wetting and 15 days drying	Corrosion study	Silica fume performed better in combined environment than OPC and metakaolin
Geng et al. 2016	0.5mol/l chloride admixed with mixing water followed by carbonation till 14, 28, 56 and 90 days (20% CO_2, RH 65-75%, Temp 20-25 ^oC)	Effect of carbonation on bound chloride	Carbonation leads to release in bound chlorides due to decomposition of Friedel's salt and C-S-H gel
Zhang et al. 2016	Early carbonation curing done in 4 steps (step 1: 5-6 hrs in-mold curing; step 2: 5.5h demold conditioning; step 3: 12 hr carbonation curing and step 4: 27 days subsequent hydration) followed by 7 day combined exposure cycle (3-day salt	Effect of early carbonation on chloride penetration and weathering carbonation on concrete	Carbonation cured concrete was not much vulnerable to weathering carbonation due to impermeability of formed carbon rich protective layer that provides resistance to chloride ingress

	immersion- 1day air drying- 3day 10% carbonation)		
Hailong et al. 2015	Testing cycle 1: 4 days NaCl (15%)- 2 days oven drying- 2 days accelerated carbonation (20%) Testing cycle 2: 4 days NaCl (15%)- 2 days oven drying- 4 days accelerated carbonation (20%)	Chloride penetration behavior was studied in combined exposure condition	Using SCM makes concrete more vulnerable to carbonation-induced chloride movement due to low portlandite content
Lee et al. 2013	14 days cyclic exposure 7 days chloride immersion (5% NaCl) 7 days carbonation exposure (10% CO_2, RH 60%, Temp 40 ^oC)	Effect of carbonation on chloride profile	Chloride penetration is more pronounced when carbonation is involved along with chloride ingress
Alonso and Andrade 1990	Addition of 2% $CaCl_2$ during casting and cured for 28 days. Specimens were carbonated for 2 months at 60% RH followed by dry and wet period	Effect of nitrite as corrosion inhibitor in contaminated and chloride free carbonated concrete	In the case of chloride and carbonation acting together, the proportion of inhibitor used were not enough to reduce the attack

From the table, it can be observed that sequence of exposure adopted by various researchers are way distinct to each other. Also, most of the studies were executed to identify the effect of carbonation on chloride distribution or redistribution within the concrete, thus effect of their redistribution and carbonation on corrosion rate of embedded steel in long term was not evaluated in detail.

2.6 METHODS TO MITIGATE CORROSION

Corrosion inhibition in RC can be achieved by selecting efficient techniques. There are various techniques available that can be effectively used either as preventive or repair strategy. These techniques can be characterized as physical, chemical, and electrochemical techniques. Table 2.2 gives the details of preventive and repair techniques used for corrosion mitigation.

The selection of an effective technique is a strenuous task as each technique has its own merits and demerits. For instance, the challenge with the electrochemical technique is that it requires constant power supply; while physical techniques like coatings on steel and concrete have limited-service life say 10 to 12 years only. Furthermore, methods such as using high quality concrete or galvanized steel need high investment initially.

Table 2.2 Corrosion mitigation techniques

S. No.	Preventive Techniques	Repair Techniques
1	High quality and Impermeable concrete	Patch repair
2	Steel coatings	Electrochemical chloride extraction
3	Galvanization protection	Electrochemical re-alkalization
4	Cathodic prevention	Cathodic protection
5	Organic coating on concrete	Corrosion inhibitors
6	Corrosion inhibitors	-

Among the available preventive and repair techniques, use of corrosion inhibitors as chemical technique is proved to better solution in terms of inhibition efficiency, cost effectiveness, ease in application and environmental concerns. A detailed literature survey on the use of corrosion inhibitors in concrete is presented in subsequent sections.

2.7 CORROSION INHIBITORS (CoI)

A chemical compound that can effectively decrease the corrosion rate of a corroded system when present at suitable concentration without significantly changing the concentration of any corrosive agent called as corrosion inhibitor (CoI) [***ISO 8044-1986 (1989)***]. Use of CoI for corrosion inhibition started in the early 1940's. Initially, their application was limited to oil and gas industry, water treatment plants and chemical related industries only. It was also reported that in oil and gas industry their application could effectively reduce corrosion rate by 90% to 95% (*Elsener et al., 1999*).

The application of CoI in controlling corrosion of rebar embedded in concrete was first reported in 1960's (*Heiyantuduwa, 2001*). In terms of concrete, it can be state that "Corrosion inhibitors are the chemical compounds that reduce corrosion rate significantly without affecting any important property of concrete and without varying the concentration of any corrosive agent" (*Goyal et al., 2021*). During its early use, CoIs were introduced in concrete in admixed form i.e., mixed during casting process and called as "admixed inhibitors". With time, their importance as a repair material also grew due to their ease in application, cost effectiveness and its inhibition efficiency. While using as repair material, CoI were applied on hardened concrete, allowed to percolate, and called as migratory inhibitors (MCoI) or surface applied inhibitors or penetrating inhibitors. Considering their inhibition mechanism, most of them protect the rebar by forming a stabilized protective film over its surface (*Ryu et al., 2016*); or by reducing the permeability of concrete (*Kaur et al., 2016*). Basically, CoI reduces the ionic

movement on the metal surface by blocking cathodic and/or anodic sites or prevent corrosion by increasing electrical resistance of the steel surface *(Lee et al. 2018*).

2.8 CLASSIFICATION OF CoI's

Based on electrochemical mechanism of action, they can be classified as anodic, cathodic, or mixed inhibitor. These inhibitors compound can be organic, or inorganic depending upon their attached functional group and can be used as an admixture or can be applied on hardened concrete surface as migratory inhibitor. All these classifications are discussed in detail in the upcoming sub-sections.

2.8.1 Based on physical mode of application:

Based on physical mode of application, CoI can be classified as admixed CoI and migratory CoI.

(a) *Admixed CoI*: Admixed CoI are a chemical compound that were used as corrosion inhibitors and introduced in concrete during mixing process. From early 1960's commercial CoI were mostly inorganic based namely, salt of nitrate, nitrite (sodium or calcium), sodium salt of phosphate, benzoate, molybdate, hydroxides, silicates, polyphosphates, phosphonates, tannins, lignins, calcium salts and chromate and zinc oxide were used as an admixed CoI (*Andrade, C. Alonso, 1990; Ann et al., 2006; Gaidis, 2004; Gouda et al., 1973*). Whereas organic compounds such as amines, urea, Mercaptobenzothiazole (MBT), benzotriazole e toliotriazol, aldehydes, heterocyclic nitrogen compounds, sulfur-containing compounds and acetylenic compounds and ascorbic acid, succinic acid, tryptamine, caffeine and extracts of natural substances. Also the other organic corrosion inhibitors such as amino-acids, alkanol-amines, unsaturated fatty acid esters of carboxylic acid and fatty acid esters were introduced later as admixed CoI *(Dariva & Galio, 2014; De Schutter & Luo, 2004; Jamil et al., 2003; Nmai, 2004*).

(b) *Migratory CoI*: They are a compound that is applied on hardened concrete surface and allowed to diffuse through concrete microstructure with time. After the application on the concrete surface, MCoI percolate through the cover concrete and protect steel either by forming a protective layer on rebar (*Ryu et al. 2016*) or/and by reducing the permeability of concrete *(Kaur et al. 2016*). Application of MCoI increases the electrical resistance of steel against corrosion which in turn postpones the initiation of corrosion/reduces the rate of on-going corrosion (*Lee et al. 2018; Goyal et al. 2021)*.

Various negative effects on the fresh and hardened concrete properties have been observed when CoI are used in admixed form (*Dharmaraj & Malathy, 2015; Gouda et al., 1973; Kannan K, Rajkumar V, 2012; Shi et al., 2022*) but when employed on to the hardened concrete no such drawbacks have been observed (*Kaur et al., 2016; Söylev et al., 2007a; Zheng et al., 2012*). Thus, it can be said that migratory inhibitors can be employed as a corrosion protection technique that will not cause any detrimental effect on concrete's important properties.

2.8.2 Based on protection mechanism:

Based on protection mechanism, CoIs can be classified as anodic inhibitors, cathodic inhibitors, and mixed inhibitors. Further details of their protection mechanism are discussed below:

a) *Protection mechanism of anodic inhibitors:* These corrosion inhibitors, also called passivation inhibitor, blocks the anodic sites, and supports the natural passivation reaction of metal surface. They help in reducing the corrosion rate by increasing the corrosion potential of steel (T*ayfun Altug Söylev et al. 2007*). There are two types of passivating inhibitors: oxidizing ions and non-oxidizing ions. Oxidizing ions can passivate in the absence of oxygen (such as chromates and nitrites), while non-oxidizing shows its efficiency in the presence of oxygen (e.g.- phosphates and molybdates) (*Lee et al. 2018*)**.** Such inhibitors attack and react with Me^{n+} produced on the anode and form an insoluble hydroxide which is deposited on the steel surface as an impermeable and insoluble to the metallic ions. Fig. 2.1a shows the mechanism of anodic inhibitors.

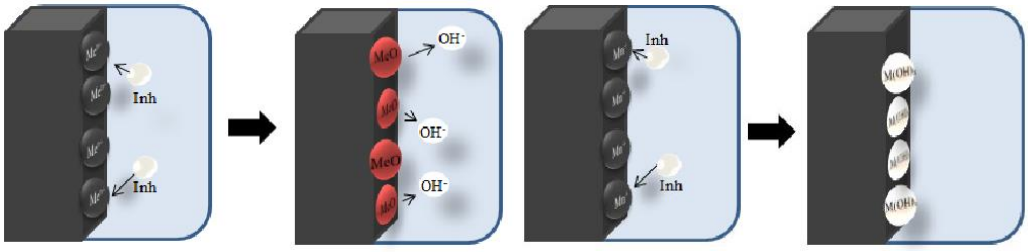

Fig. 2.1 Mechanism of action of (a) anodic inhibitor (b) cathodic inhibitor
(*Dariva and Galio 2014*)

For the effective inhibition, such inhibitors must be in high concentration within the solution, and it should be higher enough to for the perfect inhibition *(Saraswathy &*

Song, 2007). Concentration must be above the critical value because inappropriate concentration affects the formation of film, and leaves site of the metal exposed as it will not cover the complete metal surface, thus causing the localized corrosion *(Dariva & Galio, 2014*). Some of the examples of anodic inhibitors are nitrates, molybdates, phosphate, chromates, hydroxide, and silicates.

b) *Protection mechanism of cathodic inhibitor:* Cathodic inhibitors block the cathodic sites thus, preventing the occurrence of cathodic reaction of the metal during the corrosion process. The prevailing mechanism suggests that the inhibitors containing metal ions lead to the formation of insoluble compounds, which selectively precipitate on cathodic sites. Consequently, this process obstructs the reduction reaction, effectively hindering corrosion. Due to their action of causing precipitation, these inhibitors are commonly referred to as "precipitation inhibitors." *(H.-S. Lee et al., 2018*). Such CoIs deposit over the metal and form an adherent protective film, restricting the diffusion of reducible species in these areas. They reduce the corrosion rate by shifting the corrosion potential towards a more negative value. Due to this inhibition mechanism, the concentration of inhibitor is not of much importance as in case of anodic inhibitors and is more secure than anodic inhibitors in terms of toxicity and negative effect on concrete properties **(***Gariva and Dalio 2014***).** Some effectively used cathodic inhibitors are the salts of magnesium, zinc, and nickel. It was also observed that they undergo hard water kind of inhibition mechanism, react with hydroxyl ions of water and form insoluble hydroxide (i.e. $Mg(OH)_2$, $Zn(OH)_2$, $Ni(OH)_2$) which are deposited on the cathodic site on the metal surface which protects it for being exposed for corrosion process (*Heiyantuduwa et al. 2006)*. Fig. 2.1b shows the mechanism of cathodic inhibitors.

c) *Protection mechanism of mixed CoI:* Mixed inhibitors are those which can block both ongoing cathodic and anodic reactions on the steel surface. Mixed CoIs reduce the corrosion rate more probably by forming a thin adsorbed hydrophobic film on metal surface through adsorption mechanism (*Kondratova et al., 2003*). Mixed inhibitors are also known as adsorption inhibitors or film-forming inhibitors, as these are the materials consist of hydrophobic group that contains effective polar groups like N, S, and OH. The effectiveness of the film depends upon molecular structure, chemical composition, and their affinities for the metal surface (*Darvia and Galio 2014; Osial 2016*). Organic inhibitors are a mixed kind of inhibitor and can form a protecting film over the steel

surface. Amines and amino alcohol are the most used mixed type inhibitors, which displace the chloride ions and form a durable passivating film (*Jamil et al., 2003, 2004, 2005*). Organic inhibitors can protect steel by either or both types of adsorption mechanism i.e., chemisorption or physisorption or physio chemisorption. Chemisorption involves the charge transfer between iron surface and heteroatoms or sharing of charge to form the coordinate bond, whereas physisorption on steel involves electrostatic interactions between the charges of rebar metal surface and charges of dipoles of organic molecules *(H.-S. Lee et al., 2018; Ormellese et al., 2009a; Osial, 2016*). In physio chemisorption, both mechanisms occur simultaneously.

2.8.3 Based on functional group present: Based on functional group in molecular structure, CoI can be categorized as inorganic CoI and organic CoI. The various functional groups used in the protection of steel along with their type of mechanism are tabulated in Table 2.3.

(a) ***Inorganic CoI*****:** Amongst various inorganic inhibitors, nitrites stand out as the most used. These inhibitors, mainly added to the blend of fresh concrete as a preventive action, began to be tested in the 1950s. Initially sodium nitrite was studied. However, due to side effects, such as poorer of concrete strength and increased occurrence of the probability of alkali-silica reaction (ASR), which have negative effects on the concrete, it was replaced by calcium nitrite, the first to be widely commercialized on a large scale. In general, the inorganic inhibitors have cathodic actions or anodic actions. Inorganic compounds such as nitrite, nitrate, chromate, and dichromate have been extensively investigated as inhibitors. The toxicity of these compounds limits their use in corrosion protection.

(b) *Organic CoI:* The use of organic compounds to inhibit corrosion of mild steel and iron has assumed great significance due to their application in preventing corrosion under various corrosive environments. A variety of organic compounds have been reported to be effective as corrosion inhibitors during acidization in industrial cleaning processes *(Al-Mehthel et al., 2009*). The development of corrosion inhibitors is based on organic compounds containing nitrogen, oxygen, sulfur atoms and multiple bonds in the molecules that facilitate adsorption on the metal surface. The corrosion inhibition efficiency of organic compounds is related to their adsorption properties *(Morris & Vázquez, 2002; Ormellese et al., 2009b*). Adsorption depends on the nature and the state of the metal surface, on the type of corrosive medium and on the chemical structure of the inhibitor. Studies report that the adsorption of the organic inhibitors mainly depends on some

physicochemical properties of the molecule related to its functional groups, to the possible steric effects and electronic density of donor atoms; adsorption is suppose also to depend on the possible interaction of p-orbitals of the inhibitor with d-orbitals of the surface atoms, which induce greater adsorption of the inhibitor molecules onto the surface of carbon steel, leading to the formation of a corrosion protecting film.

Organic inhibitors cover the entire surface area of the corroding metal with a thick film consisting of several monolayers and change the structure of the double layer at the metal interface, decreasing depolarization rate. They may also act as a barrier film by blocking anodic and cathodic active sites or decreasing electro active species transport rate to or from the metal surface. *Morris et al. 2003* states that organic inhibitors offer protection by absorbing and forming a protective film on the passive steel surface. The organic molecule usually contains a polar group that adsorbs on the metal and a non-polar, hydrophobic chain oriented perpendicular to this surface. On one hand these chains act by repelling aggressive contaminants dissolved in the pore solution and on the other, forming a tight film (barrier) on the metallic surface.

2.9 PERFORMANCE OF CoI IN DIFFERENT ENVIRONMENTS

In the past, there was an enormous list of chemicals which have been used either in chloride contaminated environment or in carbonated environment. They introduced in concrete either in admixed form or by applying on surface as migratory inhibitor. The performance of these inhibitors in different corrosive environments has been discussed in detail in succeeding sections.

2.9.1 Performance of CoI in chloride contaminated environment

In early studies, the focus of researchers was to investigate the effectiveness of these chemicals in chloride rich environment, as it was considered that most prominent cause of corrosion in RC. For preventing chloride induced corrosion they admixed during mixing process and for the repairing of chloride effected structure, chemicals were applied on the concrete surface after the corrosion encountered. (*Rosenberg & Gaidis, 1979*) studied the effectiveness of calcium nitrite on chloride contaminated concrete structure by using polarization technique. From the study it was concluded that calcium nitrite reduces the corrosion rate by 15 times when mixed at 2% and 4% concentration. *(Bolzoni et al., 2004*) investigated the influence of calcium nitrite-based inhibitor to study their effectiveness against

rebar corrosion along with three different organic inhibitors. They observed that, all the inhibitors were effective in reducing the corrosion rate, but calcium nitrite-based inhibitor showed the best inhibition effect among these in terms of reducing corrosion rate as well as weight loss of steel but at higher dosage. Similar observations were also made by *(Al-Amoudi et al., 2003; Ann et al., 2006*)**.** They also concluded that the inhibitive effectiveness of calcium nitrite-based inhibitor depends on [NO^-/Cl^-] molar ratio, which should be higher than 0.5-0.6 to prevent corrosion that confirms the study of (*Berke & Hicks, 2004; Elsener, 2000*). *(Sideris & Savva, 2005*) studied the influence of calcium nitrate-based inhibitor on the corrosion of reinforcing steel embedded in 14 mortars and found that the addition of calcium nitrite increases the chloride induced corrosion resistance of all mixtures, but protection offered strongly depends on the quality of cement used. Similar conclusions were also made by (*Montes et al., 2004*)

Apart from nitrite, other inorganic inhibitors such as phosphate, molybdate, chromate has also been investigated extensively in the past.(*Y. Zhou & Zuo, 2015*) studied the inhibitive mechanism of NO^{2-} and MoO_4^{2-} on the initiation and propagation of pitting corrosion for mild steel in chloride solution by using electrochemical methods and X-ray photoelectron spectroscopy (XPS). Based on the result author concludes that molybdate is able to protect pitting corrosion by effectively promoting passivation of mild steel. *Omotosho et al. 2010* examined the effectiveness of potassium dichromate and potassium chromate inhibitors on the corrosion of steel rebar embedded in concrete (admixed in different concentrations) partially immersed in sulfuric acid and NaCl medium. The results acquired showed that there were much less fluctuations observed in the potential readings when the concrete was mixed with CoI. The inhibition mechanism of phosphate is not clearly understood yet. Some researcher reported while using monoflourophosphate, it behaves as an anodic inhibitor and cause formation of passive layer of Fe_3O_4, γFe_2O_3, and $FePO_4.H_2O$ *(Alonso et al., 1996; Chaussadent et al., 2006a; Génin et al., 2002*). While another study concludes that this functional group has a dual action i.e., at low value of inhibitor to chloride ratio, phosphate acts as a cathodic inhibitor, whereas at higher ratio its acts as mixed inhibitor *(Dhouibi et al., 2003; Nahali et al., 2014; Yohai et al., 2013*)**.** *Yohai et al. (2013)* studied the inhibition efficiency of phosphate ions in chloride contaminated pore simulating solution, keeping equal concentration of phosphate and chloride ion (i.e. $[PO_4^{3-}]/[Cl^-] = 1$).

Table 2.3 Various functional groups used as corrosion inhibitor

	Functional group	Molecular structure	Inhibition type	Inhibition mechanism
Inorganic	Nitrites	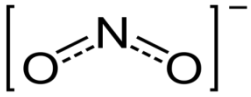	Anodic	Nitrite ions battle with chloride ions for ferrous ions to form protective ferric oxide film
	Molybdate	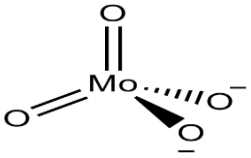	Anodic	Molybdate ions help promote the passivation of steel's active site through more effective film. They lessen the passivation current through the passive film, increase passive region area by displacing the corrosion potentials to more anodic values, promoting re-passivation of corroded regions
	Chromates	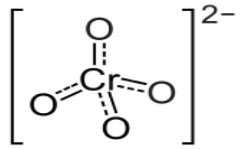	Anodic	Chromate helps maintain rebar in passive state preventing its disruption and impairment that can instigate pitting.
	Phosphates	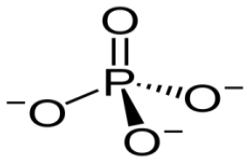	Anodic	By forming a passive layer of Fe_3O_4, γFe_2O_3, and $FePO_4.H_2O$.
	Phosphates		Mixed or cathodic	Behave as cathodic inhibitors for $[PO_4^{-3}]/[Cl^-]< 0.6$; behave as mixed inhibitors for $[PO4^{-3}]/[Cl^-] >0.6$.
Organic	Amines	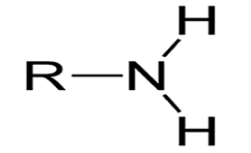	Mixed	Adsorption process is instigated as lone pairs of electron and polar nature become the reaction centre.
	Carboxylic Acid	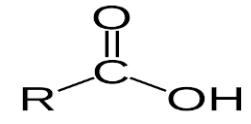	Mixed	A protective barrier is established on the steel surface through chelation process; carboxyl group (-

				COOH) being a good chelating agent.
	Aldehyde	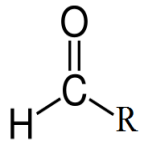	Mixed	Physically absorb on the steel surface via functional aldehydic oxygen atom of the inhibitor
Multifunctional	Alkanolamines	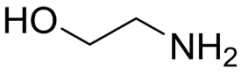	Mixed	Amino-alcohols absorb on the steel surface forming a film against erodic species like chloride or sulphate ions
	Amine-ester	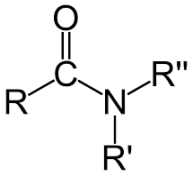	Mixed	The amine compound acts as an inhibitor while the carboxylate ester compound blocks the concrete pores, which further blocks the ingress of the aggressive ions; exhibiting a twin action of inhibition.

In addition to this, some organic inhibitors have also been used effectively to inhibit chloride induced corrosion. DMEA (Dimethyl ethanolamine) and AMA (amino-alcohol) were reported to be absorbed on rebar surface forming a protective layer of thickness 2-10 nm (*Söylev & Richardson, 2008*). *(Rakanta et al., 2013*) investigated the protective effect of N,N'-dimethylaminoethanol (DMEA) in chloride-contaminated pore solution using electrochemical and fiber optical microscopic methods. By comparing the test results with weight loss data, they concluded that DMEA creates an interfacial layer, effectively reducing the corrosion rate and mass loss of the steel rebar. (*Gaidis, 2004*) suggests that amino-alcohol (i.e., ethanolamine and diethanolamine) decreases corrosion by blocking cathodic sites only where O_2 picks up electrons and is reduced to OH^- ions. On the other hand, *Jamil et al., 2003* concluded that an inhibitor film was formed on the surface hindering the anodic sites and acts as an anodic inhibitor. (*Ormellese et al., 2009b*) studied the inhibition efficiency of several compounds like amines, amino acids, alkanolamines and carboxylates. Carboxylates (mono- and polycarboxylates) was concluded to be the best among all in terms of inhibition capacity. It was found that despite the electrostatic character and steric effect of carboxyl groups, the carboxylates compounds are also able to form complexes due to chelation process. *(Ormellese et al., 2011*) studied the inhibition properties of 2 amines, 4 amino acids and 3 carboxylate compounds in pore solutions and concrete with chloride induced corrosion. Test results revealed that amino acids perform better than amines. Sodium aspartate and sodium glutamate

enhanced critical chlorides content upto 0.4 mol/L. after analyzing all the tests performed, sodium glutamate and sodium tartrate were amongst the best inhibiting compounds. Cabrini et al. 2015 investigated the inhibitive property of aspartic acid in comparison with nitrite in alkaline pore solution (chloride containing). The tests were performed on carbon steel specimens in simulated pore solutions with an initial pH range of 12.6 to 13.8 and admixed with critical chloride threshold concentration. The investigation discloses that the aspartate ions probably adsorb on Fe (II) oxide surface due to its chelating property and inhibits corrosion through negative charge repulsion by its non-adsorbed carboxylate group. This may also effectively increase the critical chloride content.

2.9.2 Performance of CoI in carbonated environment

Literature on the use of CoI suggest that most of the compounds used to inhibit carbonation induced corrosion was organic based compounds. (*Trabanelli et al., 2005*) examined the efficacy of benzoic acid (BEN) and its derivatives (2-aminobenzoic acid (2AMB), dicarboxylic acid and dicyclohexaylammonium) in synthetic solution and in carbonated concrete. Electrochemical results conclude that BEN and its derivatives form a long-lasting layer on the steel surface in synthetic pore solution, but in concrete only benzoic acid and 2-aminobenzoic acid was able to perform efficiently. On comparing two, benzoic acid lost its inhibitive action after 400 days of carbonation exposure, while 2AB maintained its inhibition efficiency (60%) even at the end of testing age. (*Criado et al., 2012*) tested combination of disodium glycerophosphate (GPH) with sodium 3 aminobenzoate (3AMB) and sodium N-phenylanthranilate (PhAMB). Results based on polarization curves and EIS analysis suggest that combination of GPH and PhAMB performs best in carbonated environment. *Heiyantuduwa et al. (2006)* investigates the inhibition performance of commercially available CoI (blend of organic amino-alcohol and inorganic component) in carbonated environment. The inhibitor was used as MCoI in different concrete mixtures (M20, M30, M40 and M50). From the results it was found that the percolation of compound was most effective in M30 grade of concrete, and its application was helpful in delaying the carbonation induced corrosion. *Kaur et al. 2016* assessed the inhibition performance of two generic compounds (ethanolamine and anthranilic acid) along with two commercially available compounds (amine-ether based (COM1) and amino-alcohol based (COM2)) in synthetic pore solution and in concrete as migratory inhibitor. Among the tested inhibitors, both commercial inhibitors and anthranilic acid were able to perform in synthetic pore solution, while in concrete only COM2 and anthranilic acid were able to inhibit carbonation induced corrosion.

2.9.3 Performance of CoI in combined environment

Till now, several chemical compounds have been tested for their use as MCoI's in isolated aggressive environments of chloride or carbonation. However, in practical field conditions, both the species can attack simultaneously increasing the severity level of combined aggressive environment is multiple times higher than the individual. (*Andrade, C. Alonso, 1990*) conducted a study to investigate the impact of nitrite as a corrosion inhibitor in carbonated mortars contaminated with chloride, as well as in chloride-free carbonated mortars. They tested two different proportions of the inhibitor but concluded that neither proportion was sufficient to effectively reduce the corrosion rate in the combined environment. *Monticelli et al. 2011* studied the inhibiting properties of two organic compounds namely, sodium 2-amino benzoate (2AMB) and sodium glycerol-phosphate (GPH), in carbonated synthetic pore solution containing 0.1M NaCl. Test results confirms that higher inhibition efficiency was obtained (>87%) by adding mixture of 2AMB and GPH when inhibitor/chloride ratio was 0.5. However, it was also concluded that in combined environment the mixture slowly develops a passive film, and the corrosion was controlled by resisting the mass transport process. In another study**,** *Cao et al. 2015* try by using phytic acid as corrosion inhibitor in simulated carbonated concrete pore solution admixed with 0.6 mol/l NaCl. Electrochemical and sophisticated surface analysis techniques (SEM, XPS) show the deposition of three-layer protective film was formed on steel surface that protects the metal from corrosion. The inhibition efficiency at the end of 72 hours of immersion in simulated solution was more than 84%.

From the referred literature, this can be concluded that in the past researchers had very much focused on mitigating chloride induced corrosion and carbonation induced corrosion by using inorganic and organic based CoI. But in real environment, both species can attack simultaneously on RC creating a more vulnerable situation for the structure. Thus, there is need to investigate a potential CoI that could mitigate combined effect of carbonation and chloride on steel rebar. Nevertheless, only a limited number of studies have explored the application of chemicals in a combined aggressive environment. Many of these studies were conducted using synthetic pore solutions or mortars, where the corrosion inhibitor was directly mixed into the system. However, these findings cannot be directly applied to real-world scenarios involving MCoI, where the pore matrix of concrete plays a crucial role in determining the inhibitor's effectiveness. Further research is needed to investigate the performance of MCoI under realistic conditions, considering the complex interactions within the concrete's pore structure. Moreover, with the introduction of supplementary cementitious materials, there are more

complexities in the pore matrix; therefore, it is important to study the inhibition mechanism of MCoI in combined aggressive environment with variable concrete matrices.

2.10 CLOSING REMARKS

This chapter deals with the understanding of basic corrosion mechanisms, causes of rebar corrosion and efficacy of corrosion inhibitors in mitigating the corrosion under various aggressive environments. From the literature it was evident that most of the previous corrosion studies was primarily focused on individual environment of either chlorides or carbonation. However, in real conditions, both the aggressive species can attack simultaneously on the RC. The combined environment may create more severe conditions for the embedded reinforcement bars compared to individual actions, as carbonation significantly affects the redistribution of chloride within the concrete system. The effect of binder also plays a significant role in corrosion studies. Existing literature indicates that blended cement concrete exhibits superior resistance to chloride-induced corrosion compared to Portland cement concrete. However, the presence of carbonation can negatively impact its performance due to reduced portlandite content. The long-term performance of blended cement concrete in combined environments, where both chloride exposure and carbonation occur, has not been extensively studied, highlighting the need for in-depth investigation in this area.

Apart from this, various physical, chemical, and electrochemical techniques available as preventive and repair strategies to mitigate corrosion of rebar are discussed. Among the various techniques, use of CoI was the best method in terms of availability, application, inhibition efficiency, low cost and environmental concern. Also, a detailed discussion on various types of corrosion inhibitors is also presented. From the literature, it was found that admixed inhibitors can interfere in the hydration process and affect the fresh and hardened concrete properties. This can be eliminated by using them as migratory form when entire hydration process has been completed. From the literature review carried out, it was also found that most of the previous research work was primarily focused on the investigation of inhibitory performance of CoI (admixed or migratory) either in chloride contaminated environment or in carbonated environment. In a combined corrosive environment, the study of their performance is in its initial stages and needs to be explored by identifying potential CoIs for such conditions. Based on the extensive literature review, proposed objectives for the present research work were finalized.

CHAPTER 3

INHIBITION EFFICIENCY IN SIMULATED PORE SOLUTION

3.1 GENERAL

The focus of the current study is to mitigate rebar corrosion through use of generic compounds as migratory inhibitors in the combined aggressive environment of chlorides and carbon dioxide. To achieve the above-mentioned objective, the study was divided into three levels: pore solution test, migration ability test and ultimate application on reinforced concrete surface. The test matrix adopted in the study is illustrated through a flow-chart shown in Fig. 3.1.

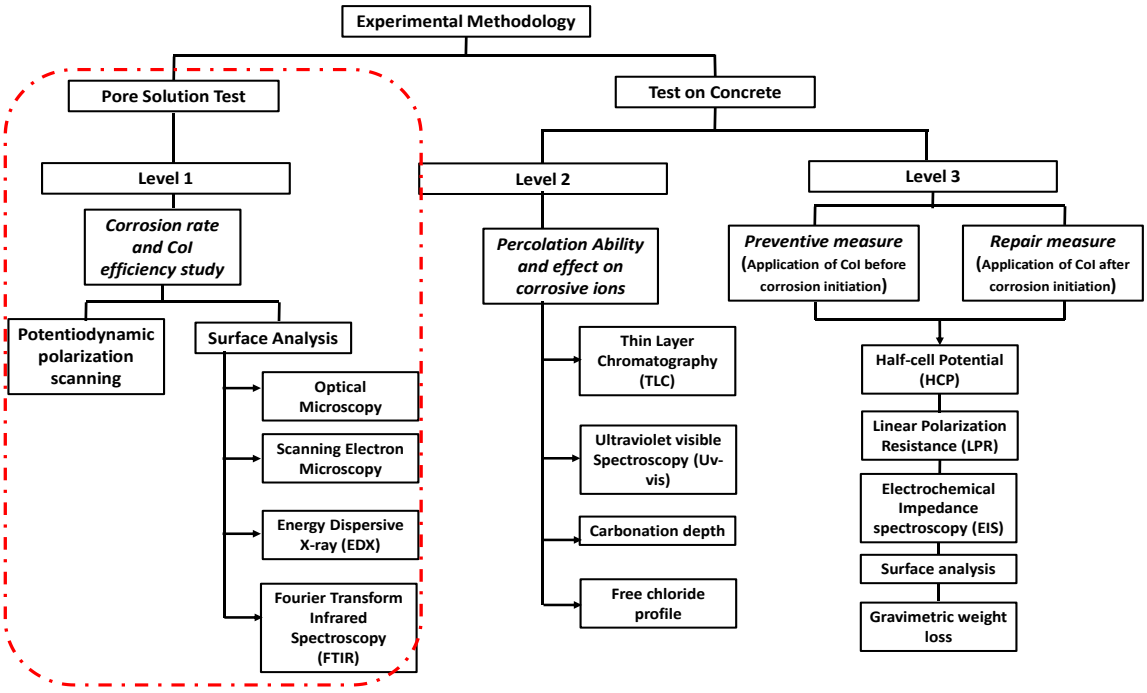

Fig. 3.1 Schematic illustration of experimental program adopted

This chapter deals with the first level of testing i.e., pore solution test where inhibition efficiency of some selected generic compounds against combined (carbonated + chloride) exposure condition was explored. In reinforced concrete (RC), the actual corrosion phenomena take a little longer for its occurrence. Therefore, alternative ways to introduce corrosion in a relatively smaller duration are thoughtfully formulated to preliminary check the efficiencies of the tested inhibitors in a short period of time. It consists of accessing the effectiveness of selected inhibitors in the simulated concrete pore solution (SCP) which is considered to imitate

the pore water chemistry of concrete that normally surrounds the rebar *(Fei et al., 2014; Monticelli et al., 2000*). Although, this system does not represent the actual condition of rebar in concrete, it can be used for comparing the inhibition efficiencies of various tested generic chemicals in relatively shorter time span. The material used in pore solution tests, experimental setup, corrosion monitoring and the test results of pore solution tests are discussed in the succeeding sections.

3.2 MATERIAL SYSTEM

The major materials used for preliminary investigation on pore solution are SCP, bare steel specimens and generic compounds. The details of all these materials are presented in the following sections:

3.2.1 Steel

12 mm diameter ribbed thermo mechanically treated (TMT) steel bars confirming to IS:1786-2008, 2008, widely used in RC structures were tested for their performance in corrosive environment. The chemical composition and properties of steel bars was provided by the manufacturer and is presented in Table 3.1 and 3.2, respectively.

Table 3.1 Chemical composition of TMT steel bars

Compound (%)	Carbon (C)	Sulphur (S)	Phosphorus (P)	S+P
TMT	0.250	0.040	0.040	0.075

Table 3.2 Physical properties of TMT bars

Property	Results obtained	As per IS 1786 Fe 500D (Minimum)
Manufacturer	Tata Tiscon	-
Diameter	12 mm	-
Yield Strength (YS)	520	500
Ultimate Tensile Strength (UTS) (N/mm^2)	580	565
Ratio of UTS/YS	1.15	1.08

3.2.2 Corrosion Inhibitors

Corrosion inhibitor (CoI) can be defined as a substance or chemical that, when used in small quantity in corrosive environment will reduce, slow down or prevent the corrosion of metal. CoIs are characterized as inorganic and organic based on functional groups present in the compound. Inorganic compounds either inhibit the anodic reaction or cathodic reaction of

the corrosion process; while organic compounds inhibit both anodic and cathodic half-cell reactions (*Dariva & Galio, 2014*). The focus of the present study is to prevent corrosion in a combined corrosive environment. Organic compounds were chosen as potential corrosion inhibitors due to the prevalence of organic-based commercial inhibitors.

The inhibition characteristics possessed by the organic CoIs depend on its molecular structure, polarity and presence of lone pair of electrons on the heteroatoms, that determines the adsorption of these molecules on the metallic surface *(El Ibrahimi et al., 2017; Schweitzer, 2017; Verma et al., 2017*). Since the proprietary corrosion inhibitors do not reveal their actual composition, generic compounds with known and effective functional groups were considered. Also, it was taken care that the chosen compounds have high solubility in the basic solution of SCP. In the present study, four generic compounds, namely, triethyl phosphate, salicylaldehyde, 2-Aminopyridine and 4-aminobenzoic acid were selected based on the presence of heteroatoms in their molecular structure. Triethyl phosphate has two heteroatoms' i.e., P and O present in the structure, salicylaldehyde contains benzene ring and one heteroatom (namely oxygen), 2-Aminopyridine consists of additional nitrogen, while 4-aminobenzoic acid consists of additional carboxylic (-COOH) functional group in the structure. These molecules are excellent candidates to study the effect of different functional groups and additional heteroatom on the corrosion inhibition properties. The molecular structure, chemical and physical properties, and reason of choice of the compounds are defined in Table 3.3.

3.2.3 Epoxy

To ensure that the corrosion is imitated over a specific area, only a small portion of the bare steel specimen was exposed to corrosion process and the remaining area was sealed with epoxy. Epoxy used in the present study was available in market with the trade name "Fevitite Rapid". It was a two-component adhesive, consisting of resin and hardener. Both the components were required to be mixed in equal proportions before use.

3.2.4 Other chemicals

Besides the generic compounds that were investigated for their use as corrosion inhibitors, some other chemicals were also used for preparation of simulated concrete pore solution that mimics the interstitial concrete pore solution. In order to prepare a synthetic pore solution, reagent grade calcium hydroxide ($Ca(OH)_2$), potassium hydroxide (KOH), and sodium

hydroxide (NaOH) were used. Along with this, analytical reagent grade hexane and methanol was used for cleaning of steel specimens and laboratory glassware.

Table 3.3 Properties of generic compounds selected for Level 1 testing

Compound Name	Triethyl-phosphate (TEP)	Salicylaldehyde (SA)	2-Aminopyridine (AP)	4-Aminobenzoic acid (ABA)
Molecular structure	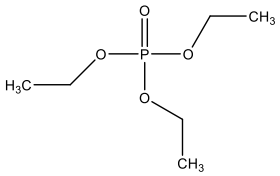	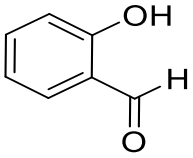	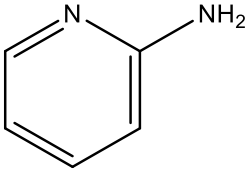	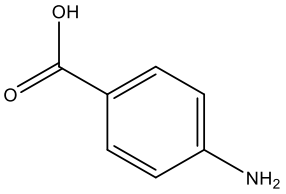
Molar Mass (g/mol)	182.15	122.12	94.117	137.14
Density (g/cm^3)	1.072	1.370	1.146	1.065
Boiling point (^oC)	215	340	197	60
Reason of choice	• Aliphatic • Presence of two heteroatoms (P and O)	• Aromatic • Two similar heteroatoms in structure with different functional groups (-OH and –CHO) • Functional groups are positioned adjacent to each other	• Aromatic • Heterocyclic compound containing amine functional group with additional heteroatom	• Aromatic • Two functional group (-COOH and $–NH_2$) attached to benzene ring are considered as multifunctional compound. • Functional groups are positioned far away from each other

3.3 PREPRATION PROCEDURE

The test set up required preparation of synthetic mixture which could simulate real concrete pore solution that surrounds the steel rebar. Also, the steel bars were to be prepared to expose a definite surface area for corrosion. The details of preparation of both bare steel specimens and of synthetic pore solution are presented in the following sections.

3.3.1 Preparation of Steel Specimens

12 mm diameter TMT bar was cut into pieces of 60 mm length. To ensure a rust-free surface, test pieces were rubbed with the help of emery paper of different grade sizes. The pieces were further washed with distilled water and cleaned by soaking in analytical reagent

grade hexane. After cleaning, the surface was allowed to dry and coated with two layers of epoxy leaving an exposed length of 4 mm at bottom for active corrosion process. In order to ensure electrical connectivity, a threaded hole was driven on top of the bar. A stainless-steel screw and nut were then inserted into the hole and a copper wire was wound around the nut (shown in Fig. 3.2(a)). For performing the surface analysis, special tablet shaped steel samples having diameter 12mm and thickness 2 mm were prepared as shown in Fig. 3.2(b). Prior to immersion, tablet surface was sequentially polished to obtain mirror finish surface by using polishing papers with grit size #600, #1000, #2000 and #3000. Finally, the tablet samples were washed with distilled water, degreased with analytical grade reagent hexane, and then dried at room temperature before subjecting to surface analysis tests.

Fig. 3.2 Bare steel specimen prepared for (a) electrochemical tests and (b) surface analysis tests in synthetic pore solution

3.3.2 Preparation of synthetic pore solution

To simulate the interstitial concrete pore solution, synthetic pore solution was prepared by mixing three alkalis; namely sodium hydroxide (0.1M NaOH), potassium hydroxide (0.3M KOH) and calcium hydroxide (0.01M $Ca(OH)_2$) in distilled water *(Alizadeh et al., 2023; Verbruggen et al., 2016*). This solution was stirred vigorously for proper mixing of hydroxides and was further left undisturbed for 24 hours. It was then filtered with the help of Whatman No. 1 filter paper and pH of solution was noted accurately with the help of pH meter. Further, to simulate the combined corrosive environment, the filtered solution was bubbled with pure carbon dioxide (CO_2) gas to reach a pH of nearly 9. The bubbling of CO_2 will cause the formation of calcium carbonate precipitate in the solution that was removed by filtering the solution again with the filter paper. The obtained solution was then admixed with 0.1M sodium chloride (NaCl). This solution containing both chlorides and carbon dioxide is referred to as the base solution (S1).

Once the corrosive solution was prepared, the desired generic compound (as mentioned in section 3.2.2) was added to it. To study the optimum concentration of each generic compound as CoI, the inhibition efficiency was investigated at three different concentration levels, viz. 0.05M, 0.1M and 0.2M. The abbreviation and concentration of various generic compounds used in the present work are listed in Table 3.4. After mixing the CoIs in the base solution, a slight change pH value of the resultant solution was observed. To maintain pH value of the solution at around 9, the solution was either bubbled with CO_2 (if the inhibitor addition increased the pH value) or sodium hydroxide was added (if the inhibitor addition lowered the pH value).

To assess the aggressiveness of the combined aggressive environment, the performance of base solution was compared with three different solutions, viz. the uncontaminated concrete pore solution, only chloride environment and only carbonated environment. Uncontaminated concrete pore solution (S0) was prepared by adding only the hydroxides (as described in the first step of preparation for base solution), chloride aggressive environment was obtained by adding 0.1M NaCl to S0, while carbonated environment was created by bubbling S0 with CO_2. The abbreviations and other details of sixteen synthetic solutions is provided in Table 3.4.

Table 3.4 Nomenclature and details of prepared synthetic pore solutions

S. No.	Nomenclature	Inhibitor name	Concentration (mol/L)	pH
1.	S0 (SCP)	-	-	13.2±0.2
2.	S0+0.1M Cl (SCP contaminated with chlorides)	-	-	13.2±0.2
3.	S0+carb (SCP with carbon-dioxide)	-	-	8.9±0.2
4.	S1 (SCP with chlorides +carbon-dioxide)	-	-	9 ± 0.2
5.	S1+TEP0.05M	TEP	0.05	9.10 ± 0.2
6.	S1+TEP0.1M		0.1	9.14 ± 0.2
7.	S1+TEP0.2M		0.2	9.15 ± 0.2
8.	S1+SA0.05M	SA	0.05	9.53 ± 0.2
9.	S1+ SA0.1M		0.1	9.52 ± 0.2
10.	S1+ SA0.2M		0.2	9.21 ± 0.2
11.	S1+AP0.05M	AP	0.05	9.13 ± 0.2
12.	S1+AP0.1M		0.1	9.16 ± 0.2
13.	S1+AP0.2M		0.2	9.32 ± 0.2
14.	S1+ABA0.05M	ABA	0.05	9.13 ± 0.2
15.	S1+ABA 0.1M		0.1	9.38 ± 0.2
16.	S1+ABA0.2M		0.2	9.50 ± 0.2

3.4 CORROSION AND ITS MONITORING

The cylindrical steel specimens were partially immersed in different pore solutions to initiate the corrosion process. While placing the steel specimen in the solution, it was ensured that the bottom exposed part of steel sample remain submerged in the solution during the investigation as shown in Fig. 3.3. The corrosion activity of the specimens was tested at 24 hours (hrs), 48 hrs, 120 hrs and 240 hrs of immersion by conducting potentiodynamic scanning. The testing duration till 240 hrs was chosen after thorough review of the existing literature. The testing duration of 240 hrs was chosen as it is a true representation of actual behavior of the compounds against corrosion (*Kaur et al., 2016*). Other researchers have also chosen similar testing ages to study the performance of different corrosion inhibitors in pore solutions (*R. Liu et al., 2014)*. Shorter testing durations of 24 and 48 hrs are reported to be not the true representation of actual behavior of the compound against protection because some time is generally taken by the compound to stabilize in the pore solution.

The corrosion monitoring was done by using Gill AC corrosion analyzer (serial number 1463). Electrochemical cell used in the monitoring consisted of a cylindrical jar with arrangement of providing necessary fittings to make connection with the reference electrode, noise reduction probe, auxiliary electrode, and the test specimen. After immersing the specimens in the aggressive pore solution, the specimens were periodically measured by using potentiodynamic polarization method with three electrode arrangement, in which TMT steel bar was used as working electrode (WE), platinum electrode as a counter electrode and saturated calomel electrode as reference electrode. A noise reduction probe was also attached to the electrochemical cell to reduce mains signal polarization and hence, minimize the reference electrode measurement noise. Noise-reducing (NR) electrodes are constructed using pure platinum set in a glass tube, with the active component sealed within the glass. Their purpose is to capacitively couple the reference electrode buffer input to the bulk electrolyte, creating a low impedance path to ground for any induced voltages in the plug-in probe or salt bridge. By using NR electrodes, unwanted polarization caused by mains-induced signals is eliminated, leading to more accurate and reliable measurement results in certain systems, such as those involving mains heaters. The electrochemical setup for corrosion monitoring is shown in Fig. 3.4. All the measurements were carried out in open-air conditions at room temperature of around 25 ± 5 ^{o}C. Polarization curve for each specimen, at a defined testing age, was recorded at a scan rate of 0.5mv/sec over a potential ranging from -250 mV to 1500 mV. The high scan

range makes the test highly perturbing to the electrodes. For this reason, the test was always conducted on undisturbed samples.

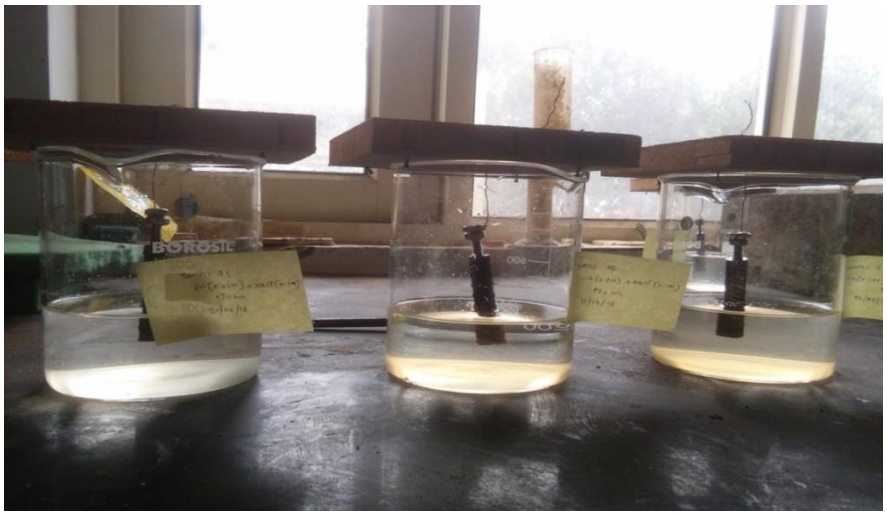

Fig. 3.3 Steel specimen immersed in synthetic pore solution

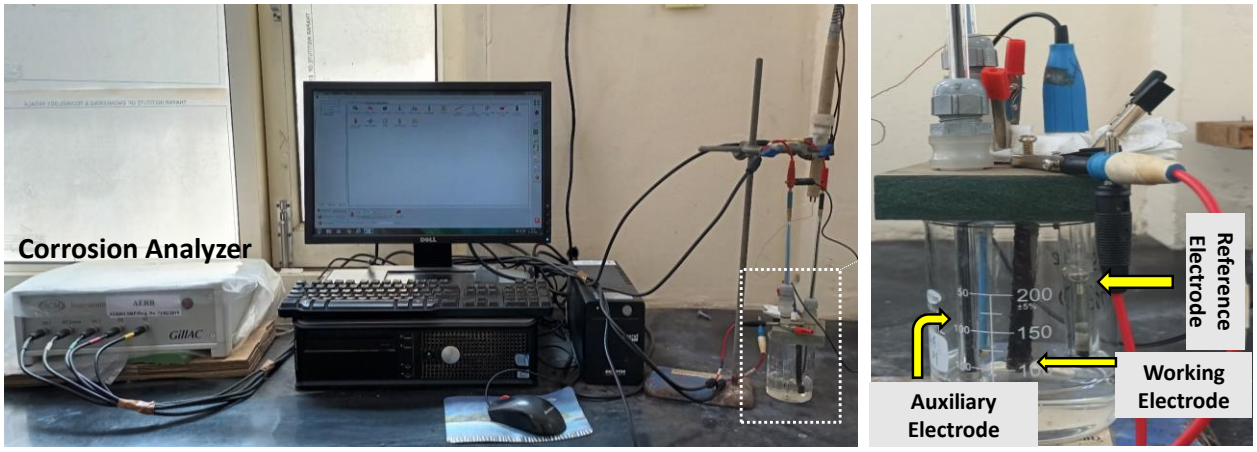

Fig. 3.4 Connection arrangement of electrochemical cell with corrosion analyser

Fig. 3.5 shows the typical polarization curve for passivating metal. The curve consists of two distinct regions namely, cathodic, and anodic region. Region AB represents cathodic behavior. The open circuit or rest potential is located at point B. At this potential the sum of anodic and cathodic reaction rates on the electrode surface is zero. As a result, the measured current will be close to zero. The anodic branch is further divided into three distinct regions namely, active, passive and transpassive region. As the potential increases from B, region BC is recorded in which dissolution of metal cause significant increase in current density with little change in potential. The region BC is referred to as the active region. Region CD is referred to as passive region, in which change in current density is relatively small with large increase

in potential. This region represents the stability of passive layer over the metal surface. Once the potential reaches a sufficiently positive value (Point D, sometimes termed the breakaway potential) the applied current rapidly increases (region DE) with small variation in potential. For some systems (e.g., iron in salt water) this sudden increase in current may be pitting (localized breakdown of passivity), while for others it may be transpassive dissolution.

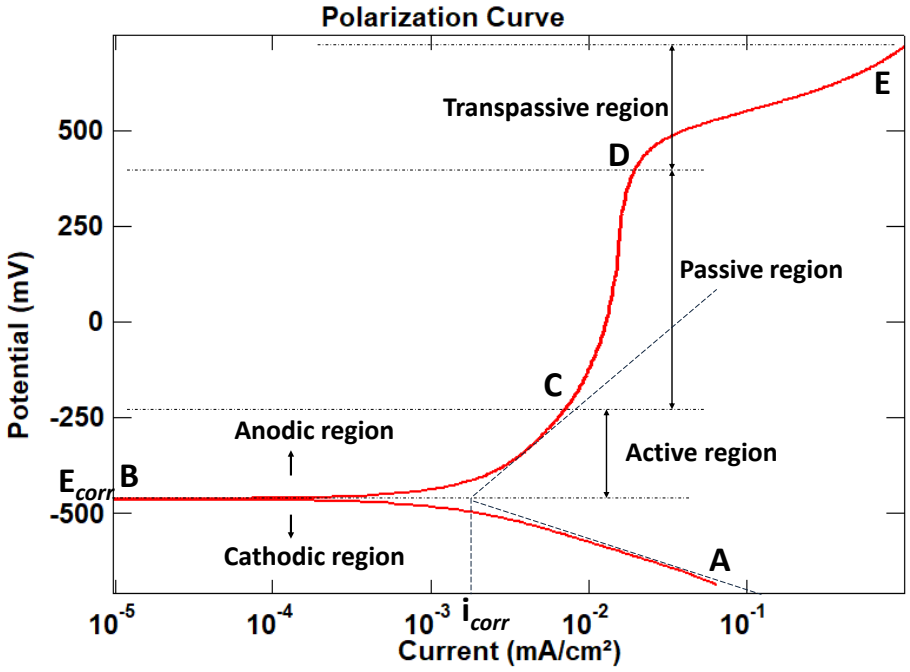

Fig. 3.5 Typical polarization curve with different regions

The Tafel extrapolation technique of all the samples were used to obtain the corrosion current density values. In the Tafel plot, the slopes of anodic and cathodic branches are generally linear up to ±50 mV, and this region is used to do the extrapolation for corrosion current measurement *(William Stephen Tait, 1994)*. The inhibitive efficiency (η%) of the compound was calculated by comparing the obtained corrosion current density with the corresponding value of S1 solution. The formula for inhibitor efficiency is given in Eq. 3.1:

$$\eta\% = \frac{i_{corr,0} - i_{corr,1}}{i_{corr,0}} \times 100 \qquad \ldots(3.1)$$

Where $i_{corr,0}$ and $i_{corr,1}$ is the corrosion current density at a defined testing age in the absence and presence of inhibitor, respectively.

3.5 SURFACE ANALYSIS TESTS

The corrosion process has an important influence on the surface of steel; thus, a thorough surface analysis of the steel tablets immersed in the respective solutions was conducted to understand the impact of inhibitor on surface characteristics and to interpret the possible

inhibition mechanism. The surface analysis was performed on one optimum concentration of inhibitor that was decided from the results of inhibitor efficiency. After deciding the optimum concentration, the steel tablets were kept in these solutions for 240 hours. After immersion, following tests were conducted to examine the surface of the tablet:

3.5.1 Optical Microscopy

The microscopic images were obtained at the end of testing duration by a SMZ 100 stereomicroscope at 10X and 20X magnification.

3.5.2 Scanning electron microscopy (SEM) with Energy dispersive X-ray spectroscopy (EDX)

The surface morphology of the dried specimens was observed by SEM (JEOL JSM-6510LV) and the elements present at the surface were obtained through EDX (EDAX octane pro). The accelerating voltage used for imaging and EDX analysis was 10 kV, with magnifications at 500X.

3.5.3 Fourier Transform Infrared Spectroscopy (FTIR)

The steel tablet sample (2 mm) to be tested was vacuum dried for 48 hrs and FTIR of the steel surface was recorded on Perkin Elmer-Spectrum RX-IFTIR spectrometer to identify and analyze the chemical composition of products formed on the top exposed surface. The absorbance determination range was 400-4000 cm^{-1}, the background noise correction involved 16 times cumulative scan and a resolution ratio of 1 cm^{-1}. The automatic baseline and the original spectral data were corrected by FTIR software.

3.6 RESULTS AND DISCUSSIONS

The results obtained by performing the above-mentioned tests in pore solution are presented in the upcoming sections. Electrochemical test results, surface analysis outcomes and a consequent mechanism are discussed in detail.

3.6.1 Potentiodynamic polarization (PDP) scans in different solutions

To investigate the severity level of different corrosive environments and effectiveness of CoI, potentiodynamic studies of bare steel specimens immersed in different solutions were carried out at 24 hrs, 48 hrs, 120 hrs and 240 hrs of immersion. Each rebar sample was immersed in its respective solution for different testing durations. Once the testing was completed, the sample was discarded. The curves are presented in Fig. 3.6, Figs. 3.8 to 3.12.

The electrochemical parameters obtained from the PDP scans are tabulated in Table 3.5. The efficiency of generic compounds was also calculated by using corrosion current density (i_{corr}) at 240 hours of immersion and the values are presented in Table 3.6. The tests were carried out in triplicate; however, only one (representative) measurement is shown because of good repeatability and better visibility.

(i) PDP curves for bare steel immersed in S0, S0+0.1M Cl, S0+carb and S1

To understand the comparative behaviour of bare steel in different environments without adding inhibitors, the steel specimens were tested in uncontaminated simulated pore solution (S0), pore solution contaminated with chlorides (S0 + 0.1M Cl), carbonated pore solution (S0 + carb) and carbonated pore solution with chlorides (S1). The comparative PDP curves obtained at 120 hrs of immersion in all these solutions are presented in Fig. 3.6. Alongside, the surface conditions of immersed bar in their respective solutions are presented in Fig. 3.7.

As can be seen from Fig. 3.6, in S0 solution, steel registered a corrosion potential (E_{corr}) of -85 mV_{sce} and a passive behavior up to 685 mV_{sce}, with the passive current density in the range of 6.5 µA/cm^2. The addition of 0.1M chloride (as NaCl) in S0 (S0 + 0.1M Cl) still permitted steel to develop passive behavior under free corrosion condition, but potential shifted towards active region and a weaker passive layer was formed. The pitting potential was recorded at around 475 mV_{sce}. The i_{corr} value was found to be one magnitude higher than S0 (i.e., 16.5 µA/cm^2). Corrosion resistance of steel diminished completely under carbonation (S0 + carb). E_{corr} shifted down to -520 mV_{sce}, the passive behavior disappeared, and current density was found to increase. These negative effects were further enhanced when chlorides were added to the carbonated solution (S1 solution), because of a marked stimulation of the anodic reaction that shifted the E_{corr} further down to -600 mV_{sce} and increased the i_{corr} to 126 µA/cm^2. When comparing the i_{corr} values of S1 with the other contaminated solutions, namely S0+0.1M Cl and S0+Carb, it was observed that the i_{corr} values of S1 were 87% and 24% higher, respectively. This indicates that the presence of both species in the vicinity of the rebar creates a more vulnerable situation for the rebar, making it more susceptible to corrosion. The addition of chloride in S0 solution weakened the passive layer and carbonation of S0 solution transformed the passive layer to pseudo-passive. The presence of both these aggressive conditions together (S1 solution) transformed the passive behavior to active corrosion conditions. All these changes in the solution chemistry were observed on the anodic part of the curve, while limited influence was observed on the cathodic reaction.

From Fig. 3.7, the rebar immersed in S0 appeared to be free from any signs of corrosion. However, those immersed in contaminated solutions show visible signs of corrosion. The rebar in S0+0.1M Cl shows pitting at various spots; while in S0+carb, the rebar shows accumulated corrosion products all over the surface. This is the typical behavior of reinforcement in chloride environment and carbonation-induced environment where localized corrosion was seen in the former while uniform corrosion in the latter. Furthermore, the rebar in S1 (i.e., combined aggressive environment) was seen to be most corroded with pits as well as uniform corrosion. This indicated that combined environment is the most severe for rebar corrosion. The surface condition correlated well with the i_{corr} values.

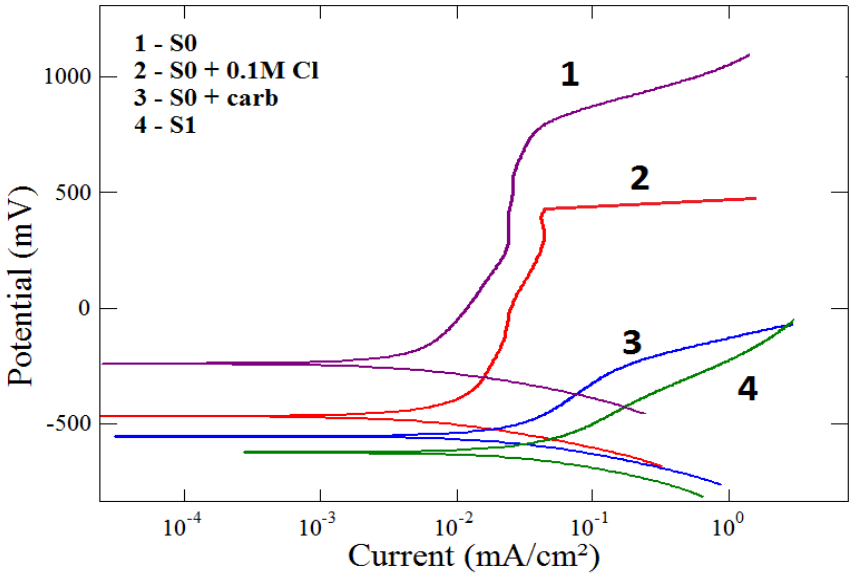

Fig. 3.6 Polarization curve recorded on steel in different solutions

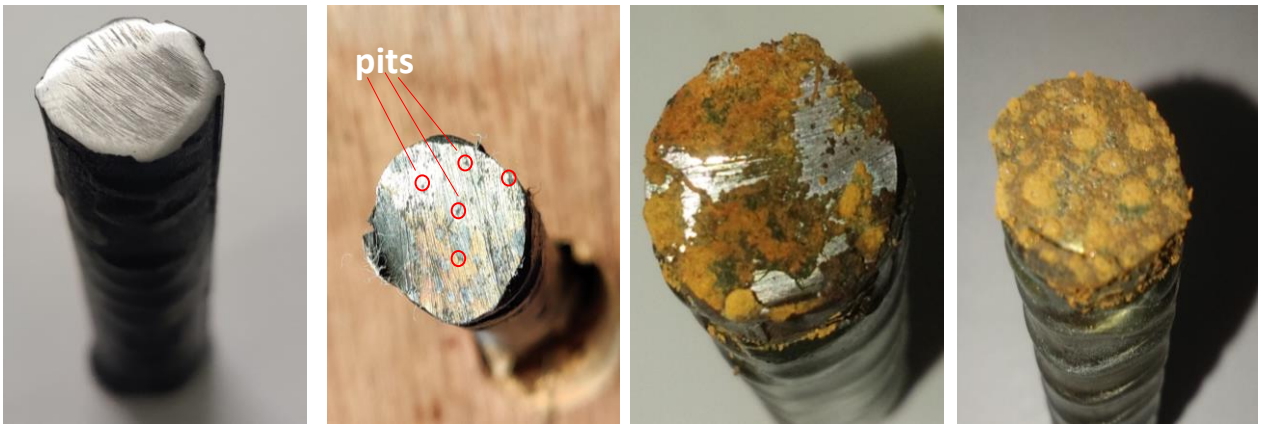

Fig. 3.7 Surface condition of rebar after 120 hrs of testing in respective solutions

Further, the base solution S1 representing a typical carbonated and chloride aggressive environment in simulated pore solution was studied in detail by taking PDP curves at 24, 48, 120 and 240 hrs separately. The progressive change in polarization curves with the immersion time in S1 solution is shown in Fig. 3.8. It can be interpreted that the Ecorr values shifted towards active region (-235 mVsce to -650 mVsce) and the current density increased from 45 µA/cm^2 at 24 hr to 220 µA/cm^2 at 240 hr indicating the active corrosion reaction on the surface of steel. Also, a well-defined pitting potential was not observed at any immersion age, indicating the absence of stable oxide layer on the surface due to low pH thus, indicating uniform corrosion at low pH environment (i.e., a uniform increase in the current value with increase in the applied potential).

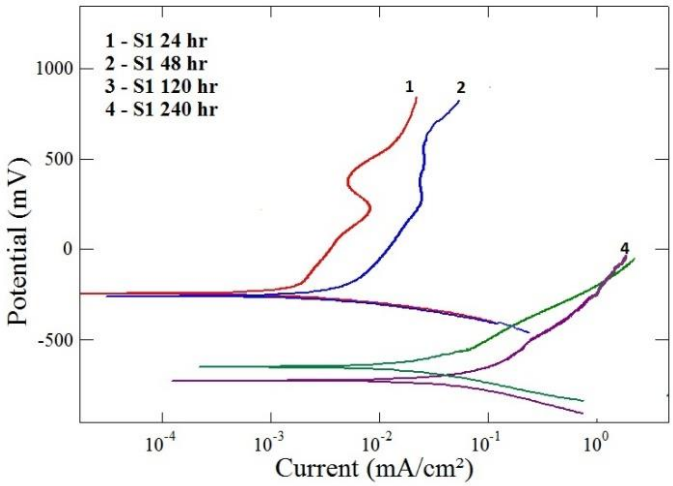

Fig. 3.8 Polarization curves recorded on steel in carbonated chloride solution (S1)

(ii) Potentiodynamic behavior for S1 + TEP

The potentiodynamic behavior of simulated pore solution mixed with TEP as CoI is represented in Figs. 3.9(a) to (c) for 0.05M, 0.1M and 0.2M concentration levels, respectively. The electrochemical parameters obtained from the curves are presented in Table 3.5. Fig. 3.9(d) shows the comparative polarization curve at the three concentration levels after 240 hr of immersion. A comparative curve is used to identify the possible inhibition mechanism on the basis of potential difference values.

Fig. 3.9 indicates that the presence of TEP, irrespective of concentration, shifted the active corrosion behavior of the base solution S1 to pseudo-passive behavior. In fact, after addition of 0.05M TEP, a typical passive behavior was observed followed by a breakdown potential near 500 mV and a transpassive behavior thereafter at the initial testing duration of 24 hr and 48 hr. With increase in testing duration, i_{corr} values increased with the final corrosion current

density at 240 hrs of 76.2 µA/cm^2, which was still one order magnitude lower than the base solution S1 (2.20E-01 mA/cm^2).

As the concentration of TEP was increased to 0.1M, the OCP of the test solution settled down at around -500 mV. The anodic curve tried to be stable towards the passive side with an increase in testing duration which indicates that corrosion inhibitor tries to form a thin layer on the surface of the rebar. Also, no typical pitting potential was observed in any of the curves.

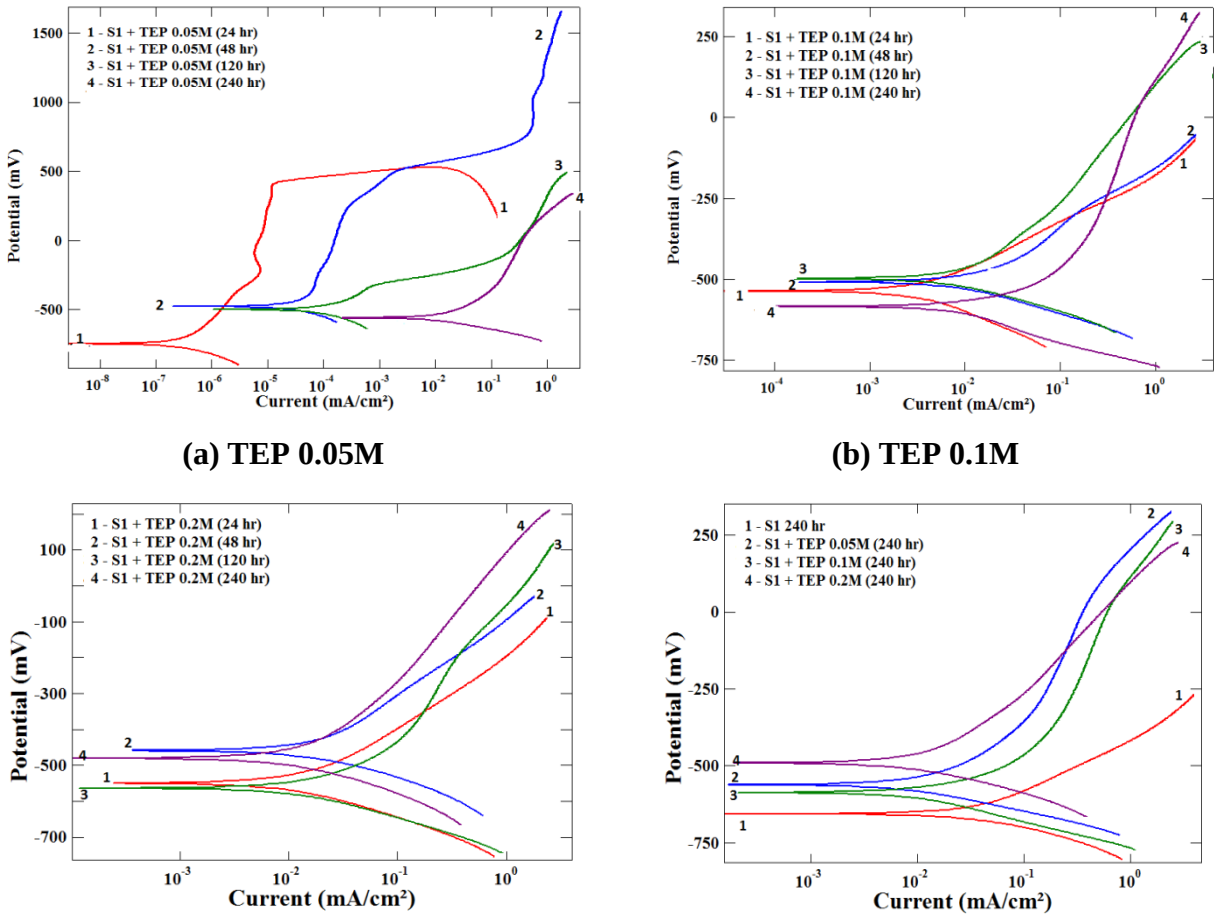

(a) TEP 0.05M **(b) TEP 0.1M**

(c) TEP 0.2M **(d) TEP Vs S1 (at 240 hrs)**

Fig. 3.9 Polarization curves of bare steel in carbonated chloride solution with TEP as corrosion inhibitor

As the concentration of TEP was increased further, the i_{corr} values increased initially (78 µA/cm^2 at 24 hours of immersion) and tended to stabilize at lower values with the increase in immersion time. The final i_{corr} value was 33.2 µA/cm^2 at 240 hr of immersion, which is one order magnitudes lower than the base solution S1. The polarization curve shows typical active corrosion behavior at 24 hr and 48 hr of immersion. With increase in test duration, the E_{corr} became nobler with shift in value from -550 mV to -436mV$_{sce}$. The polarization curve started

showing pseudo-passive behavior, with the typical absence of a well-defined passive region. It can, therefore, be concluded that the presence of TEP at higher concentration reduced the corrosion rate by shifting potential towards anodic side but failed to form a stable protective layer on the electrode surface.

A comparative polarization scan obtained in base solution without inhibitor and with variable concentration of TEP as inhibitor after 240 hr of immersion is shown in Fig. 3.9(d). The curves show that the current density values of TEP admixed solutions remained on nobler side as compared to the base solution, indicating the inhibition capacity of TEP as corrosion inhibitor. The i_{corr} value decreased by one order magnitude lower than the base solution with the addition of TEP, irrespective of the concentration level. The i_{corr} value at 0.05M, 0.1M and 0.2M concentration after 240 hr is 76.5 µA/cm^2, 53.2 µA/cm^2, 33.7 µA/cm^2. Also, the active behavior of the polarization curve for base solution was seen to shift towards pseudo-passive behavior in TEP admixed solutions. From these curves, it can be observed that the change in potential values in most of the curves was smaller than ±85mV. This small change in potential indicates that TEP acts like a mixed kind of inhibitor *(Ansari et al., 2015; Jayaperumal, 2010; H. S. Lee et al., 2018; Yadav et al., 2016*). The results indicate that phosphate group of TEP possibly retards the corrosion by promoting the growth of protective iron oxide film on the rebar surface; thereby healing the defects in protective film due to aggressive exposure. The protective oxide layer formed by the phosphate ions from the inhibitor however got damaged by the presence of the chloride ions. Similar observations have been reported by *(Nahali et al., 2014*)**.**

(iii) Potentiodynamic behavior of S1 + SA

The potentiodynamic behavior of steel rebar immersed in simulated pore solution mixed with *SA* as CoI inhibitor is represented in Figs. 3.10(a) to 3.10(c) for 0.05M, 0.1M and 0.2M concentration levels, respectively. The electrochemical parameters obtained from the curves are presented in Table 3.5. The polarization curves obtained at 0.05M concentration of SA (Fig. 3.12(a)) exhibited pseudo-passive behaviour at later testing durations. PDP curves indicate active rate of corrosion at initial testing durations with high i_{corr} value. However, with the increase in testing duration, active corrosion was arrested, and pseudo-passive behavior was noted. The i_{corr} values obtained were 78 µA/cm^2 and 82 µA/cm^2 respectively, at 24 hrs and 48 hrs of testing. But at the later testing duration, the i_{corr} values have been reduced to 44 µA/cm^2

at 120 hr and 7.8 µA/cm^2 at 240 hr of testing duration. The obtained i_{corr} values were lower than the corresponding values obtained in base solution S1 after 120 hr of immersion.

As the concentration was increased to 0.1M (Fig.3.10(b)), pseudo-passive behavior was observed at 48 hr of testing duration and the inhibitor seemed to be more effective. Active-passive transition was observed after 120 hr of testing along with drastic decrement in i_{corr} value. The i_{corr} value obtained at 120 hour of testing duration was four order magnitude lower than that obtained at 24 hr and 48 hr of testing duration. At 240 hr of testing, a positive hysteresis was observed after a stable passive region and breakdown potential of around 1050 mV_{sce}. This states that a passive layer was formed via adsorption of SA on the rebar surface which is stable up to 1050 mV.

At higher concentration of 0.2M (Fig. 3.10(c)), the slope of the anodic curve increased, and the curve became stable with the immersion age. After 240 hr of immersion, the very stable passive region was observed that remained stable at even very high scanning potential. The polarization curves indicate that SA was able to resist the localized as well as uniform corrosion (characteristics typical to chloride and carbonation induced corrosion, respectively) by forming a protective layer, which became very stable with the immersion age. The current density value decreased from 60 µA/cm^2 at 24 hr to 0.14 µA/cm^2 at 240 hr and corrosion potential shifted towards a more negative value due to formation of passive layer on the rebar surface.

The obtained test results indicate that Salicylaldehyde as a corrosion inhibitor has a persistently good inhibition efficiency for prolonged immersion period as well as on higher concentration. The initial values of corrosion current density were higher than the base solution S1, irrespective of the concentration level; but final values were two to three orders of magnitude lower than the base solution. Also, at lower concentration (i.e., 0.05M), the curve showed pseudo-passive behavior after 240 hr of testing duration, while with increase in the concentration (i.e., 0.1M), the pseudo-passive behavior was noticed at 48 hrs of testing duration. The passive region became stable with the concentration as shown in Fig. 3.10(d). When compared to the base solution S1, corrosion potential difference remained within ±85 mV that shows the mixed kind of inhibition.

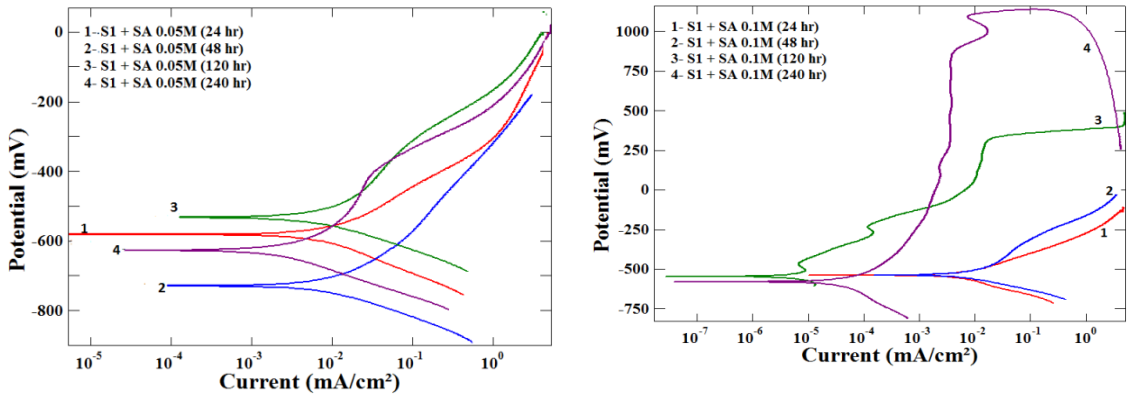

(a) SA 0.05M **(b) SA 0.1M**

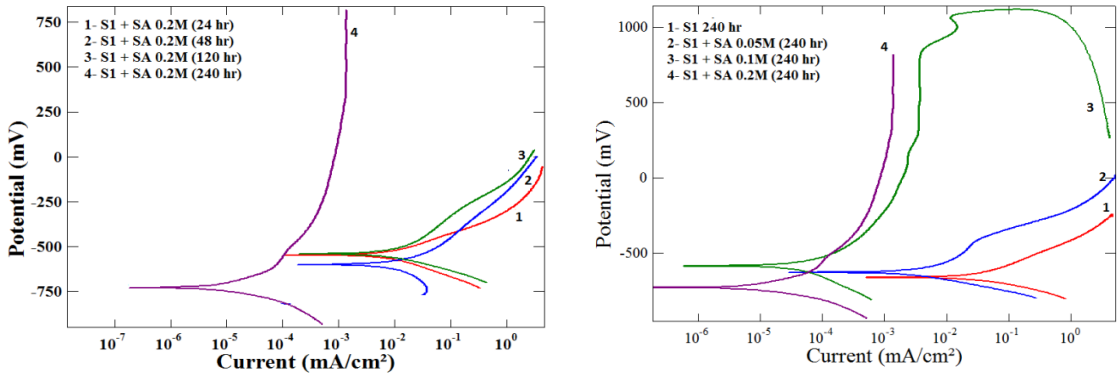

(c) SA 0.2M **(d) SA Vs S1 (at 240 hrs)**

Fig. 3.10 Polarization curve of bare steel in carbonated chloride solution with SA as corrosion inhibitor

(iv) Potentiodynamic behavior of S1 + AP

The potentiodynamic polarization curves of bare steel in simulated pore solution admixed with AP as CoI are presented in Fig. 3.11(a) to 3.11(c) for 0.05M, 0.1M and 0.2M concentration levels of the admixed compound, respectively. Fig. 3.11(d) shows the comparative polarization curves at the three concentration levels after 240 hrs of immersion.

Fig. 3.11(a) depicts a typical transpassive behavior of PDP curves at lower concentration of AP, wherein E_{corr} values shifted towards more negative side with the increase in testing duration. Also, the corrosion current density increased from 2.4E-02 µA/cm^2 at 24 hours to 34 µA/cm^2 at 240 hrs of immersion. All the curves displayed pseudo-passive behavior followed by transpassive zone. At 24 hrs and 48 hrs, it appeared that the passive layer was metastable. The transpassive zone shifted towards lower values (750 mV at 24 hrs to 300 mV at 240 hrs) indicating that the inhibition potential decreased with the immersion age. The current density obtained at 240 hrs was still lower than the corresponding value in the base solution S1, indicating inhibition capacity of AP at this concentration level.

As the concentration of AP was increased to 0.1M, the compound provided better inhibition. The polarization curve at 24 hrs of exposure, although, showed uniform increase in current density due to active dissolution of rebar in pore solution. At the later testing durations, the polarization curve illustrated a distinct pitting potential that indicated the effect of chlorides on the corrosion kinetics. The pitting potential shifted towards more positive values with immersion period indicating a high tendency of inhibition. The curve obtained at 48 hrs of testing duration shows active-passive transition that might be due to surface film formation. But after 120 hrs of immersion, a distinct passive region was noticeable and i_{corr} decreased to 0.14 µA/cm^2. At 240 hrs of immersion, the anodic curve was observed to be stable up to 1000 mV and i_{corr} value decreased by two order magnitudes lower than initial testing age.

As the concentration level further increased to 0.2M, the passive behavior was further reinforced. The anodic curve showed slightly transpassive behavior at 24 hrs, an active passive behavior after 48 hrs of immersion along with transpassive zone. A well-defined and stable passive region was obtained after 240 hr of immersion. It clearly indicates the tendency of AP to form passive layer on steel surface which stabilized with time. The corrosion current density decreased by five orders of magnitude as compared to the initial current density obtained at 24 hrs (i.e. 6.7E-02 at 24 hrs to 1.38E-07 at 240 hrs). The OCP values remained stable up to 120 hrs of testing duration (-479.34 mV_{sce} at 24 hrs and -476.94 mV_{sce} at 120 hrs) and shifted towards more negative (-590.95 mV_{sce}) value after 240 hrs of test duration. The final corrosion density was six orders of magnitude lower than the base solution S1.

A comparative polarization scan obtained in base solution without inhibitor and with variable concentrations of AP as inhibitor after 240 hrs of immersion is shown in Fig. 3.11(d). The curves displayed almost a constant open circuit potential. The i_{corr} value at 0.05M, 0.1M and 0.2M concentration after 240 hrs was 34 µA/cm^2, 5.75E-02 µA/cm^2 and 1.38E-04 µA/cm^2 in comparison to corresponding value of the base solution S1 (220 µA/cm^2), the current density values remained on nobler side, indicating the inhibition capacity of AP as corrosion inhibitor. Also, the active behavior of the polarization curve for base solution shifted towards pseudo-passive behavior to stable passivation with increase in concentration of inhibitor. From the curves, it can be observed that change in potential value is smaller than ±85 mV for all solutions. This small change in potential indicates that AP acts like a mixed kind of inhibitor.

Table 3.5 Electrochemical parameter at different inhibitor concentrations

Solutions	24 hours			48 hours			120 hours			240 hours		
	i_{corr} ($\mu A/cm^2$)	E_b (mV)	E_{corr} (mV)	i_{corr} ($\mu A/cm^2$)	E_b (mV)	E_{corr} (mV)	i_{corr} ($\mu A/cm^2$)	E_b (μV)	E_{corr} (μV)	i_{corr} ($\mu A/cm^2$)	E_b (mV)	E_{corr} (mV)
S1	45.1	-	-250.6	73.3	-	-265.2	126	-	-600.56	220	-	-650
0.05M												
S1 + TEP	5.4E-04	480	-714	4.46E-02	500	-449	3.3E-01	-	-499	76	-	-570
S1 + SA	78		-572	82	-	-708	44	-	-495	7.8	-	-626
S1 + AP	2.40E-02	-	-150.4	0.50	-	-237.02	1.25	-	-218	34	-	-579.7
S1 + ABA	39	-	-785.1	140	-	-718.68	103	-	-570.05	8.90E-04	-	-560
0.1M												
S1 + TEP	190	-	-529	47	-	-501	50	-	-489	53	-	-580
S1 + SA	39	-	-520	38	-	-515	2.85E-03	-	-515	1.65E-04	-	-570
S1 + AP	1.39E-04	300	-279.3	4.16E-03	-150	-282.5	2.61E-03	-200	-407.8	5.70E-02	1000	-560.2
S1 + ABA	61	-	-749.7	94	-	-774.1	91	-	-626.4	9.40E-02	740	-760.5
0.2M												
S1 + TEP	78	-	-550	53	-	-436	53	-	-570	33	-	-488
S1 + SA	60	-	-545	9	-	-535	4	-	-580	0.14	-	-730
S1 + AP	19.3	-	-479.3	9.5	-	-476.9	0.19	-	-410.9	1.38E-04	-	-590.9
S1 + ABA	40	-	-517.9	63	-	-759.91	59	-	-762.3	5.77E-03	-	-783.25

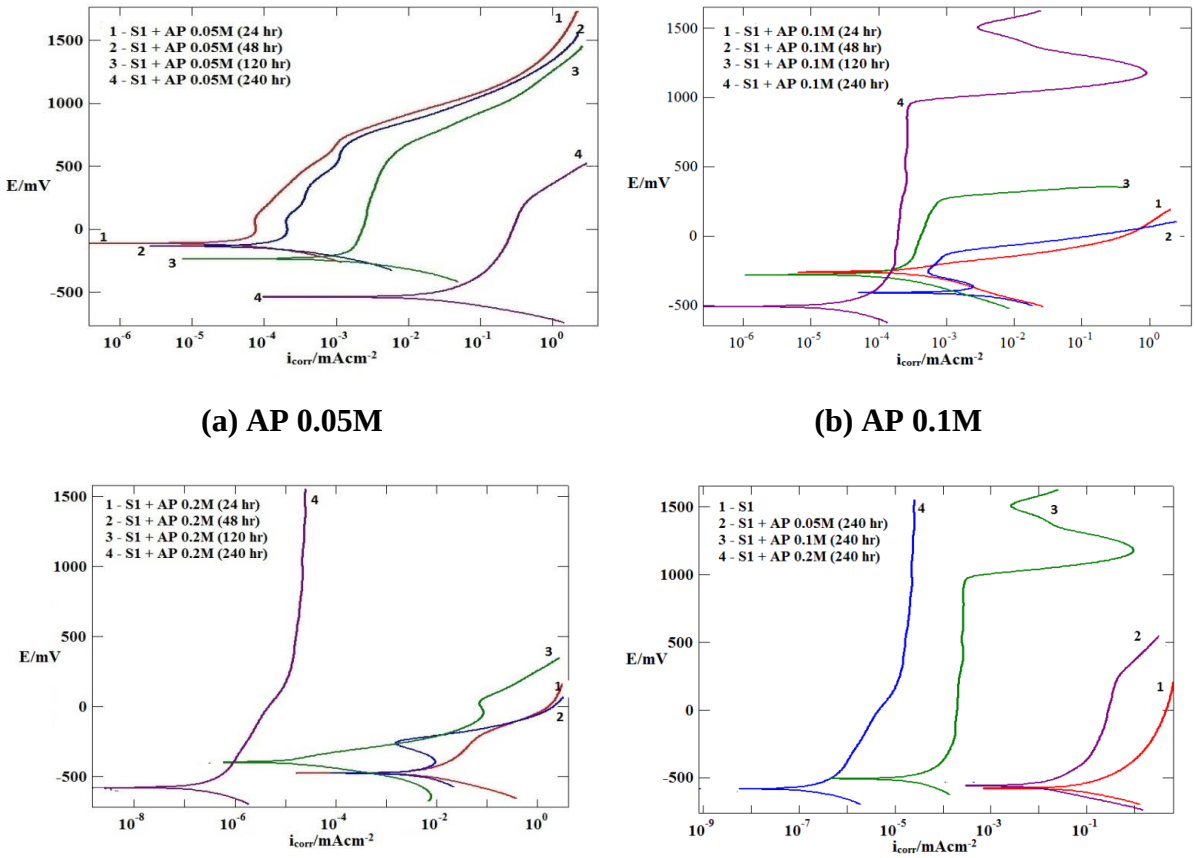

(a) AP 0.05M **(b) AP 0.1M**

(c) AP 0.2M **(d) AP Vs S1 (at 240 hrs)**

Fig. 3.11 Polarization curves of bare steel in carbonated chloride solution with AP as corrosion inhibitor

(v) Potentiodynamic behavior of S1 + ABA

The potentiodynamic polarization curves of steel specimen in ABA admixed solution are presented in Figs. 3.12(a) to 3.12(c) for 0.05M, 0.1M and 0.2M concentration levels, respectively. Fig. 3.12(d) shows the comparative polarization curve of steel immersed in base solution S1 and in different concentrations of ABA admixed solution at 240 hrs of immersion.

The polarization curve obtained at 0.05M concentration of ABA (Fig. 3.12(a)) after 24-hours of exposure displayed active corrosion behavior followed by transpassive region around -350 mV_{sce}. After 48 hrs of immersion, the curve appeared to stabilize itself by increasing the slope of the anodic polarization curve and marked pseudo-passive behavior, which remained up to 240 hrs of testing duration. This indicates that the addition of ABA at low concentration levels tried to form a stabilized passive layer on the electrode surface, and the inhibition capacity was

demonstrated by the pseudo-passive behavior. The corrosion current density initially increased from 39 µA/cm^2 (at 24 hrs) to 140 µA/cm^2 (at 48 hrs) and then decreased drastically to 8.9E-04 µA/cm^2 at 240 hrs. The potential values shifted towards anodic side with immersion age, i.e., from -785.1 mV$_{sce}$ at 24 hours to -573.5 mV$_{sce}$ after 240 hr of testing duration. It can be inferred that initially ABA was not able to counter the metal dissolution effect, but on later stage anodic reaction was arrested to provide inhibition. Anodic and cathodic current density decreased at later ages, showing the inhibition efficiency of ABA at longer duration.

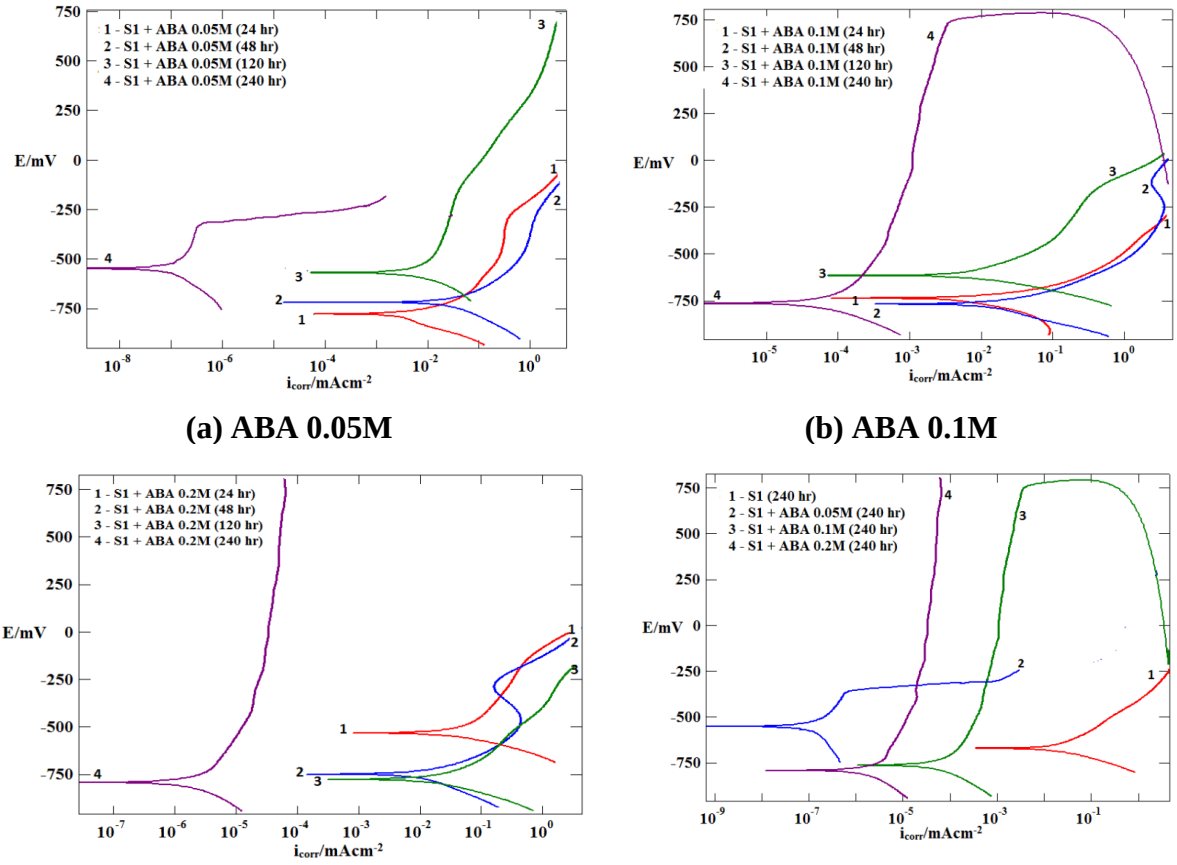

(a) ABA 0.05M **(b) ABA 0.1M**

(c) ABA 0.2M **(d) ABA Vs S1 (at 240 hrs)**

Fig. 3.12 Polarization curves of bare steel in carbonated chloride solution with ABA as corrosion inhibitor

As the concentration of ABA was increased to 0.1M, the efficiency of admixture increased with the testing duration. The i$_{corr}$ value was stable up to 120 hours and decreased further at 240 hrs of testing duration (i.e., 1 to 10^{-2} µA/cm^2). The OCP remained on nobler side as compared to the base solution S1. The curve recorded at 24 hrs of immersion illustrated a uniform increase in current density due to active dissolution, but at 48 hrs of immersion, active-passive transition was

observed. The anodic curve became more stable at 240 hrs of testing, in which breakdown potential of 740 mV was observed, followed by reverse potential at large scan range signifying a damaged passive film that was unable to repair itself due to formation of pits (*William Stephen Tait, 1994*)**.** The potentiodynamic curves clearly indicate that at this concentration level, ABA had the potential to form a passive layer on steel surface, which stabilized itself with testing age.

The performance of ABA at 0.2M concentration level is shown in Fig. 3.12(c). Similar behavior was observed at 0.2M concentration level, in which the passive layer stabilized with the increase in testing duration. The PDP curves illustrated typical active corrosion behavior at 24 hrs of immersion followed by active-passive transition at 48 hrs and stable passive region at 240 hrs of immersions. This shift of mechanism from active to passive side was due to formation of stable protective layer on the rebar surface. The i_{corr} value decreased from 39 µA/cm^2 at 24 hrs to 5.77E-03 µA/cm^2 at 240 hrs of testing duration and achieved five orders magnitude lower corrosion current density than the base solution S1.

Fig. 3.12(d) shows the polarization curves obtained at 240 hr of immersion in solution S1 and in solution having different concentrations of ABA. There was very large decrease in corrosion current densities in ABA admixed mixes, with the values registered four to six order of magnitude decreases in i_{corr} as compared to the base solution S1. The i_{corr} value recorded at 0.05M, 0.1M and 0.2M are 8.9E-04 µA/cm^2, 9.4E-02 µA/cm^{2}and 5.77E-03 µA/cm^2.

3.6.2 Inhibition efficiency of generic compounds

The efficiency of the tested generic compounds as CoIs was also calculated at 240 hrs with respect to S1 by using equation 3.1 and the values are presented in Table 3.6. The inhibition efficiency of TEP was seen to rise with the increase in concentration (from 65.36% at 0.05M to 85.18% at 0.2M). From the table and from the PDP curves together, it can be inferred that the surface coverage by the inhibitor ions over the rebar surface increased with the increase in concentration thereby providing increased protection at higher concentration. The increase in efficiency of inhibitor can be due to increase in degree of surface coverage by the absorbed organic molecule (*Awad, 2006*). The interaction of the compound's heteroatoms with the Fe ions of the steel surface resulted in high degree of adsorption.

The inhibition efficiency after mixing SA and AP in S1 was seen to increase with the increase in concentration from 0.05M to 0.1M, at which it reached a saturation value of 99.9%. In ABA, the efficacy was observed to be 99.9% even at the concentration of 0.05 M. The adsorption of inhibitor molecules on the steel surface is the most probable reason for the protection against corrosive media. This was further confirmed through SEM and FTIR tests and discussed in the upcoming sections.

Table 3.6 Percentage Efficiency (%η) of generic compounds after 240 hours

	Efficiency (%)		
Concentration / Solution	**0.05M**	**0.1M**	**0.2M**
S1 + TEP	65.36	75.9	83.18
S1 + SA	96.45	99.92	99.93
S1 + AP	84.54	99.97	99.99
S1 + ABA	99.99	99.97	99.98

3.7 SURFACE ANALYSIS RESULTS

In order to get a further insight into the inhibition mechanism, a thorough analysis of the steel surface was carried out after dipping the steel tablets in the tested solution for 240 hours. The surface characteristics were assessed by optical microscopy, SEM-EDX and FTIR. The inhibition efficiency at different concentration levels illustrated that the generic chemicals show performance even when used at lower concentration levels. SA, AP and ABA displayed saturation in their inhibition efficiency at 0.1M concentration therefore, 0.1M was used for surface analysis testing. Although, for TEP highest efficiency was obtained at 0.2M, but for comparison purpose and if the composition of the layer formed on steel at either of the concentrations would be same, the surface analysis tests for TEP were also performed at 0.1M concentration. The results of surface analysis are discussed in the following sections:

3.7.1 Optical Microscopy and SEM-EDX

The morphologies of steel tablets were determined by a SMZ 100 stereomicroscope at 10X and 20 X magnifications and by SEM at different magnifications (i.e., 500X and 1000X). Along

with SEM images, energy dispersive X-ray spectroscopy (EDX) was also performed to identify the main differences in chemical compositions of the solid phases (different crystalline deposits) that were formed on the steel surface.

(i) Morphology of steel surface for specimens immersed S1

The optical microscopy image of the steel tablets immersed in base solution S1 (Fig. 3.13(a)) shows extensive corrosion and the entire surface was covered with corrosion products demonstrating uniform corrosion of the steel surface. It confirms that the combined exposure of chlorides and carbon dioxide was highly detrimental to the steel, and completely devoid of its corrosion resistance. It is supported by the result findings of (*Monticelli et al., 2011b*). From the physical condition of the rebar surface, it can be inferred that the effect of carbonation (low pH) is more dominant than chloride ions. The image has three different regions in different colors of yellow, red, and black. The corrosion products formed over the surface were of red and yellow color which indicated the presence of geothite (FeOOH) and ferric oxide (Fe_2O_3) (*Verbruggen et al., 2016*) along with some black megnatite (Fe_3O_4) on the surface (*Antunes et al., 2014*). Close inspection of the tablet surface by the SEM image (Fig. 10(b)) indicated the emergence of corroded, rough, coarse, and uneven surface. The dense surface is due to the accumulation of corrosion product over the steel surface in the form of magnetite, hematite, etc. (Fig. 3.13(b)). The argument was further authenticated by EDX spectral analysis, where the concentration of Fe and O were 57.71% and 32.5%, respectively (Table 5). The obtained ratio of Fe/O was 1.68, which corresponds to the molecular composition of FeOOH, (goethite) (*Verbruggen et al., 2016*).

(ii) Morphology of steel surface for specimens immersed in S1 + TEP

The optical image of tablet specimen immersed in S1 + TEP solution (Fig. 3.14(a)) showed some visible pits formed on the steel surface. SEM image (Fig. 3.14(b)) confirmed the presence of certain products on the surface. The EDX data is summarized in Table 3.7, and it was observed that Fe and O content has been reduced to 49.07% and 21.37% as compared to the base solution S1. Also, the Cl^- content at pitting site has been increased to 1.27%. The SEM image and EDX data confirmed that the addition of TEP reduced the formation of corrosion product but increase in chloride content near pits suggests the attack of this aggressive ion predominate in S1 + TEP solution on the exposed surface. This suggests that phosphate was able to restrict corrosion by

forming a protective layer that blocked the anodic and cathodic reaction on the exposed surface. However, obtained data also states that Cl^- ion still has the capacity of destroying this passive film**.** (*Nahali et al., 2014*) confirms that presence of higher chloride content can change the morphology of protective layer formed by phosphate and has a capacity to delaminate this layer at certain point of the surface.

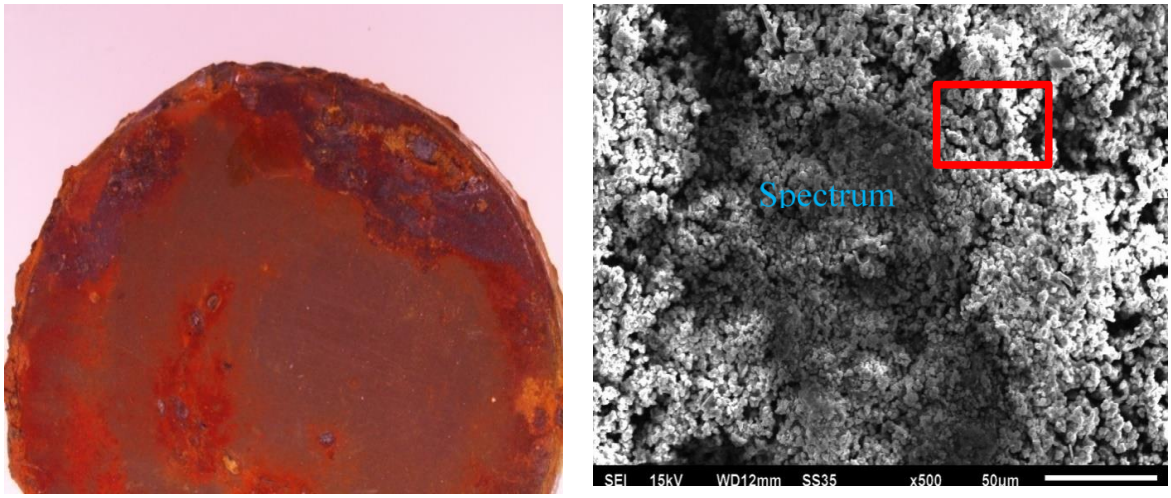

(a) **(b)**

Fig. 3.13 Surface magnified image in base solution S1 (a) Optical micrograph; (b) SEM image

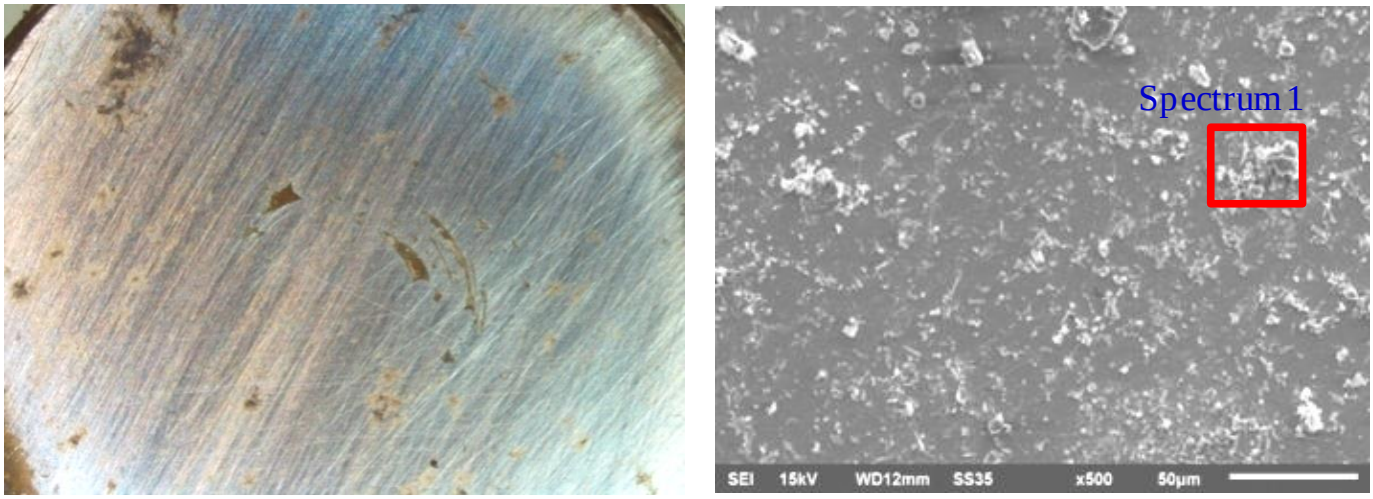

(a) **(b)**

Fig. 3.14 Surface magnified image in S1 + TEP solution (a) Optical micrograph; (b) SEM image

(iii) Morphology of steel surface for specimens immersed in S1 + SA

Optical image of the tablet immersed in S1 + SA solution (Fig. 3.15(a)) shows that in this solution a black layer was formed over the steel surface. The presence of some protective layer was also confirmed from the polarization curves of steel specimens immersed in solution containing SA, where the active-passive behavior of the curve became more stable with immersion time. The SEM micrograph (Fig 3.15(b)) also indicates the presence of a thin layer with some dense product formed on the steel surface. The EDX spectra confirmed that the layer consisted of higher C (26%) and O (55.03%) concentration, but the Fe (0.78%) concentration was very low. The increase in content of element C and O on the test group specimen (S1 + SA) were far higher than the contents on the specimen immersed in base solution S1. It means that a great deal of organic substance existed on the surface of carbon steel. The organic substance most probably referred to is the film formed by the active component (heteroatoms) of the inhibitor. Also, very low Fe content indicates that the film does not involve the participation of iron but is formed above it. The reduction in i_{corr} values, presence of black film and absence of iron contents in formed film clearly demonstrate that the film is protective in nature. Besides, the presence of heteroatom (i.e., O) strongly confirmed the corrosion resistant capacity of SA inhibitor in preventing the steel surface by developing a protective thin layer over the steel surface.

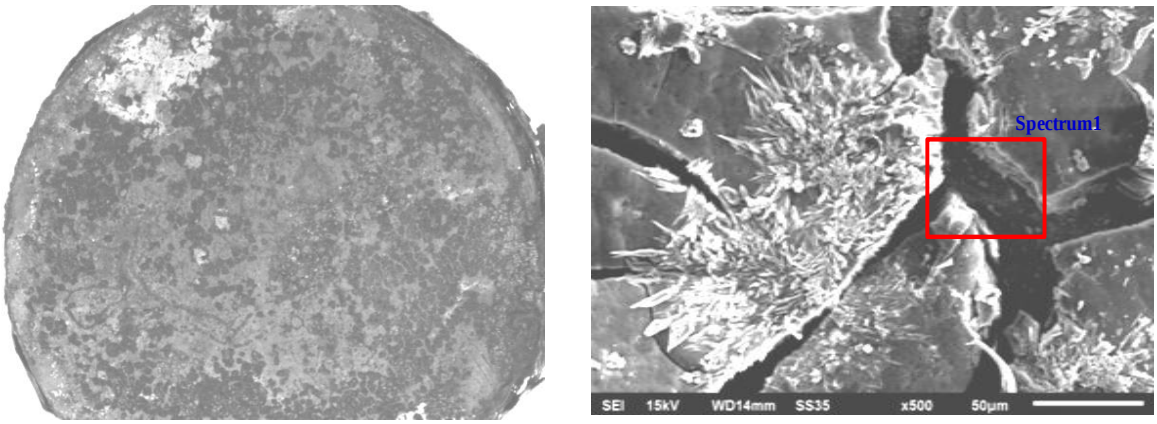

(a) **(b)**

Fig. 3.15 Surface magnified image in S1 + SA solution (a) Optical micrograph; (b) SEM image

(iv) Morphology of steel specimen surface immersed in S1 + AP

Fig. 3.16(a) shows the optical image of sample immersed in S1 + AP solution. The rebar surface was observed to be neat with no noticeable corrosion pits or any corrosion product. The SEM micrograph exhibited smoother surface morphology (shown in Fig. 3.16(b)). The EDX spectral analysis of S1 + AP shows the presence of Fe (88.07%) only, which confirmed that AP has not allowed the corrosion products to form and has shown remarkable corrosion inhibition efficiency.

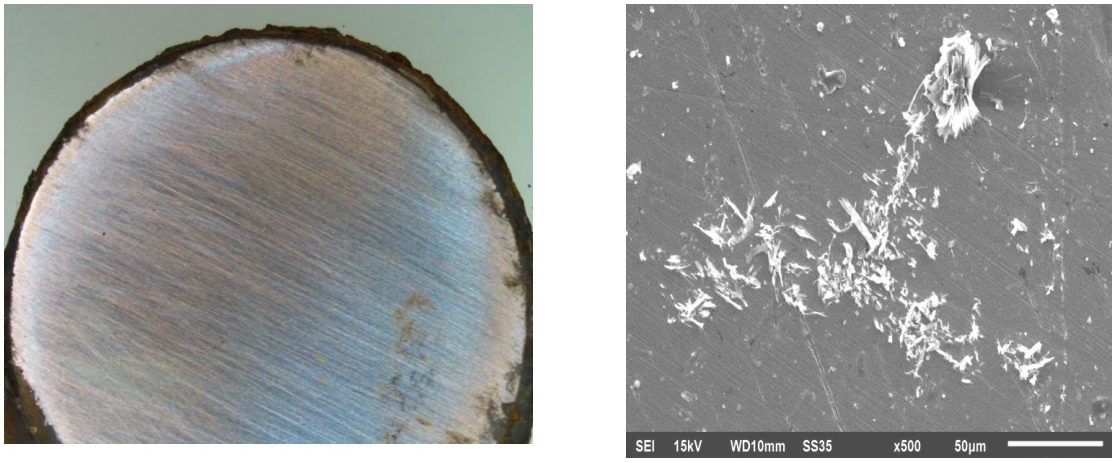

(a) (b)

Fig. 3.16 Surface magnified image in S1 + AP solution (a) Optical micrograph; (b) SEM image

(v) Morphology of steel specimen surface immersed in solution with S1 + ABA

The optical image of sample submerged in solution containing ABA is shown in Fig. 3.17(a). It is evident that a film was formed on the steel surface in ABA (Fig. 3.17(a)), which could be an influencing factor in lowering lower corrosion rate and validate the PDP curves behavior. The magnified SEM image of ABA inhibited specimen is shown in Fig. 3.17(b). The close inspection of sample indicates a physically absorbed protective layer and some dispersed products were also to be seen due to additives in solution. The concentrations of Fe, O, and C in ABA were 30.24%, 20.27%, and 22.42%. Content of element C and O were higher than the base specimen S1, while the content of Fe decreased. The increase in content means a great deal of organic substance present on the steel surface. The presence of organic substance most probably refers to the protective film formed by the active components of the inhibitor, which isolates the attack of aggressive ions on the surface (*X. Zhou et al., 2011)*. The EDX spectra of ABA verified that the

presence of such inhibitors could provide a protective layer via the adsorption of inhibitive species and reduced the corrosion rate by preventing the Cl^- attack in such low pH environment.

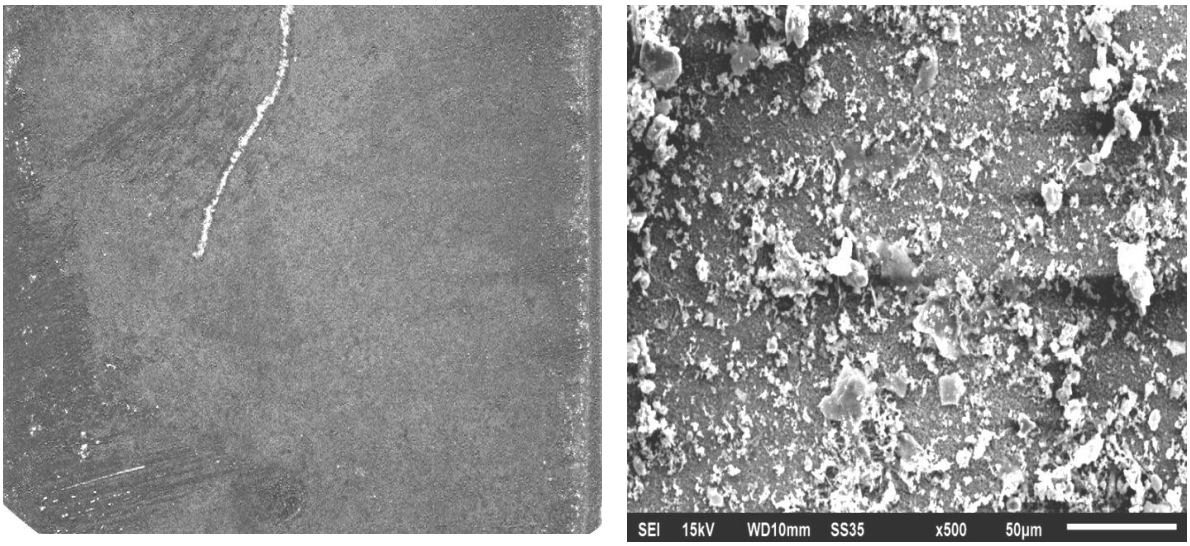

(a) **(b)**

Fig. 3.17 Surface magnified image in S1 + ABA solution (a) Optical micrograph; (b) SEM image

Table 3.7 Energy-Dispersive X-ray (EDX) Analysis Data for

Elements	S1	S1 + TEP	S1 + SA	S1 + AP	S1 + ABA
C	06.85	00.87	26.00	02.23	9.24
O	32.55	21.37	55.03	04.27	49.83
Na	04.35	03.00	00.42	01.01	03.20
K	05.54	05.56	33.54	01.50	04.10
Fe	54.70	49.07	00.78	88.07	33.67
Cl	00.26	01.27	00.18	00.23	00.15

3.7.2 Fourier-transform infrared spectroscopy (FTIR)

The chemical bond of the surface product formed on the steel surface immersed in different solutions was characterized using FTIR to analyse the functional groups by vibrational modes and the results are provided below:

(i) FTIR spectrum of specimen immersed in S1

Fig. 3.18 represents the FTIR spectrum obtained from the product formed on specimen immersed in solution S1. The FTIR spectra of steel tablet immersed in the base solution S1 shows

a broad peak around 3338 cm^{-1}. This is the peak of –OH stretching represents the polymorphic form of FeOOH (*Cabrini et al., 2015*). Spectra in the range of 1650-1540 cm^{-1} and peak observed at 958 and 840 cm^{-1} are respectively due to amorphous or crystalline Fe (II) and Fe(III) hydroxides and carbonates *(Inam et al., 2018; Kasperek et al., 1998*). Spectra peaks at 1069 and 858.7 cm^{-1} are the peaks of γFeOOH and αFeOOH (*Kumar & Balasubramaniam, 1998*). The peak appeared at 1360 $cm^{-1}$is attributed to the bending vibration of the hydroxyl group associated with Fe *(Inam et al., 2018*). Peaks observed at 695 cm^{-1} represented the corresponding peak of Fe_3O_4 and at 470 cm^{-1} represents the corresponding peak of Fe_2O_3 (*Fabis et al., 1981; Neufeld & Cole, 1997*). The spectrum obtained by FTIR on the specimen immersed in base solution S1clearly indicates the corrosion product contains FeOOH, Fe_2O_3 and Fe_3O_4.

(ii) FTIR spectrum of specimen immersed in S1+TEP

Fig. 3.19 represents the FTIR spectrum obtain from the product formed on specimen immersed in solution S1+TEP. In comparison with the spectra obtained by the product formed on steel tablet immersed in solution S1 + TEP, there was shift in a peak from 3338 cm^{-1} to 3151 cm^{-1} which characteristics–OH present in chelate form due to intermolecular H-bonding. While the spectra obtained at 1600 cm^{-1} cm and 1543 cm^{-1}characteristicsthat the compound contains Fe(II) and Fe (III) hydroxides. A similar band peak observed at 1365 $cm^{-1}$was attributed to the bending vibration of hydroxyl group associated with Fe. While peak of Fe_3O_4 and Fe_2O_3 was observed in the spectra at 695 cm^{-1} and 470 cm^{-1}. This clearly states that the product formed on rebar consisted of hydroxides of Fe(II) and Fe(III) that might be the corrosion products formed on the rebar surface. But. the bands in the range of 1400–800 cm^{-1} and 670–500 cm^{-1} obtained are due to the vibrations of the $[PO_4]^{3-}$ groups (*Jastrzbski et al., 2011*). This clearly demonstrates that the presence of phosphate promotes the growth of protective iron oxide film and tries to heal the defect caused by aggressive species. Although, peak obtained in spectra indicates the formation of hydroxide in the form of corrosion product as well, phosphate was able to inhibit the dissolution of ion as suggested by electrochemical parameters and polarization curves.

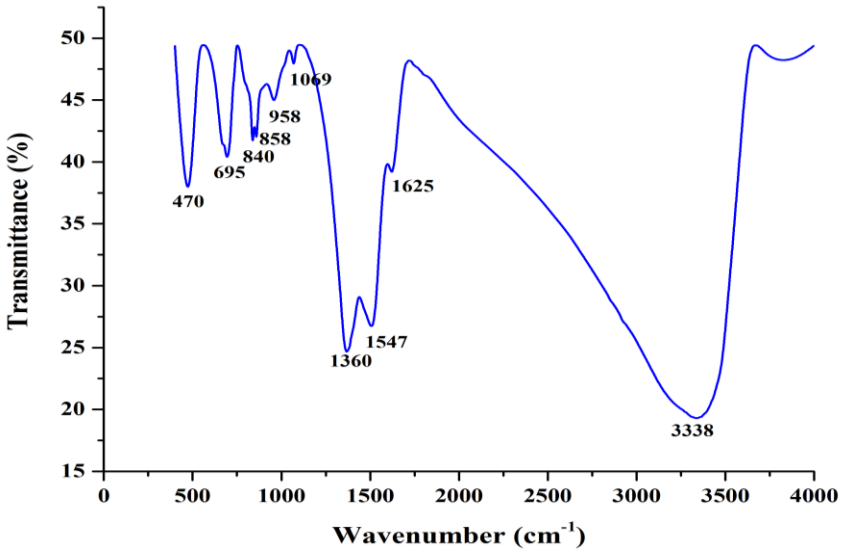

Fig. 3.18 Infrared spectrum of steel surface immersed in S1

(iii) FTIR spectrum of specimen immersed in S1+SA

The spectra obtained from the product formed on the tablet immersed in S1 + SA solution is shown in Fig. 3.20. The broad band obtained at 3410 cm^{-1} is in the range of the stretching frequency of the –OH group (*Al-Saleh, 2015; Y. Liu et al., 2019*) supported by the band of C-O stretching at 1152 cm^{-1} and 1255 cm^{-1}. The hydrogen bonded –OH band appears as a broad peak between 3400 and 3300 cm^{-1}. The broad peaks around 1620 cm^{-1}, 1527 cm^{-1} and 1463 cm^{-1} are the characteristic peaks due to chelate complex formation with Fe^{2+} along with two medium adsorption band at 850 cm^{-1} and 760 cm^{-1} that can be assigned to C-H out of plane bending on an aromatic ring (Y. Liu et al., 2019). The spectra at these wave numbers (between 1600 cm^{-1} and 1400 cm^{-1}) also indicate the presence of aromatic ring but because of the complex formation these peaks overlapped and resulted in a broad peak rather than sharp band of aromatic ring. Since the band is obtained around 750 cm^{-1} indicates its ortho substitution. The band obtained at 1384 $cm^{-1}$is related to the adsorption of SA, through the interaction of –CHO and phenolate ion with the metal surface.

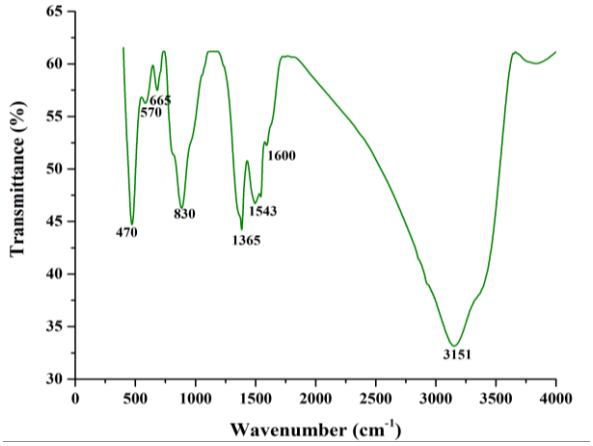

Fig. 3.19 Infrared spectrum of steel surface immersed S1 + TEP

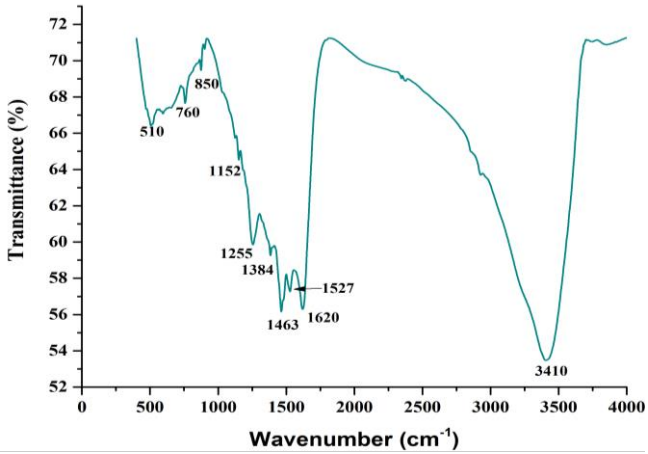

Fig. 3.20 Infrared spectrum of steel surface immersed S1+SA

(iv) FTIR spectrum of specimen immersed in S1+AP

Since the surface of steel immersed in S1 + AP was very clean, no product could be obtained in this case for the FTIR analysis.

(v) FTIR spectrum of specimen immersed in S1+ABA

The FTIR analysis was carried out for only S1+ ABA and the results are presented in Fig. 3.21. The spectra for the specimen kept in ABA admixed solution had two broad peaks at 3390 and 3250 cm^{-1}. These bands are the characteristic bands of the –NH group present in ABA at para position (*Perencatan et al., 2014*). These peaks overlapped, thus giving a broad band peak. The band obtained at 1605 and 1533 $cm^{-1}$is due to the complex formation of ABA with Fe^{2+}. The band at 1450$cm^{-1}$is attributed to C=C stretching vibration (*Al-Saleh, 2015*). The peak at 1384 cm^{-1} is attributed to deformation vibration of C-N stretch (aromatic ring). Also, presence of band at 850 cm^{-1} and 680 cm^{-1} confirmed that the compound contains an aromatic ring as these peaks can be assigned to C-H out-of-plane bending on an aromatic ring. For simple structures, it is possible to differentiate mono-, di- (ortho, meta and para), and certain poly-substitutions. Note that a single, strong band may support simple ortho (around750 cm^{-1}) or para (around 830 cm^{-1}) substitution (*Coates, 2006*). The weak band visible in spectra at 1170 $cm^{-1}$is attributed to –C-O stretch. On the other hand, the presence of band attributable to –C=O is not evident in the spectrum when the sample was treated with ABA. This confirms the absence of free carboxylic group and the presence

of protective film in the form of chelate ring formed by $–COO^-$ on the surface of rebar. This chelates ring blocked chloride ions due to chemical structure. Then they form coating on rebar surface as esters react in alkali medium and forms alcohols and carboxylic ions which then reacts with Fe^{2+}ions (*Y. Wang et al., 2018*).

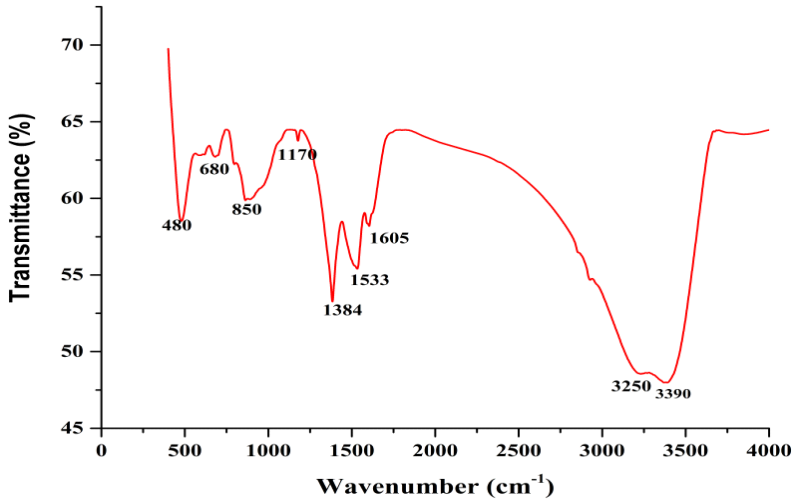

Fig. 3.21 Infrarred spectrum of steel surface immersed S1 + ABA

3.8 CORROSION INHIBITION MECHANISM

The polarization curves obtained for steel immersed in base solution confirmed uniform corrosion due to dissolution of Fe^{2+} ions, which was supported by microscopic image. SEM-EDX, and FTIR data confirmed the presence of various corrosion products formed on the rebar surface in combined contaminated environment. Further, the inhibition mechanism of tested chemicals was formulated based on electrochemical and surface analysis results and the mechanism is discussed in preceding sections.

3.8.1. Inhibition mechanism of TEP

TEP in pore solution was able to inhibit the corrosion process, resulting in lower current density values than those recorded in the base solution. Phosphate is a chemical derivative of phosphoric acid. It is a molecule that contains one atom of phosphorus covalently bound to four oxygen residues. Phosphate based inhibitors are reported to reduce both pitting corrosion due to the presence of chlorides and uniform corrosion due to carbonation *(Alonso et al., 1996; Andrade et al., 1999; Chaussadent et al., 2006b; Ngala et al., 2003*). The PDP curves registered pseudo-

passive behavior that represents the possible formation of week protective layer that inhibit corrosion up to some extent.

This performance can be ascribed with the study that (*Yohai et al., 2013*) made. Here, when carbon steel is exposed to a solution containing phosphate group, firstly in the surface layer formation they form a precipitate of ferrous phosphate (i.e. $Fe_3(PO_4)$) by dissolution-precipitation mechanism. The mechanism by which formation of ferrous phosphate take place is shown in Eq. 3.2:

$$3Fe + 2PO_4^{-3} \rightarrow (Fe)_3(PO_4)_2 + 6e^- \quad \ldots(3.2)$$

Along with this, a passive layer (i.e. Fe_3O_4) is formed via solid state process beneath this layer. Other authors *(Sieber et al., 2006*) also proposed this kind of duplex film formation when $PO4^{3-}$ ions are present in phosphate buffer at pH = 8.4 and acidic or neutral media. (*Sancy et al., 2010*) states that this phosphate layer could delay oxygen diffusion through the duplex interface and hinder the consumption of electrons produced by the anodic reaction taking place at the metal–film interface**.**

From the data obtained by electrochemical measurements and surface analysis, it can be observed that phosphate-based corrosion inhibitors retards corrosion by promoting the growth of protective iron oxide films and healing the defects in protective films. The effectiveness of phosphate inhibitor is reduced by chloride ions which damage the protective film formed by phosphate.

3.8.2 Inhibition mechanism of SA

PDP curves show the formation of stable passive layer over the exposed surface with decrease in the i_{corr} values with immersion. Surface analysis using a stereo microscope revealed the presence of a distinctive black layer on the rebar surface. Further confirmation through SEM-EDX results established that this layer predominantly consisted of carbon (C) and oxygen (O) with less amount of Fe (0.78%). The identification of these constituents eliminates the possibility of magnetite formation, which is a common black corrosion product. The band obtained in FTIR results further confirm the presence of complex product formed by SA with Fe in the alkaline environment. Salicylaldehyde contain aldehyde functional group and –OH at ortho position on benzene ring. The presence of phenolic group reacts with alkali to give first phenolate ion which is then attached

to the anodic Fe^{2+} on the rebar surface through electrostatic attraction (*Talati & Joshi, 1978*). The inhibitor having less activation energy is firmly held on the metal surface either by force of specific adsorption or by chemisorption and as a result, surface film of the reaction product is formed on the metal surface. The inhibition mechanism reaction in alkaline media is shown in Fig. 3.22.

The presence of this layer effectively inhibits rebar corrosion.

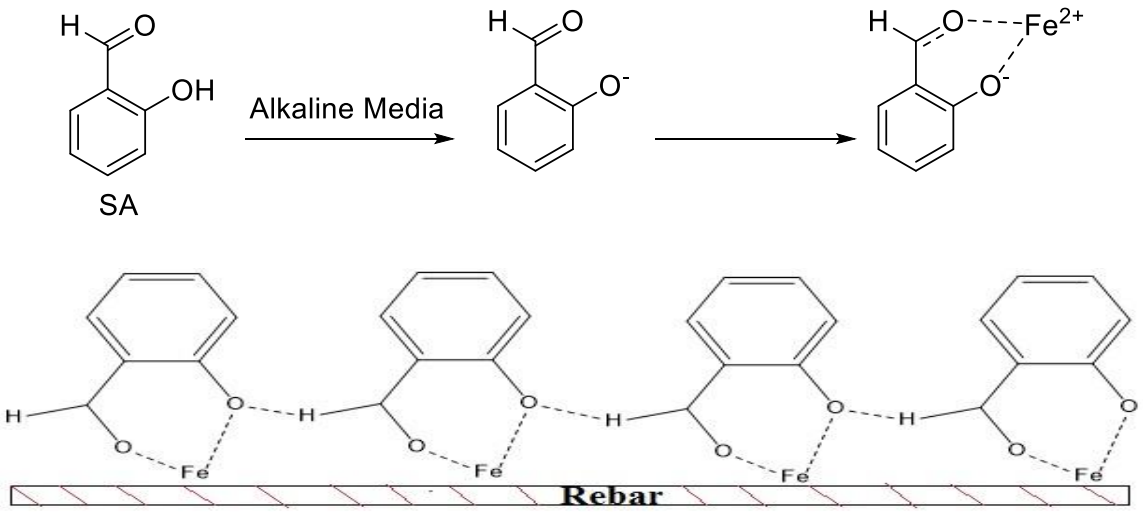

Fig. 3.22 Inhibition mechanism of salicylaldehyde

3.8.3 Inhibition mechanism of AP

Potentiodynamic polarization curves in S1+ AP demonstrated a stable passivation region at higher concentration levels. The obtained electrochemical parameters show decrease in current density values as compared to the base solution S1. Also, the inhibition efficiency increased with the increase in concentration of inhibitor.

It is generally accepted that the primary action in the inhibition process by organic compounds is the adsorption of these compounds onto the metal surface (*Awad, 2006*) by the action of at least one functional group, considered as a reaction center for the adsorption process. Typically, the adsorption of inhibitors is attributed to the presence of nucleophilic atoms (such as nitrogen, oxygen, phosphorus, and sulfur) with a triple bond or aromatic ring in their molecular structure. In the corrosive environment, the rebar develops a region of positively charged ions due to

dissolution of metal. Literature suggests that there occurs an intermolecular attraction whenever there is +ve and -ve charge isolation. Therefore, the negative charge on the nucleophilic atoms of the inhibitor probably interacts with the metal surface (+ve charged) making these atoms the reaction center of the ongoing chemical interaction. There is also a probability of multilayer formation over the working electrode due to accumulation of other inhibitor molecule on the first inhibitor layer by the positively charged atom's bridge. Most probably the protonated amine group accumulated on the rebar surface after the first layer formation would attract the –ve charge of the center of the other molecule of the inhibitor, hence, leading to the formation of multilayer. *(Mert et al., 2014*) studied the effect of 2-amino-4-methylpyridine on the corrosive behavior of mild steel in highly corrosive medium and thermodynamic data indicates physical adsorption of inhibitor in addition to electrostatic attraction. The two probable ways of inhibiting the mechanism of 2-aminopyridine are shown in Fig. 3.23.

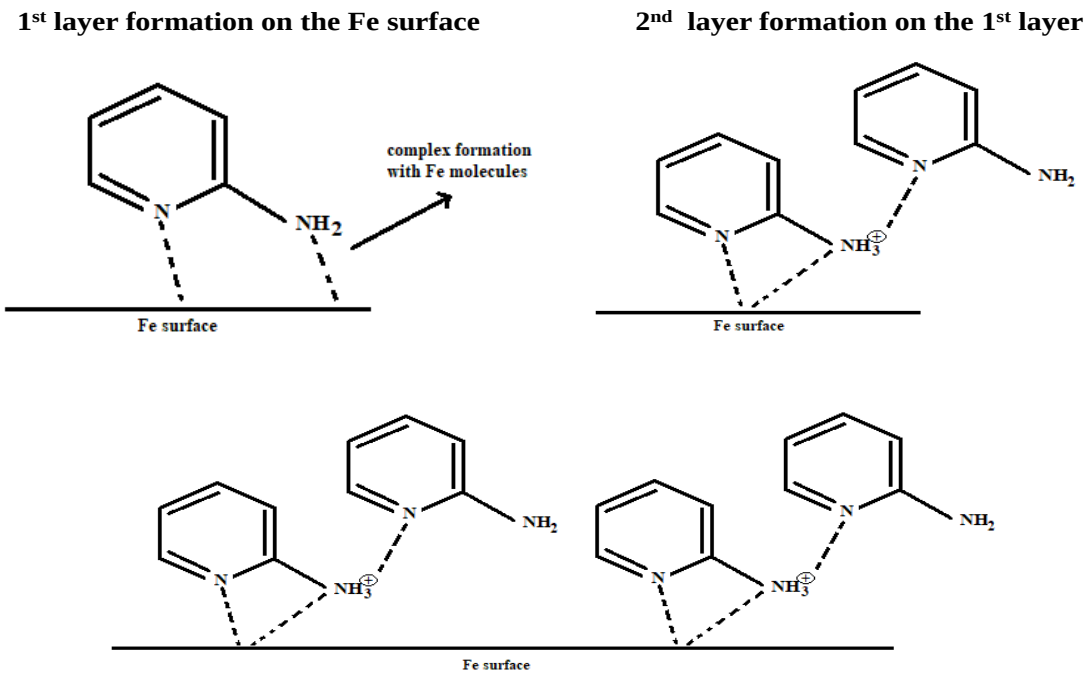

Fig. 3.23 Inhibition Mechanism of 2-Aminopyridine

It is assumed that a Lewis-Base-acid type bond generally develops between metal (as e^- acceptor) and the inhibitor being the Lewis base (as e^- donor). Also, the basis of the adsorption of the inhibitor molecules is chemisorption. Further, the adhesiveness of the adsorbed layer/multilayer

will be dependent upon the e^- density at the reaction center of the organic compound chosen as an inhibitor.

3.8.4 Inhibition mechanism of ABA

PDP curves obtained in the presence of ABA show the formation of protective film with stable passivation during the immersion age. With the surface analysis, a light grey layer is clearly visible on the steel surface that protects the rebar from undergoing corrosion in harsh environment. The behavior of ABA can be interpreted by considering their chelating properties. 4ABA is a multifunctional organic inhibitor and it has been proved to be more efficient because of their two-fold mechanism of corrosion inhibition. In the first stage, carboxylic group under the highly alkaline condition gets deprotonated to form 4-amino benzoate ion ($RCOONa \leftrightarrow RCOO^- + Na^+$) and becomes highly polar in nature.

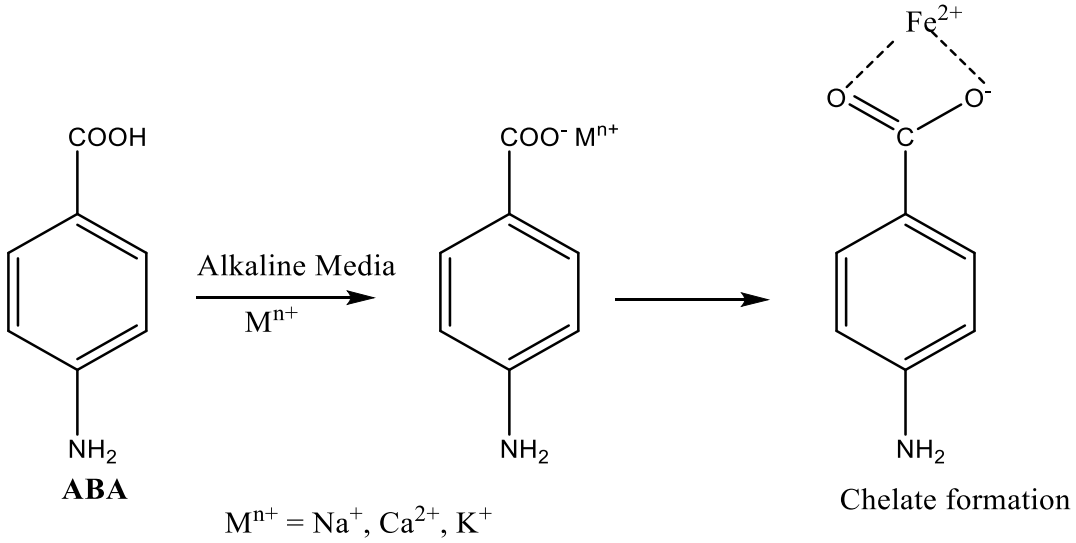

Fig. 3.24 Inhibition Mechanism of amino benzoic acid

Due to the polar nature, it can easily form six-membered chelate rings (38*). Ormellese et al., 2009* stated that organic compounds having carboxyl as their functional group can inhibit corrosion by adsorption of carboxyl group on the metal surface by delocalized charge on the oxygen atoms. Since the surface of carbon steel contains positively charged Fe on the surface in simulated concrete pore solution. The polar end of $RCOO^-$ anion tends to diffuse and adsorb on the steel surface (*Y. Wang et al., 2018; Zomorodian et al., 2021*), which would exclude the adsorption of

chloride ion on the surface. The surface analysis result confirms this behavior and is illustrated in Fig. 3.24.

3.9 COMPARATIVE PERFORMANCE EVALUATION OF COIs

From the electrochemical tests, surface analysis tests and the developed inhibition mechanism, it can be inferred that the presence of heteroatoms and rings in the chemical structure of an organic compound plays a vital role in the inhibition performance. Among all the tested generic compounds, a ring was present in AP, SA, and ABA, while no ring was present in TEP. The results confirmed that the protection of TEP in comparison with SA, AP and ABA was lower. Also, the layer formed on steel surface in the presence of TEP in S1 was less stable than the layer formed in the presence of other three generic compounds. This further provides an insight that the presence of ring in an organic compound leads to the development of more adherent layer on metal surface.

3.10 CLOSING REMARKS

The pore solution test was conducted to check the corrosion behavior of bare steel in carbonated pore solution in the presence of chloride and inhibition efficiency of generic compounds in a short period of time.

The potentiodynamic polarization curve behavior and surface analysis confirmed that the combined environment causes more severe corrosion as compared to individual environments. Also, selected generic compounds effectively inhibit corrosion process in combined aggressive environment. From the test data, it was established that the inhibition efficiency of generic compounds depends upon the molecular structure, presence of functional group and number of heteroatoms. Based on pore solution testing, three generic compounds ABA, AP and SA that ahave the inhibitor effecicy of > 99% were finalized for the Level 2 of study i.e. percolation ability on concrete.

CHAPTER 4

MIGRATION OF PROTECTIVE AND CORROSIVE SPECIES THROUGH CONCRETE

4.1 GENERAL

There are two processes by which inhibitors can be introduced in reinforced concrete structures i.e., admixed, and migratory. The former can be considered as preventive measure, in which inhibitors are directly added into a freshly mixed concrete; while the latter is usually adopted in repair systems where inhibitors are applied onto the surface of hardened concrete. Studies reveal that the inhibitors, when used in admixed form, affects the concrete properties by interacting with hydrated and un-hydrated phases of cement (*Ann et al., 2006; Dharmaraj & Malathy, 2015; Saraswathy & Song, 2007; Shi et al., 2022*)**.** The negative effect of the inhibitors on the properties of concrete can be avoided by applying inhibitors in migratory form either as preventive (application before corrosion initiation) measure or as repair material (application after corrosion initiation). The two main factors about migratory corrosion inhibitors (CoI) are the doubts related to their ability to migrate through concrete cover (*Ngala et al., 2003; Tritthart, 2003*). Also, migratory CoI's can provide a physical barrier for the ingress of aggressive ions into the concrete by blocking the pores (*Söylev et al., 2007b; Söylev & Richardson, 2008*); both these parameters of migratory inhibitors are studied in this chapter.

In this chapter, the focus is on the changes in migratory parameters upon application of the generic compounds. For this purpose, the compounds that were effective in simulated pore solution of Level 1 testing were applied on the surface of concrete. The penetration ability of the compounds was investigated at regular intervals. Further their effect on the penetration of corrosive agents was also studied in terms of chloride profile and carbonation profile after periodic exposure. The testing done at this stage is designated as Level 2 of the experimental program. The test matrix for investigating the percolation ability and concentration of generic compound is presented in Fig. 4.1.

4.2 MATERIAL SYSTEM

The major material used for the experimental program includes cement, aggregates, water, and generic compounds. Along with this, chemicals required for testing carbonation depth and chloride profile are phenolphthalein and silver nitrate solution, respectively. The details are presented in the section below.

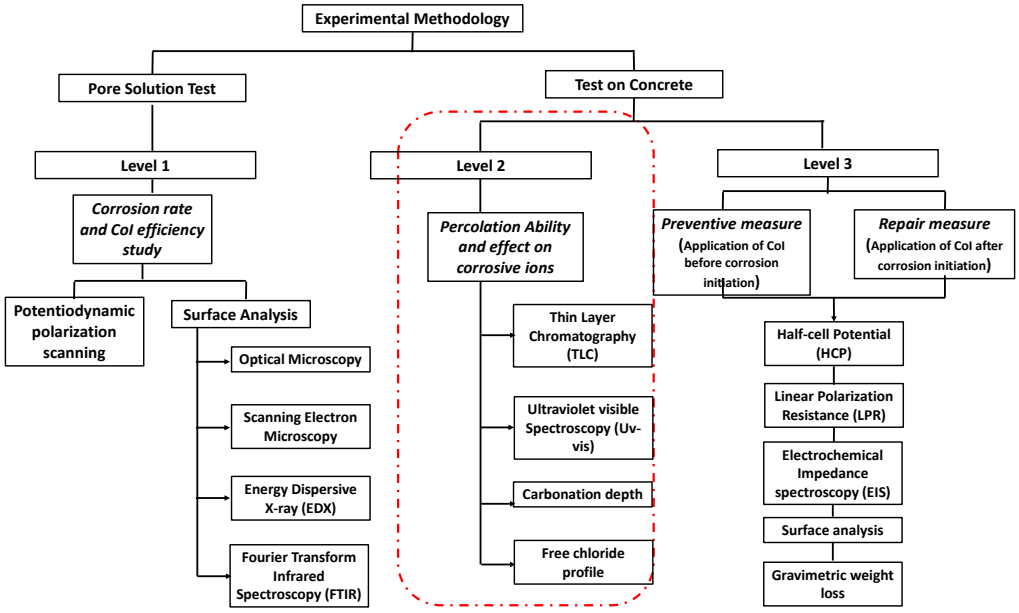

Fig. 4.1 Schematic illustration of test program for Level 2 of testing: Migratory parameters of concrete with application of migratory generic compounds

4.2.1 Cement

This type of cement can influence the microstructure of concrete, and hence can affect the penetration of compounds. Therefore, the migratory parameters were studied on concrete prepared by separately using two types of cement; Ordinary Portland Cement (OPC) conforming to (*IS:8112:2013*) and Pozzolana Portland Cement (PPC) confirming to BIS:1489 (Part 1), 1991 . The chemical composition of OPC and PPC used in this study is presented in Table 4.1.

4.2.2 Aggregates

Two types of aggregates, i.e., coarse, and fine aggregate were used in the present study. The basic properties of both the aggregates are presented in the following sections.

a) Coarse aggregates: Crushed gravel of size 20mm and 10mm was used in the ratio of 1:1. The specific gravity and water absorption of 20 mm aggregates were 2.82 and 0.53%; while the corresponding properties for 10 mm aggregates were 2.84 and 0.65% respectively. The sieve analysis for 20 mm and 10 mm aggregates are presented in Tables 4.2 and 4.3, respectively.

b) Fine aggregates: The fine aggregates used in the present study confirmed to Zone-II as per IS: 383-2016 (IS:383, 1970). The values of specific gravity, water absorption and fineness modulus were 2.64, 3.02% and 0.87, respectively. The test results of sieve analysis are presented in Table 4.3. From sieve analysis result it can be seen that the percentage finer for all sieve sizes lies within the range of values recommended for Zone II sand.

Table 4.1 Chemical composition and Physical properties of cement

Properties			**OPC**	**PPC**
Chemical compounds (%)	SiO_2		20.65	26.84
	Al_2O_3		4.85	9.10
	Fe_2O_3		3.32	4.86
	CaO		62.15	49.75
	MgO		1.72	0.95
	SO_3		2.45	2.34
	Na_2O		0.20	0.18
	K_2O		0.68	1.24
	LOI		2.05	1.72
Physical properties	Fineness (m^2/kg)		290	340
	Specific gravity		3.16	3.04
	Setting Time (min)	Initial	125	190
		Final	170	210

Table 4.2 Sieve analysis for coarse aggregate (20 mm)

S.No	IS Sieve size (mm)	% weight retained	Cum. % wt retained	% passing
1	40	0.00	0.00	100
2	20	0.40	0.40	99.6
3	10	97.2	97.6	2.4
4	4.75	2.1	99.7	0.3
5	Pan	0.3	100	0

Table 4.3 Sieve analysis for coarse aggregate (10 mm)

S.No	IS Sieve size (mm)	% weight retained	Cum. % wt retained	% passing
1	20	0.00	0.00	100
2	12.5	8.1	8.1	91.9
3	10	38.2	46.3	53.7
4	4.75	52.6	98.9	1.1
5	Pan	1.1	100	0

Table 4.4 Sieve analysis for fine aggregates

S.No	IS Sieve size (mm)	% weight retained	Cum. % wt retained	% passing	IS Limit for Zone II
1	10	0.00	0.00	100	100
2	4.75	2.5	2.5	97.5	90-100
3	2.36	8.1	10.6	89.4	75-100
4	1.18	25.3	35.9	64.1	55-90
5	0.6	17.6	53.5	46.5	35-59
6	0.3	29.4	82.9	17.1	8-30
7	0.15	14.4	97.3	2.7	0-10
8	Pan	2.7	100	0	0

4.2.3 Water

In the present study, tap water was used during casting and curing purposes. The utilized water was free from organic material, turbidity, other impurities, and negligible amount of chloride.

4.2.4 Generic Compounds

The focus of the present study is to investigate the percolation ability of generic compounds to act effectively as migratory CoIs; and to study their effect on carbonation depth and chloride concentration. For selecting and finalizing the generic compounds, preliminary investigations were done on four generic compounds in the simulated concrete pore solution, details of which are presented in Chapter 3. In the first level of testing, among the four selected generic compounds three of them namely, 4-aminobenzoic acid (ABA), 2-aminopyridine (AP) and salicylaldehyde (SA) were highly efficient in combined aggressive environment. Thus, these three generic compounds were further taken for level 2 of testing i.e., Migration test and its effect on migration of corrosive ions. The detail of these three generic compounds is briefly discussed hereunder:

a) **4-Aminobenzoic acid:** ABA consists of benzene ring substituted with amino and carboxyl as functional group. The chemical formula for ABA is $C_7H_7NO_2$ and molecular structure is shown in Fig. 4.2. The density and molar mass of the compound is 1.37 g/cm^3 and 137.14 g/mol, respectively. The generic compound ABA was available in the solid form and its solubility of ABA in water was 6.1 g/l, which is very low. Thus, to convert the compound in aqueous form for effective application on concrete surface, methanol was used as solvent.

b) **2-Aminopyridine:** 2AP is a white or clear colored crystalline solid. It is an aromatic compound with chemical formula $H_2NC_5H_4N$ and molecular structure as given in Fig. 4.2. From the molecular structure the structure consists of aromatic ring with amine as functional group. Also, additional heteroatom N is attached to the aromatic ring providing additional adsorption center. The compound was available in solid form and was highly soluble in water. Thus, for making a viscous solution for application on concrete surface, 2AP was dissolved in distilled water (solvent) in required concentration.

c) **Salicylaldehyde:** It is an organic compound with the formula $C_7H_7O_2$ and the molecular structure is given in Fig. 4.2. As can be seen from the structure, the compound contains benzene ring and one heteroatom i.e., O in different hybridization state in molecular structure. The density and molar mass of the compound is 1.17 g/cm^3 and 122.12 g/mol, respectively. This compound was available in liquid form and mixed with distilled water (solvent) to prepare solution of required concentration for effective application on concrete surface.

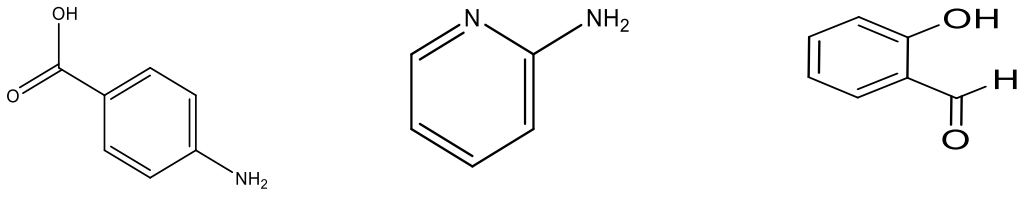

4-Aminobenzoic acid 2-Aminopyridine Salicylaldehyde

Fig. 4.2 Molecular structure of the generic compounds

4.2.5 Silver Nitrate Solution

Silver nitrate ($AgNO_3$) solution is widely used in the titration of chloride to estimate the amount of chloride present in testing solution. The silver ions from the silver nitrate react with chloride ions from testing solution to give white precipitate of silver chloride. The amount of silver ions consumed in titration gives the chloride concentration in the given solution. In the present

study, 0.05N $AgNO_3$ was used for titration of solution obtained from concrete. For the preparation of 0.05N $AgNO_3$ solution, 8.5 gm of silver nitrate were dissolved in water and was diluted to 1L in volumetric flask. The solution obtained was mixed thoroughly and standardized against 5 mL of standard 0.05N sodium chloride solution with titration.

4.2.6 Phenolphthalein Indicator

Phenolphthalein is a chemical compound used primarily as an indicator for acid-base titration. When phenolphthalein encounters concrete having high pH interstitial pore solution (pH>10), the solution shows bright pink color, whereas, in low pH (<10), concrete surface shows no color change after its application and concrete. Since the carbonated concrete has pH of less than 10, the bright pink color after phenolphthalein spray on freshly exposed concrete surface indicates un-carbonated concrete, while zone with no color change indicates carbonated concrete. Phenolphthalein solution can be prepared by mixing ethanol solution (1%) with phenolphthalein powder (1g) and 90 ml ethanol (95 V/V%) diluted in water to 100 ml. In the present study, phenolphthalein indicator was procured from the local market as it is easily available in the solution form.

4.3 CONCRETE MIX PROPORTIONING

A concrete mix was designed as per IS standards (IS 456, 2000) for a w/c ratio of 0.45 and mix proportion are presented in Table 4.5. Two types of mixes were prepared; one by using OPC and other by using fly-ash based cement (PPC).

Table 4.5 Mix proportions of concrete specimens

w/c ratio	Cement (kg/m^3)	Water (kg/m^3)	Fine Aggregate (kg/m^3)	Coarse Aggregate (kg/m^3)	
				20 mm	10 mm
0.45	410	184.5	572.4	598	598

4.4 CASTING OF SPECIMENS

100 mm concrete cubes were cast for migration ability test, carbonation depth and chloride concentration test. For preparation of cube specimens, the constituents were mixed in the required proportions in a mixer and were transferred into molds in 3 layers after subsequent compaction of each layer on the vibration table. To prevent evaporation loss from the unhardened concrete, all

samples were covered with wet jute bags and maintained at standard temperature till demolding. The specimens were demolded after 24 hours of preparation and moist cured for 7 days in curing tank. After 7 days of wet curing, specimens were kept in the laboratory environment for 7 days at RH of 60-80%. Triplicate cube specimens were prepared for each test at each testing age. With two types of cement, a total of 360 cubes were cast for checking penetration capacity and 240 concrete cubes were cast (120 OPC and 120 PPC) for carbonation depth and chloride profile measurement. The test matrix along with sample size and testing duration is shown in Fig. 4.3 and Fig. 4.4. The nomenclature used for each inhibitor is summarized in Table 4.6.

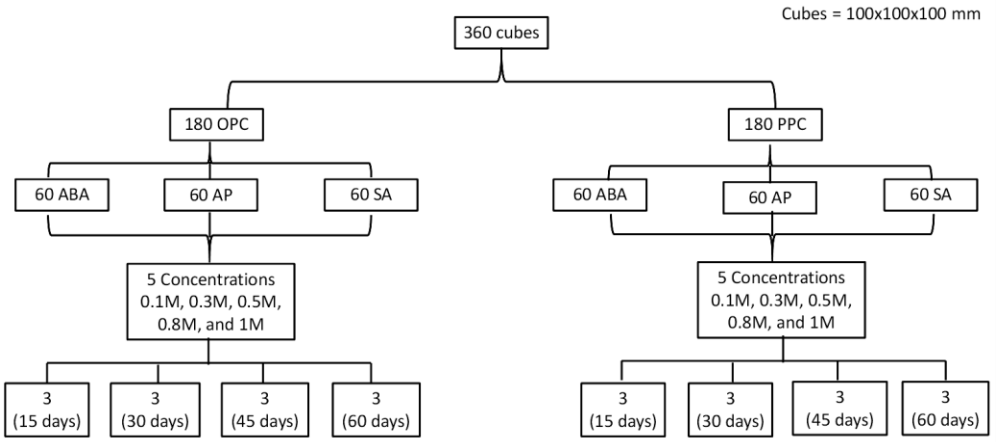

Fig. 4.3 Schematic illustration for the determination of percolation ability of generic compounds

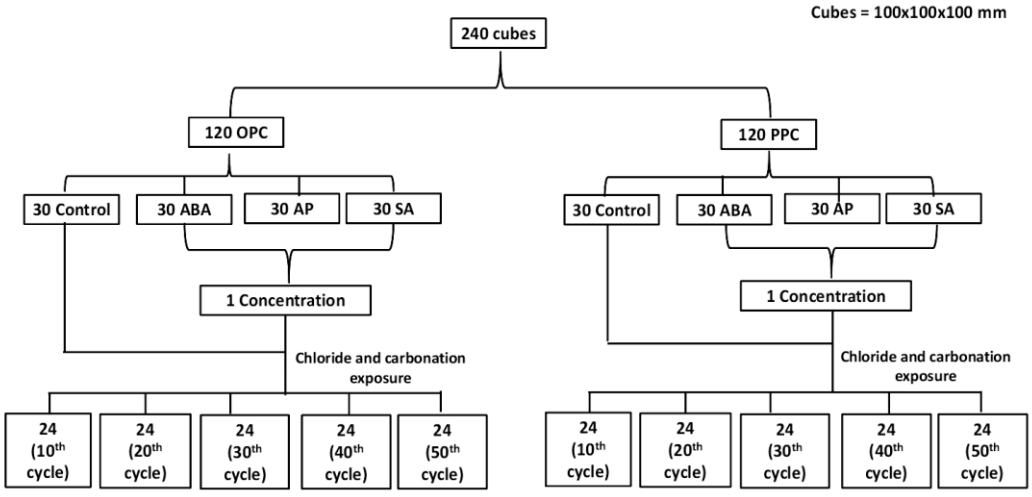

Fig. 4.4 Schematic illustration for the determination of carbonation depth and chloride profile

4.5 PRECONDITIONING OF SPECIMENS AND INHIBITOR APPLICATION

In the present work, concrete cubes were cast for migration ability test, carbonation depth test and chloride profile test. After 14 days of curing, the side surfaces and the bottom of cube specimens were sealed with a layer of sealant to ensure penetration from top surface only. The specimens were then kept in an environment chamber for preconditioning at controlled temp (30±2℃) and RH (60-70%) for 14 days to achieve an even distribution of moisture within the specimens. The inhibitor application, exposure condition and testing duration for different tests are discussed in the succeeding section.

Table 4.6 Nomenclature used for concrete cube specimens

Cement Type	Inhibitor used	Nomenclature
OPC	-	OC
	4-Aminobenzoic acid	O-ABA
	2-Aminopyridine	O-AP
	Salicyaldehyde	O-SA
PPC	-	PC
	4-Aminobenzoic acid	P-ABA
	2-Aminopyridine	P-AP
	Salicyaldehyde	P-SA

4.5.1 Preparation for percolation ability test

After preconditioning, the viscous solution of selected inhibitor was applied by brush on the top surface of cube at five different concentrations of 0.1M, 0.4M, 0.6M, 0.8M and 1.0M to identify the optimum concentration reached at the rebar level. The inhibitor was applied at a rate of 500ml/m^2 in three layers, in which the surface was allowed to dry out between consecutive coats. This method of application was adopted from *(Kaur et al., 2016; Kaur, Goyal, Bhattacharje, et al., 2017*). After applying the chemical, the cubes were kept in the laboratory environment till the testing age. The penetration capacity of inhibitor was monitored after 15, 30, 45 and 60 days of application (mentioned in Fig. 4.3).

4.5.2 Carbonation depth and chloride profile

In the present investigation, the effect of inhibitor application was studied on the two properties related to the corrosive exposure of RC viz. carbonation depth and water-soluble

chloride profile. For this 100 mm cubes of concrete were cast with the same procedure as mentioned in previous section. Through percolation test, the best concentration was identified for application. The chosen concentration was applied on concrete cubes using the same procedure as mentioned in Section 4.5.1. After application, the concrete cubes were kept in the laboratory environment for 15 days to allow the migration of inhibitor. After 15 days, the cubes were subjected to carbonation and chloride exposure. The exposure cycle was decided by a thorough literature review. It is reported that the alternate wetting (chloride ponding) and drying exposure cycles cause a more severe effect on corrosion rate than continuous exposure to chloride. Similarly, the carbonation of concrete could be deleterious only on certain conditions. Relative humidity ranging between 60-70% in combination with temperature variation between 25-30 ^{o}C and CO_2 concentration between 3-5% are considered to be most favorable condition for carbonation acceleration (*B. Q. Dong et al., 2014; Glass et al., 1991)*. Considering the above, a typical 7-day exposure cycle (shown in Fig. 4.5) was used in this study that includes 2 days of chloride ponding (3.5% NaCl solution), followed by 2 days of air drying, 2 days of CO_2 exposure in a closed chamber (maintained at a concentration of 5% by volume at 30 ± 2˚ C temperature and 60-70% relative humidity) and 1 day of air drying.

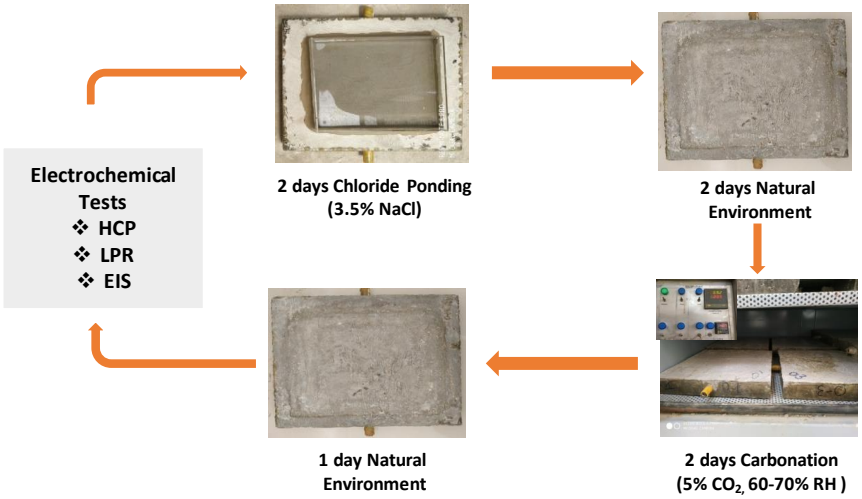

Fig. 4.5 Exposure cycle for corrosive ions penetration

4.6 TESTING OF SPECIMENS

Prepared specimens were tested for determining the migration capability of generic compound and penetration of aggressive ions in the presence of generic compound. For percolation test,

carbonation depth and chloride ions profile test, 100mm concrete cubes were utilized. For percolation test, at their respective test duration, samples were drilled using rotary hammer drilling machine to collect the powdered samples. Considering the rebar location of 15 mm in the present study, the percolation ability of generic compounds was tested up to 15 mm depth (i.e., 0-5, 5-10, and 10-15 mm). Powder from each depth was collected and stored separately in airtight packets. The samples were collected by drilling at nine points as shown in Fig. 4.6. For carbonation depth measurement phenolphthalein tests were used, whereas, for chloride determination samples were collected at depths of 0-5mm, 5-10mm, 10-15mm and 15-20mm from the top exposed face. The collected samples were tested by using titration method that will be discussed in succeeding section.

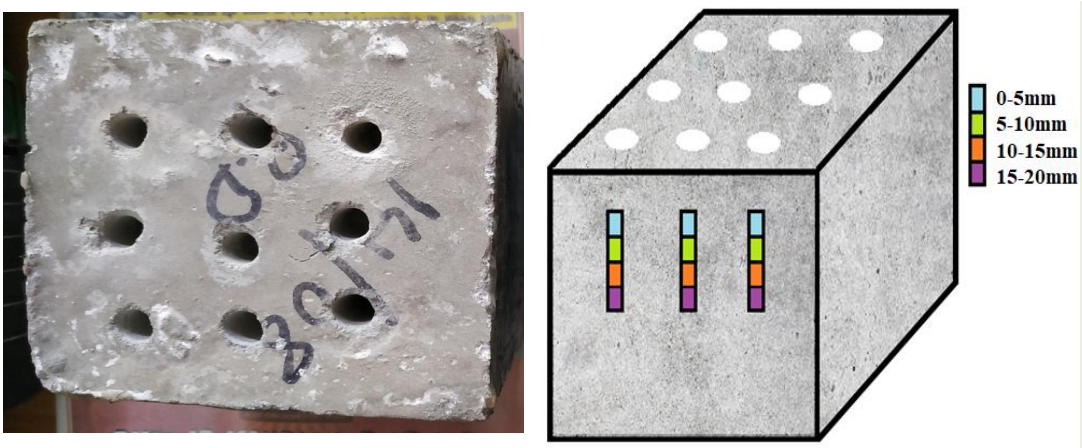

Fig. 4.6 Location of measurement for Free chlorideconcentration in concrete

4.6.1 Percolation ability test

In the present study, percolation ability of generic compounds was tested by thin layer chromatography and ultraviolet visible spectroscopy method; former is considered as a qualitative method of testing and later is stated as a quantitative method. The detail procedure is described in following subsections:

(a) Thin Layer Chromatography (TLC)

The presence of compound at a given depth in concrete was monitored through thin-layer chromatography (TLC). The method is helpful in identifying the presence of compound and its purity. The test was conducted on TLC plate as shown in Fig. 4.7(a), which is coated with silica

gel to form an absorbent layer on the top. The identification of compounds by TLC method consists of 3 steps: viz., spotting, development and visualization as shown in Fig. 4.7(b). The step-by-step procedure is described below:

First, the extracted concrete powder which needs to be analyzed is dissolved in a volatile solvent to produce a very dilute solution. The mixture was prepared with concrete/solvent ratio of 1:3. Various solvents namely, ethyl acetate, methanol, hexane, and chloroform in their pure form or in combination of two different solvents in varying solute percentage were tried. After various trial and error methods, ethyl acetate was chosen for ABA, whereas for AP and SA, chloroform and 50% solution of hexane and ethyl-acetate was finalized as volatile solvents, respectively. The small amount of dilute solution is then transferred to one end of a TLC plate to form a spot by using a micropipette. The spotting solvent quickly evaporates and leaves behind a small spot of the material. In the second stage (i.e., development stage) TLC plate is placed into a shallow pool of development solvent, which then travels up the plate by capillary action. In the present study, hexane was used as a development solvent. Due to the movement of solvent over the absorbed silica gel layer, the spots on plate were also moved from the original position. The polar silica gel tries to hold the spot and the solvent tries to move the spot with it as it travels up the plate. Once the solvent has travelled up-to top of the plate, the plate is removed and visualized under UV lamp.

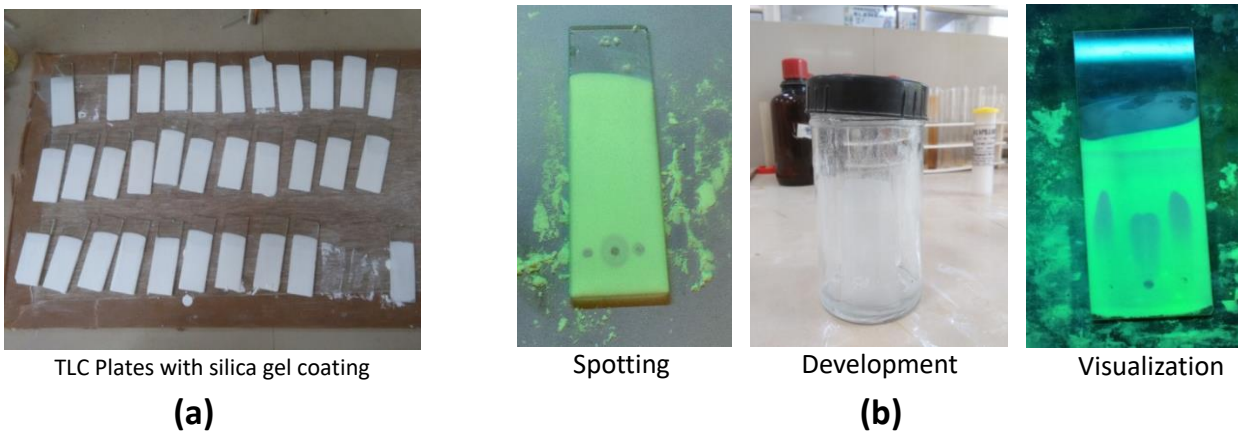

Fig 4.7. TLC method for analyzing mixtures (a) TLC plates (b) Procedure for identification

.

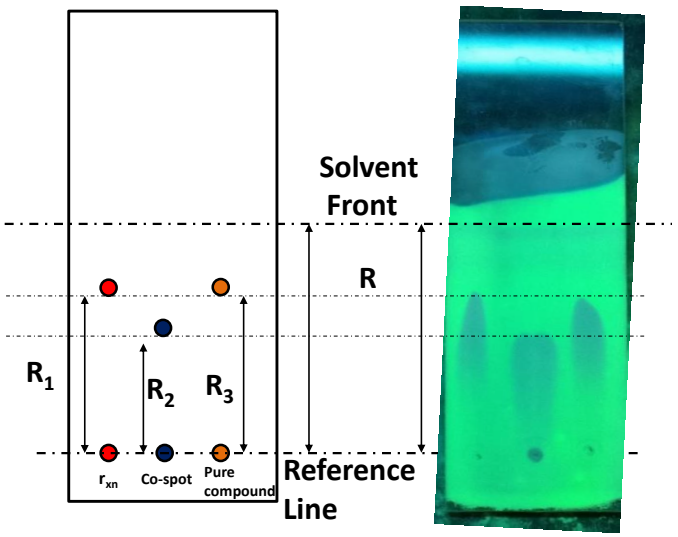

Fig. 4.8. Movement of spots on TLC plates

The movement of three spots along with the movement of solvent is shown in Fig. 4.8. The retention factor (R_f) values obtained by TLC was used to analyze the presence of the compound at required depth. The R_f value is simply the ratio of migration distance of substance to migration distance of solvent front, and it is dimensionless quantity. The obtained R_f value was compared with the corresponding value of the pure compound. If R_f value of filtered mixture matches with the pure compound, it confirms the presence of compound in concrete. The samples for which measured R_f value was like that of the pure compound, the quantitative analysis by UV-vis spectroscopy was done to get the concentration of the compound at a particular depth.

(b) Ultraviolet Visible Spectroscopy (UV-vis)

The quantitative analysis for determining concentration of compound is done by using UV-Vis spectroscopic technique. It is referred to as a molecular spectroscopy which involves the study of interaction of UV-vis radiation with molecules. The absorption spectra were recorded on SHIMADZU-2600 spectrophotometer and quartz cuvettes with path length of 1cm. The concentration of the compound. The working mechanism of UV spectrometer is shown in Fig. 4.9. The detailed procedure for sample preparation and concentration determination is discussed below:

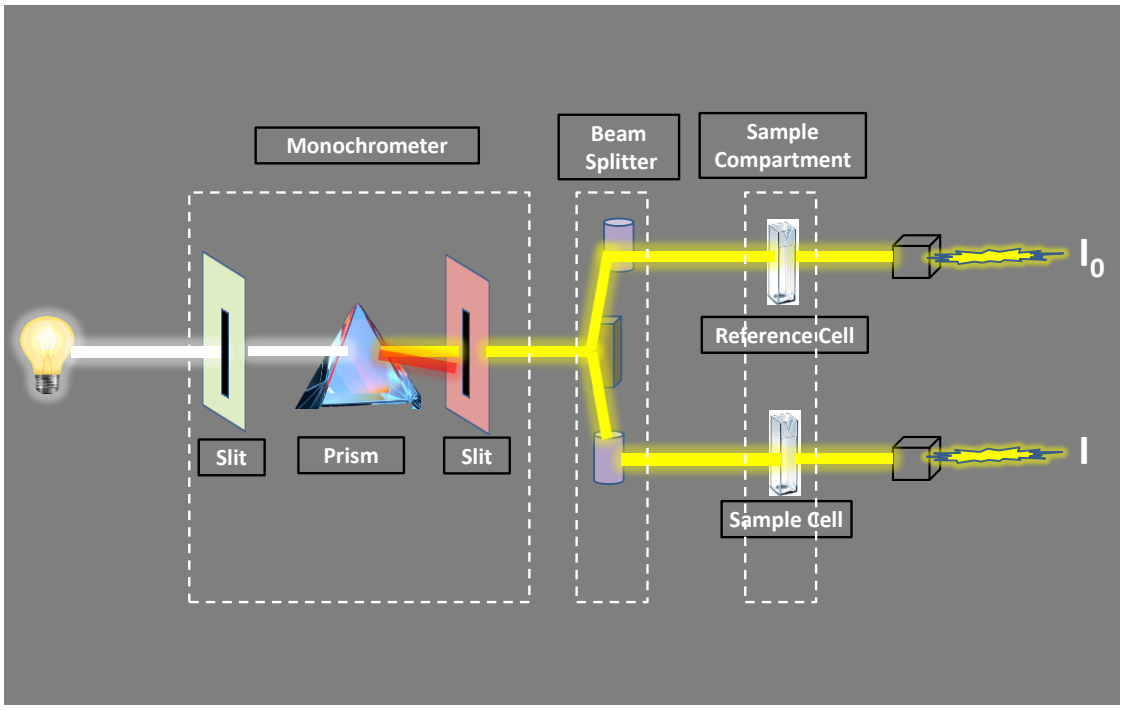

Fig. 4.9 Mechanism of UV-vis spectroscopy

For concentration profiling in concrete, the sample for UV- Vis analysis were prepared by adding drilled concrete powder in water (solvent) in same ratio as mentioned in TLC sample preparation and solution were further mixed with stirrer for two minutes. The prepared solution was placed in oven at 50-60 ^{o}C for 30 minutes. After pre-heating it was allowed to cool down for 10 minutes and then filtered by using what-man filter paper. The filter solution along with reference solvent (in the present case water is used as solvent) was filled in separate cuvette for measuring the absorbance peak and corresponding wavelength. The spectra were measured in 200nm to 700nm range so that their absorbance peak could be easily detected. The absorbance peaks of pure compounds for reference and concrete samples were recorded carefully. After recording the absorbance value from different samples, concentration of compound was found by using Beer-lamberts relationship. According to this, absorption is proportional to the concentration of absorbing molecules and the path length of the light through the sample (at a given wavelength).

$$A = \log (I_o/I) = \varepsilon bc \qquad \ldots 4.1$$

Here, I_o and I are the intensity of incident and transmitted radiation respectively, ε is known as the molar absorptivity, b is the path length and c is the concentration expressed as moles/lit.

4.6.2 Carbonation Depth

Carbonation depth was measured at 10, 20, 30, 40 and 50 exposure cycles, with each cycle having a duration of 7 days. At the testing age, triplicate cube specimens were split into two halves under UTM. Phenolphthalein solutions were sprayed on the specimens immediately after splitting the cubes. The depth of uncolored region vertically from the exposed surface was measured using vernier caliper at 5 different points along the edge of broken surface (shown in Fig. 4.10) and the average value was taken as the carbonation depth for each sample. Markedly, the measurement locations were chosen to eliminate the impermeability effect of coarse aggregate in carbonation depth of concrete (*Anon, 1988; Q. Huang et al., 2012*).

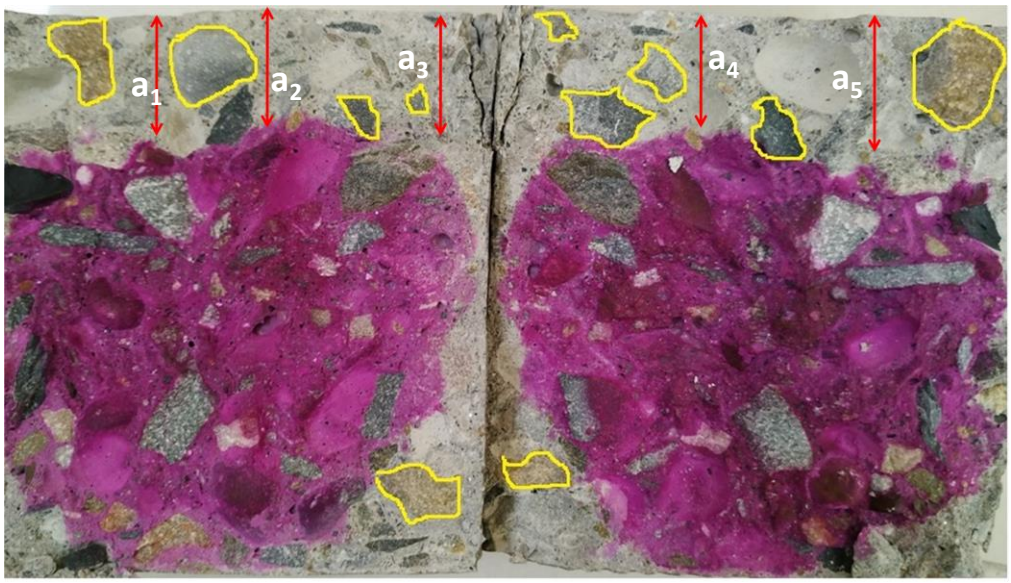

Fig. 4.10 Cross-section of split cube specimen and depth measurement location

4.6.3 Free chloride concentration

Penetration of chloride ions from external source are found in concrete as bound chloride and free chloride. Carbonation has significant effect on chloride as they convert bound chloride into free radicals and make them available for accelerating the corrosion process *(Aguirre-Guerrero et al., 2016; Y. Wang et al., 2017; Ye et al., 2016)*. Free chloride diffuses through the cementitious matrix and upon reaching the rebar level causes localized destruction of passive layer. Thus, it can be stated that chloride in its free form accelerates the corrosion process by activating the surface of the steel to form anode and the passivated surface being the cathode. After the formation of

$Fe(OH)_2$, Cl^- ions regenerate and reacts with another Fe ion and process continuous. Free chloride concentration was measured at 10, 20, 30, 40 and 50 exposure cycles. The Free chloride contents were determined by the potentiometric titration method as per ASTM standard *(ASTM C1218*)**.**

4.7 RESULTS AND DISCUSSIONS

The migration capacity of generic compound and penetration of corrosive ions in the absence and presence of generic compound is discussed in the following sections.

4.7.1 Percolation ability of generic compounds

The percolation capacity of generic compound in different concrete systems was analyzed both qualitatively and quantitatively by TLC and UV-vis spectroscopy respectively. The test results are discussed in the following sub-section.

(a) Thin Layer Chromatography

The presence of the compound was assessed based on the comparison of R_f values of concrete powder and the pure compound (ABA, SA, and AP). The R_f values obtained at 5mm, 10mm and 15 mm depth for different concentrations of the compound in different concrete systems (made with two different cement types) were obtained at 15, 30, 45 and 60 days of inhibitor application. The test results obtained at all the testing durations are presented in Annexure I (Tables A1 to A3 for ABA, AP and SA respectively). To determine the presence of compound at depth, R_f value of pure compound were compared with the value obtained by concrete samples. The R_f value obtained for a pure compound were 0.67, 0.68 and 0.70 for ABA, AP, and SA, respectively. From the R_f values presented in the annexure, it was clear that the inhibitor percolated within 15 days of its application. Therefore, the test results at 15 days of application for all compounds are presented separately in Table 4.7. From the table, the R_f value of the powder matched with the corresponding value of pure compound at the concentration level of 0.8 M and above.

Table 4.7 Retention factor (R_f) for ABA, AP, and SA at 15 days of application for OPC and PPC concrete

Cement↓	Depth↓	Concentration				
		0.1	0.3	0.5	0.8	1
		ABA				
OPC	5	0.13	0.27	0.35	0.65	0.69
	10	0.12	0.17	0.28	0.68	0.68
	15	0.25	0.27	0.38	0.66	0.67
PPC	5	0.25	0.27	0.31	0.68	0.65
	10	0.25	0.34	0.31	0.66	0.64
	15	0.25	0.34	0.41	0.67	0.66
AP						
OPC	5	0.17	0.27	0.40	0.69	0.71
	10	0.16	0.25	0.42	0.67	0.66
	15	0.27	0.37	0.34	0.67	0.65
PPC	5	0.15	0.25	0.37	0.69	0.63
	10	0.15	0.22	0.24	0.66	0.65
	15	0.17	0.22	0.32	0.67	0.65
SA						
OPC	5	0.14	0.16	0.33	0.48	0.70
	10	0.24	0.26	0.40	0.42	0.67
	15	0.14	0.26	0.30	0.42	0.69
PPC	5	0.22	0.24	0.30	0.44	0.70
	10	0.12	0.14	0.22	0.42	0.68
	15	0.12	0.24	0.26	0.32	0.68

It can be seen from Table 4.7 that the Rf value of concrete powder coincided with the pure compound at the application level of 0.8 M and 1 M. Similarly, presence of AP was identified at 0.8 and 1 M concentration, while SA was identified at 1M concentration level only. This clearly suggests that at higher concentration these compounds were able to penetrate within 15 days of its application. The pore structure of concrete consists of interconnected pores that allowed the movement of generic compounds by diffusion in the dissolved state.

The summarized observations of TLC results are presented in Table 4.8 for easy understanding.

Table 4.8 Thin layer chromatography results at 5mm, 10mm, and 15mm depth

Concentration (M)	Testing Duration (Days)			
	15	30	45	60
	4-Aminobenzoic acid			
0.1	×	×	×	×
0.4	×	×	×	×
0.6	×	×	×	×
0.8	Present	Present	Present	Present
1.0	Present	Present	Present	Present
	2-Aminopyridine			
0.1	×	×	×	×
0.4	×	×	×	×
0.6	×	×	×	×
0.8	Present	Present	Present	Present
1.0	Present	Present	Present	Present
	Salicylaldehyde			
0.1	×	×	×	×
0.4	×	×	×	×
0.6	×	×	×	×
0.8	×	×	×	×
1.0	Present	Present	Present	Present

(b) Ultraviolet visible spectroscopy

Since the TLC method confirms that the compound is present at 0.8M and 1.0M concentration, the next step involved the quantification of reached amount at different levels within concrete. This was done by using UV-*vis* spectroscopy technique on the powder sample obtained at 5mm, 10mm and 15mm depth. In this method, the absorbance peaks of concrete sample were obtained and compared with the peaks of the reference compound. The absorbance peaks of pure compounds are shown in Fig. 4.11. As can be seen from the figure, the absorbance peak of ABA, AP and SA is identified at 288 nm, 290 nm and 325 nm, respectively.

Thereafter, the absorbance peaks of the concrete samples were recorded at definite durations. The obtained absorbance peak of ABA, AP and SA applied concrete specimen at different depth and duration is shown in Annexure 1 (Fig. A1 to A5). The careful examination of the obtained spectra indicated that absorbance peak of ABA and AP applied samples overlapped with pure compound, while a shift in peak for SA samples towards higher wavelength (325nm to 375nm)

was observed. This shift towards the lower energy and longer wavelength is known as '*bathochromic shift'* or '*red shift'* that happens due to increasing polarity of compound i.e., change in molecular structure properties due to basic medium of concrete. Further, to confirm that red shift, pure SA mixed with the basic constituents of interstitial pore solution i.e. $Ca(OH)_2$, NaOH and KOH individually, and absorbance peak was recorded. The overlay of the corresponding peak of pure compound (SA), SA with NaOH (SA+ NaOH) and concrete sample (SAC) is shown in Fig. 4.12(a). From the figure, it is observed that the absorption spectra of Pure SA in the presence of Na^+ overlapped with the absorption spectra of SAC which clearly indicates the deprotonation of hydroxyl group of salicylaldehyde as shown in Fig. 4.12(b).

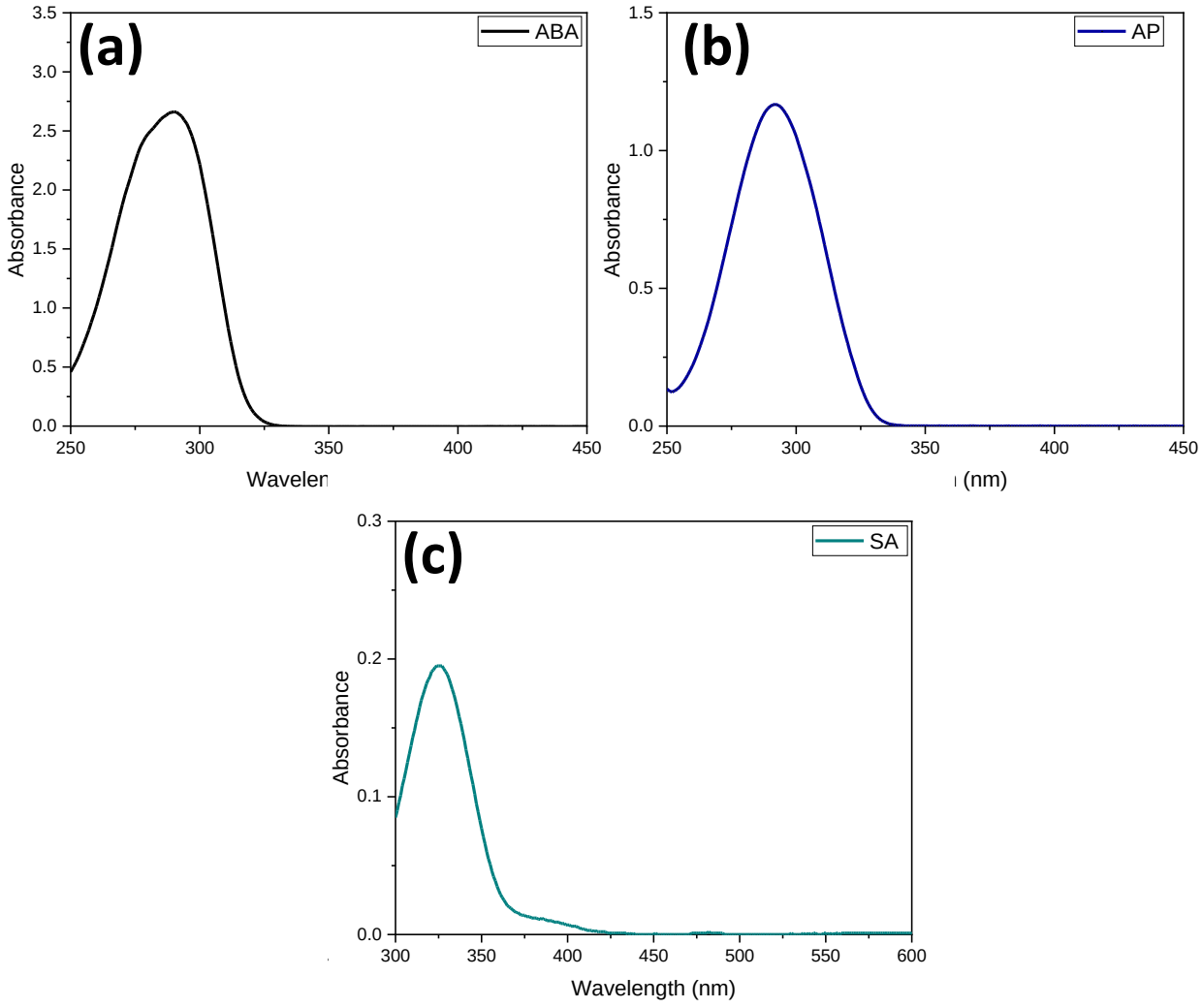

Fig. 4.11 Absorbance peak of pure compounds (a) ABA; (b) AP; (c) SA

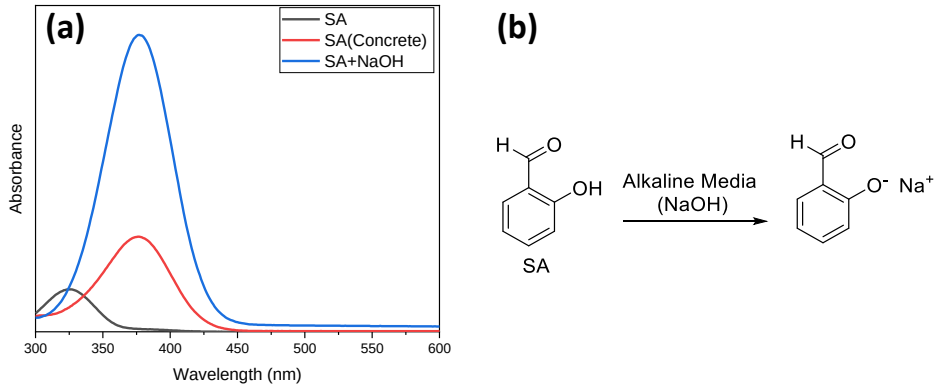

Fig. 4.12 (a) Peak shift in SA applied concrete (b) Mechanism reaction of SA in concrete

Further, the absorbance values obtained from the adsorption spectra were utilized for measuring the reached concentration at different depth by using Beer-lamberts relationship (equation 4.1). The concentration profile of generic compounds at different depths and durations is shown in Fig. 4.13 to 4.15.

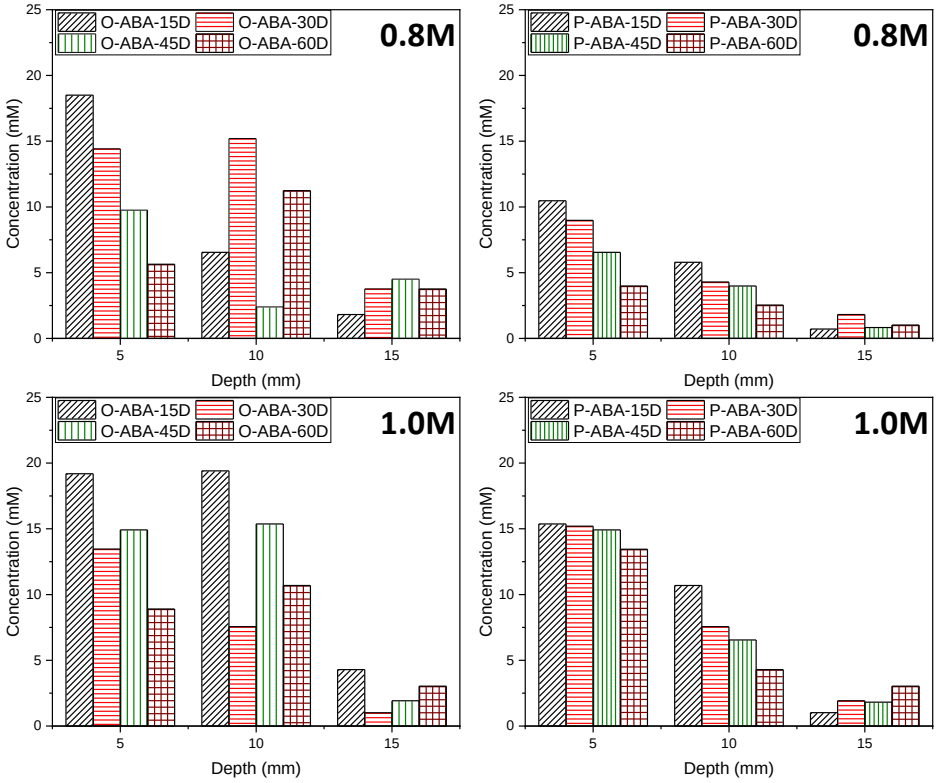

Fig. 4.13 Concentration of ABA in OPC and PPC based concrete systems

As can be seen from the figures, the concentration of the compounds was observed to be higher in OPC concrete system as compared to PPC at all testing durations. Measured higher concentration values in OPC concrete can be attributed to the porous microstructure as compared to PPC that allows free movement of generic compound. Whereas addition of pozzolanic material improved the microstructure properties of concrete by the secondary pozzolanic reaction, thus making it more resistant towards the penetration of external ions. From the variation in percolation data, it is inferred that due to the densified pore structure of PPC based concrete, penetration ability of generic compound was reduced resulting in low concentration recorded at various depths. From the concentration profile, it was also observed that the concentration of ABA was higher among the tested generic compounds at all depths irrespective of cement type. This suggests that ABA percolate at much faster rate than AP and SA. ABA has the highest migration rate in both cement systems because of its high molecular weight. As the percolation was being induced by gravity only, molecular weight played a vital role. Due to low molecular weight of AP, the diffusion rate was lower in AP as compared to ABA, thus low concentration was achieved at various depths. The interaction of SA with Na^+ ions in concrete led to decrease in its percolation capacity. Thus, from the obtained profile it can be said that the migration potential of compound depends upon type of concrete system and molecular structure properties of generic compound.

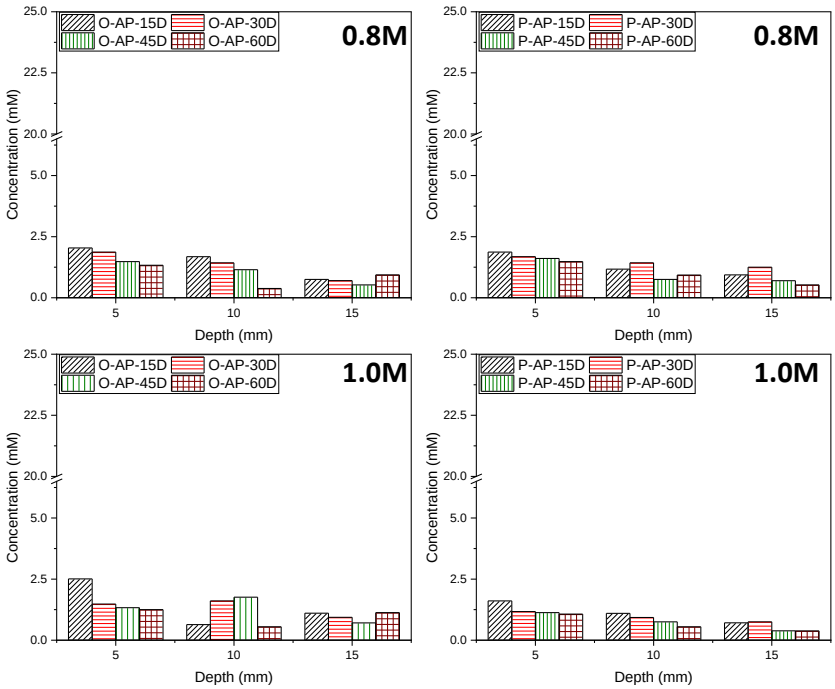

Fig. 4.14 Concentration of AP in OPC and PPC based concrete systems

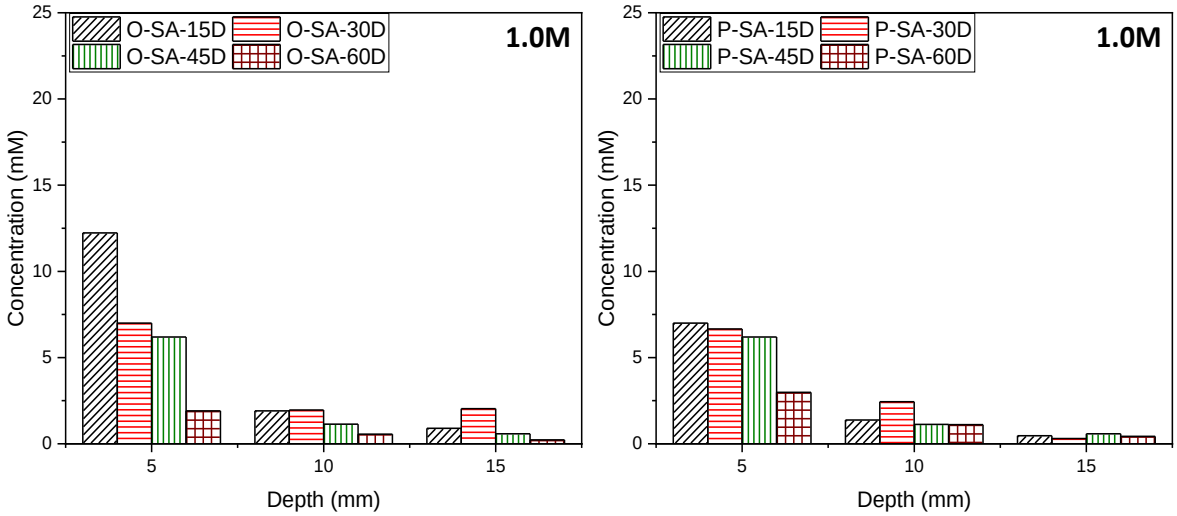

Fig. 4.15 Concentration of SA in OPC and PPC based concrete systems

4.7.2 Carbonation Depth results

To study the effect of cement type and generic compound application on carbonation depth, OPC and PPC cement based concrete cubes were exposed to carbonation during the aggressive exposure. The carbonation depth was measured after 10, 20, 30, 40 and 50 exposure cycles by using a phenolphthalein indicator. The variation in carbonation depth of both concrete systems i.e., OPC and PPC are compared and shown in Fig. 4.16.

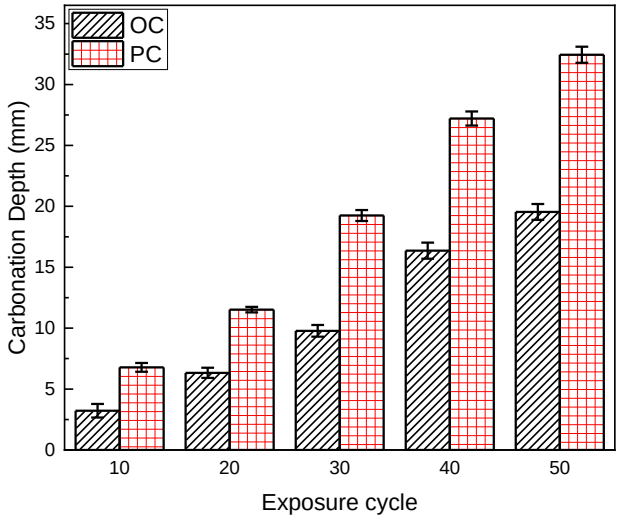

Fig. 4.16 Effect of cement type on carbonation depth

It was observed that carbonation depths of all the specimens increased with increase in exposure duration. The figure also shows that PPC concrete has higher carbonation depth than

OPC at all exposure cycles. This can be explained by the fact that replacement of cement by pozzolanic materials decreases the content of portlandite ($Ca(OH)_2$) in hydrated products due to secondary pozzolanic reaction. Due to the presence of lesser amount of portlandite, PPC concrete shows higher values of carbonation depth than OPC. Similar observation was made by various other researchers (*Hren et al., 2021; Nicolas et al., 2014; Ye et al., 2016*). Further, during carbonation, portlandite reacts with CO_2 and leads to formation of $CaCO_3$ precipitates which blocks the concrete pores due to its low solubility and lead to densification of pore matrix *(Luo et al., 2017*). This densification helps in reducing the progressive exposure in OPC based systems. However, initial lower content of $Ca(OH)_2$ in PPC leads to lesser amount of $CaCO_3$ precipitate with time as compared to OPC, leading to lesser densification. Therefore, carbonation front in PPC concrete ingresses at a much faster rate at later ages, hence, higher carbonation depth than OPC concrete.

The variation in carbonation depth after the application of different generic compounds was also measured and is shown in Figs. 4.17 to 4.19 for ABA, AP and SA applied specimens, respectively.

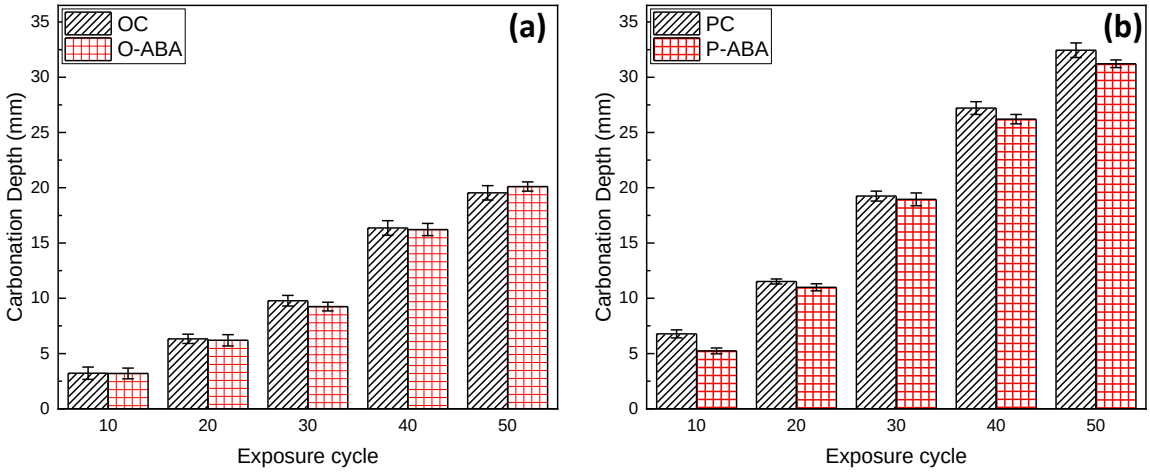

Fig. 4.17 Effect of ABA application on carbonation depth of (a) OPC and (b) PPC concrete at different exposure cycles

From the measured carbonation depth, it can be said that the application of inhibitors did not reduce the CO_2 ingress in OPC concrete system, whereas in PPC specimens, slight reduction in the carbonation front was recorded for all the inhibitors. This improvement could be attributed to the denser pore structure of PPPC concrete which acted as a barrier for CO_2. OPC concrete is more porous than PPC that allows the free movement of inhibitors thus, causing no layer formation

on its surface whereas in the case of PPC, due to its dense structure the inhibitor stayed on the surface for some time which reduced the carbonation depth. This phenomenon can also be validated from slow percolation of inhibitors in PPC specimens in concentration evaluation tests.

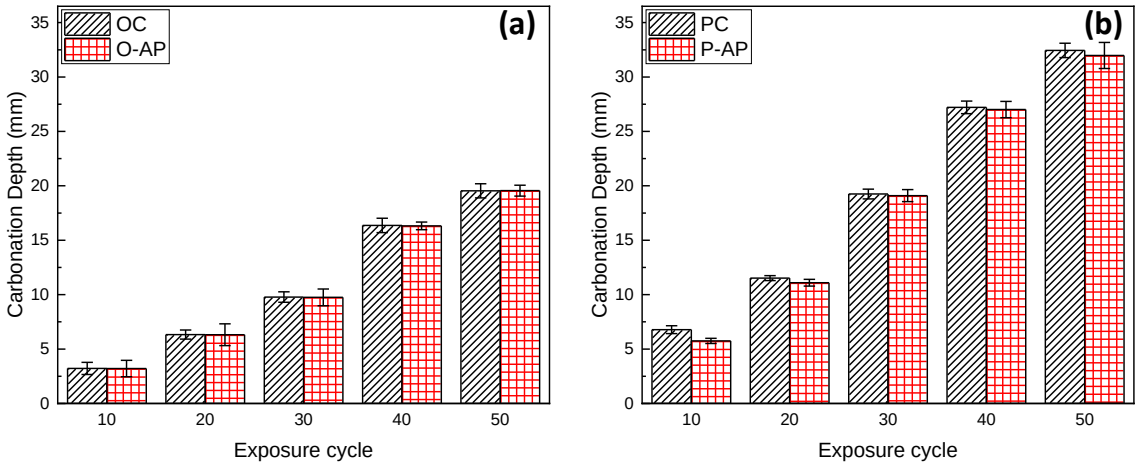

Fig. 4.18 Effect of AP application on carbonation depth of (a) OPC and (b) PPC concrete at different exposure cycles

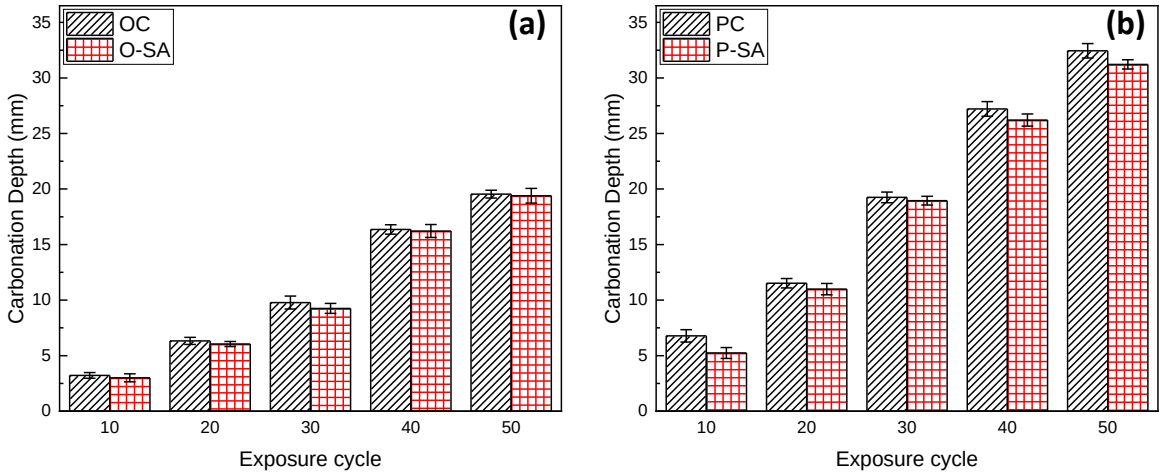

Fig. 4.19 Effect of SA application on carbonation depth of (a) OPC and (b) PPC concrete at different exposure cycles

4.7.3 Free chloride concentration

To study the effect of CoI application on Free chloride concentration of different concrete systems, the chloride concentration was measured after 10, 20, 30, 40 and 50 exposure cycles at various depths. The chloride profiles were plotted based on the measured data and are presented in Fig. 4.20 to 4.22. Fig. 4.20 describes the effect of cement type on chloride penetration and

distribution within concrete microstructure, whereas Fig. 4.21 and 4.22 present the water-soluble chloride concentration and distribution of inhibitor applied OPC and PPC concrete system. The obtained test results are discussed in the following section:

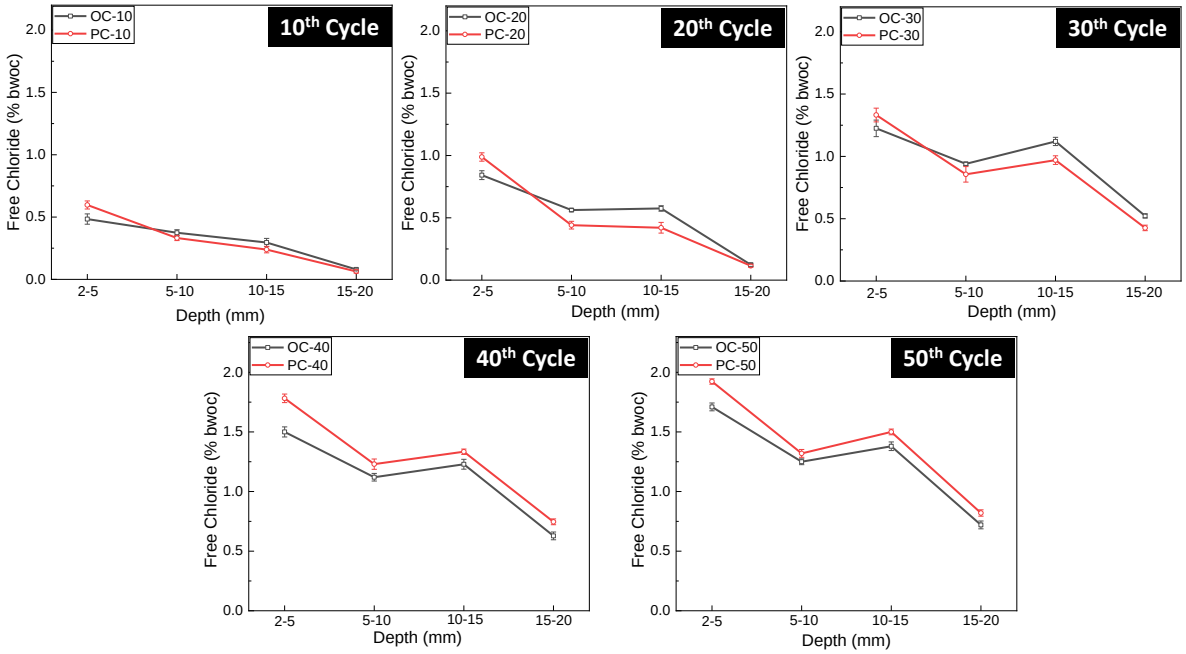

Fig. 4.20 Free chloride concentration variation in OPC and PPC concrete system

From Fig. 4.20, Free chloride content at each depth increases with increasing number of cycles regardless of cement type. The chloride content measured in PPC concrete was lower than OPC up to 30th exposure cycle (except for 5 mm depth). Along with this, the chloride binding capability of PC is higher than OC due to its high Al_2O_3 content *(Kwon et al., 2017; Montemor et al., 2002; Vedalakshmi & Palaniswamy, 2010*). This trend got reversed with continuous exposure cycles where the chloride content in PC was found to be higher than OC at all depths with further exposure (after 40 exposure cycle). It is opposed to the general observation in chloride environment which suggest the lower chloride diffusion in PPC concrete (*Montemor et al., 2000*). This might be due to combined exposure to CO_2 and Cl^- and further suggests that CO_2 is playing a predominant role in deciding the free Cl^- content (*Montemor et al., 2002*). The exception of higher chloride content obtained near the surface of PPC concrete (at 5mm) might be associated with the accumulation of chloride ions on the surface of PC due to its dense pore structure. Another prominent feature observed that at 10th cycle the concentration of chlorides at 15mm is lesser than that at 10mm, which is a usual observation as per the literature. At 20th cycle, the amounts of chloride ions

present at 10mm and 15mm depth is almost similar to each other. However, at 30th cycle, the concentration of chlorides at 15mm is higher than that obtained at 10mm. This observation is quite pronounced from 30th cycle and consequent exposure cycles as well. This could be attributed to the release of bound to free chlorides with the progression of CO_2 at deeper depths. During the initial exposure cycles, chloride tends to accumulate on the top surface, and continuous carbonation affects the concrete through a dual mechanism: altering the porosity and increasing the content of free chloride (*Angst et al., 2020; Byung Hwan Oh, Sang Hwa Jung, 2013; Geng et al., 2016; Ramezanianpour et al., 2014; D. Zhang & Shao, 2016*). This phenomenon of conversion will be applicable to both the cement types. However, the lower chloride content of OC as compared to PC, is because of continuous pore refinement of OC due to calcite precipitation which is less in PPC (*Ye et al., 2016*). The effect of the application of CoI on chloride concentration was also recorded at different durations. Free chloride concentration of CoI applied specimens was measured at similar duration and the obtained concentration is shown in Fig. 4.21 and 4.22. From the figures, it was found that application of CoI does not alter the penetration of chloride ion and the variation in chloride content was also insignificant except at 10 exposure cycle in PPC concrete. This insignificant behavior in OPC is attributed to the diffusion phenomena of CoI inside the concrete. The OPC concrete is porous than PPC, that allows free movement of CoI; whereas dense pore structure of PPC restricts the uniform dispersion of CoI leading to layer formation on the topmost surface of concrete that causes significant change in chloride content of PA after 10 exposure cycles. Further, the chloride concentration of inhibitor applied specimen increases in similar manner as recorded for control specimens.

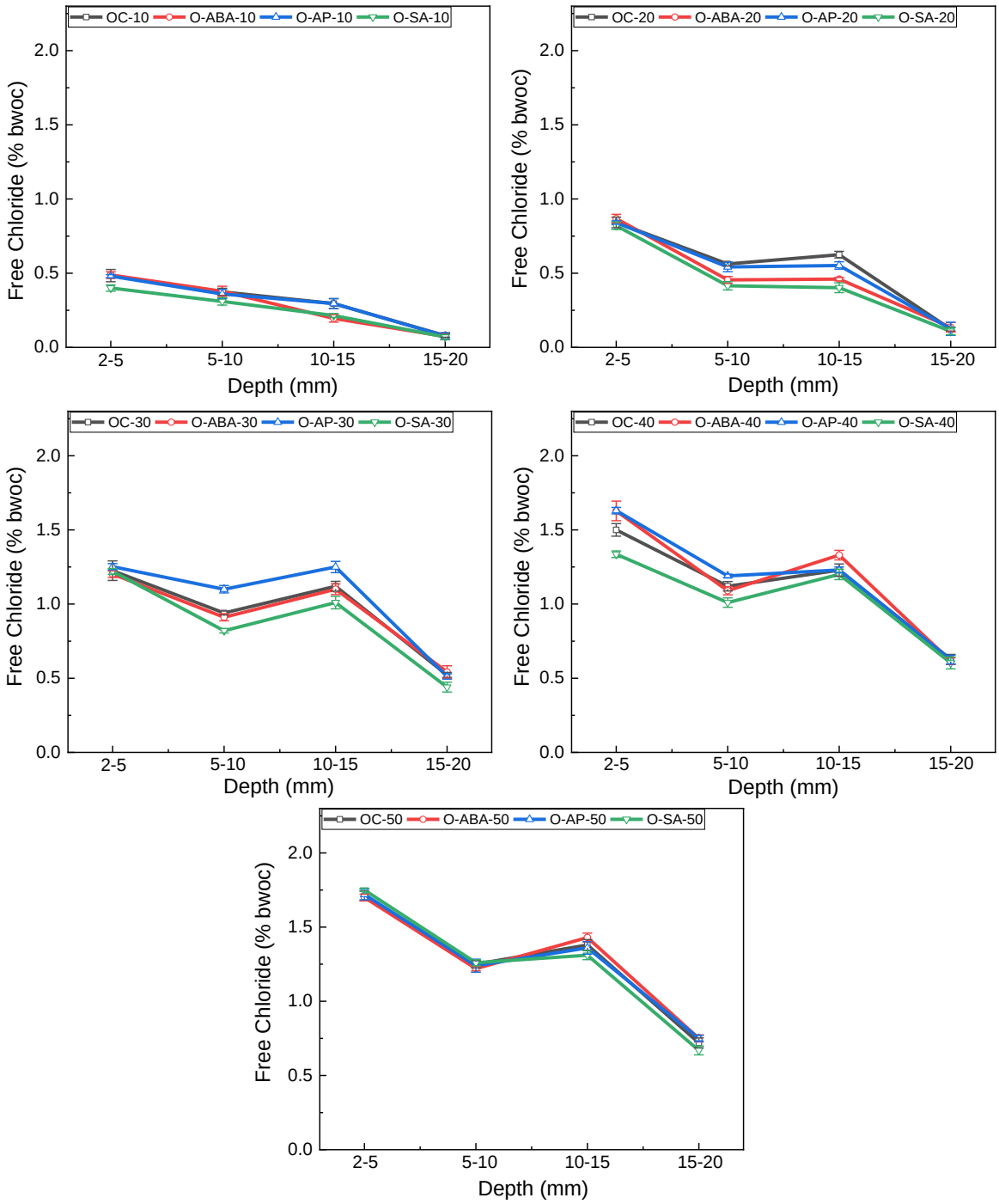

Fig. 4.21 Variation in free chloride concentration in OPC concrete specimens

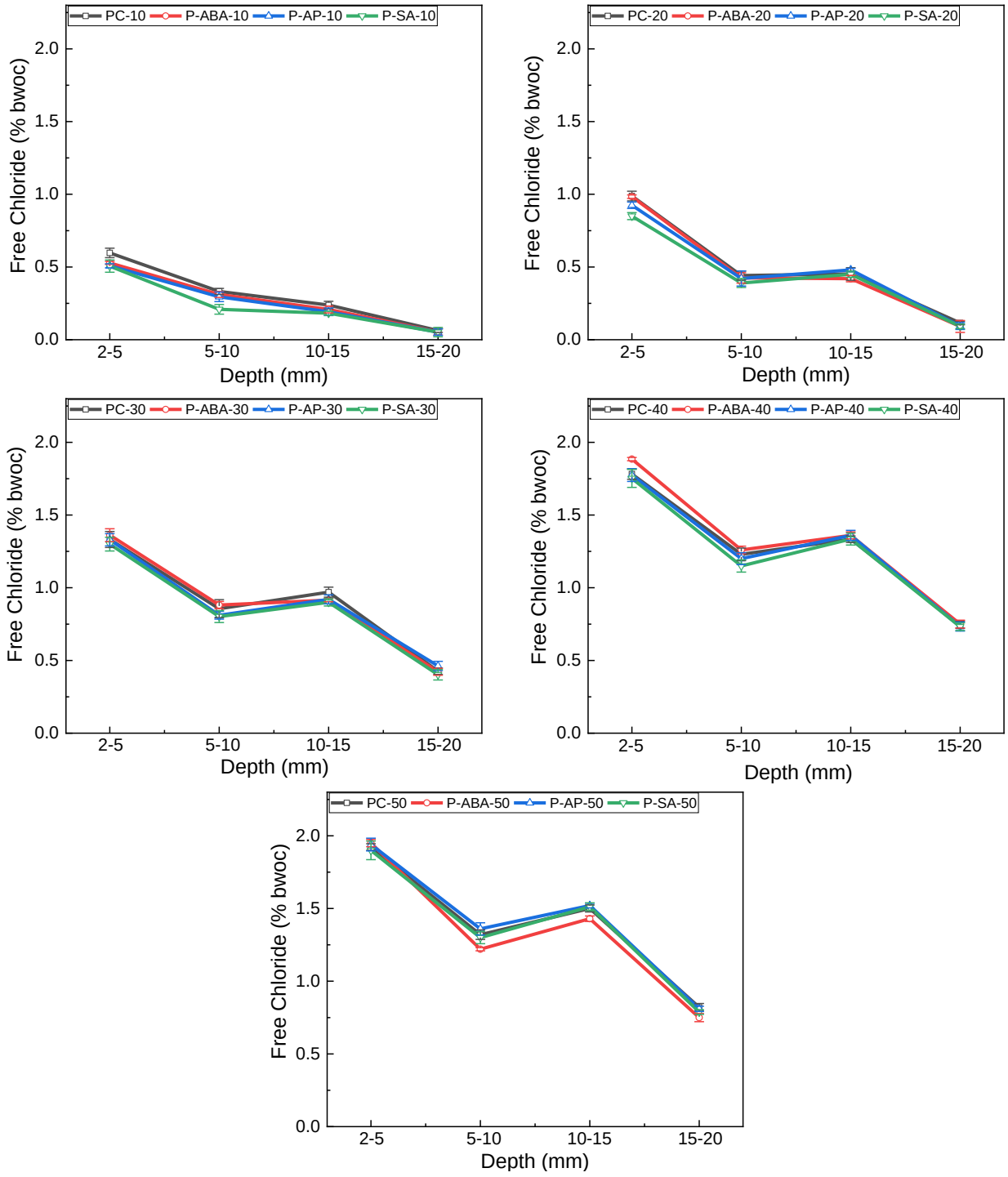

Fig. 4.22 Variation in free chloride concentration in PPC concrete specimens

It is clear from the carbonation depth and chloride profile data that in addition to the reduction of pore solution alkalinity, carbonation could aggravate chloride penetration and increase the risk of chloride corrosion. The aggravation effect was more severe for pozzolanic based concrete than OPC based. Further, with the application of CoI, the variation in the data of both tests was insignificant indicating no modification of pore matrix by the application of CoI in any cement type.

4.8 CLOSING REMARKS

The present study focuses on investigating the potential ability of generic compounds to percolate through concrete microstructure and the effect of their application on penetration of aggressive ions. The percolation ability test confirms that generic compounds tend to migrate through cover concrete via diffusion in liquid state. The concentration reaches a different level in concrete depends on their molecular weight, molecular structure, and type of cement.

Carbonation depth results and chloride profile confirmed that PPC based systems are more vulnerable to the combined exposure environment. Carbonation depth of PPC based concrete was higher than OPC concrete system due to lower portlandite content in PPC cement. Along with this, chloride concentration was observed to be higher in OPC concrete due to porous microstructure as compared to PPC concrete. However, continuous alternate chloride and carbonation exposure changes this trend. It is clear from the carbonation depth and chloride profile data that in addition to the reduction of pore solution alkalinity, carbonation could aggravate chloride penetration and increase the risk of chloride corrosion. The aggravation effect was more severe for pozollanic based concrete than OPC based. Further, insignificant variation in carbonation depth and chloride profile on both concrete systems after compounds application suggest that they are not acting as pore blocker.

Depending upon the obtained results, all the tested compounds have potential to act as migratory corrosion inhibitors and further taken for Level 3 testing i.e., test on reinforced concrete prisms.

CHAPTER 5

POTENTIAL ABILITY OF GENERIC COMPOUNDS TO MITIGATE CORROSION: PREVENTIVE vs. REPAIR MEASURE

5.1 GENERAL

Rebar in concrete can be safeguard from corrosion by using various corrosion mitigation techniques. Amongst the available methods, application of corrosion inhibitors (CoI) is the most economical and widely adopted technique. CoI can be introduced in concrete in either admixed form (called admixed CoI) or they can be applied on hardened concrete after construction termed as migratory CoI). When used in admixed form, various negative effects have been observed on different concrete properties such as workability, air entertainment, water adsorption, microstructure and strength properties; but when employed in migratory form, no such drawbacks have been observed. Thus, it is preferable to employ CoI in migratory form for the corrosion protection measure. The present study focuses on the use of three generic compounds namely, 4-amino benzoic acid (ABA), 2-aminopyridine (AP) and salicylaldehyde (SA) as migratory CoIs as preventive and repair measure.

Further, for employment of CoI in migratory form, its percolation capacity through cover concrete should be such that it reaches the rebar level in sufficient quantity so as to perform the inhibitory action. Therefore, the percolation capacity of the CoIs finalized for the current study was investigated as Level 2 of testing and the results have been presented in Chapter 4. Based on the percolation studies, a concentration of 1M of the chosen generic compounds was finalized for application on RC specimens. This part of the experimental program is referred to as Level 3 of testing and is shown in Fig. 5.1.

Furthermore, the application of CoI in migratory form can be utilized in two formats: preventive and repair. The CoI is said to be applied in preventive format when the rebar in concrete is still its passive state (non-corroded); whereas in repair strategy, the inhibitor is applied on the concrete surface when the rebar has reached the active state of corrosion. The Level 3 of testing program deals with the application of CoIs as both preventive measure and as repair measure. The test matrix for Chapter 5 is presented in Fig. 5.2.

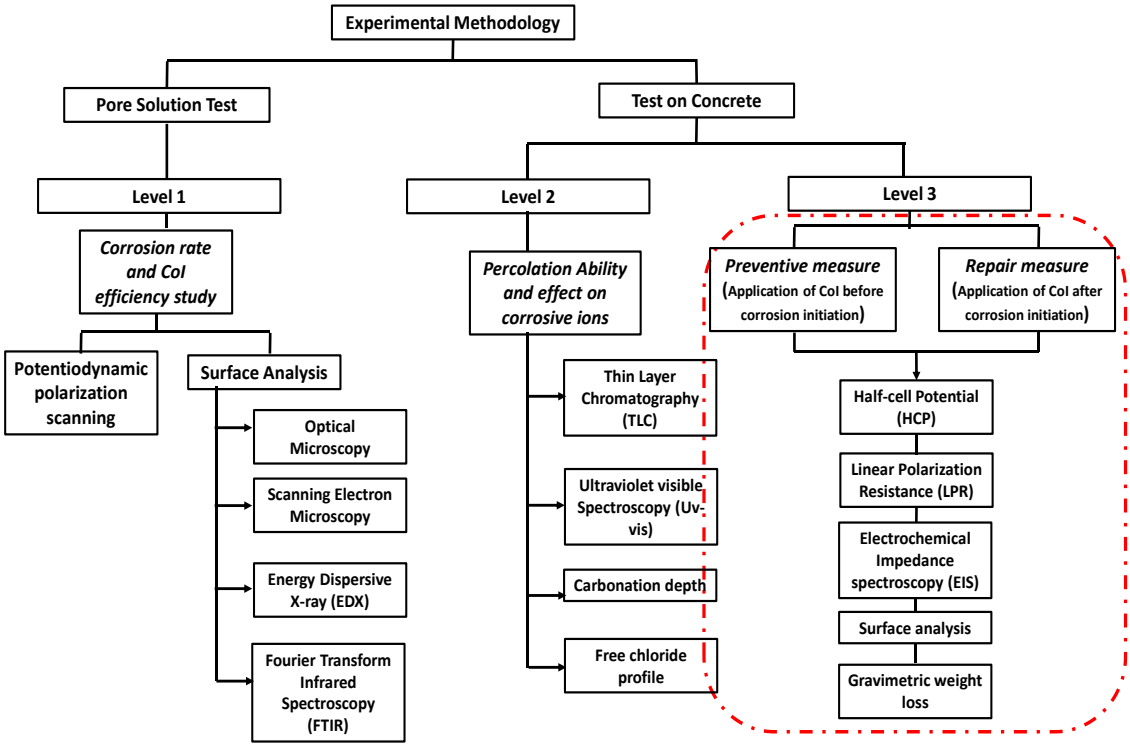

Fig. 5.1 Schematic representation of experimental methodology

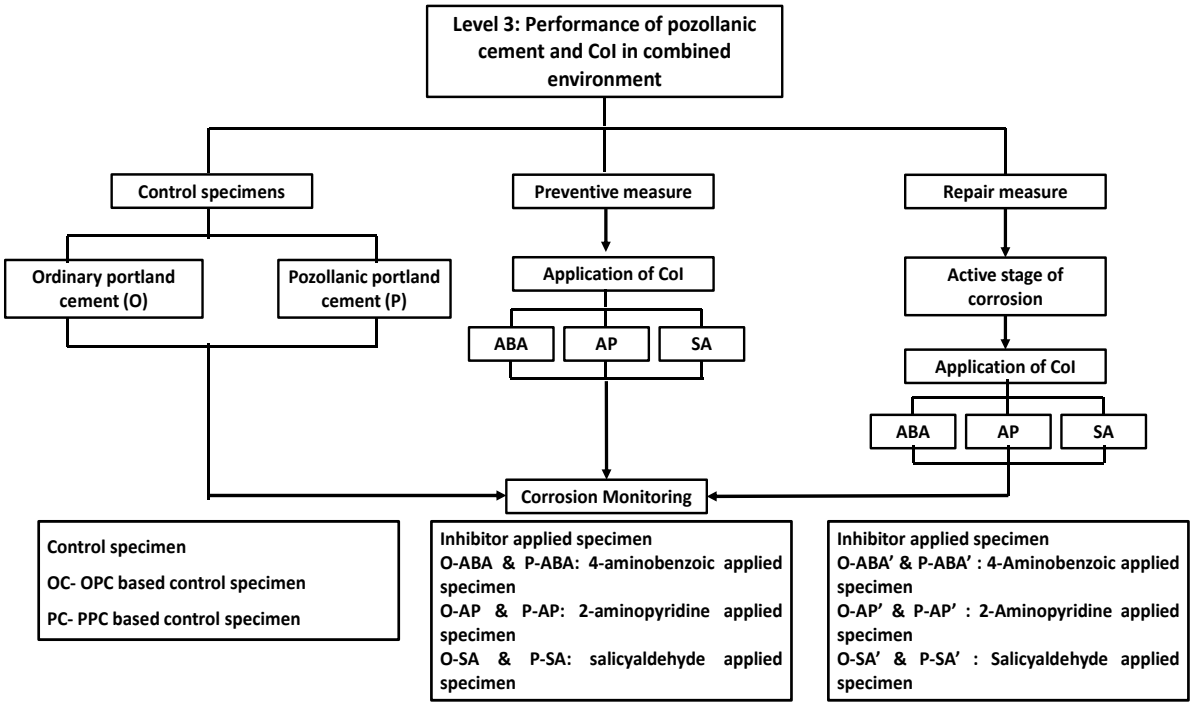

Fig. 5.2 Schematic illustration for determination of corrosion inhibitor performance against combined chloride and carbonation ingress: Preventive and repair measure

5.2 MATERIALS

The experimental program consisted of the preparation of reinforced concrete (RC) prisms. The materials used for making prism specimens consisted of two cement types (ordinary portland cement and pozzolanic portland cement), fine aggregates, coarse aggregates, three generic compounds and TMT steel bars. The properties of the cement, fine aggregates, coarse aggregates, and generic compounds had already been discussed in Chapter 4 under section 4.3. The w/c ratio and mix proportions are also the same as discussed in Chapter 4.

Further, Thermo Mechanically Treated (TMT) bars of 12 mm diameter conforming to *IS:1786-2008* were used in the preparation of RC prisms. The chemical composition of rebar obtained from the manufacture has already been present in Chapter 3 under section 3.2. The bars were cut in the length of 360 mm and a threaded hole was made at one end of the bar to assure electrical connectivity. Before embedding the bars in concrete, they were prepared according to ASTM guidelines (*ASTM G109:2013*). The preparation started with rubbing the surface with a wire brush to remove any rust. They were then degreased by soaking in analytical grade reagent, hexane and allowing to air dry for some time. Out of 360 mm length, central 200 mm was exposed to corrosion. The remaining 80 mm length on each side was insulated by applying epoxy and insulating tape on this portion, followed by mounting a 3 mm thick neoprene rubber tube over the insulating tape. The line diagram and actual prepared steel specimens are shown in Fig. 5.3.

5.3 REINFORCED CONCRETE SPECIMEN PREPRATION

To study the corrosion behavior of embedded steel under combined exposure of carbonation and chlorides, RC prisms of size 300 × 300 × 42 mm were cast. The prism specimens were prepared with one rebar embedded at a clear cover of 15 mm. Special type of molds was procured for casting of the prism specimens. To maintain rebar cover depth, holes with appropriate diameter were drilled at the exact location in the steel mold. Since 20 mm size aggregate was used in the concrete mix, care was taken that aggregate did not come in the cover zone during casting.

The line diagram and prepared prism specimens are shown in Fig 5.4. With two types of cement and three CoI application, two sets of specimens were prepared: first set had a total of 24 prisms for preventive strategy; 12 for OPC based concrete and 12 for PPC based concrete. Further, the prisms were divided into control and CoI applied specimens. Out of 12 specimens for each

cement type, 9 specimens were treated with CoI (triplicate specimen for each inhibitor) and remaining 3 were considered as control specimens. A similar set of 24 prisms were also prepared for CoI to be applied in repair strategy. Details of prism specimen along with their nomenclature used are given in Table 5.1.

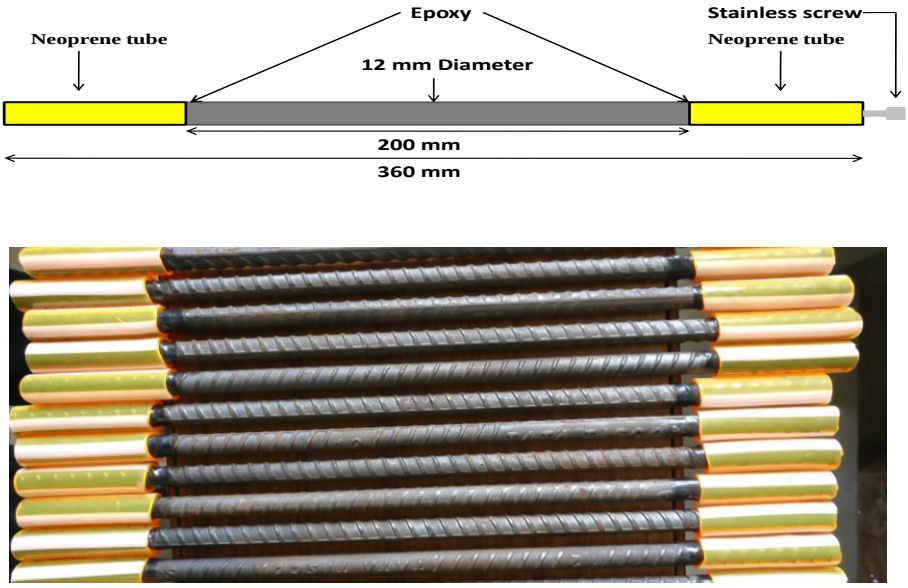

Fig. 5.3 Line diagram and actual prepared TMT steel bars

The prisms were demolded after 24 hours of casting and moist cured for 7 days by using wet jute bags. The specimens were then kept in laboratory environment for 7 days at RH of 60-70% after which preconditioning of the specimens was done at a temperature of 30 ± 2 °C and RH of 60-70% for 14 days to achieve an even distribution of moisture within specimens. All the sides of prisms except one top surface (300 x 300 mm^2) was applied with epoxy to ensure unidirectional flow of the CoI and corrosive species (CO_2 and chlorides). Finally, the inhibitor was applied by brush on the exposed surface of RC prisms of first set of specimens immediately after preconditioning and on the other set of specimens, CoI was applied after assuring that the rebars have entered the active state of corrosion (corrosion got initiated on rebars after 10^{th} exposure cycle as indicated by the electrochemical tests). For inhibitor application, 1M solution of CoI (i.e., ABA, AP and SA) was prepared and applied on the exposed face of hardened concrete in three layers at the rate of 500 ml/m^2. The details of solution preparation have already been discussed in Chapter 4 under Section 4.5. The surface was allowed to dry out between consecutive coats. This method of application was adopted from (*Kaur et al., 2016; Kaur, Goyal, Bhattacharje, et al., 2017*)**.**

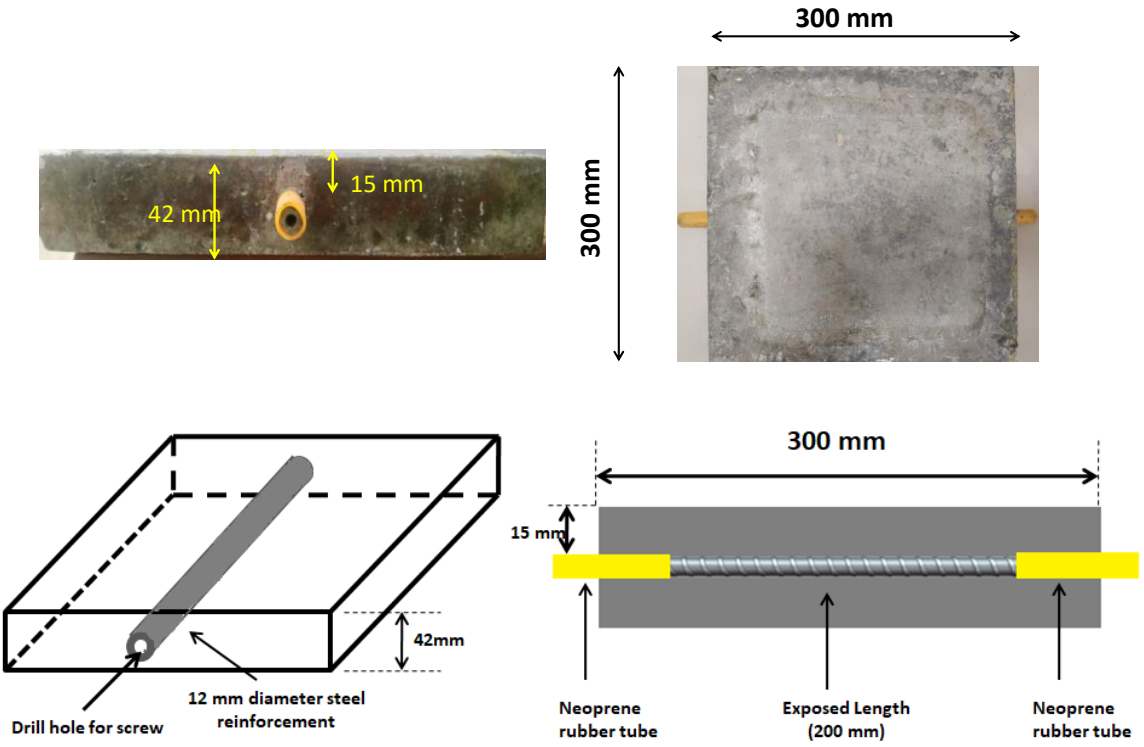

Fig. 5.4 Line diagram and cast prism specimens

Table 5.1 Nomenclature and description of specimens

Inhibitor applied	Cement Type	Nomenclature	Cement Type	Nomenclature	Description
-	OPC	OC	PPC	PC	Control specimens
ABA		O-ABA		P-ABA	Preventive
		O-ABA’		P-ABA’	Repair
AP		O-AP		P-AP	Preventive
		O-AP’		P-AP’	Repair
SA		O-SA		P-SA	Preventive
		O-SA’		P-SA’	Repair

5.4 EXPOSURE CONDITIONS

To study the corrosion behavior of embedded steel under combined exposure of carbonation and chlorides, it is necessary to ensure that the specimens must be subjected to both the aggressive environments. In the present study, a typical 7-day exposure cycle has been adopted as shown in Fig. 5.5 and the reason of choice has been discussed in Chapter 4 under Section 4.5. For chloride exposure, a plexiglass reservoir of size 200 × 200 × 70 mm was fabricated on the top surface to ensure one-dimensional penetration of chlorides and the prepared chloride solution was poured in the reservoir for required exposure duration. To avoid any evaporation loss, the reservoir was covered with plastic sheet. For carbonation exposure, the specimens were kept in a closed chamber maintained at a CO_2 concentration of 5% by volume at 30 ± 2˚ C temperature and 60-70% relative humidity.

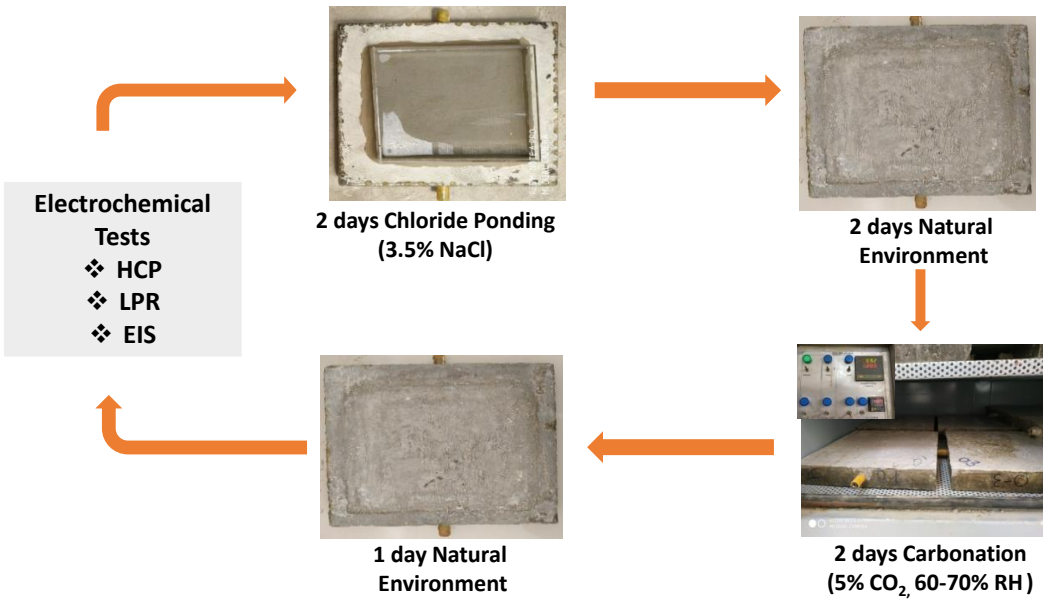

Fig. 5.5 Schematic representation of seven-day exposure cycle used in the study

5.5 CORROSION MONITORING BY ELECTROCHEMICAL TECHNIQUES

To study the long-term effect of combined environment and inhibition effect of migratory inhibitor the test program was continued up to 50 exposure cycles (total 350 days≈ 1 year). From Chapter 4, it was also observed that the water-soluble chloride content after 50 exposure cycles was as 1.5% by weight of cement at the cover depth (15 mm) for both concrete type (with and without inhibitor treated specimens), whereas average carbonation depth for OPC and PPC based

concrete was 20 mm and 30 mm, respectively. These values suggest that the severity level was very high after 50 cyclic exposures. Therefore, the testing program was discontinued after 50 exposure cycles.

Corrosion behavior of embedded rebar in concrete exposed to combined chloride and carbonation environment was monitored by various electrochemical techniques. Potential measurement of rebar was evaluated by half-cell potential technique, whereas corrosion rate was determined by performing Tafel extrapolation (LPR) measurements. To get the insight details of concrete microstructure and steel concrete interface, EIS technique was used effectively. The detailed procedure for each of the technique is described in the succeeding sections.

5.5.1 Half-cell potential (HCP)

Half-cell Potential measurement was measured periodically after every second exposure cycle till the end of test program for all specimens till 50 exposure cycles. The HCP of the rebar was measured with reference to the Saturated calomel electrode (SCE). Before initiating the test, pre-wetting of the testing surface was done by using methods explained in *(ASTM C876-22b)*. For HCP, conducting sponge wetted with soap solution was placed on the surface of the prism to ensure proper electrical contact of embedded rebar with reference electrode. The measurements were made by placing the SCE along the length of bar at five different positions and average value was considered as HCP value of the specimen. Test setup for half-cell potential measurement is shown in Fig. 5.6.

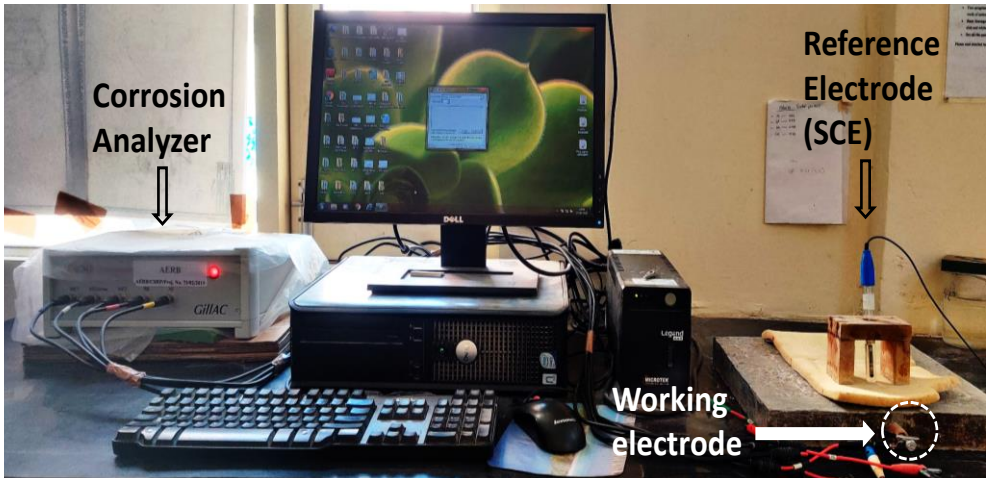

Fig. 5.6 Experimental arrangement for Half-cell potential measurement

5.5.2 Linear Polarization Resistance (LPR)

LPR method was employed on the prism specimens with the help of guard ring arrangement provided along with Gill AC corrosion analyzer. Polarization tests were performed immediately after HCP by polarizing the working electrode (steel rebar) to ±25 mV at a sweep rate of 10 mV/min. Before commencement of test, specimens were saturated to obtain a uniform moisture content on the cover concrete. This was done by placing a wetted sponge on the top of the prism specimen for two hours. After achieving a desired saturation, guard ring was placed along with wet sponge on the top of the prism. The wet sponge provides the proper ionic conductivity during the test. The working electrode and guard ring were connected to the corrosion analyzer with the help of connection wires. The arrangement for performing LPR test by using guard ring method is shown in Fig. 5.7.

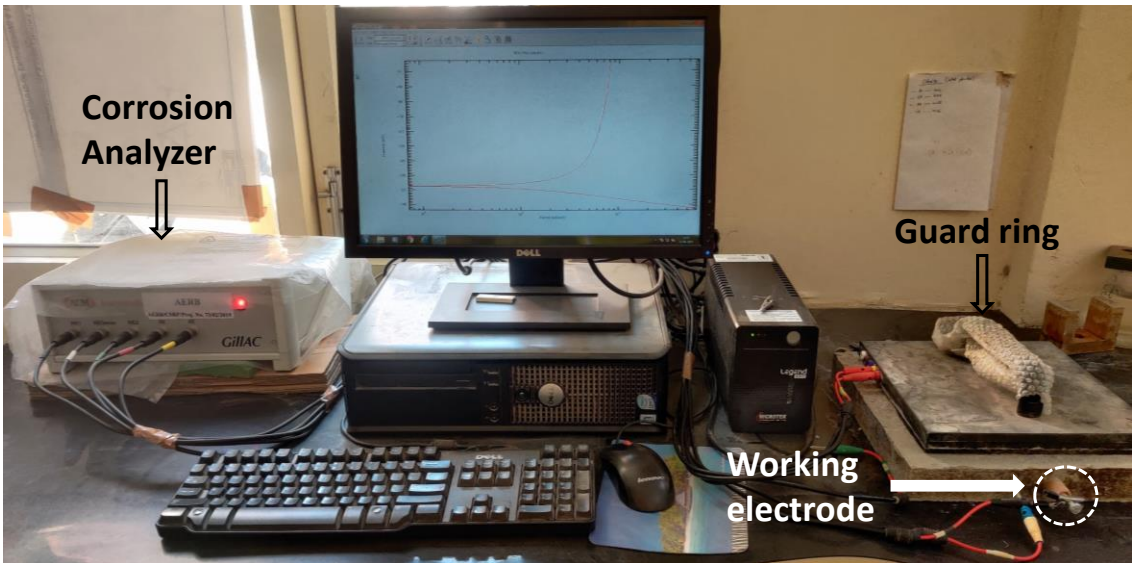

Fig. 5.7 Experimental arrangement of electrochemical measurements LPR and EIS

Typical polarization curve obtained by using LPR technique is shown in Fig 5.8. The curve consists of two branches i.e., anodic branch representing anodic dissolution reaction and cathodic branch representing cathodic reaction on steel surface. The slope of the two branches represented in figure as anodic Tafel slope and cathodic Tafel slope are obtained by extrapolating linearly and the point of intersection of these two slopes at x-axis gives the corrosion current density (i_{corr}) while the potential (at y-axis) at which it lies gives the potential of rebar called as corrosion

potential (E_{corr}). Based on the obtained Tafel plots and Tafel extrapolation technique, corrosion current density (i_{corr}) was obtained for all the specimens.

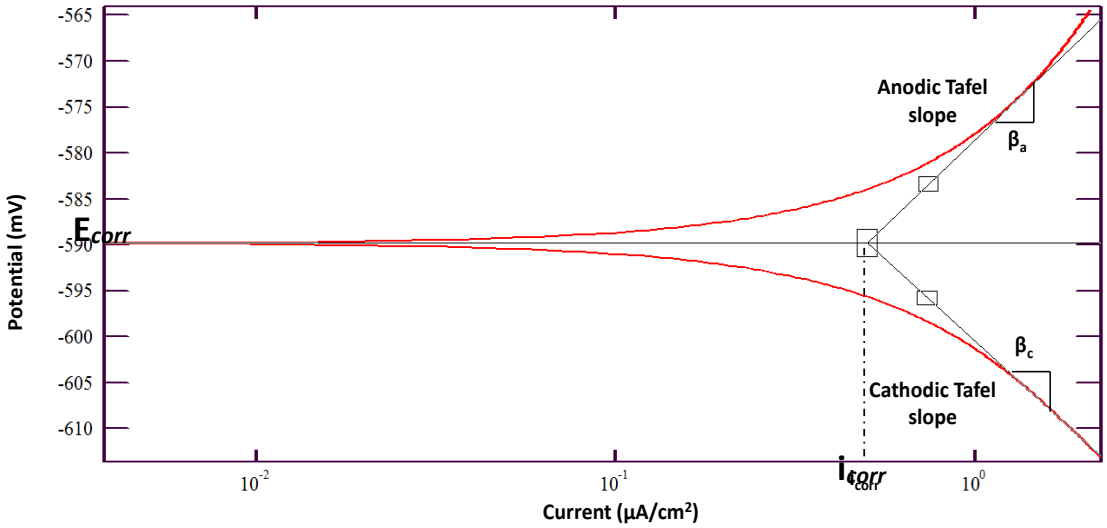

Fig. 5.8 Typical polarization curve for RC specimen

5.5.3 Electrochemical Impedance Spectroscopy (EIS)

The principle of the EIS technique is to apply AC signal amplitude to the working electrode (rebar) embedded in an electrolyte (concrete). It provides abundant information about concrete pore structure and corrosion mechanism i.e. electrical resistivity, dielectric properties of concrete, rate of corrosion, steel/concrete interface properties and the kinetic information *(Montemor et al., 2003; Rodrigues et al., 2021; Song & Saraswathy, 2007*). *Herrera Hernández et al., 2019* concludes that EIS can be used as non-destructive tool to analyze the changes occurring in concrete as well as steel surface when carbonation is involved. The results validated with carbonation depth obtain by phenolphthalein spray test and it successfully predict the time of corrosion initiation. EIS test was performed on the prism specimens after 10 exposure cycles till the end of testing age i.e., until 50 exposure cycles. The measurement was carried out with the help of guard ring arrangement provided with ACM Gill AC corrosion analyzer. The test setup used for EIS measurement was like that used in LPR measurement and represented in Fig. 5.7. The test was performed at a sinusoidal voltage of 25mV, applied in the frequency range of 100 KHz to 3 mHz. According to (*ASTM G3-14, 2019*) EIS data can be represented in two formats, Nyquist and Bode plot. Nyquist plot corresponds to graph of $Z = Z' + jZ''$ (where Z' is the real part and Z'' is the imaginary part) plotted at different frequencies. Bode plot format further has two representations

(i) Bode magnitude plot (ii) Bode phase angle plot. In this study, EIS test was performed at 0, 10 and 50 exposure cycles and represented in the form of Nyquist and Bode magnitude plots.

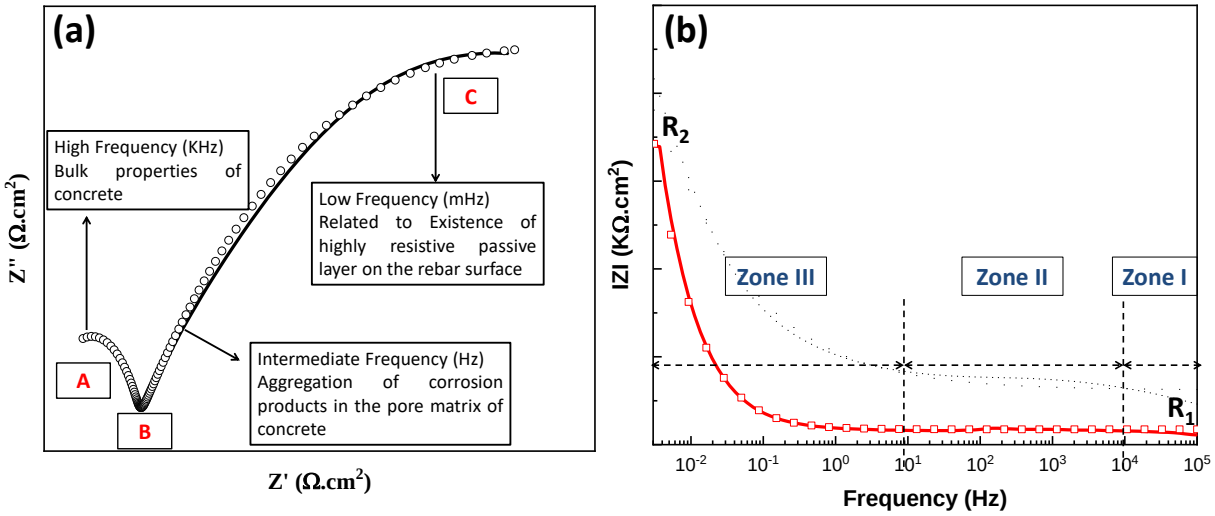

Fig. 5.9 Distinguish features of (a) Nyquist plot (b) Bode plot

Fig. 5.9(a) shows a typical Nyquist plot with three distinct traits (A, B, C). These traits are frequently seen in impedance spectra (Ford et al., 1998) and each trait defines the distinct feature of Nyquist plot. Most often, trait B is not distinctively visible as it gets veiled by C. Divergence of the actual curve from straight line is indicative of the existence of trait B. The changes in the capacitive arc of Nyquist and impedance in Bode plot display the ongoing process in concrete matrix as well as on steel surface. In Nyquist plot, the increase and decrease in radii of HF arc displays the changes occurring in concrete matrix while changes in LF arc describes the condition of embedded rebar surface (B. Q. Dong et al., 2014; Ford et al., 1998; Kaur, Goyal, Bhattacharje, et al., 2017). Also, shift in spectra w.r.t. the x-axis shows the dominant process of either chloride or carbonation. Similarly in Bode magnitude plots (shown in Fig. 5.9(b)) the distinguished region can be divided in three zones i.e. Zone I corresponds to High frequency (HF) region (100KHz-10KHz) and changes in impedance in this region correlates to the change in concrete matrix, Zone II corresponds to Mid frequency region (10KHz-10Hz) and change in this region is attributed to change in concrete microstructure and its composition at steel/concrete interface, Zone III corresponds to Low frequency (LF) region (10Hz-3mH) in which impedance change is associated with the changes in passivity of steel. In studies related to application of migratory inhibitors, mid frequency range which is attributed to the steel/concrete interface properties is important as the

inhibitor is expected to reach the rebar and form a protective layer that affects steel/concrete interface.

Equivalent electrical circuit

The impedance pot was further interpreted by modelling an equivalent circuit that represents the condition of electrolyte, corrosion reactions and passive film by means of involving various resistance and capacitance in the circuit. For obtaining the equivalent circuit in the present study, Z-man software has been utilized for mathematical analysis of the obtained EIS plots. The basic equivalent circuit was proposed by John Edward Brough Randel, also known as Randel circuit, composed of pore solution resistance (R_s) in series with parallel combination of impedance (known as charge transfer resistance (R_{ct})) and double layer capacitance (C_{dl}) (*Ribeiro & Abrantes, 2016*). Fig. 5.10 shows the typical Nyquist plot and its equivalent circuit.

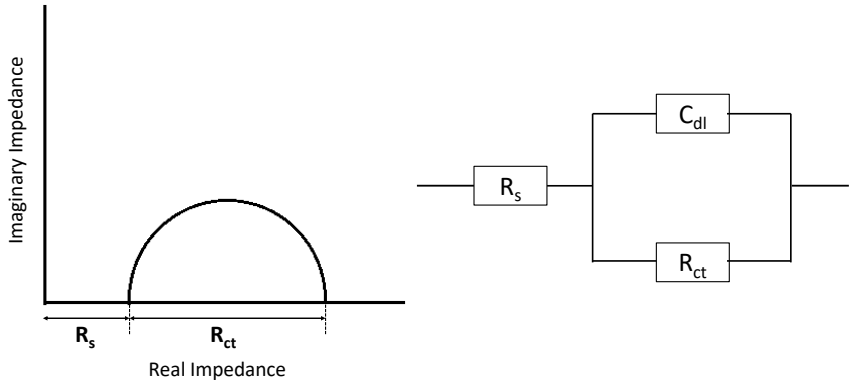

Fig. 5.10 Typical Nyquist plot and its equivalent circuit

Fig. 5.11 Schematic representation of steel-concrete interface

The equivalent circuit represented in Fig. 5.10 cannot be applied to reinforced concrete due to complexity of the reinforced concrete interface. A schematic representation that describes the typical steel-concrete interface is shown in Fig. 5.11 and it consists of various interface layers such as compact iron-oxide layer and interfacial film layer adjoining the concrete matrix. The interfacial layer consists of calcium hydroxides, calcium carbonate and other cement hydration products on the steel surface *(Kaur, Goyal, Bhattacharje, et al., 2017*).

Since the corrosion process in aggressive environment and inhibition process by corrosion inhibitor involves various physical process, therefore, simple Rendell circuit cannot be used to interpret the EIS data of reinforced concrete. Previous research has proposed different models defining different stages of reinforced concrete corrosion process that had already discussed in Chapter 2 under Section 2.11.4.

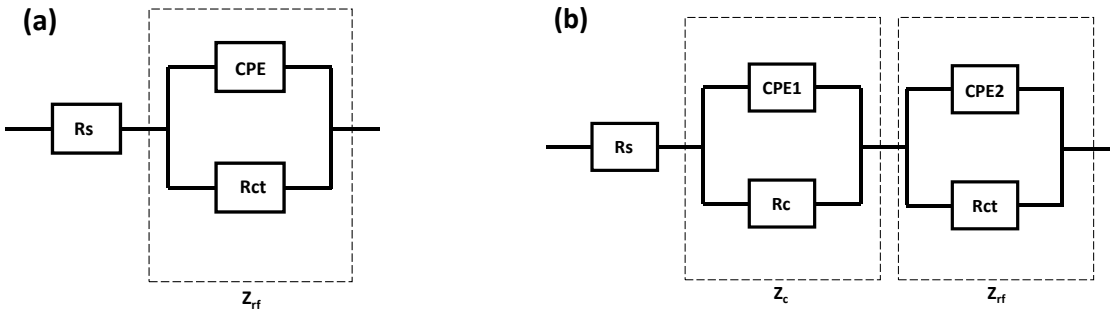

Fig. 5.12 Electrochemical equivalent circuits (a) EEC1 (b) EEC2

In the present work, several models were tried to obtain the best fit electrochemical equivalent circuit (EEC). Two EEC models namely, EEC1 and EEC2 were found to fit best for the obtained experimental data. These circuits are presented in Fig, 5.12. EEC1 is representative of those conditions where only one impedance arc is obtained in the Nyquist spectra (LF arc in this research) and EEC2 was used when both high and low frequency arcs were acquired. In the equivalent circuit, R_s represents the electrolytic pore solution resistance in concrete followed by series of Impedances (Z). EEC1 consist of one impedance (Z_{rf}) and EEC2 consist of two impedances, Z_c and Z_{rf}. Impedance Z_c corresponds to process inside the concrete matrices, whereas impedance Z_{rf} corresponds to Faradaic procedure between the interfacial film and rebar. Impedance Z_c consist of resistance (R_c) and constant phase element (CPE_c) between solid/liquid phase in the concrete bulk. Similarly, Z_{rf} consist of resistance (R_{ct}); also known as charge transfer resistance and constant phase element (CPE_{dl}) between the interfacial film and steel. In the present

circuit CPE is used instead of pure capacitor for fitting a depressed semi-circle. The depression in semi-circle is due to surface reactivity, in-homogeneity, porosity of concrete, roughness, and irregularities on rebar surface. The impedance of CPE depends upon the angular frequency and is determined by equation 5.1.

$$Z = 1/Q(j\omega)^{\alpha} \quad \ldots.5.1$$

Where Q is the admittance, ω is the angular frequency and α is the exponent for constant phase element due to depressed semicircle. When α equals 1, CPE behaves as pure capacitor and α equals 0, CPE behaves as pure resistor.

5.6 RESULTS AND DISCUSSION FOR CONTROL SPECIMENS

In the present study, corrosion monitoring of RC prism specimens was done by using various electrochemical techniques namely, HCP, LPR and EIS method. Along with this, surface condition of rebar was assessed by optical images at the end of testing age. Weight loss of embedded rebar was measured to identify the corrosion rate in combined exposure condition. The obtained results for control specimens are discussed in the following sections:

5.6.1 HCP and LPR for control specimens

The HCP values and the determined corrosion current density values (i_{corr}) for OC and PC specimens up to 50 exposure cycles were recorded and are shown in Fig. 5.13(a) and (b), respectively.

From Fig. 5.13(a), it is observed that the HCP values of OC and PC remain at low corrosion risk zone initially i.e., before being exposed to the aggressive environment, which clearly demonstrates that a passive layer is present over the steel surface before exposure. A sudden drop in potential was seen after 2nd exposure cycle in OC, whereas in PC, the drop was observed after 4th cycle. Although the drop in PC is two cycles later than OC but PC specimens fell directly in the severe corrosive zone, whereas in OC the shift of zone from high risk to severe is steady and that too after a much longer time. The results thus, indicate that in combined aggressive environment, concrete made with pozzolanic cement is more susceptible to corrosion than OPC.

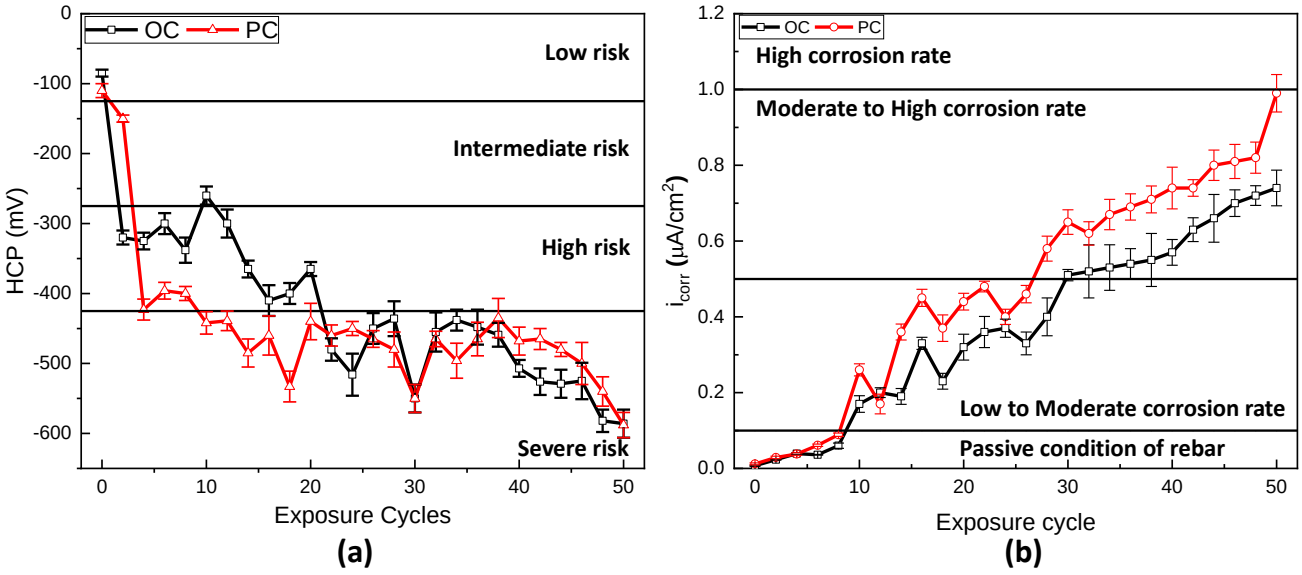

Fig. 5.13 Variation in (a) HCP and (b) i_{corr} for OC and PC specimens with exposure duration

From Fig. 5.13(b), it can be seen that i_{corr} values remained in passive zone upto the 8th exposure cycle for both OC and PC specimens. After 10th cycle, both OC and PC enter the 'low to moderate' corrosion region. From the graph, OC specimens took 32 exposure cycles to shift from moderate to high corrosion rate, while PC recorded the same shift after 28th exposure cycle. Also, at all exposure durations, PC specimens registered higher corrosion rate than OC specimen; clearly indicating more severe corrosion in pozzolanic cement concrete under combined exposure to chlorides and carbonation. The results are also in agreement with HCP values.

5.6.2. EIS for control specimens

Apart from getting the information regarding rebar corrosion, EIS is important to understand the progressive changes occurring in the properties of concrete pore structure and at steel/concrete interface. According to (*ASTM G3 2012*), EIS data can be represented in two formats, Nyquist and Bode plot. The changes in the capacitive arc of Nyquist and impedance in Bode plot displays the ongoing processes in the concrete matrix as well as on the rebar surface. In Nyquist plot, increase or decrease in radii of high frequency (HF) arc displays the changes occurring in concrete matrix; while changes in low frequency (LF) arc describes the condition of embedded rebar surface *(B. Q. Dong et al., 2014; Ford et al., 1998; Kaur, Goyal, Bhattacharje, et al., 2017*). Also, shift in spectra w.r.t. the x-axis shows the dominant process of either chloride or carbonation. During the dominant carbonation effect, the spectra is seen to shift towards the right w.r.t. x-axis however, in chloride

dominant reactions, left shift in the spectra is recorded with increasing number of testing ages (Kaur, Goyal, Bhattacharje, et al., 2017; Sohail et al., 2020). Similarly, in Bode magnitude plots, changes in HF (100KHz-10KHz) impedance show the change in bulk concrete, change in intermediate frequency (IF) region (10KHz-10Hz) is attributed to changes at steel/concrete interface and LF (10Hz-1mH) impedance is associated with the changes in passivity of steel.

In the present study, EIS test was performed after every 10 exposure cycles. The Nyquist plots obtained for OC and PC are presented in Figs. 5.14(a) and (b), respectively. From the figures, a clear shift in the spectra towards the left side i.e., towards the lower frequency values can be seen. This signifies that the effect of chloride ions and its conductivity in the concrete matrix is dominant than the carbonation effect. Further, the shift in the spectra with increasing cycles, is more pronounced in PC as compared to OC signifying that PC has more conductivity of chloride ions than OC and would have more corrosion levels than OC. In PC, the chloride ions are expected to get accumulated at the surface of concrete due to its initial dense pore structure. They are then pushed by CO_2 during carbonation exposure. This push led to an increase in chloride ion concentration of PPC concrete with increase in exposure duration. Further, for the comparison purpose of OC and PC, the Nyquist and Bode plots at 0, 10, 30 and 50 cycles are shown cycle-wise in Figs. 5.15 and 5.16 and the behavior is discussed in detail in the following sections.

Nyquist plots

Before exposure, large diameter LF arc was witnessed for both cement types, which indicates the presence of a highly resistive passive layer on the steel surface before exposure because of high pH of pore solution *(Kaur, Goyal, Bhattacharje, et al., 2017; Sohail et al., 2020; Vedalakshmi & Thangavel, 2011)*. The reduction in diameter of LF arc was observed from 0 to 10^{th} cycle of exposure in both the cement type specimens which clearly indicates that the protective film on the rebar vanished quickly, and the corrosion started in shorter duration. Afterwards, a gradual decrease in diameter of LF arc was witnessed due to progressive decrease in charge transfer resistance of steel and active corrosion process.

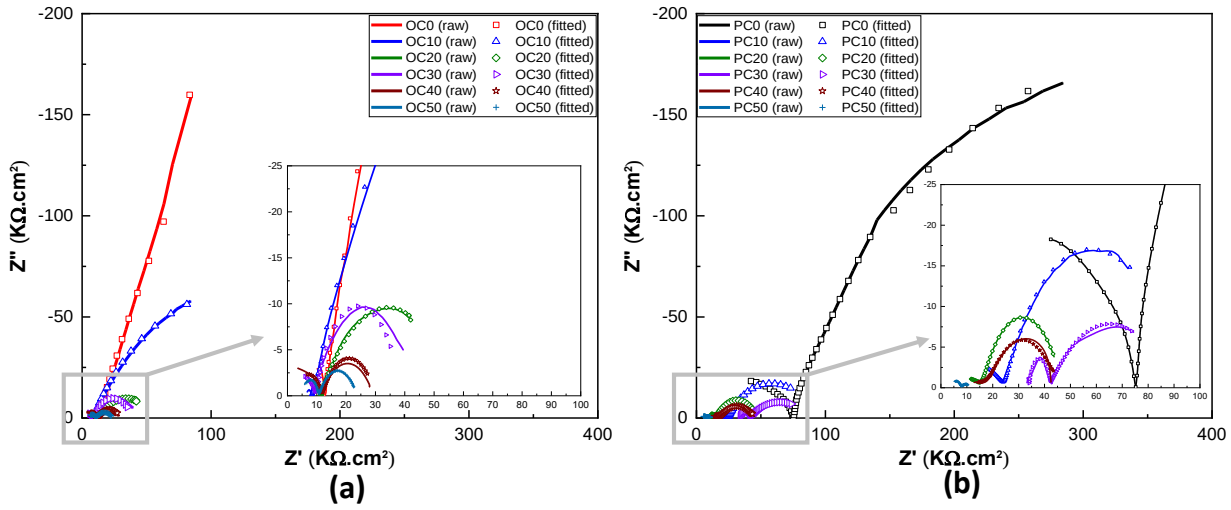

Fig. 5.14 Nyquist spectra of (a) OC and (b) PC specimen at 0, 10, 20, 30, 40 and 50 exposure cycle

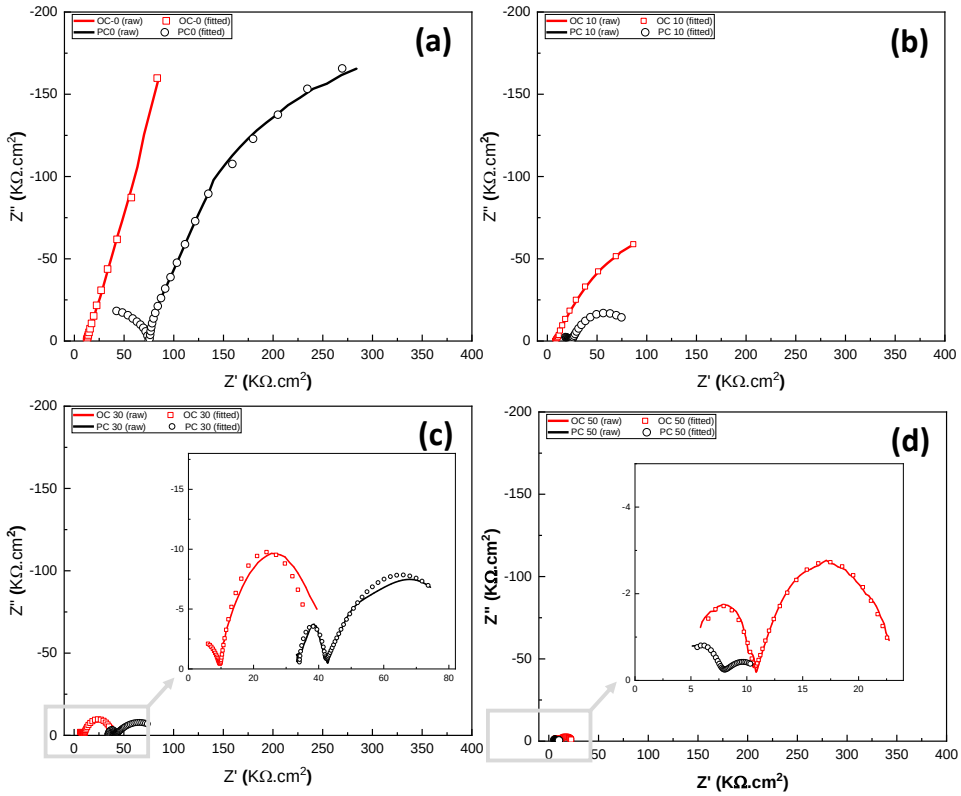

Fig. 5.15 Nyquist plots for OC and PC at (a) 0; (b) 10; (c) 30 and (d) 50 exposure cycles.

When observing the Nyquist spectra in HF region, a larger diameter in PC as compared to OC specimens is seen before exposure. From this, it can be said that PC was denser as compared to OC during the initial testing (*Aguirre-Guerrero et al., 2016*). In OC progressive increase in HF arc were observed indicating densification of concrete matrix owing to precipitation of $CaCO_3$ in its pores during carbonation reaction *(Aguirre-Guerrero et al., 2016; B. Q. Dong et al., 2014; Montemor et al., 2003*); on the contrary, small decrease in HF arc was noticed in PC with continuous exposure. This is due to the consumption of $Ca(OH)_2$ in the secondary pozollanic reaction in PC specimens and/or due to the increase in pore size volume caused by the decomposition of C-S-H (*Hren et al., 2021; Morandeau et al., 2015).*

Bode Plots

The initial resistance to charge transfer of rebar due to presence of passive layer is further validated by high impedance values in Bode plot (shown in Fig. 5.16) at LF i.e. 340 $K\Omega cm^2$ and 540 $K\Omega cm^2$ for OC and PC, respectively. The modulus of impedance, |Z| of PC is 1.58 times higher than OC initially. It was seen that the impedance value of PC at LF decreased by 85.18% after 10 exposure cycles and for OC the value decreased by 77.05%. Although, |Z| value is higher for PC than OC initially, but after exposure to combined environment, it reduced to reach similar impedance. It can be said that the rebar passivity in both OC and PC was destroyed after 10 cyclic exposures. The LF impedance modulus continuously decreased which is the indication of the active corrosion state of steel in both concrete types. At the end of the 50^{th} cycle, OC displays more impedance than PC i.e. 21.56$K\Omega cm^2$ and 10.62$K\Omega cm^2$. This observation is in compliance with Nyquist observations. In the intermediate frequency range, |Z| values are seen to decrease for both OC and PC at all testing durations, with an exception at 20^{th} exposure cycle in OC (shown in Fig.5.16(a)). The continuous reduction in |Z| is attributed to the change in composition at steel/concrete interface due to aggressive ion attack on the passive film. Exceptionally, an increase of |Z| in OC at 20^{th} exposure cycle is witnessed that might be due to the precipitation of corrosion products and calcium carbonate at the steel-concrete interface *(Sohail et al., 2020*). Also, |Z| value noted at HF for PC was 70 $K\Omega cm^2$ which is higher in comparison to OC (i.e., 22 $K\Omega cm^2$) due to its dense pore structure of PC. The |Z| values are observed to decrease for both OC and PC with the continuous cyclic exposure (shown in Fig.5.16(b)). Decrease in HF impedance resulted from

the higher conductivity of the solution due to presence of chloride ions (Królikowski & Kuziak, 2011).

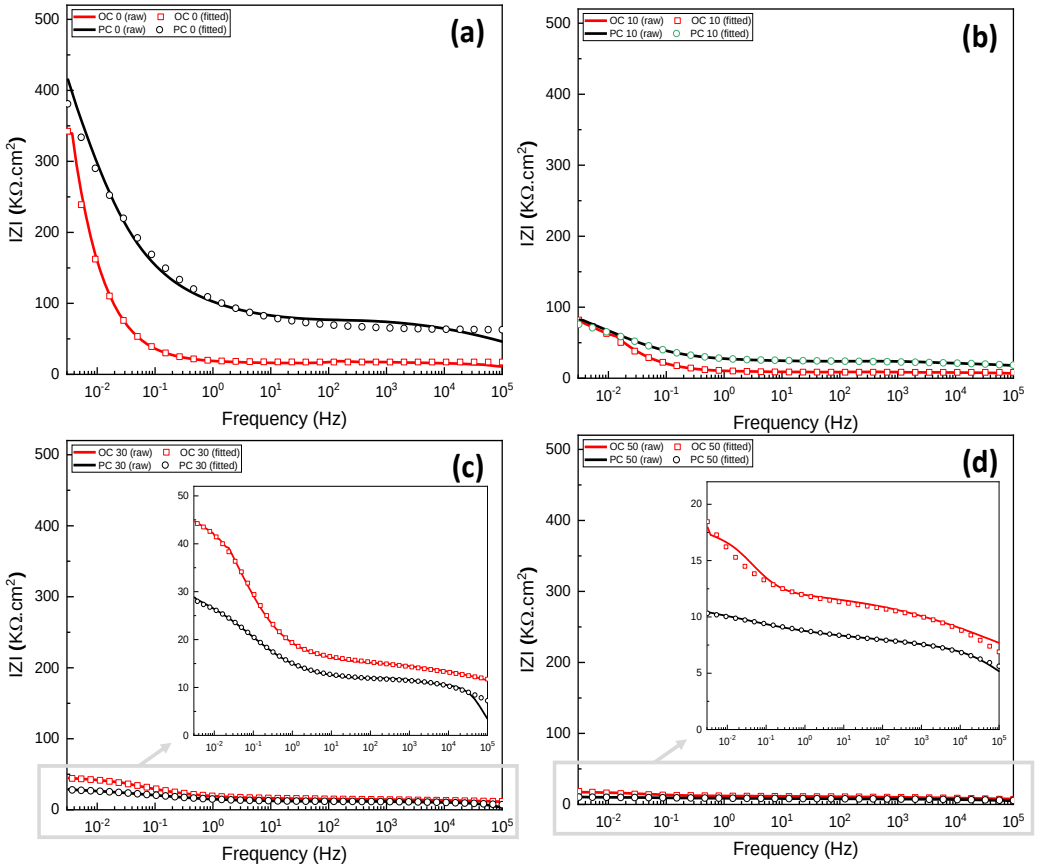

Fig. 5.16 Bode plots for OC and PC at (a) 0; (b) 10; (c) 30 and (d) 50 exposure cycles.

5.6.3 Electrochemical parameters and equivalent circuits for control specimens

Further, the obtained Nyquist and Bode magnitude plots were fitted by using Zman view software. Two electrochemical equivalent circuits (EEC) were used for fitting, that are discussed in Section 5.5.3. EEC1 was applicable to OC for 0 and 10th cycle and EEC2 was found to be suited for all the other cycles; EEC2 is valid for all the cycles of both OC and PC. In the equivalent circuit, R_s represents the electrolytic pore solution resistance in concrete followed by series of Impedances (Z). EEC1 consist of one impedance (Z_{rf}) and EEC2 consist of two impedances, Z_c and Z_{rf}. Impedance Z_c corresponds to Faradaic procedure inside the concrete matrices, whereas impedance Z_{rf} corresponds to Faradaic procedure between the interfacial film and rebar. Impedance Z_c consist of resistance (R_c) and constant phase element (CPE_c) between solid/liquid phase in the concrete bulk. Similarly, Z_{rf} consist of resistance (R_{ct}); also known as charge transfer

resistance and constant phase element (CPE_{dl}) between the interfacial film and steel. The EIS fitted parameters for control specimens are represented in Table 5.2.

Table 5.2 Resistive parameters obtained after fitting Nyquist plots

Sample	Cycle	Rs ($k\Omega.cm^2$)	Rc ($k\Omega.cm^2$)	Rct ($k\Omega.cm^2$)	Sample	Cycle	Rs ($k\Omega.cm^2$)	Rc ($k\Omega.cm^2$)	Rct ($k\Omega.cm^2$)
OC	0	10.99	-	329.06	PC	0	62.87	354.2	353.46
	10	6.74	-	74.6		10	17.92	143.01	62.48
	20	8.22	7.25	55.34		20	10.35	92.36	52.43
	30	11.45	23.84	33.25		30	3.44	45.13	25.41
	40	9.42	17.22	18.54		40	4.21	25.24	15.66
	50	7.69	10.95	10.29		50	5.17	3.43	5.26

It can be stated that any changes in the bulk concrete will be reflected in the changes in pore solution resistance (R_s) and ion transfer resistance of the bulk concrete (R_c). As can be observed from Table 5.2, the values of R_s and R_c decreased with progressive exposure in both the control specimens (i.e., OC and PC), which is representative of increase in ionic movement in the concrete matrix. It is worth mentioning that R_c is not found in some of the OC samples as the high frequency arc was missing in their corresponding Nyquist plots. Gu et. al. (*Gu et al., 1997*) reported that the size of high frequency arc (which represents the properties of concrete matrix) decreases with the increase in ion concentration in the concrete electrolyte or due to the increase in porosity of concrete systems. On further exposures, R_s and R_c decreased progressively which suggests the presence of highly conductive ions inside the different concrete matrices (i.e., OPC and PPC based specimens).

The resistive parameter obtained after fitting of the LF ($R_{ct)}$ is representative of the phenomenon happening at the rebar level and is analyzed to study the changes in the charge transfer mechanism. It is considered as the most important parameter and has a direct relationship with the corrosion rate. The value decreases when the resistance against the charge transfer decreases, indicating an active state of corrosion. As can be seen from the table, the R_{ct} value of both the specimen was high (329.06 $k\Omega.cm^2$ for OC and 353.46 $k\Omega.cm^2$ for PC) initially indicating formation of passive layer on the rebar due to high alkalinity. After the 10^{th} exposure cycle the values reduced drastically for both the concrete type. The value of R_{ct} decreases about 77% in OC (from 329.06 $k\Omega.cm^2$ to 74.6 $k\Omega.cm^2$) and 82% in PC (353.46 $k\Omega.cm^2$ to 62.48 $k\Omega.cm^2$) which is directly related to the

depletion of initially formed passive layer on the rebar surface. Further, progressive decrease in value was recorded with exposure duration indicating decrease in surface resistance against charge transfer mechanism and formation of porous corrosion products on the rebar surface. At the end of exposure, R_{ct} value of PC recorded to be lower than OC indicating higher severity level in PPC based concrete system.

5.6.4 Visual and microscopic observations of concrete surface and exposed rebar surface for control specimens

Fig. 5.17 shows the measured crack width of the top exposed surface of reinforced concrete of different specimens at the end of exposure duration of fifty cycles. The formation of corrosion products on the steel surface cause expansive stresses in concrete. From the visual inspection it was seen that a surface crack was formed throughout the length of the bar in control specimens i.e. OC and PC. The magnified image shows that the width of the crack on the surface of OC is smaller than PC. The average crack width in OC and PC was 0.377 mm and 0.535 mm, respectively as shown in Fig. 5.17(a) and (b). This suggests that the PC specimen undergoes higher stress due to formation of corrosion product in more severe condition as suggested by electrochemical investigation.

The visual and microscopic images of steel rebars before embedding in concrete and after extraction from OC and PC specimens at the end of the experimental program are shown in Fig. 5.18. The initial condition of rebar was free from any defect (Fig. 5.18(a) and (a')), whereas pits due to chloride attack are visible on the extracted rebar along with corrosion products formed throughout the surface at the end of testing as shown in Fig.5.18 (b), (b'), (c) and (c'). The continuous carbonation caused reduction in pH and uniform corrosion on rebar surface, while continuous chloride attack on rebar surface caused pitting at various locations. The surface observation clearly shows that mixed environment cause more severe condition for embedded rebar as it cause localized and uniform corrosion of the reinforced steel. Further, the condition of rebar from PC specimens is more severe than OC. This is in compliance with the electrochemical tests to find corrosion rate.

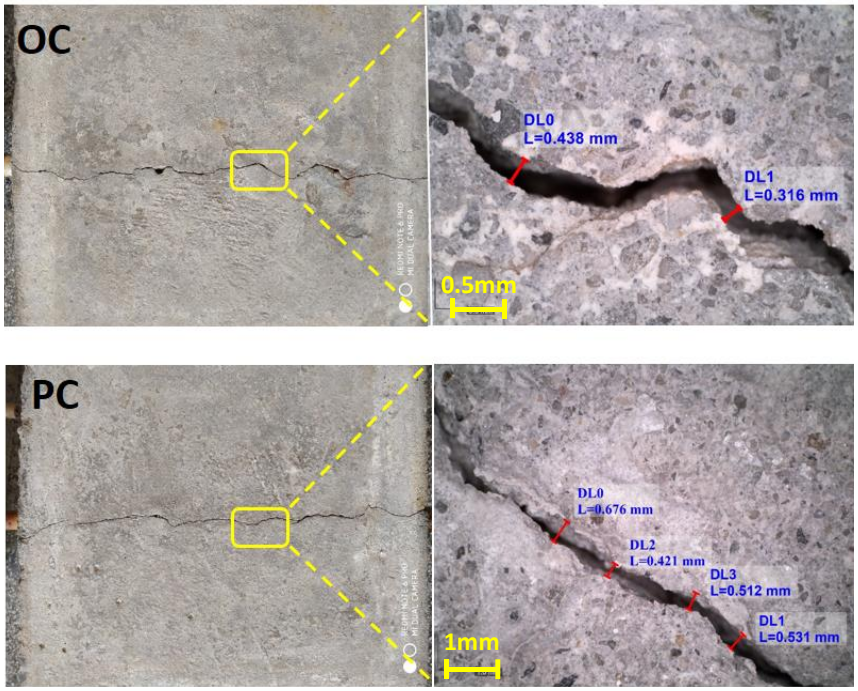

Fig. 5.17 Magnified images of concrete surface at the end of exposure

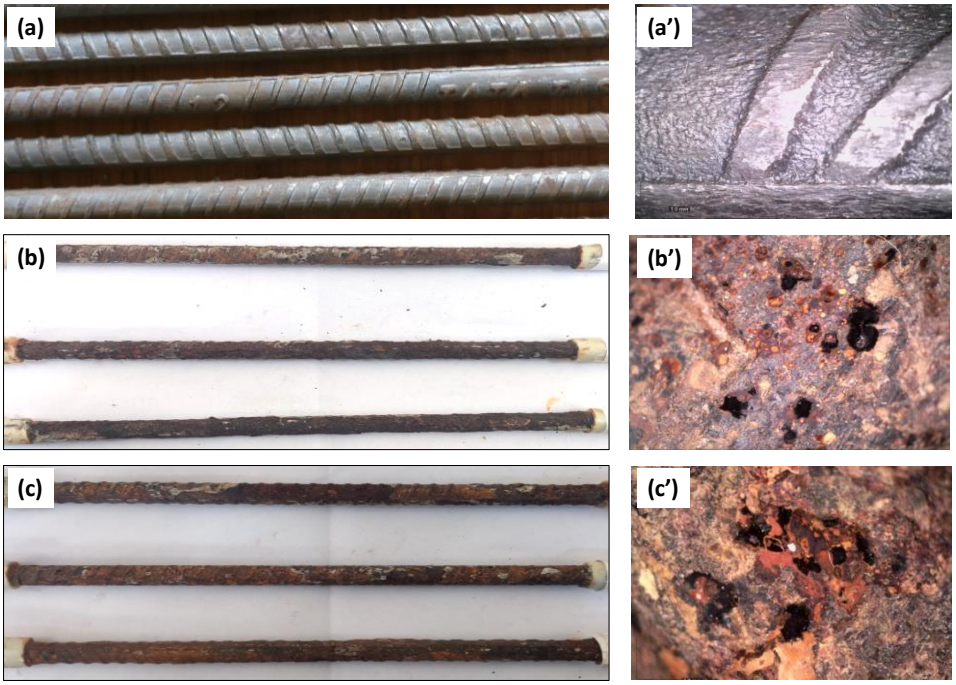

Fig. 5.18 Visual and microscopic images of (a), (a') rebar before embedding in concrete; extracted bars from (b), (b') OC and (c), (c') PC, respectively

5.7 RESULTS AND DISCUSSION FOR ABA APPLIED SPECIMENS

The efficacy of the selected inhibitor against rebar corrosion was examined by using electrochemical methods: namely HCP, LPR and EIS. It was followed by surface condition assessment by optical images at the end of testing age and weight loss measurements of embedded rebar to measure corrosion rate in combined exposure condition. The various test results of ABA applied specimens are discussed in the following sections:

5.7.1 HCP for ABA applied specimens

The HCP values of inhibitor applied specimens are shown in Fig. 5.19; in which Fig. 5.19(a) represents data OPC system; while Fig. 5.19(b) represents data for PPC based system in which inhibitor was applied before corrosion initiation and after the rebar has reached active state of corrosion. In comparison with HCP of control specimens, it can be noted that OC specimens shifted to severe risk zone after 22 exposure cycles (see Fig. 5.19(a)), while inhibitor applied specimens remained in high-risk zone for most of the testing duration. Among the two series of inhibitor application, O-ABA shifted to severe zone at 38th cycle, while O-ABA' showed the shift after 46th cycle. In PPC based specimens, PC shifted to severe region after 10th exposure cycle, while CoI applied P-ABA and P-ABA' specimen showed shift after 20th and 40thexposure cycle (see Fig. 5.20).

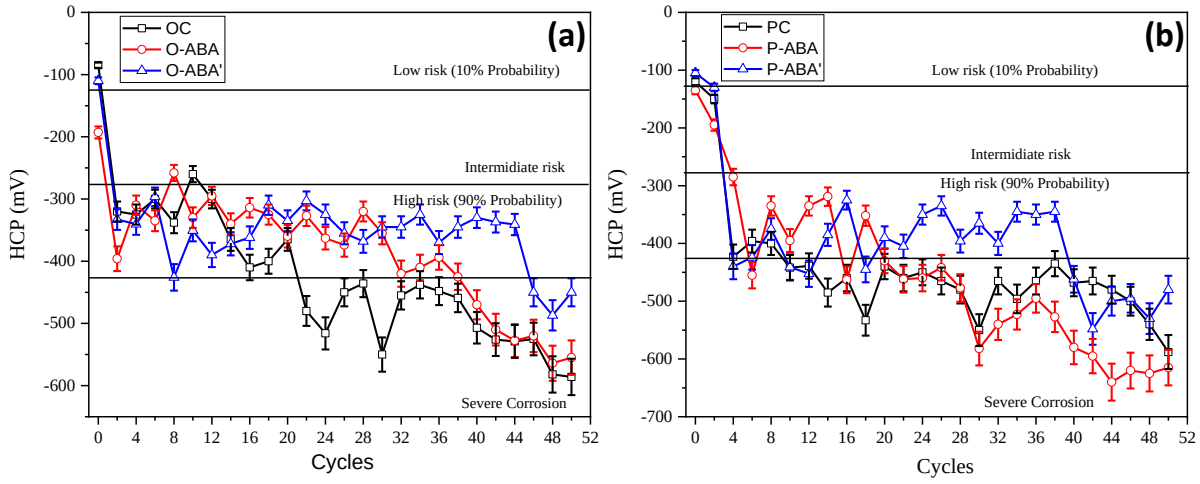

Fig. 5.19 Half-cell potential of control and ABA applied specimens (a) OPC based concrete system(b) PPC based concrete system

The HCP results indicate that in combined environment, both concrete types, OC as well as PC, become vulnerable to corrosion as indicated by the potential values; however, inhibitor application could reduce the risk to corrosion process.

5.7.2 LPR for ABA applied specimens

LPR test was performed to get variation in corrosion current density (i_{corr}) of rebar with the continuous cyclic exposure. The obtained results for ABA applied specimens are shown in Fig. 5.20. In control specimens exposed to combined environment, i_{corr} values showed that rebar remained in passive zone up to the 8th exposure cycle for both OC and PC specimens. After 10th cycle, both OC and PC entered 'low to moderate' corrosion region. Further OC specimen took 32 exposure cycles to shift from moderate to high corrosion rate, while PC recorded the same shift after 28th exposure cycle. Also, at all exposure durations, PC specimens registered higher corrosion rate than OC specimen; clearly indicating more severe corrosion in pozzolanic cement concrete under combined exposure to chlorides and carbonation.

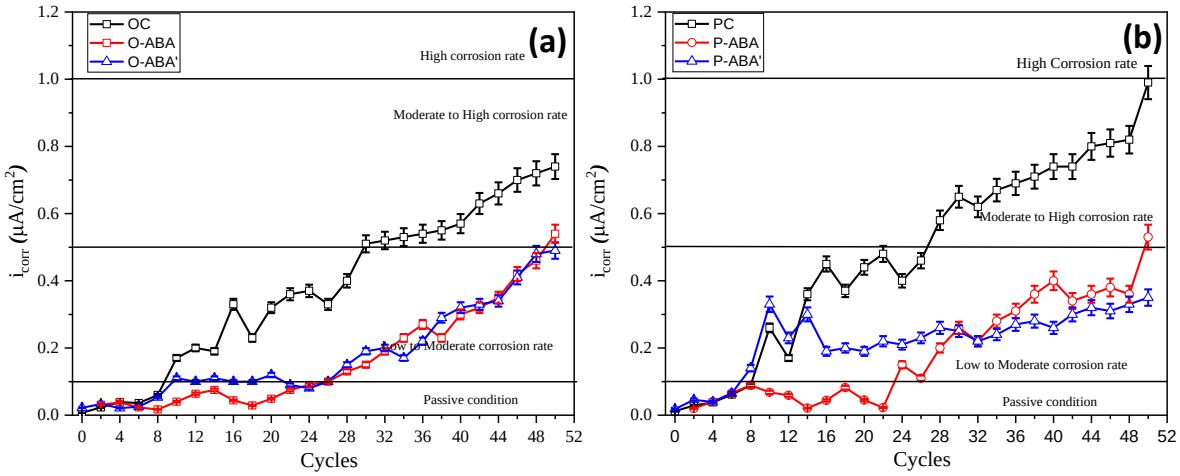

Fig. 5.20 Variation in corrosion current density with exposure duration for control and ABA applied specimens (a) OPC based concrete system(b) PPC based concrete system

Further, in specimens where CoI was applied on concrete before exposure for preventive measure (O-ABA and P-ABA), the passivity was seen to prolong till 24 exposure cycles in both type of concretes. Later, the i_{corr} shifted to active corrosion zone. Even after 50 exposure cycles, the i_{corr} recorded was 44.6% (for O-ABA) and 56.9% (for P-ABA) lower than the corresponding control specimens. It clearly demonstrates that the inhibitor performed efficiently throughout the test

exposure. For specimens where CoI was applied after the rebars got de-passivated (O-ABA´ and P-ABA´), the i_{corr} was seen to be steady up to 28 cycles. This indicated that 4ABA can restrain the ongoing corrosion process. Further, in O-ABA´, the i_{corr} increased in similar manner as in O-ABA after 28 cycles. On the other hand, in PPC based concrete the i_{corr} is seen to be constant till the end of testing age for P-ABA´. In comparison with the control specimens, the ABA treated specimens as repair strategy displayed 33.78% (for O-ABA´) and 64.64% (for P-ABA´) lower i_{corr} values even at the end of testing duration. On comparing the two stages of inhibitor application, it can be said that 4ABA performed either similar to or better when used as repair strategy. The results are also in agreement with HCP test.

5.7.3 EIS for ABA applied specimens

Apart from getting the information regarding rebar corrosion, EIS is important to understand the progressive changes occurring in the properties of concrete pore structure and at steel/concrete interface.

5.7.3.1 EIS spectra for ABA applied specimens as preventive measure:

The Nyquist impedance spectra for the set of specimens in which CoI was applied before exposure to aggressive environment are shown in Fig. 5.21 and the corresponding bode magnitude plot are shown in Fig. 5.22. In this set, the inhibitor was allowed to percolate after application for 15 days. After 15 days of natural penetration, EIS test was performed as reference and the specimens were then exposed to corrosive environment. The test results for this set are discussed hereunder:

Nyquist plots

It was observed from the Fig. 5.21 that there was a four-fold (from 150 KΩcm^2 to 600 KΩcm^2) and two-fold (from 150 KΩcm^2 to 300 KΩcm^2) increase in diameter of LF arc in O-ABA and P-ABA, respectively, as compared to control specimens. This is associated with the formation of better protection provided by the inhibitor over steel surface (Chaussadent et al., 2006b; Cui et al., 2021). It further suggests that the inhibitor could percolate through the concrete cover with 15 days of application to form protective layer on the steel surface. This statement can also be confirmed from the migration ability test results of ABA which are presented in Chapter 4 under Section 4.7. On comparing the performance in O-ABA and P-ABA, it can be seen that the diameter of LF arc

in O-ABA is very large as compared to P-ABA. This is related to the diffusion process of CoI inside the concrete. Blended cement concrete is reported to be denser initially and because of this the dispersion of the inhibitor is slow and steady with the continuous alteration of pore matrix. Unlike this, OPC based concrete is less dense thus, allowing the inhibitor to migrate easily. With the continuous exposure, the LF capacitive arc kept on decreasing which indicates the breakdown of passive layer steadily unlike the abrupt breakdown in case of control specimens. When HF region is observed, unlike in OC, HF capacitive arc is absent in O-ABA at all exposure durations (shown in Fig. 5.21(a)). It indicates that 4ABA was not acting as pore blocker and got dispersed easily into concrete to reach the rebar surface. However, in P-ABA an abrupt rise in diameter of HF arc is observed after the 10^{th} cycle (shown in Fig. 5.21(b)). This arc is again noticed to decrease with time as the inhibitor was getting uniformly dispersed. The whole process indicates that the refined pore structure of PPC offered some initial hindrance to penetration of ABA. The diameter of arc decreased later after the uniform dispersion was achieved with time. Similar pore blocking effect is reported by. (*Kaur, Goyal, Bhattacharje, et al., 2017*) in PPC concrete subjected to carbonated environment. Similar to the control specimens, the Nyquist spectra of P-ABA shifted towards left due to highly conductive chloride ions.

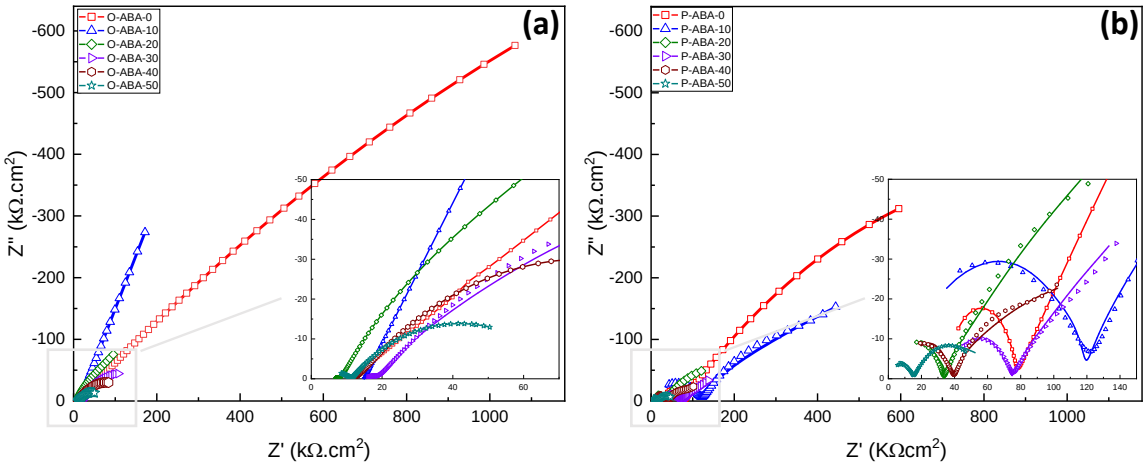

(a) OPC based concrete system **(b) PPC based concrete system**

Fig. 5.21 Nyquist spectra for ABA applied specimens as <u>preventive measure</u>

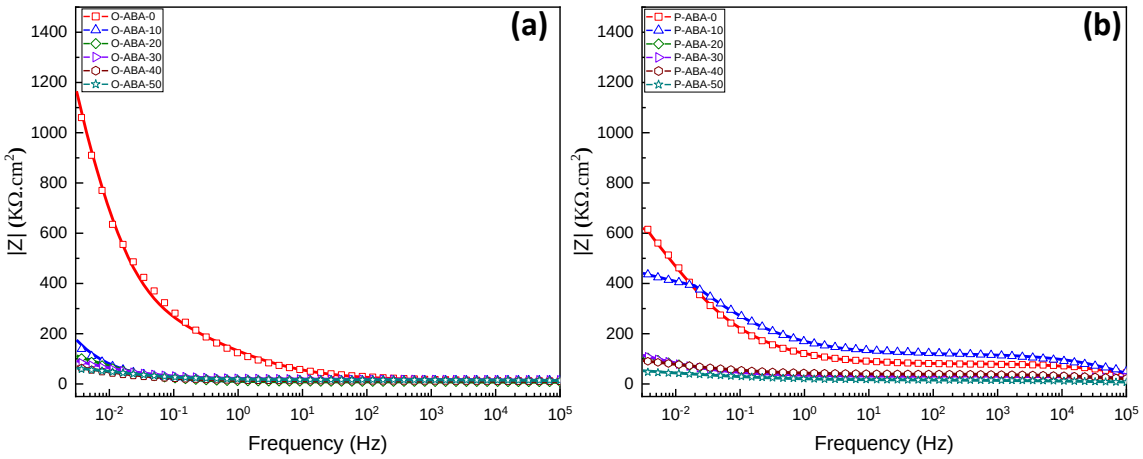

(a) OPC based concrete system **(b) PPC based concrete system**

Fig. 5.22 Bode plot for ABA applied specimens as <u>preventive measure</u>

Bode magnitude plots

Bode magnitude plot shows increase in LF impedance values for both O-ABA and P-ABA as compared to control specimen (shown in Fig. 5.22). The impedance value of O-ABA and P-ABA are observed to be 1550 KΩcm^2 and 650 KΩcm^2 respectively, as compared to the corresponding values of 340 KΩcm^2 in OC and 530 KΩcm^2 in PC. This represents the increase in the charge transfer resistance of embedded rebar by the action of inhibitor. In O-ABA, the concentration of CoI that reached the surface of rebar was possibly more due to its less dense structure as compared to P-ABA hence, the higher impedance. Another prominent feature is the progressive reduction in impedance values with number of exposure cycles. Fig. 5.22 show that LF impedance value of O-ABA decreased abruptly from 1550 KΩcm^2 to 300 KΩcm^2 after 10 exposure cycles. It further indicates that OPC specimens do not offer much hindrance to penetrating species, either inhibitive or corrosive. On the other hand, impedance in P-ABA specimen decreased gradually. The similar behaviour was recorded in the Nyquist plot which is related to the steady dispersion of CoI in P-ABA that reduces the corrosion rate by retarding the diffusion and charge transfer process on the rebar surface. The LF impedance value for O-ABA and P-ABA at the end of 50 exposure cycles were recorded as 50 KΩcm^2 and 52 KΩcm^2, respectively. The recorded values at last testing age are higher than the corresponding values of control specimens, which suggest that application of

inhibitor reduced the charge transfer process and delayed the de-passivation time of the passive film on rebar surface.

Another prominent feature of Bode plot in P-ABA is higher impedance modulus in the intermediate frequency range (i.e., 10 KHz to 10 Hz), even after large number of exposure cycles. This indicates that the inhibitor refined the steel/concrete interface. However, such increase in mid frequency region was absent in case of O-ABA specimen, which might be due to higher porosity of O-ABA that allowed unrestricted percolation of CoI without much refinement of the steel/concrete interface. With continuous exposure, |Z| value at intermediate frequency region for P-ABA increased after 10 cycles of exposure and after that decreased gradually throughout the testing age. This shows the better protection ability of CoI in blended cement concrete due to continuous and gradual diffusion of CoI after application. Similar behavior was also witnessed in HF impedance region of Bode plot. The change in impedance value at HF for O-ABA was negligible; while in P-ABA this value increased after 10 exposure cycles which then decreased with exposure duration. As the inhibitor percolates through the concrete cover gradually and forms a protective film upon reaching the rebar surface, the HF and intermediate frequency ranges are likely to be affected and so was observed in the Bode magnitude plots.

5.7.3.2 EIS spectra for ABA applied specimens as repair measure:

In this set of specimens, CoI was applied after the active corrosion stage was reached and allowed to percolate for 15 days. After 15 days of natural penetration, the specimens were again exposed to corrosive environment and EIS was performed at definite durations. The Nyquist impedance spectra for this set of specimens are shown in Fig. 5.23 and the corresponding Bode magnitude plot are shown in Fig. 5.24.

Nyquist plots

After CoI application, a large increase in diameter of LF arc for both the cement types after 15 days of application was witnessed which is owed to development of some protective layer by ABA over the rebar. From the slope of the capacitive arc, it can also be said that the layer formed in both the cement types is equally adherent. With the continuous cyclic exposure, the diameter of LF capacitive arc kept on decreasing gradually due to the negative effect of the corrosive species. When HF capacitive arc was observed, in O-ABA´, the diameter of HF arc did not show much

change with the exposure cycles, similar to its behavior in O-ABA and control specimens. In P-ABA´, the diameter increased upto 30th exposure cycle after the application of CoI which was further observed to reduce till 50th exposure cycle. Such behavior defines the alteration of concrete matrix by multiple mechanisms (i.e., due to CoI dispersion or due to carbonation) that are happening simultaneously. The prominent mechanism might be the diffusion of CoI with time in P-ABA´. This indicates that the CoI is still getting dispersed in the matrix of PC due to its dense structure; but in OC, the inhibitor reached earlier and the depletion due to the aggressive environment also started occurring early.

Bode magnitude plots

The LF impedance value shifted from 350KΩcm^2 to 75KΩcm^2 and 550KΩcm^2 to 80KΩcm^2 after 10 cycles in O-ABA´ and P-ABA´, respectively (shown in Fig. 5.24). However, on applying CoI, a drastic increase (75 KΩcm^2 to 500 KΩcm^2) was observed in O-ABA' after 15 days of application. Similarly, in P-ABA´ the value increased from 80 KΩcm^2 to 575 KΩcm^2 during the same period. This increase in LF impedance demonstrated that ABA had the ability to effectively delay the corrosion process by increasing the charge transfer resistance of the rebar (Ford et al., 1998; Jamil et al., 2004). The further decrease in LF impedance value indicates the decrease in the resistivity of rebar surface due to continuous aggressive attack of chloride and carbonation. In P-ABA´ the value of LF impedance at the end of the testing duration is 85 KΩcm^2 and for O ABA´ this value was 65 KΩcm^2. These values are 83.6% (for O ABA´) and 74.6% (for P-ABA´) higher as compared to the corresponding control specimens which shows that the inhibitor application reduced the corrosion rate to a good extent. When comparing with the set of specimens in which ABA was applied as preventive measure, these values are 23.07% (for O-ABA´) and 38.82% (for P- ABA´) higher than O-ABA and P-ABA, respectively.

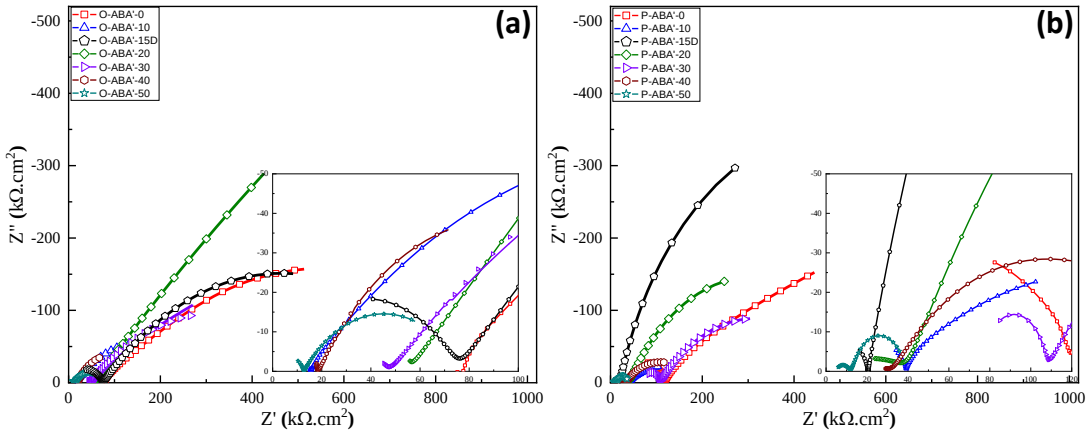

(a) OPC based concrete system **(b) PPC based concrete system**

Fig. 5.23 Nyquist spectra for ABA applied specimens as repair measure

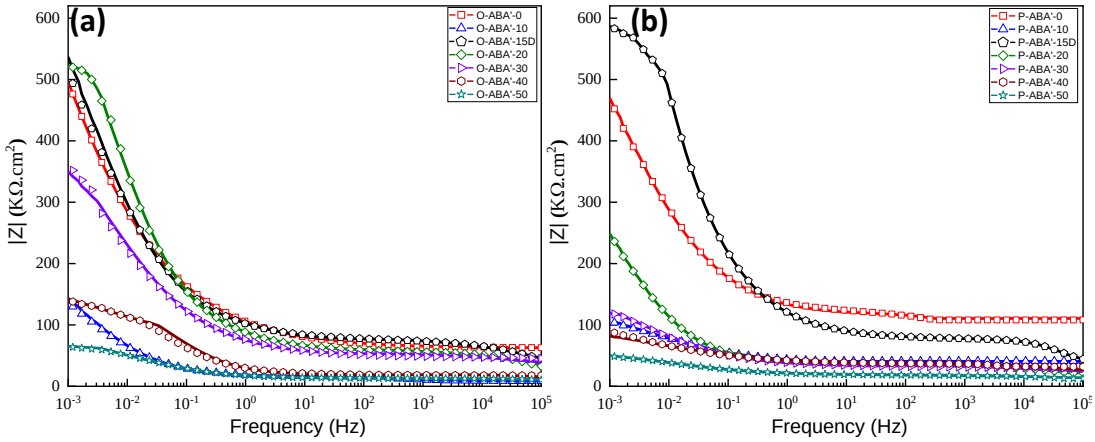

(a) OPC based concrete system **(b) PPC based concrete system**

Fig. 5.24 Bode plot for ABA applied specimens as repair measure

.

The increase in |Z| value at intermediate frequency region indicates that the application of CoI effectively refined the steel/concrete interface. In like manner, increase in HF impedance was recorded after the application of CoI due to alteration in concrete matrix made by ABA during its dispersion through the cover concrete. Thereafter, decrease in HF impedance value was recorded for O- ABA´ after 30th exposure cycle and for P- ABA´ after 40th exposure cycle because of slow dispersion in P- ABA´ as compared to O- ABA´. Thus, from the Nyquist and Bode plot it can be inferred that ABA can be employed as repair strategy as well.

5.7.4 Electrochemical parameters for ABA applied specimens

The electrochemical parameters were obtained by fitting Nyquist and Bode magnitude plots of ABA applied specimens by using Zman view software. The used circuits are described in Section 5.5. EEC1 is applicable to OPC control and inhibitor applied specimens for 0 and 10th exposure cycle and EEC2 is valid for all the other cycles. The EIS fitted parameters for control and inhibitor applied specimens are represented in Table 5.3.

Table 5.3 Resistive parameters obtained from Nyquist spectra for control and ABA applied specimens

Sample	Cycles	Rs (kΩ.cm^2)	Rc (kΩ.cm^2)	Rct (kΩ.cm^2)	Sample	Cycles	Rs (kΩ.cm^2)	Rc (kΩ.cm^2)	Rct (kΩ.cm^2)
OC	0	10.99	-	329.06	PC	0	62.87	354.2	353.46
	10	6.74	-	74.6		10	17.92	143.01	62.48
	20	8.22	7.25	55.34		20	10.35	92.36	52.43
	30	11.45	23.84	33.25		30	3.44	45.13	25.41
	40	9.42	17.22	18.54		40	4.21	25.24	15.66
	50	7.69	10.95	10.29		50	5.17	3.43	5.26
O-ABA	0	12.51	-	1537.5	P-ABA	0	41.21	375	579.04
	10	12.12	-	162.88		10	41.20	190.28	398.81
	20	12.65	8.55	123.45		20	42.25	115.46	245.68
	30	13.39	23.39	78.71		30	44.56	54.26	83.81
	40	12.21	15.22	65.27		40	24.33	35.12	64.11
	50	12.57	13.94	50.55		50	9.04	17.22	45
O-ABA´	0	10.99	-	329.06	P-ABA´	0	62.87	354.2	353.46
	10	6.74	-	74.6		10	17.92	143.01	62.48
	20	44.73	35.43	467.16		20	54.16	95.21	542.84
	30	45.39	12.36	214.61		30	29.41	35.12	90.32
	40	23.25	10.43	113		40	18.24	24.35	63.52
	50	10.41	7.22	43.70		50	12.41	18.57	36.79

The values of R_s and R_c given in Table 5.3 shows declination from initial to final exposure durations for all mixes, which is representative of increase in chloride ions in the concrete matrix. When ABA is applied on concrete initially (O-ABA and P-ABA), no significant change in R_c value

was been recorded in O-ABA due to porous nature of the concrete microstructure; whereas, an increase in the R_c values was observed in the case of inhibitor applied P-ABA which might be due to the slow dispersion of inhibitors in the blended concrete because of its lower porosity. Further, for the repair specimens i.e., O-ABA´ and P-ABA´, no change in Rc was seen that indicates the resistance offered by concrete remains unchanged when ABA is applied after 10 cycles of exposure. On more observation is the significant rise in the R_s values when ABA was applied in repair measure, indicating the modification in pore solution of concrete matrix during percolation. Decrease in pore solution resistance and ion transfer resistance of bulk concrete suggest the formation of different reaction products inside the concrete and presence of highly conductive ion inside the different concrete matrices (i.e., OPC and PPC based control and inhibitor applied specimens).

The resistive parameter obtained after fitting of the LF arc ($R_{ct)}$ is representative of the phenomenon happening at the rebar level and is analyzed to study the changes in the charge transfer mechanism for control and inhibitor applied specimens. It is considered as the most important parameter and has a direct relationship with the corrosion rate. The value R_{ct} decreases when the resistance against the charge transfer decreases, indicating an active state of corrosion. As can be seen from the table, in control specimens R_{ct} decreased (from 329.06 $k\Omega.cm^2$ to 10.29 $k\Omega.cm^2$ for OC and from 353.46 $k\Omega.cm^2$ to 5.26 $k\Omega.cm^2$ for PC) with the increase in exposure duration, which clearly indicates higher corrosion rate. The application of ABA increased R_{ct} value for both the concrete system, indicating its efficiency to act as migratory inhibitor in preventive as well as repair strategy. The rise in R_{ct} values after ABA application in preventive format is 4.67 times for O-ABA and 1.63 times in P-ABA; on the other side in repair format the rise is 6.45 times in O-ABA´ and 3.55 times in P-ABA´. This clearly indicates ABA could perform better in controlling the rate of on-going corrosion than being used as preventive strategy in combined exposure condition. Increase in the R_{ct} values in either form of application conveys that ABA increases the resistance of rebar against corrosion which can be due to combined effect of concentration reached at the rebar level and the chemical bonding that the inhibitor makes with the rebar. These values unveil an important aspect that with inhibitor application PPC concrete turns out to be more corrosion resilient as discussed in the section of EIS spectra of inhibitor applied specimens.

5.7.5 Corrosion rate (CR) from gravimetric weight loss for ABA applied specimens

The corrosion rates of embedded steel rebar obtained from different concrete specimens are reported in Table 5.4. From the table, it can be observed that the steel embedded in OC and PC concrete showed corrosion rates of 0.086 and 0.121 mm/yr, respectively. This shows the severity level is high for steel embedded in fly ash based concrete specimens. Further, the observed values of gravimetric mass loss and corrosion rate show that the application of ABA reduced the corrosion rate irrespective to their application stage. The corrosion rate of O-ABA and P-ABA were 0.069 and 0.104 mm/yr, while for O-ABA´ and P-ABA´ these values were 0.052 and 0.076 mm/yr, respectively. Further, on comparing the CR of preventive and repair measure, it was observed that CR of specimens in preventive measure (i.e., O-ABA and P-ABA) were 24.67% and 26.9% higher than the corresponding values for repair measure. It conveys that 4ABA performed better when used in repair strategy.

Table 5.4 Gravimetric weight loss

Specimen	Mass Loss (%)	CR (mm/year)
OC	1.5	0.086
PC	2.1	0.121
O-ABA	1.23	0.069
O-ABA´	0.92	0.052
P-ABA	1.84	0.104
P-ABA´	1.30	0.076

5.7.6 Surface Inspection (Visual and Optical) of ABA applied specimens

Fig. 5.25 shows the measured crack width of the top exposed surface of RC of different specimens at the end of exposure duration. From the visual inspection it was seen that surface crack was formed throughout the length of the bar in control specimens i.e., OC and PC. The magnified image shows that the width of the crack on the surface of OC is smaller than PC. The average crack width in OC and PC was 0.377 mm and 0.535 mm, respectively. This suggests that the PC specimen undergoes higher stress due to formation of corrosion product in more severe condition as suggested by electrochemical investigation.

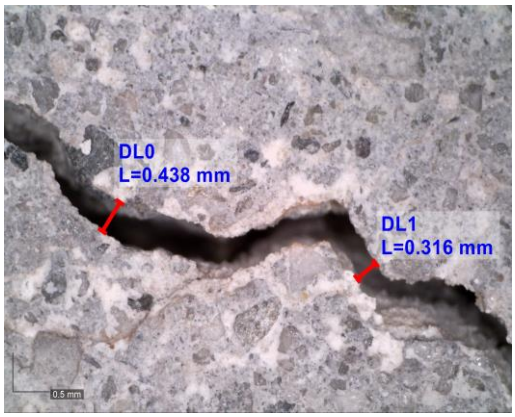

OC

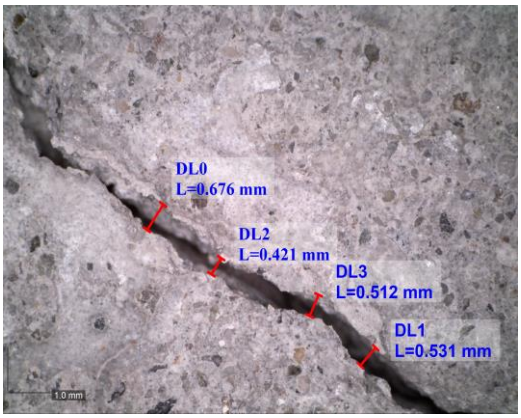

PC

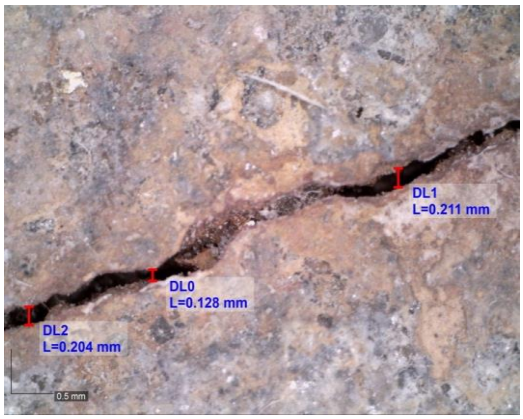

O-ABA

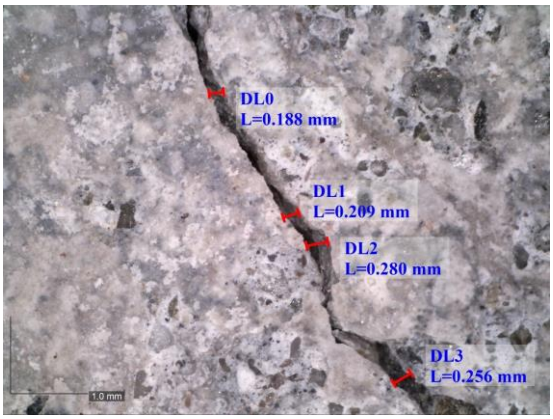

P-ABA

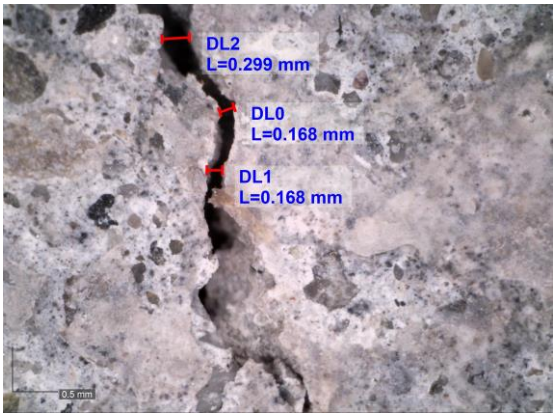

O-ABA´

P-ABA´

Fig. 5.25 Crack width of control and ABA applied specimens

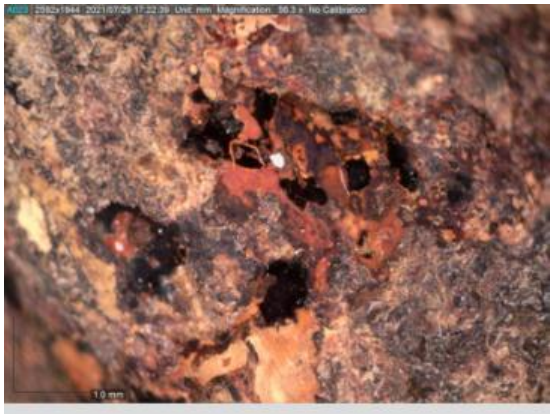

OC

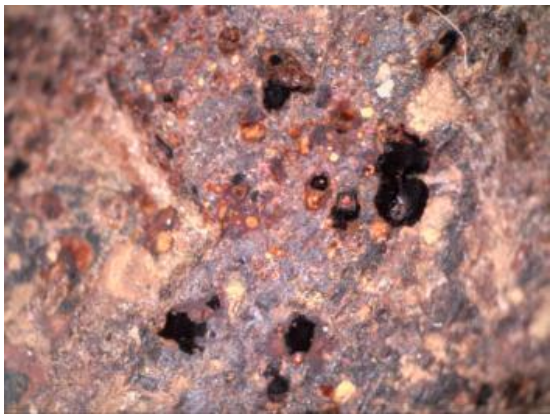

PC

O-ABA

P-ABA

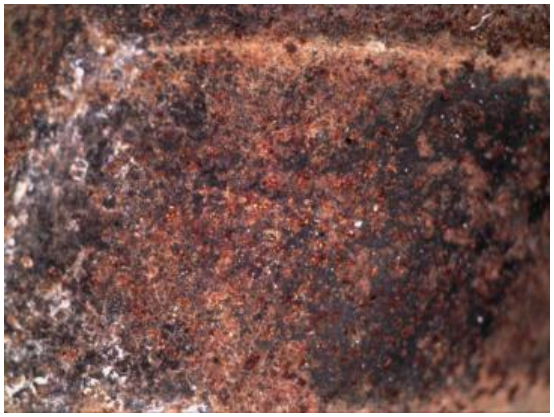

O-ABA´

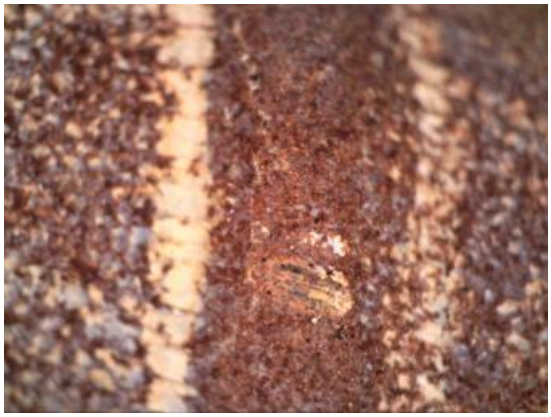

P-ABA´

Fig. 5.26 Magnified image of rebar surface extracted from different specimens at 50x magnification

The average crack width in O-ABA and P-ABA was noted to be 0.217 mm and 0.233 mm, respectively. The average crack width in O-ABA´ was 0.211 mm, while no crack was observed in P-ABA´. This suggests that application of CoI caused reduction in formation of corrosion products on the rebar surface which in turn reduced the expansive stresses in concrete.

The microscopic images of the rebar surface taken at a magnification of 50x are shown in Fig. 5.26. The pits due to chloride attack were visible on the rebar surface of the control specimens, also corrosion products formed on the surface of steel was observed throughout the surface. Similarly, pits were also visible in inhibitor applied specimens, but the size of pits is observed to be smaller than control specimens. This shows the presence of CoI on rebar surface reduces the effect of chloride attack up to some extent, as suggested by electrochemical results.

5.8 RESULTS AND DISCUSSION FOR AP APPLIED SPECIMENS

The various test results of AP applied specimens as preventive and repair measure are discussed in the following sections:

5.8.1. HCP for AP applied specimens

The HCP values of AP applied specimens are shown in Fig. 5.27; in which Fig. 5.27(a) corresponds to the use of inhibitor as preventive measure while Fig. 5.27(b) represents the values for specimens in which inhibitor was applied as a repair measure. In comparison with HCP of control specimens, in which OC and PC shifted to severe corrosion risk zone after 22 and 10 exposure cycles; O-AP and P-AP remained in high-risk zone for most of the testing duration. In O-AP´ and P-AP´ (in which CoI was applied after active stage of corrosion had reached), HCP values showed trend similar to control specimen. HCP indicates that initial CoI application could reduce the corrosion process as indicated by HCP values but unable to reduce the ongoing corrosion process.

Further, where CoI was applied initially before exposing the prisms to corrosive environment as preventive measure (O-AP and P-AP), the passive state of rebar was seen to prolong in both types of concretes. Later, the i_{corr} shifted to active corrosion with 'low to moderate' corrosion zone. Even after 50 exposure cycles, the i_{corr} recorded was 27% (for O-AP) and 46% (for P-2P) lower than the corresponding control specimens, indicating that AP performed efficiently throughout the test exposure. For specimens when CoI was applied after the rebars got de-passivated as repair

measure (O-AP′ and P-AP′), the i_{corr} was seen to be increased at the same rate as recorded in the control specimens. This indicated that the application of AP could not curb the rebar corrosion when it is applied on the surface of concrete with a rebar in active state of corrosion. In other words, AP worked effectively as a preventive measure but could not perform as a repair measure. The results are also in agreement with HCP test.

5.8.2 LPR for AP applied specimens

LPR test was performed to get variation in corrosion current density (i_{corr}) of rebar with continuous cyclic exposures. The obtained results for AP applied specimens are shown in Fig. 5.28 (a) for OPC based systems and Fig. 5.28 (b) for PPC based systems, along with the results of corresponding control specimens. In control specimens exposed to combined environment, i_{corr} values showed that rebar remained in passive region upto the 8th exposure cycle for both OC and PC specimens. After 10th cycle, both OC and PC entered 'low to moderate' corrosion region. Further OC specimen took 32 exposure cycles to shift from 'moderate to high corrosion rate', while PC recorded the same shift after 28th exposure cycle. Also, at all exposure durations, PC specimens registered higher corrosion rate than OC specimen; clearly indicating more severe corrosion in PPC concrete under combined exposure of chlorides and carbonation.

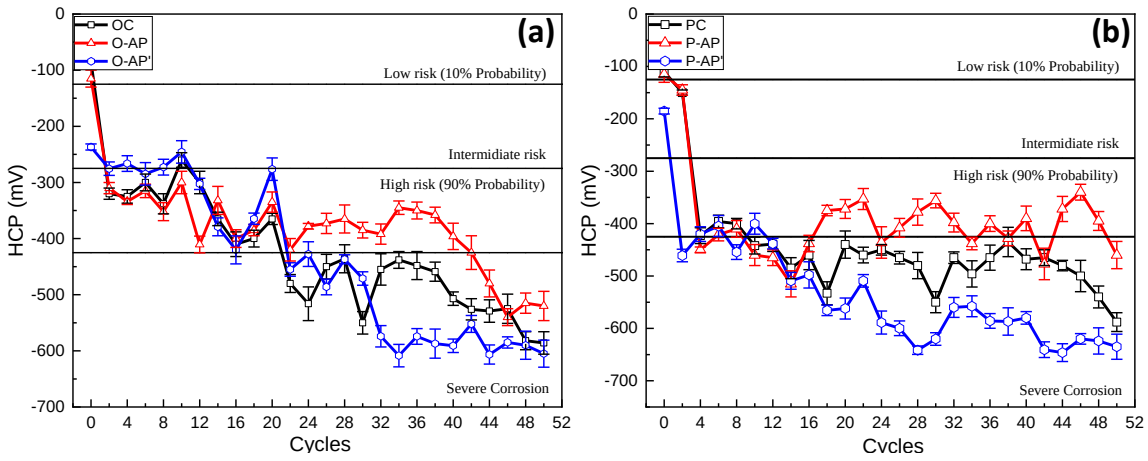

(a) OPC based concrete system **(b)** PPC based concrete system

Fig. 5.27 Variation in half-cell potential with exposure duration for control and AP applied specimens

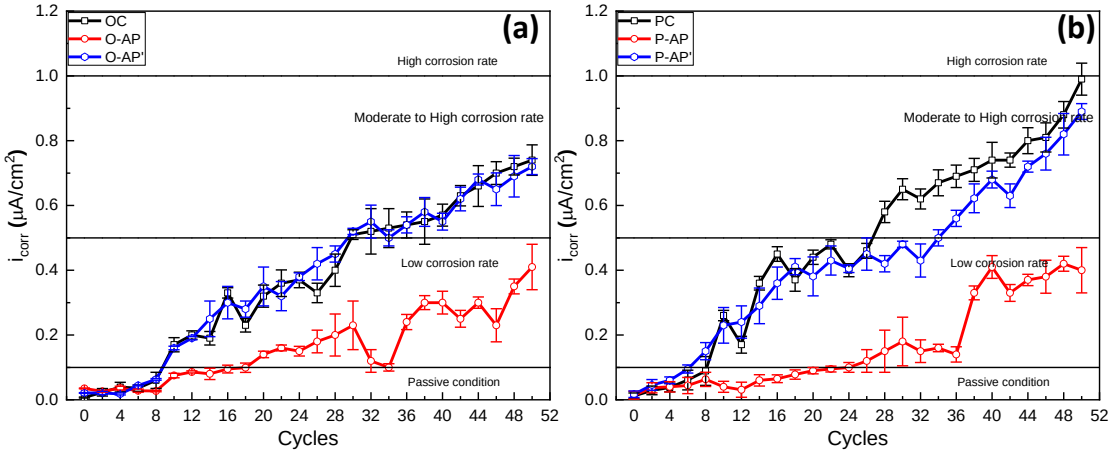

(a) OPC based concrete system **(b)** PPC based concrete system

Fig. 5.28 Variation in corrosion current density with exposure duration for control and AP applied specimens

5.8.3 EIS for AP applied specimens

Apart from getting the information regarding rebar corrosion, it is important to understand the progressive changes occurring in the properties of concrete pore structure and at steel/concrete interface. EIS is a useful technique that provides information about concrete pore structure and corrosion mechanism. EIS test was performed after every 10 exposure cycles and represented in the form of Nyquist and Bode magnitude plot. The EIS test results for AP applied specimens are discussed in the following sections:

5.8.3.1. EIS spectra for AP applied specimens as preventive measure:

In this set of specimens, CoI was applied before exposure to aggressive environment and was allowed to percolate naturally for 15 days before exposure. After 15 days, EIS test was performed as reference and the specimens were then exposed to corrosive environment.

Nyquist plots

The Nyquist impedance spectra for this set of specimens are shown in Fig. 5.29. In CoI applied specimens, there was three-fold (from 150 KΩcm^2 to 450 KΩcm^2) increase in diameter of low frequency arc in O-AP as compared to the corresponding control; while approximate two-fold

(from 150 KΩcm^2 to 250 KΩcm^2) increase was witnessed in P-AP. This is associated with the formation of better protective layer by the inhibitor over steel surface. The higher increase in LF arc of O-AP specimen as compared to P-2AP is associated with the initial pore structure of the concrete. Blended cement concrete is reported to have denser pore structure, because of which the diffusion of the CoI was slow and steady with the continuous alteration of pore matrix. Unlike this, OPC based concrete is less dense thus, allowing the CoI to migrate easily. With the continuous exposure, the LF capacitive arc kept on decreasing which indicates the breakdown of passive layer as observed in case of control specimens (shown in Figs. 5.29 (a) & (b)). On comparing the LF arc of control and CoI-applied specimens after 50 exposure cycles, it was observed that the diameter of LF arc of AP applied specimens was higher than the corresponding control. This suggests that even at the end of testing duration, AP applied specimens have better resistivity against the corrosive species.

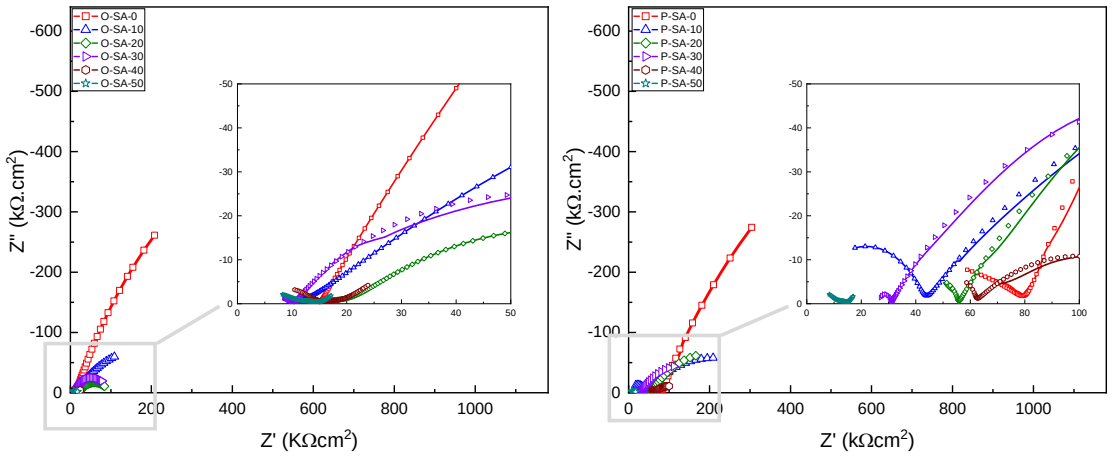

(a) OPC based concrete system **(b)** PPC based concrete system

Fig. 5.29 Nyquist spectra for AP applied specimens at 0, 10, 20, 30, 40 and 50 exposure cycle as <u>preventive measure</u>

When HF region is observed, capacitive arc was absent initially in both O-AP and P-AP. It indicates that AP was not acting as pore blocker and got dispersed easily into concrete to reach the rebar surface. As the corrosive exposure is continued, a small increase in diameter of HF arc was observed in both specimens. It can be due to densification of concrete matrix due to precipitation of $CaCO_3$ upon exposure to CO_2 environment. However, in P-2AP an abrupt rise in diameter of HF arc was observed typically after the 10th cycle due to some kind of blockage offered by the

refined pore matrix of PPC based concrete, Cl^- ions and calcium carbonate precipitates. This arc was again noticed to decrease with the continuous exposure cycle. The decrease in HF arc can be attributed to the movement of accumulated Cl^- ions due to carbonation of concrete. Similar to the control specimens, the Nyquist spectra of P-AP shifted towards left due to highly conductive chloride ions.

Bode magnitude plots

Bode magnitude plot (Fig. 5.30) shows increase in LF impedance values for AP applied specimens as compared to the corresponding control. The impedance values of O-AP and P-AP were 490 $K\Omega cm^2$ and 502 $K\Omega cm^2$ respectively as compared to the corresponding values of 340 $K\Omega cm^2$ and 420 $K\Omega cm^2$ of OC and PC. This represents an increase in charge transfer resistance of embedded rebar by the action of inhibitor. Another prominent feature is the progressive reduction in impedance values with number of exposure cycles. Fig. 5.30 (a) show that LF impedance value of O-AP decreased abruptly from 490 $K\Omega cm^2$ to 120 $K\Omega cm^2$ after 10 exposure cycles. It further indicates that OPC based specimens do not offer much hindrance to penetrating species, either inhibitive or corrosive. On the other hand, impedance in P-AP specimen decreased gradually (502 $K\Omega cm^2$ to 195 $K\Omega cm^2$) as shown in Fig. 5.30 (b). The similar behavior was recorded in the Nyquist plot which is related to the steady dispersion of CoI in P-AP that reduced the corrosion rate by retarding the diffusion and charge transfer process on the rebar surface. The LF impedance value for O-AP and P-AP at the end of 50 exposure cycles were recorded as 26.8 $K\Omega cm^2$ and 35.7 $K\Omega cm^2$, respectively which is 1.24 and 25.08 times higher than the corresponding values for control specimens. Further, it was observed that efficiency of 2AP was lower in OPC concrete than PPC concrete at the end of testing age due to easy percolation of corrosive species. Similar observation was made by ABA application as preventive measure. In comparison to ABA, efficiency of AP seems to be lower than ABA application when used as preventive measure. This might be due to the reason that, ABA percolate with much higher diffusion rate and reached at rebar level with significantly higher amount than of AP.

In the intermediate frequency range, |Z| values are seen to decrease for AP applied specimens at all testing durations. The continuous reduction in impedance modulus is attributed to the continuous destruction of passive film at steel/concrete interface due to aggressive ion attack.

Similarly, reduction in HF impedance was noticed in P-AP and O-AP due to attack of highly conductive chloride ion.

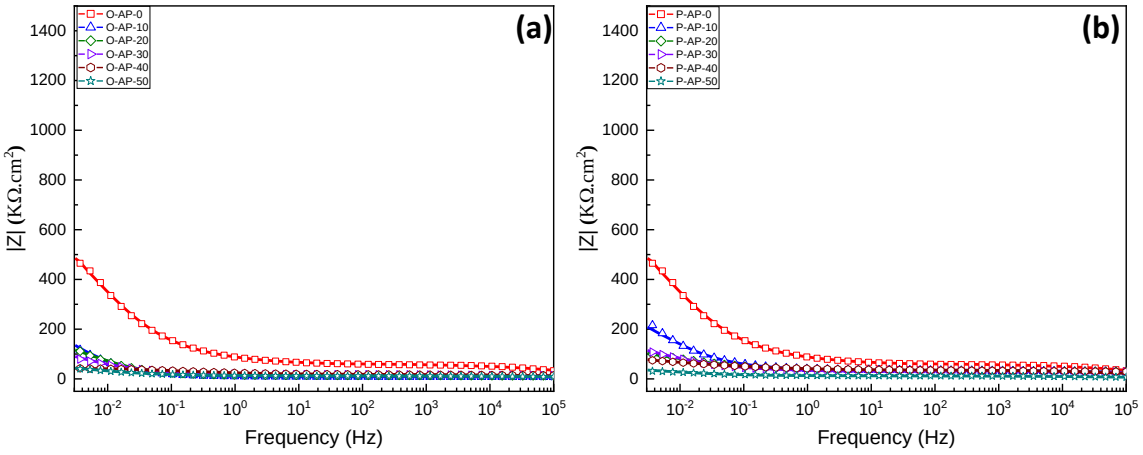

(a) OPC based concrete system **(b) PPC based concrete system**

Fig. 5.30 Bode magnitude plot for AP applied specimens at 0, 10, 20, 30, 40 and 50 exposure cycle as <u>preventive measure</u>

The EIS plot suggest that AP started showing its inhibition effect just after the application. This can be explained by the basic inhibition mechanism of AP which is related to the formation of lewis-base-acid type bond between electron acceptor (metal) and electron donor (inhibitor)(Tiwari et al., 2021).

5.8.3.2. EIS spectra for AP applied specimens as repair measure

In this set of specimens, AP was applied after the active corrosion stage had been reached and was allowed to percolate for 15 days. After 15 days of natural penetration, the specimens were again exposed to corrosive environment and EIS was performed at definite durations.

Nyquist plots

The Nyquist impedance spectra for this set of specimens are shown in Fig. 5.31. After the inhibitor application, no significant increase in diameter of LF arc for both the cement types at 20th cycle were witnessed which indicated the ineffectiveness of AP in preventing corrosion. With the continuous cyclic exposure, the diameter of LF capacitive arc kept on decreasing gradually due to the negative effect of the corrosive species. When HF capacitive loop was observed, in O-AP′, the diameter of HF arc had similar behavior as observed in O-AP and OC specimens. In P-AP′, the

diameter of HF arc was more than the corresponding diameter in PC. It can be attributed to the dispersion of AP through the concrete matrix. The diameter of HF arc reduced with increase in exposure cycles.

Bode magnitude plot

In Bode magnitude plot (shown in Fig. 5.32), the LF impedance value shifted from 343 KΩcm^2 to 152 KΩcm^2 (O-AP′) and 425 KΩcm^2 to 75 KΩcm^2 (P-AP′) after 10 cycles. On applying AP, no significant change in LF impedance value was witnessed after 20 exposure cycles in both concrete systems. This suggests that AP failed to increase the charge transfer resistance of rebar against ongoing corrosion activity. The further decrease in LF impedance value indicates the decrease in resistivity of rebar surface due to continuous aggressive attack of chloride and carbonation. In O-AP′ the value of LF impedance at the end of the testing duration was 20.28 KΩcm^2 and for P-AP′ this value was 18 KΩcm^2. The value in O-AP′ was very much like the value of control specimens after 50 exposure cycles that defines the ineffectiveness of AP in OPC. While in P-AP′, a value was slightly higher than PC which can be attributed to steady dispersion of AP as witnessed in P-AP specimens.

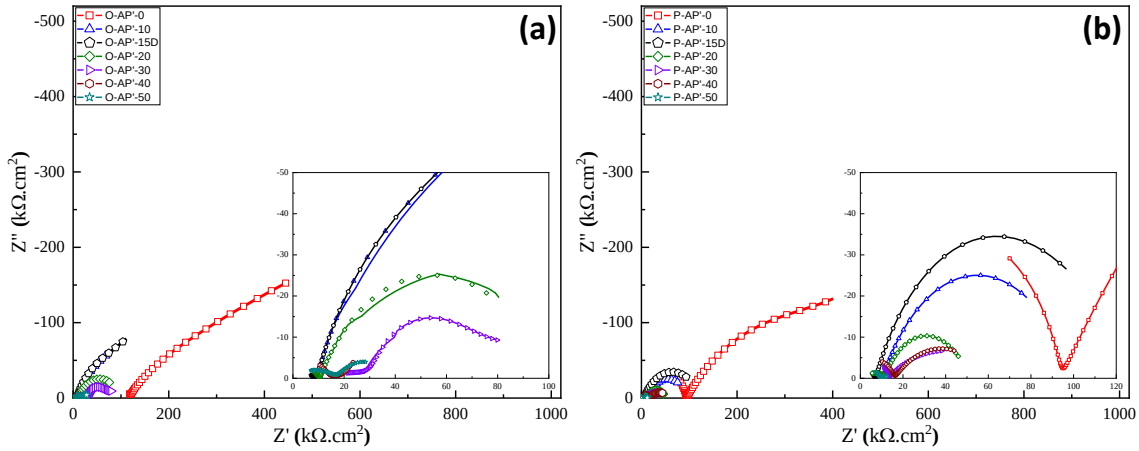

(a) OPC based concrete system **(b)** PPC based concrete system

Fig. 5.31 Nyquist spectra for AP applied specimens at 0, 10, 20, 30, 40 and 50 exposure cycle as repair measure

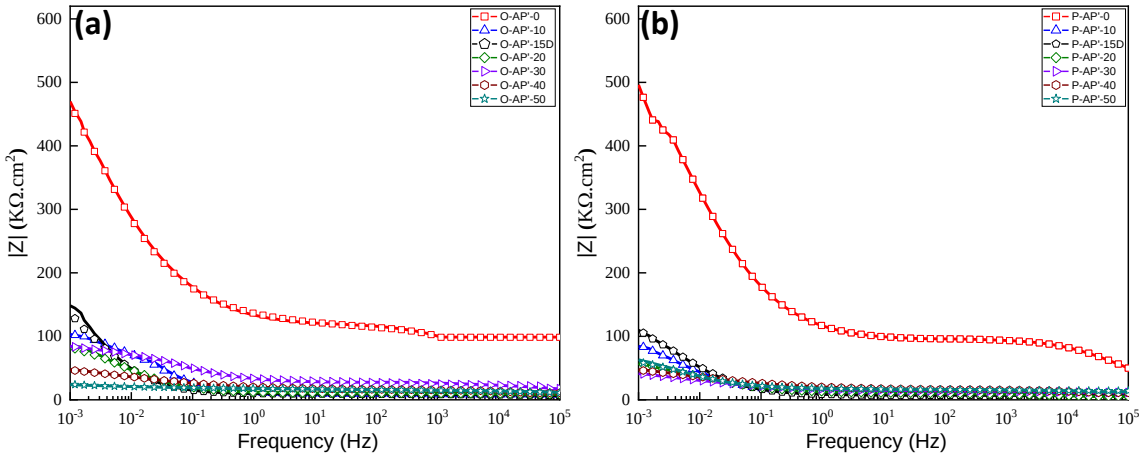

Fig. 5.32 Bode magnitude plot for AP applied specimens at 0, 10, 20, 30, 40 and 50 exposure cycle as repair measure; (a) OPC based (b) PPC based

In the intermediate frequency range, |Z| values were seen to decrease for specimens as repair measure at all testing durations, with an exception at 30th exposure cycle in O-AP´ which might be due to the precipitation of corrosion products and $CaCO_3$ at the steel-concrete interface. In like manner, increase in HF impedance was recorded after the application of AP due to alteration made by calcite precipitation in concrete matrix of O-AP´. While in P-AP´, the |Z| values at HF region decreased with continuous cyclic exposure. The above recorded data shows that AP was not effective in reducing the corrosion rate in OPC and PPC based concrete after the activation of corrosion process.

It can be concluded that in specimens where AP was applied after the corrosion had been initiated, the corrosion products formed on the rebar surface hindered the inhibition mechanism by not allowing the bond formation. Thus, from the Nyquist and Bode plot it can be inferred that application of 2AP failed to inhibit the ongoing corrosion mechanism and become ineffective when used as repair strategy.

5.8.4 Electrochemical parameters for AP applied specimens

The electrochemical parameters were obtained by fitting Nyquist and Bode magnitude plots of ABA applied specimens by using Zman view software. The used circuits are described in Section 5.5. EEC1 is applicable to OPC control and inhibitor applied specimens for 0 and 10th exposure

cycle and EEC2 is valid for all the other cycles. The EIS fitted parameters for control and inhibitor applied specimens are represented in Table 5.5.

The values of R_s and R_c given in Table 5.5 shows declination from initial to final exposure durations for all mixes, which is representative of increase in chloride ions in the concrete matrix. When AP is applied on concrete initially (O-AP and P-AP), no significant change in R_c value was recorded in both concrete systems. Further, for the repair specimens i.e., O-AP´ and P-AP´, no change in Rc was seen that indicates the resistance offered by concrete remains unchanged when AP is applied after 10 cycles of exposure. Decrease in pore solution resistance and ion transfer resistance of bulk concrete suggest the formation of different reaction products inside the concrete and presence of highly conductive ion inside the different concrete matrices (i.e., OPC and PPC based control and inhibitor applied specimens).

While comparing the value of charge transfer resistance in control specimens R_{ct} decreased (from 329.06 kΩ.cm^2 to 10.29 kΩ.cm^2 for OC and from 353.46 kΩ.cm^2 to 5.26 kΩ.cm^2 for PC) with the increase in exposure duration, which clearly indicates higher corrosion rate. The application of AP increased R_{ct} value for both the concrete system, indicating its efficiency to act as migratory inhibitor in preventive strategy. The rise in R_{ct} values after AP application in preventive format is 1.47 times for O-AP and 1.27 times in P-AP; on the other side in repair format the rise is not that much significant in both concrete systems. This clearly indicates AP could not be able to perform in controlling the rate of on-going corrosion. Decrease in the R_{ct} values further indicates that once the corrosion got initiated, ability of AP forming chelate with Fe ions reduces which in turn, eliminates its efficiency in combined environment.

Table 5.5 Resistive parameters obtained from Nyquist spectra for control and AP applied specimens

Sample	Cycles	Rs (kΩ.cm^2)	Rc (kΩ.cm^2)	Rct (kΩ.cm^2)	Sample	Cycles	Rs (kΩ.cm^2)	Rc (kΩ.cm^2)	Rct (kΩ.cm^2)
OC	0	10.99	-	329.06	PC	0	62.87	354.2	353.46
	10	6.74	-	74.6		10	17.92	143.01	62.48
	20	8.22	7.25	55.34		20	10.35	92.36	52.43
	30	11.45	23.84	33.25		30	3.44	45.13	25.41
	40	9.42	17.22	18.54		40	4.21	25.24	15.66
	50	7.69	10.95	10.29		50	5.17	3.43	5.26
O-AP	0	12.38	-	472.5	P-AP	0	34	360	450.56
	10	6.62	-	128.28		10	25.66	146.25	182.6
	20	7.45	13.22	98.33		20	23.24	82.54	135.85
	30	11.12	25.24	78.97		30	24.65	49.11	89.40
	40	10.21	14.28	57.77		40	12.16	25.34	45.95
	50	8.58	7.84	33.13		50	6.86	12.25	28.86
O-AP´	0	10.99	-	329.06	P-AP´	0	62.87	354.2	353.46
	10	6.44	-	72.2		10	17.92	143.01	62.48
	20	7.16	28.86	89.33		20	5.87	106.64	73.77
	30	6.25	21.36	74.22		30	6.24	65.32	53.25
	40	7.22	10.74	34.36		40	6.77	38.95	24.66
	50	7.36	8.49	17.75		50	5.49	18.578	4.92

5.8.5 Corrosion Rate (CR) by gravimetric weight loss method for AP applied specimens

The embedded steel rebars were extracted from different prism specimens and the corrosion rate was calculated from gravimetric mass loss values. The results are reported in Table 5.6. From the table, it can be observed that the steel embedded in OPC and PPC showed a corrosion rate of 0.086 and 0.121 mm/yr, respectively. The corrosion rate of O-AP and P-AP were 0.069 and 0.104 mm/yr, while for O-AP´ and P-AP´ these values were 0.0868 and 0.120 mm/yr, respectively. Further, on comparing the CR of AP applied specimens as preventive and repair measure, it was observed that CR of O-AP and P-AP were 25.7% and 15.3% higher than the corresponding

specimens of repair measure. It conveys that AP performed better when used as preventive measure.

Table 5.6 Gravimetric mass loss of control and AP applied specimens

Cement type	Specimen	Mass Loss (%)	CR (mm/year)	Cement type	Specimen	Mass Loss (%)	CR (mm/year)
OPC	OC	1.5	0.087	PPC	PC	2.1	0.121
	O-AP	1.24	0.069		P-AP	1.84	0.104
	O-AP´	1.48	0.0868		P-AP´	1.98	0.120

5.8.6 Surface Inspection (Visual and Optical) of AP applied specimens

Fig. 5.33 shows the magnified image of the top exposed surface of reinforced concrete of different specimens at the end of exposure duration. From the visual inspection it was seen that surface crack was formed throughout the length of the bar in control specimens i.e., OC and PC.

The average crack width in OC and PC was 0.377 mm and 0.535 mm, respectively. While comparing with the inhibitor applied specimen, it was observed that the cracks formed on O-AP and P-AP had a smaller width than the corresponding control specimens. The average crack width in O-AP and P-AP are 0.181 mm and 0.268 mm, respectively. Also, crack width on surface of O-AP´ was 0.331 mm, which is almost similar to the corresponding control specimen; while the crack width measured on P-AP´ ((i.e., 0.35 mm) was smaller than PC. The crack widths suggest that the application of AP worked effectively as a preventive measure by reducing the formation of corrosion products on the rebar surface, thereby causing lesser expensive stresses in concrete. However, AP failed to restrict the ongoing corrosion process in a repair measure.

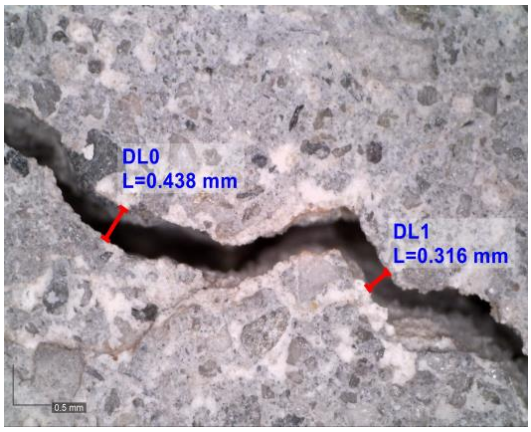

OC

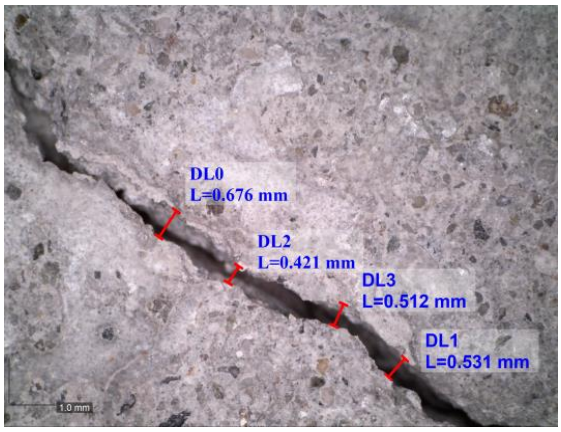

PC

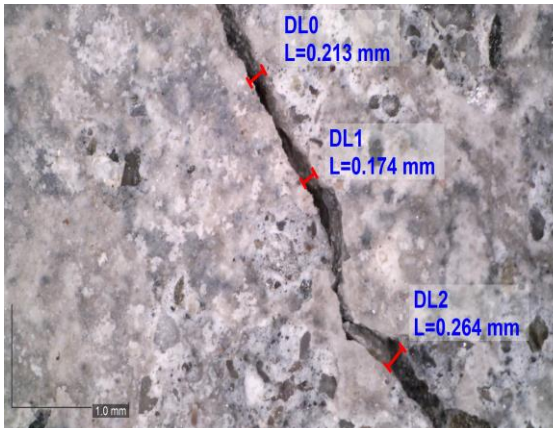

O-AP

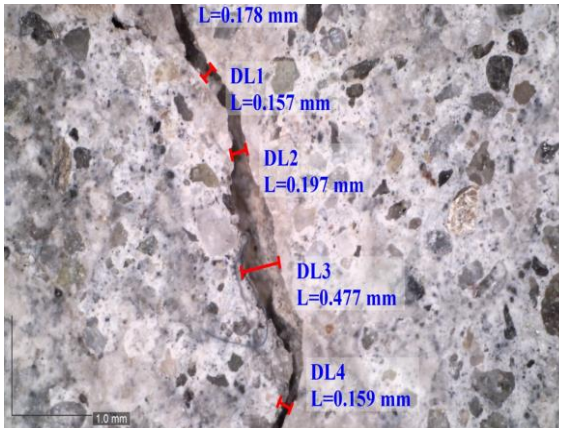

P-AP

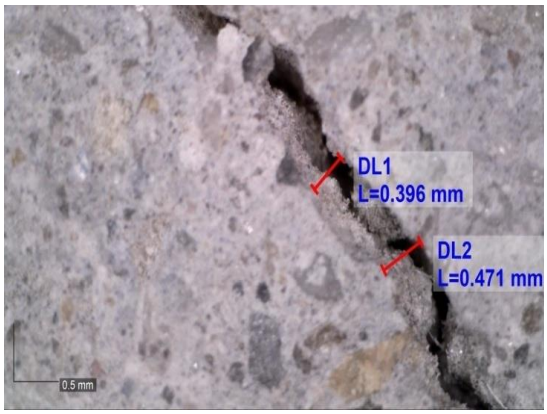

O-AP´

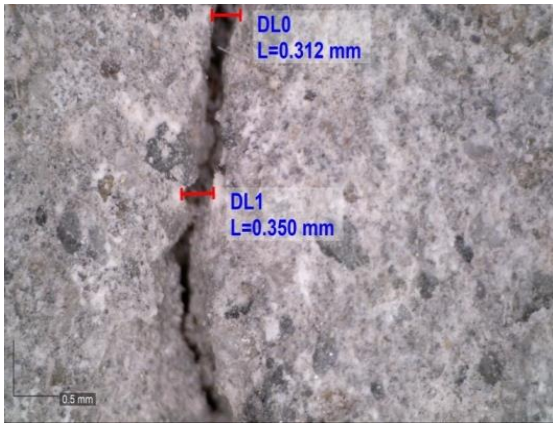

P-AP´

Fig. 5.33 Crack width of control and AP applied specimens

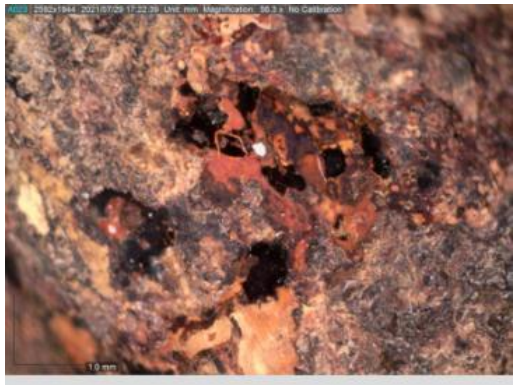

OC

PC

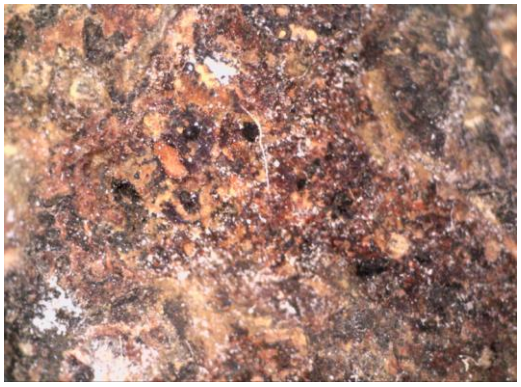

O-AP

P-AP

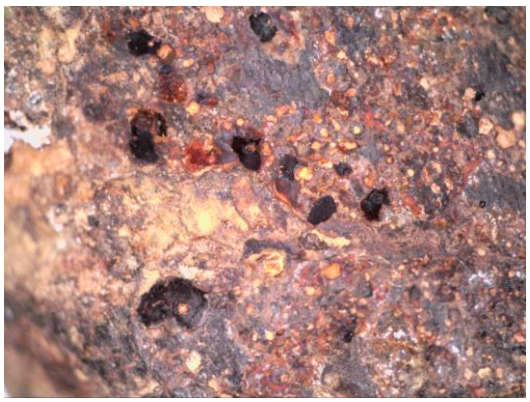

O-AP′

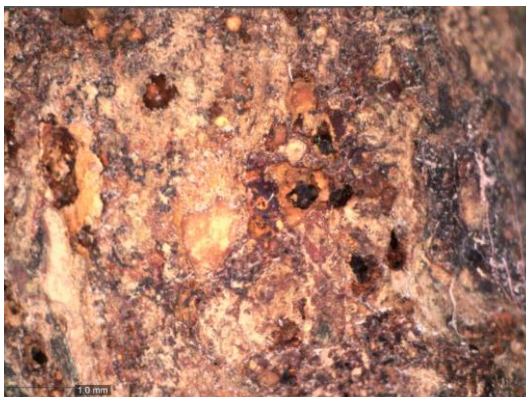

P-AP′

Fig. 5.34 Magnified image of rebar surface extracted from different specimens at 50x magnification.

The microscopic images (taken at a magnification of 50x) of the rebar surface taken after extracting it from the prism specimens at the end of exposure are shown in Fig. 5.34. In control specimens, corrosion pits were visible on the rebar surface along with some corrosion products all along the steel surface. It clearly showed the severity of combined aggressive exposure. The

application of AP as a preventive measure reduced the corrosion activity in both cement systems, as indicated by lesser amount of corrosion pits and a cleaner rebar surface. However, application of AP as repair measure could not arrest the ongoing corrosion activity as was visible from the surface condition of O-AP′ and P-AP′ specimens.

5.9 RESULTS AND DISCUSSION FOR SA APPLIED SPECIMENS

The various test results of SA applied specimens as preventive and repair measure are discussed in the following sections:

5.9.1 HCP for SA applied specimens

The HCP values of inhibitor applied specimens are shown in Fig. 5.35; in which Fig. 5.35a represents data OPC system; while Fig. 5.35b represents data for PPC based system in which SA was applied before corrosion initiation and after the rebar has reached active state of corrosion. In comparison with HCP of control specimens, it can be noted that SA applied specimen shows almost similar values irrespective to their application age in both concrete systems. At the end of testing age, potential values both preventive and repair application of SA shifted to sever corrosion zone. This is the indication that SA does not able to combat the corrosion process in any of the concrete system.

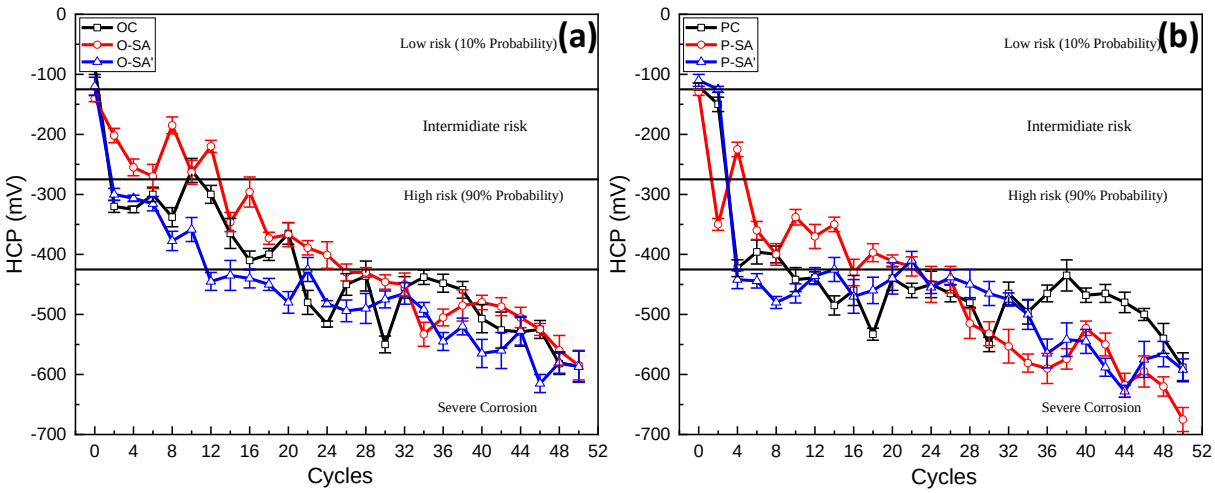

(a) OPC based concrete system **(b)** PPC based concrete system

Fig. 5.35 Variation in half-cell potential with exposure duration for control and SA applied specimens

5.9.2 LPR for SA applied specimens

LPR test was performed to get variation in corrosion current density (i_{corr}) of rebar with continuous cyclic exposures. The obtained results for SA applied specimens are shown in Fig. 5.36 (a) for OPC based systems and Fig. 5.36 (b) for PPC based systems, along with the results of corresponding control specimens.

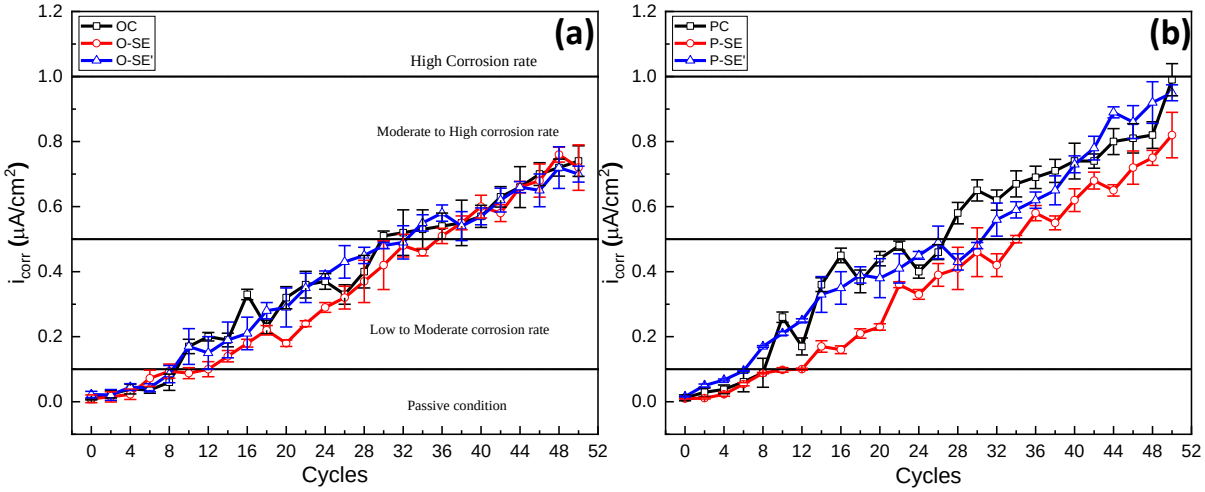

(a) OPC based concrete system **(b)** PPC based concrete system

Fig. 5.36 Variation in corrosion current density with exposure duration for control and SA applied specimens

On comparing the i_{corr} values of inhibitor applied specimen with corresponding control specimen, it was observed that application of SA, either preventive or repair strategy, not able to reduce the corrosion phenomena in any of the concrete system. The increase trend in inhibitor applied specimen is like that of control specimen in both OPC and PPC concrete system. In other words, SA become ineffective weather used as a preventive measure or as a repair measure. The results are also in agreement with HCP test.

5.9.3 EIS for SA applied specimens

Apart from getting the information regarding rebar corrosion, it is important to understand the progressive changes occurring in the properties of concrete pore structure and at steel/concrete interface. EIS is a useful technique that provides information about concrete pore structure and corrosion mechanism. EIS test was performed after every 10 exposure cycles and represented in

the form of Nyquist and Bode magnitude plot. The EIS test results for SA applied specimens are discussed in the following sections:

5.9.3.1. EIS spectra for SA applied specimens as preventive measure:

In this set of specimens, CoI was applied before exposure to aggressive environment and was allowed to percolate naturally for 15 days before exposure. After 15 days, EIS test was performed as reference and the specimens were then exposed to corrosive environment.

Nyquist plots

The Nyquist impedance spectra for this set of specimens are shown in Fig. 5.37 and 5.38. In inhibitor applied specimens, there was increase in diameter of LF arc of O-SA and P-SA, respectively, as compared to control specimens. This is associated with the formation of better protective layer by the inhibitor over steel surface. On comparing the performance of SA in both OPC and PPC, it can be seen that the diameter and slope of LF arc in O-SA is similar to P-SA that suggests that the layer formed on both cement type is equally adherent. With the continuous exposure, the LF capacitive arc kept on decreasing which indicates the breakdown of passive layer as observed in case of control specimens (shown in Fig 5.37(a) & (b)). Another prominent feature that was witnessed was the decrement rate of the diameter of LF arc in O-SA and P-SA. The diameter decreases at the same rate in both the specimen that shows the rebar losing its passivity in OPC and PPC specimen in similar manner.

On comparing the LF arc of control and inhibitor applied specimen after 50 exposure cycle it was observed that the diameter of LF arc of SA applied specimen completely diminished similar to that obtained in control specimens. When a high frequency region is observed, HF capacitive arc is absent in O-SA that can be due to presence of pores. However, in P-SA, diameter of HF arc decreases in similar manner as observed in PC specimen and the Nyquist spectra shifted towards left due to highly conductive chloride ions.

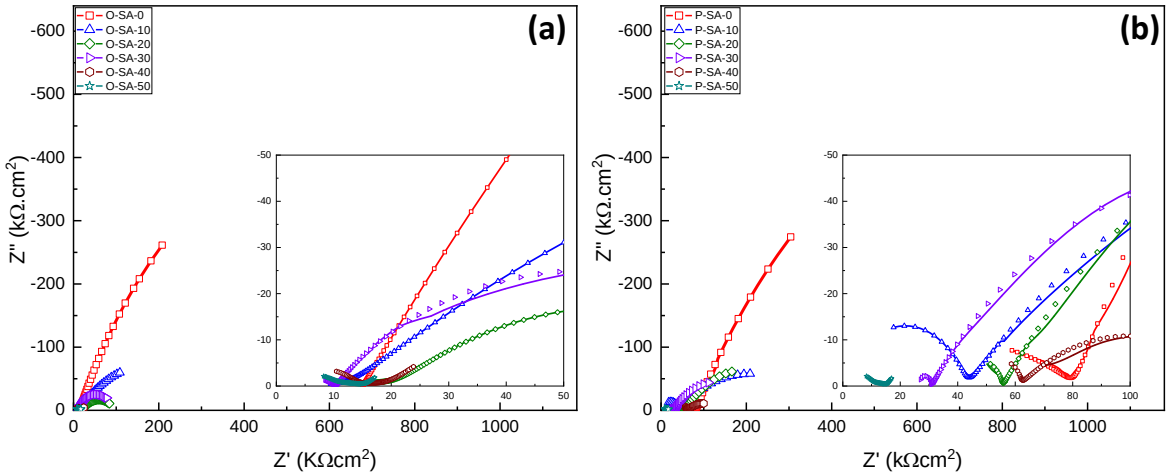

(a) OPC based concrete system **(b)** PPC based concrete system

Fig. 5.37 Nyquist spectra for SA applied specimens at 0, 10, 20, 30, 40 and 50 exposure cycle as <u>preventive measure</u>

Bode magnitude plot

In Bode magnitude plot (shown in Fig. 5.38), increase in LF impedance values for O-SA and P-SA as compared to OC and PC specimen was witnessed after the application. The impedance value of O-SA and P-SA was 450 KΩcm^2 and 490 KΩcm^2 respectively as compared to the corresponding values of 340 KΩcm^2 and 420 KΩcm^2. This represents the increase in the charge transfer resistance of embedded rebar in specimens by the action of inhibitor. Another prominent feature that was observed are the progressive reduction in impedance values with number of exposure cycles. Figure 5.38 show that LF impedance value of O-SA decreased abruptly from 450 KΩcm^2 to 120 KΩcm^2 after 10 exposure cycles. It further indicates that OPC based specimens do not offer much hindrance to penetrating species. On the other hand, impedance in P-SA specimen decreased gradually (490 KΩcm^2 to 210 KΩcm^2). The LF impedance value for O-SA and P-SA at the end of 50 exposure cycles were recorded as 16.31 KΩcm^2 and 26.4 KΩcm^2, respectively. The recorded value in both concrete systems suggests that the SA failed to inhibit in highly corrosive environment and long-term exposure. Similarly, while comparing its performance as repair material, no significant improvement was observed after SA application. The represented Nyquist and Bode plot suggest that CoI application in OPC based specimen seems to be effective initially as it does not restrict the movement of CoI and allows it to reach at steel-concrete interface in short duration, but also unrestricted movement of aggressive ions destroy this protective layer early.

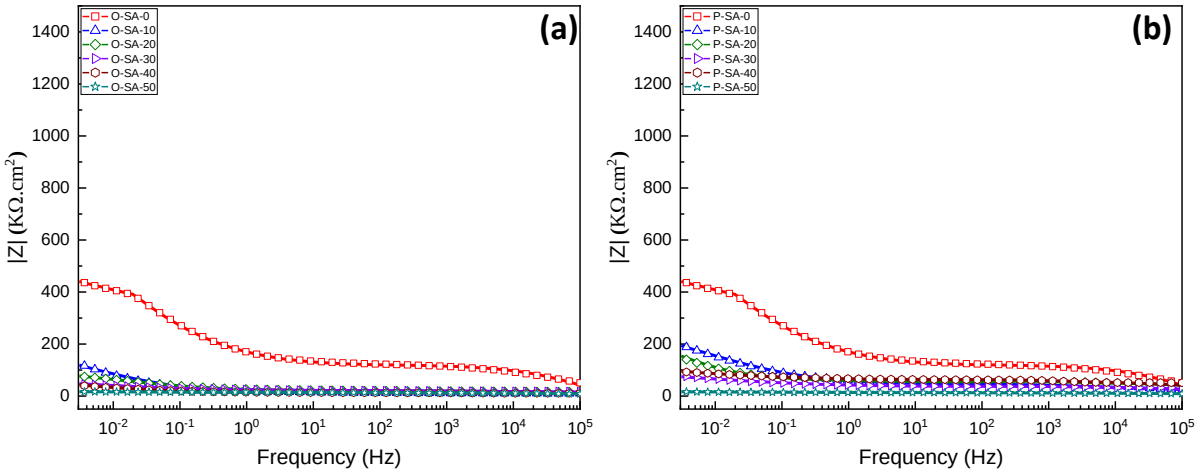

(a) OPC based concrete system **(b)** PPC based concrete system

Fig. 5.38 Bode plot for SA applied specimens at 0, 10, 20, 30, 40 and 50 exposure cycle as preventive measure

5.9.3.2. EIS spectra for SA applied specimens as repair measure:

In this set of specimens, SA was applied after the active corrosion stage had been reached and was allowed to percolate for 15 days. After 15 days of natural penetration, the specimens were again exposed to corrosive environment and EIS was performed at definite durations.

Nyquist Plots

The obtained Nyquist plots for this set is shown in Fig. 5.39. From the Figure, it is seen that application of SA does not cause any significant changes in LF arc. This means application of SA does not have any beneficial effect against combined rate of corrosion. Also, no modification in HF arc was witness at any testing age. Similar to control specimen, decrease in LF arc suggests the severe attack of corrosive ions on the rebar surface. At the end of testing age, the LF arc completely diminishes signifies the inefficient performance of SA as repair material.

Bode magnitude plot

Similar observation was also made by Bode magnitude plots. Initial passivity decreased with the introduction of corrosive ions. After SA application, no significant improvement is impedance value was observed. Continuous decrease in impedance value suggests that application of SA does

not able to cause any positive impact on the reduction of corrosion rate. Results obtained are in agreement with HCP and LPR observations.

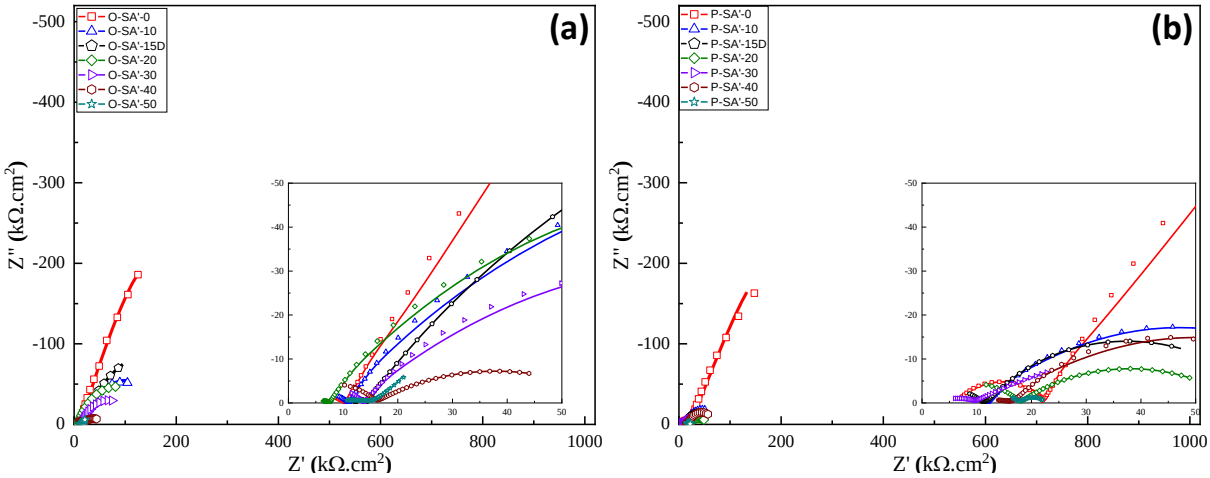

(a) OPC based concrete system **(b)** PPC based concrete system

Fig. 5.39 Nyquist spectra for SA applied specimens at 0, 10, 20, 30, 40 and 50 exposure cycle as <u>preventive measure</u>

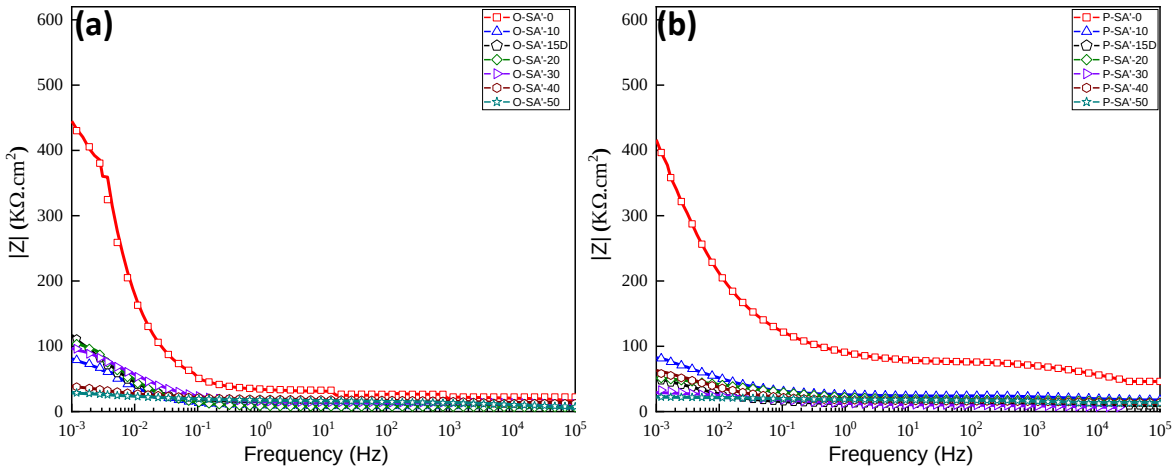

(a) OPC based concrete system **(b)** PPC based concrete system

Fig. 5.40 Bode plot for SA applied specimens at 0, 10, 20, 30, 40 and 50 exposure cycle as <u>preventive measure</u>

5.9.4 Electrochemical parameters for SA applied specimens

The electrochemical parameters were obtained by fitting Nyquist and Bode magnitude plots of ABA applied specimens by using Zman view software. The used circuits are described in Section 5.5. EEC1 is applicable to OPC control and inhibitor applied specimens for 0 and 10th

exposure cycle and EEC2 is valid for all the other cycles. The EIS fitted parameters for control and inhibitor applied specimens are represented in Table 5.7.

The values of R_s and R_c given in Table 5.7 shows declination from initial to final exposure durations for all mixes, which is representative of increase in chloride ions in the concrete matrix. When SA is applied on concrete initially (O-SA and P-SA), no significant change in R_c value was recorded in both concrete systems. Further, for the repair specimens i.e., O-SA´ and P-SA´, no change in Rc was seen that indicates the resistance offered by concrete remains unchanged when AP is applied after 10 cycles of exposure. Decrease in pore solution resistance and ion transfer resistance of bulk concrete suggest the formation of different reaction products inside the concrete and presence of highly conductive ion inside the different concrete matrices (i.e. OPC and PPC based control and inhibitor applied specimens).

While comparing the value of charge transfer resistance in control specimens R_{ct} decreased (from 329.06 kΩ.cm^2 to 10.29 kΩ.cm^2 for OC and from 353.46 kΩ.cm^2 to 5.26 kΩ.cm^2 for PC) with the increase in exposure duration, which clearly indicates higher corrosion rate. The application of SA does not cause any significant modification in R_{ct} values. This clearly indicates SA could not able to perform in preventive the corrosion and control the rate of on-going corrosion. Decrease in the R_{ct} values further indicates that once the corrosion got initiated.

5.9.5 Corrosion Rate (CR) by gravimetric weight loss method for SA applied specimens

The embedded steel rebars were extracted from different prism specimens and the corrosion rate was calculated from gravimetric mass loss values. The results are reported in Table 5.8. From the table, it can be observed that the steel embedded in OPC and PPC showed a corrosion rate of 0.086 and 0.121 mm/yr, respectively. The corrosion rate of O-SA and P-SA were 0.086 and 0.117 mm/yr, while for O-SA´ and P-SA´ these values were 0.086 and 0.120 mm/yr, respectively. Further, on comparing the CR of SA applied specimens as preventive and repair measure, it was observed that CR are almost similar in both measure techniques (preventive or repair). It conveys that SA become inefficient in combined exposure condition as compared to other used compounds.

Table 5.7 Resistive parameters obtained from Nyquist spectra for control and SA applied specimens

Sample	Cycles	Rs (kΩ.cm^2)	Rc (kΩ.cm^2)	Rct (kΩ.cm^2)	Sample	Cycles	Rs (kΩ.cm^2)	Rc (kΩ.cm^2)	Rct (kΩ.cm^2)
OC	0	10.99	-	329.06	PC	0	62.87	354.2	353.46
	10	6.74	-	74.6		10	17.92	143.01	62.48
	20	8.22	7.25	55.34		20	10.35	92.36	52.43
	30	11.45	23.84	33.25		30	3.44	45.13	25.41
	40	9.42	17.22	18.54		40	4.21	25.24	15.66
	50	7.69	10.95	10.29		50	5.17	3.43	5.26
O-SA	0	14.44	-	405.56	P-SA	0	41.85	415	398.81
	10	8.88	-	110.29		10	25.35	149.13	168.67
	20	11.25	16.32	75.24		20	24.43	88.47	112.25
	30	15.5	23.1	38.24		30	26.49	32.19	47.89
	40	12.25	14.36	18.34		40	13.37	20.15	23.33
	50	8.67	9.19	8.06		50	7.59	11.43	7.18
O-SA´	0	10.99	-	329.06	P-SA´	0	62.87	354.2	353.46
	10	6.44	-	72.2		10	17.92	143.01	62.48
	20	10.19	28.60	62.77		20	8.96	48.12	43.74
	30	11.73	12.49	46.38		30	6.40	39.65	28.1
	40	11.24	10.46	32.21		40	5.22	24.36	16.52
	50	12.41	9.56	16.43		50	4.07	17.92	8.22

Table 5.8 Gravimetric mass loss of control and AP applied specimens

Cement type	Specimen	Mass Loss (%)	CR (mm/year)	Cement type	Specimen	Mass Loss (%)	CR (mm/year)
OPC	OC	1.5	0.087	PPC	PC	2.1	0.121
	O-SA	1.22	0.086		P-SA	2.02	0.117
	O-SA´	1.38	0.086		P-SA´	1.97	0.120

5.9.6 Surface Inspection (Visual and Optical) of SA applied specimens.

Fig. 5.41 shows the magnified image of the top exposed surface of reinforced concrete specimens at the end of exposure duration. The magnified image of rebar extracted from SA applied specimen are shown in Fig. 5.42. The average crack width in O-SA and P-SA are 0.412 mm and 0.268 mm, respectively. Also, crack width on surface of O-SA´ was 0.233 mm; while the crack width measured on P-SA was 0.437 mm. The crack widths suggest that the CR was high in these specimens leading to expansive stresses even after the application of SA. However, SA failed to arrest and restrict the corrosion process in concrete. The surface condition of rebar shows the sign of uniform corrosion along with pitting at different locations throughout the rebar. It clearly suggests that SA failed to inhibit in the aggressive environment.

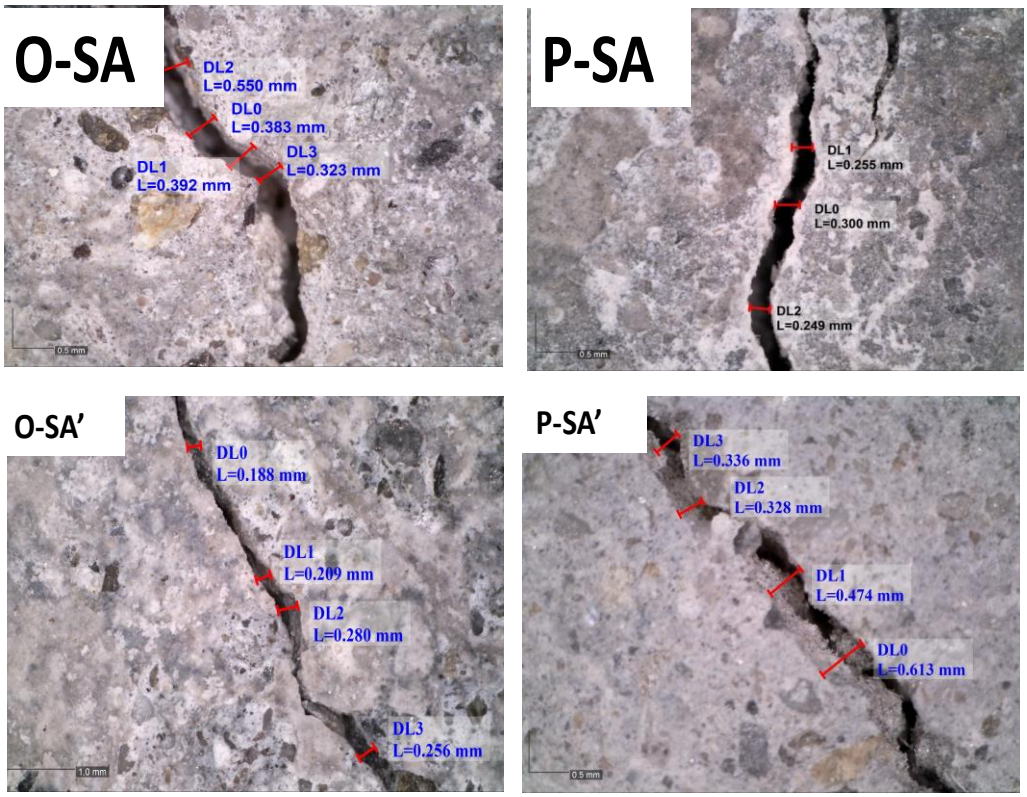

Fig 5.41 Crack width of SA applied specimens

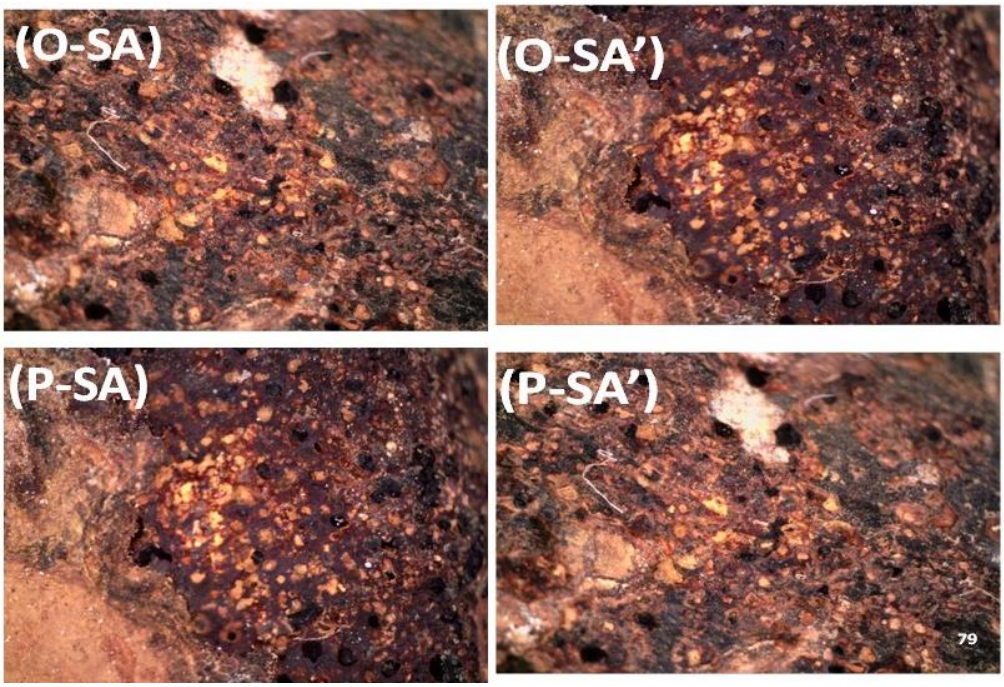

Fig. 5.42 Magnified images of rebar surface at the end of exposure

5.10 PERFORMANCE EVALUATION OF GENERIC COMPOUNDS: PREVENTIVE vs. REPAIR

Based on the test results obtained from Level 1, Level 2 and Level 3 of testing, probable reasons for the performance/non-performance were analyzed and presented in a summarized form in Table 5.9.

ABA was able to perform well in preventive as well as repair strategy. The performance is owed to its highest percolation ability through concrete in OPC as well as PPC concrete systems as explained in Chapter 4. The inhibitor protected the rebar surface even in the presence of accumulated corrosion products (repair measure). Further, AP successfully when applied as preventive measure but was unable to perform in the repair measure. This was owed to the concentration of AP reaching the rebar which was lesser than ABA. It is probably due to this reason that AP successfully formed an adsorbed layer on rebar surface in the absence of the corrosion products; but when accumulation of rust was present the concentration available at the rebar level got consumed during the reaction between rust and AP. No concentration of AP molecules was left to interact with the Fe ions that got exposed thereafter. SA, unlike ABA and SA, was unable to perform in either of the two strategies. The reason could be that SA percolated through the cover concrete but in a modified structural form and in minimum amount as discussed in Chapter 4 under

Section 4.7.1. It is due to this modification that the compound was not able to able curb the corrosion.

Table 5.9 Summary of the performance of generic compounds: preventive vs. repair

Inhibitor	Application of CoI		Reason for performance/non-performance of CoI
	Preventive measure	Repair measure	
ABA	✓	✓	Percolated through the cover concrete in its pure form and protected the rebar in preventive as well as repair measure by forming an adherent protective via adsorption.
AP	✓	✕	Percolated through the cover concrete but the concentration reaching the rebar was lesser than ABA. Performed successfully as in preventive measure but in-sufficient concentration must have got consumed while reacting with the accumulated corrosion products. No amount of AP ions was available to adsorb on the rebar surface for protective action.
SA	✕	✕	Percolated through concrete but in the least concentration and that too in modified form, hence, could not perform the inhibitory action in either of the strategies. The modification in the molecular structure led became the reason for non-performance.

Therefore, it was concluded that there are three factors on which the performance of any compound to work as a corrosion inhibitor would depend:

i. The performance of the compound in pore solution testing.
ii. The concentration of the compound reaching the rebar level when applied on hardened concrete surface.
iii. The form of the inhibitor in which it reaches the rebar level.
iv. The condition of the rebar: passive state or corroded.

Based on these findings, it was deduced that Level 1 of testing should also be performed with corroded rebar as working electrode. Therefore, pore solution testing was redone.

Pore solution testing with corroded rebars

Before initiating the test, the rebar specimens were firstly taken and dipped in S1 till corrosion got imitated. To get an idea about the corrosion initiation time, a set of steel coupons (3 coupons) were immersed in S1 and monitored through optical microscopy after each hour. Once the occurrence of corrosion products/pit embryo formation was witnessed, the samples were carefully taken out, dried and subjected to SEM-EDX testing and the time to initiate corrosion was noted. The optical image of coupon before immersion and after formation of corrosion product is shown in Fig. 5.43 (a_1) and (b_1). From the figure, it can be seen that the initial surface was shiny and lustrous, whereas; after 10 hours of immersion some red brown products were visible over the entire surface. The morphological images of top surface (Fig. 5.43 (a_2) and (b_2)) also indicated the development of hydroxides and oxides after 10 hours. The argument was further authenticated by EDX spectral analysis which shows the decrease in concentration of Fe (97.78% to 45.72%) and increase in concentration of O (0 to 42.47%) along with C (2.22% to 7.58%). Therefore, a duration of 10 hours was considered to initiate corrosion on immersed rebars. After corrosion has been initiated, CoI's were added in S1 to assess their inhibition efficiencies on already corroded rebars.

The optical images and SEM-EDX results after 240 hours of immersion of steel coupons in CoI-free and CoI-admixed pore solution are presented in Fig. 5.44. As can be seen from Fig. 5.44a_1, the surface of the coupon immersed in CoI-free pore solution is severely corroded with red brown corrosion product accumulation all over the surface. The SEM image of the same sample (Fig. 5.44a_2) displays the presence of globular loose products which are confirmed as corrosion products by the elemental analysis. With the addition of CoI, the corrosion is seen to reduce. For ABA and AP, the coupon surface exhibits clear steel surface along with the presence of some product formation whereas for SA, a black layer region and a few products assemblage is observed from the optical images (Figs. 5.44b_1, c_1 and d_1). From the SEM and EDX results, it is confirmed that maximum exposed area of the coupons was protected from corrosion in the presence of CoI. In CoI-admixed specimens, the concentration of Fe reduced from 45% to near 20% (for ABA and AP; while it reduced drastically to 1.09% for SA) with the corresponding increase in concentration

of C (Figs. 5.44b$_2$, c$_2$ and d$_2$). This indicates the presence of CoI molecules on Fe surface due to some chelate formation as organic molecules are the only source of C atoms in pore solution.

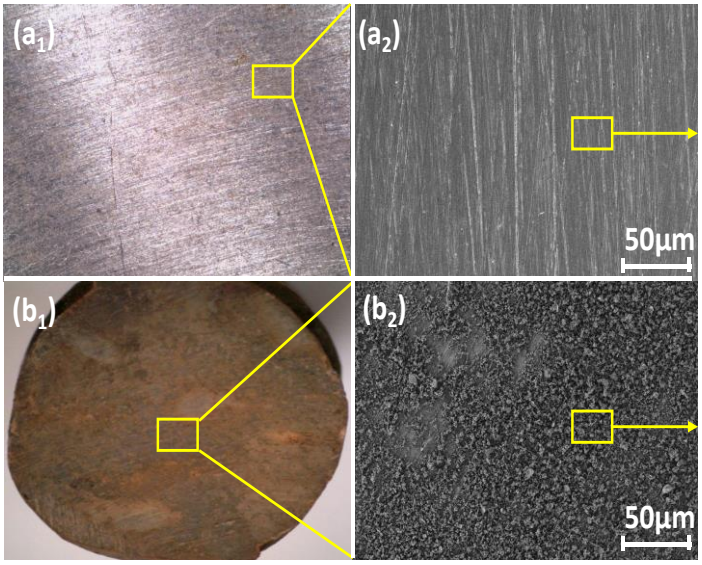

Element	Atomic %	Element	Atomic %
Fe	97.78	K	-
C	2.22	Na	-
O	-	Cl	-

Element	Atomic %	Element	Atomic %
Fe	45.72%	K	1.32
C	7.58%	Na	1.35
O	42.47%	Cl	1.56

Fig. 5.43 Surface inspection of steel coupons before and after 10 hours of immersion (a) Optical images (b) SEM-EDX

To validate the inhibition efficiency of the selected CoI's by more reliable test methods, electrochemical test was performed, and the efficiency of the compounds is presented in Table 5.10. From the Table, SA displayed the highest efficiency followed by ABA and AP when corroded bars were taken as working electrodes. When the CoI were added as preventive technique in corrosive pore solution, the adsorption sites of the CoI were attracted electrostatically and chemically towards the metal surface. For comparison, the corrosion inhibition efficiency of CoI obtained on non-corroded bars during Level 1 testing (presented in Chapter 3, Section 3.6.2, Table 3.6) is also presented in Table 5.10. As the CoI were added before corrosion initiation, the entire surface of the metal was available for interaction with the CoI molecules hence, the complete coverage by CoI which led to the high inhibition efficiency. On the other hand, in repair strategy, the accumulation of the corrosion products on the rebar before the addition of CoI, acted as some sort of barrier for CoI molecules to interact with the Fe ions. As the number of interaction sites reduced, so did the surface coverage by the CoI and hence, the decrease in inhibition efficiency was recorded during the PDP tests.

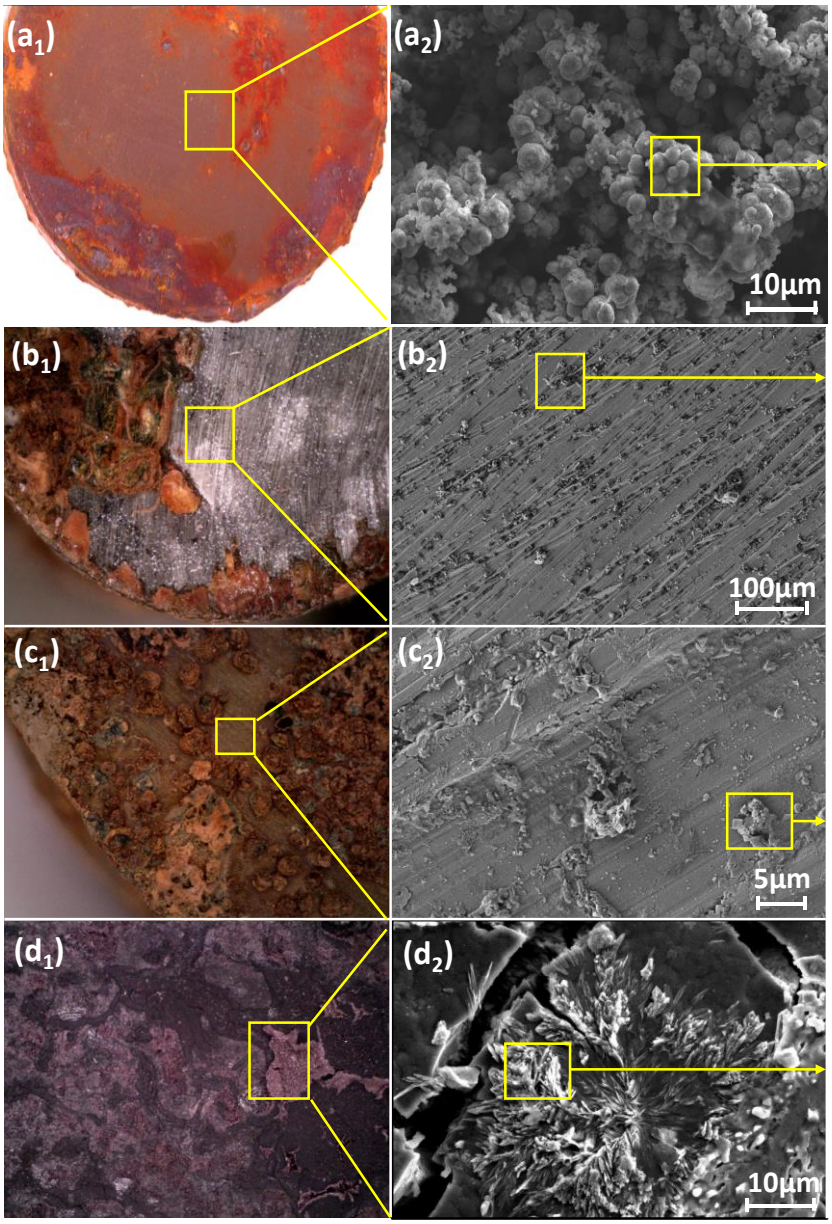

Element	Atomic %	Element	Atomic %
Fe	45.72%	K	1.32
C	7.58%	Na	1.35
O	42.47%	Cl	1.56

Element	Atomic %	Element	Atomic %
Fe	22.4	K	3.32
C	29.24	Na	2.52
O	42.19	Cl	0.33

Element	Atomic %	Element	Atomic %
Fe	20.4	K	4.98
C	31.11	Na	5.20
O	38.25	Cl	0.06

Element	Atomic %	Element	Atomic %
Fe	1.09	K	5.90
C	11.29	Na	23.12
O	58.22	Cl	0.38

Fig. 5.44 Optical microscopy images of (a_1) Control (inhibitor-free) (b_1) ABA (c_1) AP (d_1) SA and SEM images with EDS results of (a_2) Control (inhibitor-free) (b_2) ABA (c_2) AP (d_2) SA admixed in pore solution

Table 5.10 Corrosion current density and efficiency of generic compounds

Sample description		S1	S1+ABA	S1+AP	S1+SA
i_{corr} (μA/cm^2)		92.57	44.05	52.85	15.62
Efficiency (%)	Repair (already corroded rebar)	-	52.41	42.90	83.12
	Preventive (non-corroded rebar)	-	99.97%	99.97%	99.9%

5.11 DEGRADATION AND INHIBITION MECHANISM IN RC

The continuous monitoring by electrochemical test followed by surface analysis and gravimetric weight loss at the end of exposure duration suggest that rebar was severely corroded in control specimen, while out of three CoI two perform efficiently as preventive measure in reducing the corrosion rate. It is worth noted that the diffusion rate of chloride ions and carbonation is different and hence the combined degradation mechanism would be different than reported in individual environment. In case of CoI, presence of different functional group and positioning of functional group influence the inhibition mechanism on the rebar surface. Thus, the degradation mechanism due to simultaneous chloride and carbonation exposure and the chemistry so involved for used CoI in the present study is discussed hereunder.

5.11.1 Degradation mechanism in combined aggressive exposure

A combination of chloride and carbonation cycle was given to the reinforced concrete samples. Although, chloride ions reach earlier than carbonation at the rebar level, CO_2 exposure had a severe impact on corrosion of rebar with testing age. Initially a very local attack (pitting corrosion) could have started when the carbonation front is very low as explained by Fig. 5.45 (a); but with continuous exposure and increasing carbonation front, widespread generalized corrosion could have started with more severe pitting (as shown in Fig. 5.45 (a)) due to increased number of chloride ions at the rebar level. As explained in earlier sections, the surface accumulated chloride ions are pushed into deeper depths by the action of CO_2. Hence, the degradation of steel rebar in combined corrosive environment can be divided into two phases; phase I- where pitting corrosion is dominant and phase II- where both uniform and pitting corrosion are at their highest severity. It can be therefore said that in simultaneous exposure conditions, chloride ions are responsible for corrosion initiation but with testing durations, carbonation aggravates the degradation process.

5.11.2 Inhibition mechanism of CoI's

Preventive measure: Application of all the CoIs reduced the degradation phenomena when applied as preventive measure as suggested by the electrochemical test, gravimetric weight loss measurements, visual and microscopic observations. The observed trend can be chemically explained by Fig. 5.45. 4ABA which is an amine and carboxylate containing aromatic compound, could have formed a protective film on the steel surface by co-ordinate bond formation between N atom of amine group and Fe^{2+} ions; in addition to this, a negative layer could also have formed by the carboxylates as shown in Fig. 5.45 (b).

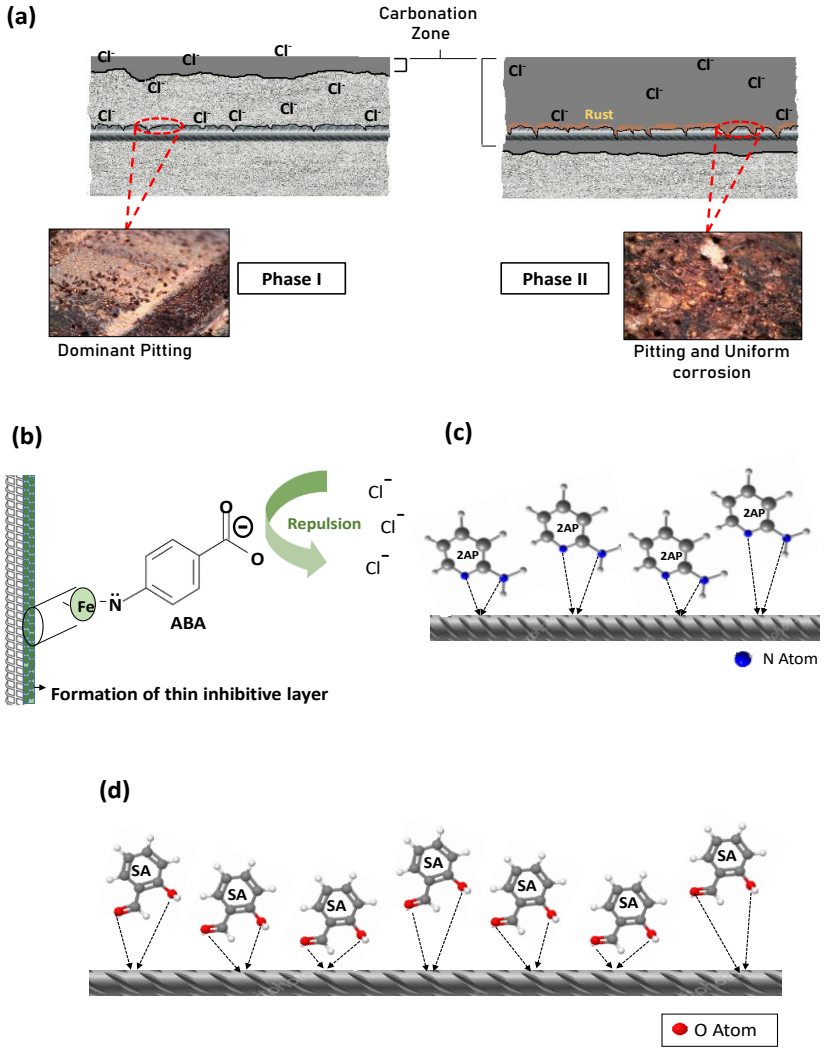

Fig. 5.45 Schematic representation of (a) Degradation mechanism in combined chloride and carbonation environment and (b), (c) & (d) Inhibition mechanism of ABA, AP, and SA

Thus, an inhibitive layer along with a repulsive layer for the corrosive chloride and bicarbonate ions must have built making 4ABA an effective corrosion inhibitor. On the other side, AP acted as a chelating agent whose structure permitted the attachment of N atom (donor atom with lone pairs) to the metal ion and produce a chelating ring as illustrated in Fig. 5.45 (c). A four membered chelate ring (two N atoms, Fe and C) has a possibility to get formed on the steel surface, thus, inhibiting the corrosion process. Whereas SA is a molecule with aldehyde (-CHO) and alcohol (-OH) group attached adjacent to each other and act as ligand for chelation with iron as shown in Fig. 5.45 (d). Both –CHO and –OH have electron donating O atom which bound the rebar site where Fe^{2+} ions were available, hence, forming a protective layer. Generally, chelation leads to the formation of more stable complex as compared to those complexes with no chelate ring formation, but in this case the development of the negative charged repulsive layer in the case of 4ABA has provided even better inhibitive properties than the other two inhibitors.

Repair Measure: When the organic compounds were applied as migratory CoI on the concrete surface after the accumulation of corrosion products, ABA performed well in suppressing the rate of on-going corrosion by forming a layer over the rebar surface. This layer sustained itself even after the exposure to harsh corrosive environment which explains the inhibitive nature of ABA molecules. On the other hand, the molecules of SA and AP was unable to perform as CoI in concrete due the modification of their ions when applied as migratory CoI. The possible mechanism in repair measure is presented in Fig. 5.46.

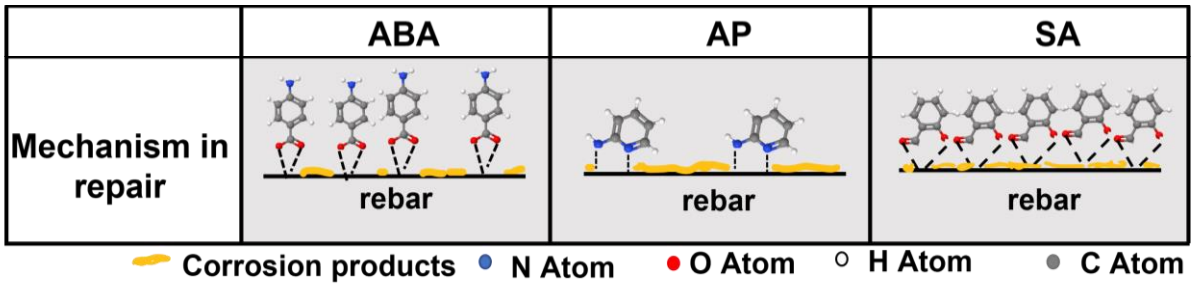

Fig. 5.46 Mechanism in repair strategy for ABA, AP and SA

5.12 CLOSING REMARKS

In the present chapter, inhibition efficiency of three different generic compounds in mitigating corrosion in preventive strategy and in repair strategy due to combined chloride and carbonation

ingress was studied. Electrochemical, gravimetric weight loss and surface studies were employed for assessing the rebar condition during the testing period. The concrete specimens treated with generic compounds, ABA, AP and SA exhibit different behavior when employed as preventive and repair measure. ABA curbed the corrosion processes in both the employed measures, AP performed successfully in only preventive measure however SA did not perform in either of the two measures. ABA performed better than AP in preventive measure.

The inhibitors which successfully inhibited the corrosion during preventive measure, protected the rebar by forming a protective layer upon reaching the rebar. Among the three generic compounds, ABA shows the best protection ability throughout the exposure duration. The percolation ability along with its advantageous molecular structural features (molecular weight, two functional groups, and ability to form covalent bond and repulsive nature for chloride) makes ABA a better CoI than other two compounds. Whereas, in AP presence of adjacent nitrogen atoms in molecular structure enhances its capability to form chelate with ferrous ions upon reaching the rebar level. In case of SA, the initial efficiency of controlling the corrosion process decreases with the continuous corrosive ion attack. Thus, the protection efficiency of SA vanished after certain period. The most probable reason behind decrement in efficiency was the unavailability of sufficient concentration of SA at the rebar level due to its high chelating ability with hydration products of cement reducing its percolation.

CHAPTER 6

CONCLUSIONS AND FUTURE SCOPE

6.1 GENERAL

The aim of the present research is to investigate the severity level of combined chloride and carbonation attack on reinforced steel and selection of potential corrosion inhibitor (CoI) to mitigate corrosion in the combined aggressive environment. To fulfil these objectives, the study was divided into three levels. Level 1 consisted of testing of selected generic compounds in simulated concrete pore solution to get their efficiency in the combined aggressive environment. Level 2 of the study focused on the migration ability of the tested genetic compounds in OPC and PPC based concrete systems, in order to check their applicability as migratory corrosion inhibitors. In Level 3 of the study, the selected generic compounds were applied on reinforced concrete (RC) prisms in both the preventive and repair measure. Based on the test results at various levels of testing, following conclusions are drawn:

6.2 PERFOMANCE OF STEEL IN SIMULATED PORE SOLUTION

During the pore solution testing, the performance of four generic compounds namely, Triethyl-phosphate (TEP), Salicylaldehyde (SA), 2-Aminopyridine (AP) and 4-Aminobenzoic acid (ABA) were explored.

1. The test conducted in synthetic concrete pore solution simulating different corrosive environments shows different potentiodynamic behavior under different exposure conditions. In uncontaminated solution, three distinct zones namely, active, passive and transpassive zone are clearly identified, whereas in chloride contaminated solution the transpassive zone has been transformed to pitting region due to chloride attack. In carbonated solution, uniform increase in current density with potential signifies the uniform corrosion on surface, with absence of explicit passive behaviors or transpassive behavior. However, potentiodynamic curve for solution simulating combined environment demonstrated highest severity level of combined attack marked with increase in corrosion current density (i_{corr}) and shift in corrosion potential (E_{corr}). The obtained i_{corr} value in combined environment was 87% and 24.4% higher than individual chloride induced, and

carbonation induced corrosion. The SEM-EDX data confirmed the presence of corrosion product on the specimen immersed in combined aggressive solution.

2. Generic compounds were efficient in retarding corrosion rate in combined aggressive environment. With increase in concentration the inhibition efficiency of TEP increased from 65.3% to 83% at 0.05Mto 0.2M concentration respectively, the inhibition efficiency of AP increased from 84.5% to 99.9%; while SA and ABA demonstrated very high efficiency even at low concentration levels.

3. The corrosion protection mechanism of generic compounds was found to depend upon the presence of heteroatoms in all the compounds. The presence of O and P as heteroatoms in TEP functionality enhanced the protection mechanism by making it more reactive with ferrous ions on the exposed surface. The presence of additional heteroatoms (i.e., N) in AP enhanced the protection mechanism by multilayer physisorption. In the case of ABA and SA, inhibition mechanism was governed by the presence of heteroatom O in their respective functional groups (i.e., carboxyl group in ABA; hydroxyl and carbonyl group in SA). This heteroatom gave them additional chelating capability that helped in their adsorption on the metal surface. Moreover, the presence of phenyl ring in the organic compounds was seen to be effective in enhancing the inhibition efficiency of AP, ABA, and SA.

6.3 PENETRATION ABILITY OF INHIBITORS AND CORROSIVE AGENTS

1. Generic compounds have a tendency to migrate through cover concrete via diffusion in liquid state. Retention factor (R_f) obtained from thin layer chromatography (TLC) method suggest that at higher concentration of compounds i.e., at 0.8M and 1.0M (for ABA, AP, and SA), the R_f value matched with the reference compound, while at lower concentration no spots were visible on TLC plate. This clearly suggests that at higher concentration, these compounds were able to penetrate within 15 days of their application. The pore structure of concrete with interconnected pores allowed the movement of generic compounds by diffusion in the dissolved state.

2. The concentration reaching at different levels of concrete was observed to be dependent on the characteristics of the generic compound (viz. molecular weight and molecular structure) and on the type of cement. ABA, due to its high molecular weight diffused at much faster rate than AP and SA. Also, AP and SA interacted with Ca^{2+} and Na^{+} ions present in the concrete matrix due to their high chelating capability that caused reduction in their diffusion rate. The order of concentration of generic compounds reaching at the rebar level in different concrete system was ABA>AP>SA.

3. The diffusion of generic compounds is higher in OPC leading to higher concentration in Portland cement than fly ash based PPC concrete.

4. While comparing the carbonation depth in the different concrete systems, it was observed that PPC concrete had higher carbonation front than OPC due to lesser portlandite content in the former. The carbonation depth of PPC was 43% higher than OPC concrete.

5. The chloride profile indicates that carbonation had a notable impact on the redistribution of chloride within the concrete system. Initially, the chloride content in PPC was lower than in OPC might be due to its dense microstructure. However, with continuous exposure to carbonation and chloride, the Free chloridecontent in PPC increased, suggesting that concrete carbonation may affect the concentration of Free chlorideions, leading to higher concentrations at deeper depths. This phenomenon was observed in both cement types. Interestingly, there was no significant variation in chloride concentration after the application of CoI.

6. The chloride and carbonation profiles show that the application of CoI did not lead to any significant variation in the data from either test. This suggests that the generic compounds did not show any sign of pore modification in any type of cement.

6.4 POTENTIAL OF GENERIC COMPOUND AS CORROSION INHIBITORS

1. From the electrochemical tests conducted on both OPC and PPC based concrete systems, it can be concluded that PPC concrete was more vulnerable to corrosion during cyclic exposure of chloride and carbonation than the OPC concrete. Also, at the rebar level, Free chloride ions reach earlier than carbonation thereby initiating pitting corrosion. However,

at later durations, carbonation played a major role in pushing the chloride ions towards deeper depths in concrete, thereby increasing the rates of corrosion (pitting and uniform corrosion) in both OPC and PPC concrete.

2. Out of three generic compounds, ABA performed the best in both preventive and repair measures. Application of ABA enhanced the corrosion resistant properties of embedded rebar by refining the steel/concrete interface, thereby preventing the aggressive corrosion reactions. Application of ABA reduced the charge transfer process and delayed the de-passivation time of the passive film on the rebar surface. As a preventive measure when ABA was applied before corrosion initiation, it increased the de-passivation time of embedded rebar; while after corrosion initiation in repair measure, it formed a protective layer on the steel surface by co-ordinate bond formation between N atom of amine group and Fe^{2+} ions. In addition to this, a negative layer could also have formed by the carboxylates. On comparing the performance of ABA as two measures, the test results confirm that the potential of ABA was higher when used in repair strategy.

3. The test results of AP applied specimens conclude that AP can effectively reduce the corrosion processes in combined aggressive environment when employed as preventive technique, as indicated by the low i_{corr} and HCP values. The inhibitor ions chelate the Fe ions via nitrogen atom in its heterocycle and amine functional group. A layer of inhibitor-Fe complex forms on the rebar surface which prevents the rebar to corrode; confirmed from the EIS results. Optical microscopy and weight loss data validated these observations. When employed as repair strategy, AP could not reduce the on-going corrosion rate due to the accumulation of the corrosion products on the rebar. The reason for the inefficiency was the insufficient concentration of 2AP that percolated and reached the rebar level. With increase in the concentration of 2AP, it can turn out to be effective in repair technique also. This was confirmed by the pore solution testing on already corroded rebars.

4. SA being a potential inhibitor in pore solution was unable to prevent and restrict the ongoing corrosion process in both the concrete systems. Initial formation of passive layer just after the application was not able to hold its inhibition capability to a long run due to

the insufficient amount of SA concentration that reached the rebar level and that too in modified form.

6.5 SCOPE FOR FUTURE WORK

The scope for future work is as follows:

1. Generic compounds have potential to mitigate corrosion in most severe environment. However, in this study percolation was checked prior to environmental exposure when there is no change in microstructure. It will be interesting to study the migration behaviour after the modification in microstructure of different concrete systems has occurred.

2. Field application of generic compounds is necessary to identify their potential as corrosion inhibitor in actual structures. Thus, efforts are required to study their efficiency on RC after onsite application.

REFERENCES

ASTM 109, G. (2011). *Standard Test Method for Determining Effects of Chemical Admixtures on Corrosion of Embedded Steel Reinforcement in Concrete Exposed to*. *07*(Reapproved 2013), 3–8. https://doi.org/10.1520/G0109-07R13.2

8112:2013. (2013). IS: 8112 – 1989, Specification for 43 grade Ordinary Portland Cement. *BIS*, 17.

Aguirre-Guerrero, A. M., Mejía-De-Gutiérrez, R., & Montês-Correia, M. J. R. (2016). Corrosion performance of blended concretes exposed to different aggressive environments. *Construction and Building Materials*, *121*, 704–716. https://doi.org/10.1016/j.conbuildmat.2016.06.038

Al-Amoudi, O. S. B., Maslehuddin, M., Lashari, A. N., & Almusallam, A. A. (2003). Effectiveness of corrosion inhibitors in contaminated concrete. *Cement and Concrete Composites*, *25*(4-5 SPEC), 439–449. https://doi.org/10.1016/S0958-9465(02)00084-7

Al-Mehthel, M., Al-Dulaijan, S., Al-Idi, S. H., Shameem, M., Ali, M. R., & Maslehuddin, M. (2009). Performance of generic and proprietary corrosion inhibitors in chloride-contaminated silica fume cement concrete. *Construction and Building Materials*, *23*(5), 1768–1774. https://doi.org/10.1016/j.conbuildmat.2008.10.010

Al-Saleh, S. A. (2015). Analysis of total chloride content in concrete. *Case Studies in Construction Materials*, *3*(10), 78–82. https://doi.org/10.1016/j.cscm.2015.06.001

Alizadeh, R., Naderi, R., Saremi, M., Hamidi, H., & Shojaei, F. (2023). Corrosion inhibition effect of sodium tri-polyphosphate on reinforcing steel in simulated concrete pore solution with different pHs. *Construction and Building Materials*, *363*(May 2022), 129819. https://doi.org/10.1016/j.conbuildmat.2022.129819

Alonso, C., Andrade, C., Argiz, C., & Malric, B. (1996). Na2PO3F as inhibitor of corroding reinforcement in carbonated concrete. *Cement and Concrete Research*, *26*(3), 405–415. https://doi.org/10.1016/S0008-8846(96)85028-9

Andrade, C. Alonso, C. (1990). Effect of Nitrite as a Corrosion Inhibitor in Contaminated and Chloride-Free Carbonated Mortar. *ACI Materials Journal*, *87*(2), 130–137.

https://doi.org/10.14359/1937

Andrade, C., Blanco, V. M., Collazo, A., Keddam, M., Nóvoa, X. R., & Takenouti, H. (1999). Cement paste hardening process studied by impedance spectroscopy. *Electrochimica Acta*, *44*(24), 4313–4318. https://doi.org/10.1016/S0013-4686(99)00147-4

Andrade, C., & Page, C. L. (1986). Pore solution chemistry and corrosion in hydrated cement systems containing chloride salts: A study of cation specific effects. *British Corrosion Journal*, *21*(1), 49–54. https://doi.org/10.1179/000705986798272415

Angst, U., Moro, F., Geiker, M., Kessler, S., Beushausen, H., Andrade, C., Lahdensivu, J., Köliö, A., Imamoto, K. I., von Greve-Dierfeld, S., & Serdar, M. (2020). Corrosion of steel in carbonated concrete: Mechanisms, practical experience, and research priorities – A critical review by RILEM TC 281-CCC. *RILEM Technical Letters*, *5*, 85–100. https://doi.org/10.21809/rilemtechlett.2020.127

Ann, K. Y., Jung, H. S., Kim, H. S., Kim, S. S., & Moon, H. Y. (2006). Effect of calcium nitrite-based corrosion inhibitor in preventing corrosion of embedded steel in concrete. *Cement and Concrete Research*, *36*(3), 530–535. https://doi.org/10.1016/j.cemconres.2005.09.003

Anon. (1988). CPC-18 Measurement of hardened concrete carbonation depth. *Materials and Structures*, *21*(6), 453–455. https://doi.org/10.1007/BF02472327

Ansari, K. R., Quraishi, M. A., & Singh, A. (2015). Pyridine derivatives as corrosion inhibitors for N80 steel in 15% HCl: Electrochemical, surface and quantum chemical studies. *Measurement: Journal of the International Measurement Confederation*, *76*, 136–147. https://doi.org/10.1016/j.measurement.2015.08.028

Antunes, R. A., Ichikawa, R. U., Martinez, L. G., & Costa, I. (2014). Characterization of corrosion products on carbon steel exposed to natural weathering and to accelerated corrosion tests. *International Journal of Corrosion*, *2014*. https://doi.org/10.1155/2014/419570

ASTM C1218/C1218M-20. (2020). Standard Test Method for Water-Soluble Chloride in Mortar and Concrete. *American Society for Testing and Materials.*, 3. https://doi.org/10.1520/C1218_C1218M-20

ASTM C876-22b. (2015). Standard test method for corrosion potentials of uncoated

reinforcing steel in concrete. ASTM C876 - 15. G01.14,. *ASTM International*, 1–8. https://doi.org/10.1520/C0876-22B.2

ASTM G3-14. (2019). Standard Practice for Conventions Applicable to Electrochemical Measurements. *ASTM Standards, Reapproved 2019*, 1–9. https://doi.org/10.1520/G0003-14R19.2

ASTM Standars. (2012). Standard Practice for Conventions Applicable to Electrochemical Measurements. *ASTM G3 2012*, *i*(Reapproved 2010), 1–9. https://doi.org/10.1520/G0003-14R19.2

Awad, H. S. (2006). The corrosion and inhibition of Zn-Al alloy in acidic media by pyridine and its methyl-containing derivatives. *Anti-Corrosion Methods and Materials*, *53*(2), 110–117. https://doi.org/10.1108/00035590610650811

Berke, N. S., & Hicks, M. C. (2004). Predicting long-term durability of steel reinforced concrete with calcium nitrite corrosion inhibitor. *Cement and Concrete Composites*, *26*(3), 191–198. https://doi.org/10.1016/S0958-9465(03)00038-6

Bertolini, L., Carsana, M., & Redaelli, E. (2008). Conservation of historical reinforced concrete structures damaged by carbonation induced corrosion by means of electrochemical realkalisation. *Journal of Cultural Heritage*, *9*(4), 376–385. https://doi.org/10.1016/j.culher.2008.01.006

BIS:1489 (Part 1). (1991). Portland-pozzolana cement-specification. *Bureau of Indian Standard (BIS)*, New Delhi,India.

Bolzoni, F., Brenna, A., & Ormellese, M. (2022). Recent advances in the use of inhibitors to prevent chloride-induced corrosion in reinforced concrete. *Cement and Concrete Research*, *154*(March 2021), 106719. https://doi.org/10.1016/j.cemconres.2022.106719

Bolzoni, F., Coppola, L., Goidanich, S., Lazzari, L., Ormellese, M., & Pedeferri, M. P. (2004). Corrosion inhibitors in reinforced concrete structures Part 1: Preventative technique. *Corrosion Engineering, Science and Technology*, *39*(3), 219–228. https://doi.org/10.1179/147842204X2871

Bowman, E., Jacobson, G., Koch, G., Varney, J., Thopson, N., Moghissi, O., Gould, M., &

Payer, J. (2016). International Measures of Prevention, Application, and Economics of Corrosion Technologies Study. *NACE International*, A-19.

Broomfield, J. P. (2006). *Corrosion of Steel in Concrete: Understanding, Investigation and Repair, Second Edition* (2nd ed.). CRC Press. https://doi.org/https://doi.org/10.1201/9781482265491

Byung Hwan Oh, Sang Hwa Jung, M. K. L. (2013). Effects of Carbonation on Chloride Penetration in Concrete. *ACI Materials Journal*, *110*(5), 559–566. https://doi.org/10.14359/51685907

Cabrini, M., Fontana, F., Lorenzi, S., Pastore, T., & Pellegrini, S. (2015). Effect of Organic Inhibitors on Chloride Corrosion of Steel Rebars in Alkaline Pore Solution. *Journal of Chemistry*, *2015*. https://doi.org/10.1155/2015/521507

Cao, F., Wei, J., Dong, J., & Ke, W. (2015). The corrosion inhibition effect of phytic acid on 20SiMn steel in simulated carbonated concrete pore solution. *Corrosion Science*, *100*, 365–376. https://doi.org/10.1016/j.corsci.2015.08.020

Chaussadent, T., Nobel-Pujol, V., Farcas, F., Mabille, I., & Fiaud, C. (2006a). Effectiveness conditions of sodium monofluorophosphate as a corrosion inhibitor for concrete reinforcements. *Cement and Concrete Research*, *36*(3), 556–561. https://doi.org/10.1016/j.cemconres.2005.09.006

Chaussadent, T., Nobel-Pujol, V., Farcas, F., Mabille, I., & Fiaud, C. (2006b). Effectiveness conditions of sodium monofluorophosphate as a corrosion inhibitor for concrete reinforcements. *Cement and Concrete Research*, *36*(3), 556–561. https://doi.org/10.1016/j.cemconres.2005.09.006

Coates, J. (2006). Interpretation of Infrared Spectra, A Practical Approach. *Encyclopedia of Analytical Chemistry*, 10815–10837. https://doi.org/10.1002/9780470027318.a5606

Criado, M., Monticelli, C., Fajardo, S., Gelli, D., Grassi, V., & Bastidas, J. M. (2012). Organic corrosion inhibitor mixtures for reinforcing steel embedded in carbonated alkali-activated fly ash mortar. *Construction and Building Materials*, *35*, 30–37. https://doi.org/10.1016/j.conbuildmat.2012.02.078

Cui, L., Hang, M., Huang, H., & Gao, X. (2021). Experimental study on multi-component corrosion inhibitor for steel bar in chloride environment. *Construction and Building Materials*, *313*(November), 125533. https://doi.org/10.1016/j.conbuildmat.2021.125533

Dariva, C. G., & Galio, A. F. (2014). Corrosion Inhibitors - Principles Mechanisms and Applications. *Developments in Corrosion Protection*, 365–379. https://doi.org/10.5772/57255

De Schutter, G., & Luo, L. (2004). Effect of corrosion inhibiting admixtures on concrete properties. *Construction and Building Materials*, *18*(7), 483–489. https://doi.org/10.1016/j.conbuildmat.2004.04.001

Deng, G., He, Y., Lu, L., Wang, F., & Hu, S. (2023). A preliminary study on the efficiency of the steel slag-based spraying carbonation layer in improving the durability of cement-based products. *Cement and Concrete Composites*, *136*(December 2021), 104899. https://doi.org/10.1016/j.cemconcomp.2022.104899

Dharmaraj, R., & Malathy, R. (2015). Performance evaluation of sodium nitrite corrosion inhibitor in self compacting concrete. *Indian Journal of Science and Technology*, *8*(36). https://doi.org/10.17485/ijst/2015/v8i36/87647

Dhouibi, L., Triki, E., Salta, M., Rodrigues, P., & Raharinaivo, A. (2003). Studies on corrosion inhibition of steel reinforcement by phosphate and nitrite. *Materials and Structures/Materiaux et Constructions*, *36*(262), 530–540. https://doi.org/10.1617/13893

Dong, B. Q., Qiu, Q. W., Xiang, J. Q., Huang, C. J., Xing, F., Han, N. X., & Lu, Y. Y. (2014). Electrochemical impedance measurement and modeling analysis of the carbonation behavior for cementititous materials. *Construction and Building Materials*, *54*, 558–565. https://doi.org/10.1016/j.conbuildmat.2013.12.100

Dong, B., Qiu, Q., Xiang, J., Huang, C., Xing, F., & Han, N. (2014). Study on the carbonation behavior of cement mortar by electrochemical impedance spectroscopy. *Materials*, *7*(1), 218–231. https://doi.org/10.3390/ma7010218

El Ibrahimi, B., Jmiai, A., Bazzi, L., & El Issami, S. (2017). Amino acids and their derivatives as corrosion inhibitors for metals and alloys. *Arabian Journal of Chemistry*. https://doi.org/10.1016/j.arabjc.2017.07.013

Elsener, B. (2000). Corrosion inhibitors for steel in concrete. *Proceedings of the International Congress on Advanced Materials*, *33*(6), 44–47. https://doi.org/10.1201/9781003076957-6

Elsener, B., Büchler, M., Stalder, F., & Böhni, H. (1999). Migrating Corrosion Inhibitor Blend for Reinforced Concrete: Part 1—Prevention of Corrosion. *Corrosion*, *55*(12), 1155–1163. https://doi.org/10.5006/1.3283953

Fabis, P., Brown, C., Rockett, T., & Heidersbach, R. (1981). An infrared and Raman spectroscopy study of the corrosion products on carbon steel and weathering steel. *Oxidation of Metals*, *16*(5–6), 399–407. https://doi.org/10.1007/BF00611352

Fei, F. L., Hu, J., Wei, J. X., Yu, Q. J., & Chen, Z. S. (2014). Corrosion performance of steel reinforcement in simulated concrete pore solutions in the presence of imidazoline quaternary ammonium salt corrosion inhibitor. *Construction and Building Materials*, *70*, 45–53. https://doi.org/10.1016/j.conbuildmat.2014.07.082

Florea, M. V. A., & Brouwers, H. J. H. (2012). Cement and Concrete Research Chloride binding related to hydration products Part I : Ordinary Portland Cement. *Cement and Concrete Research*, *42*(2), 282–290. https://doi.org/10.1016/j.cemconres.2011.09.016

Ford, S. J., Shane, J. D., & Mason, T. O. (1998). Assignment of features in impedance spectra of the cement-paste/steel system. *Cement and Concrete Research*, *28*(12), 1737–1751. https://doi.org/10.1016/S0008-8846(98)00156-2

Gaidis, J. M. (2004). Chemistry of corrosion inhibitors. *Cement and Concrete Composites*, *26*(3), 181–189. https://doi.org/10.1016/S0958-9465(03)00037-4

Geng, J., Easterbrook, D., Liu, Q. F., & Li, L. Y. (2016). Effect of carbonation on release of bound chlorides in chloride-contaminated concrete. *Magazine of Concrete Research*, *68*(7), 353–363. https://doi.org/10.1680/jmacr.15.00234

Génin, J. M. R., Dhouibi, L., Refait, P., Abdelmoula, M., & Triki, E. (2002). Influence of phosphate on corrosion products of iron in chloride-polluted-concrete-simulating solutions: Ferrihydrite vs green rust. *Corrosion*, *58*(6), 467–478. https://doi.org/10.5006/1.3277637

Glass, G. K., Page, C. L., & Short, N. R. (1991). Factors affecting the corrosion rate of steel in carbonated mortars. *Corrosion Science*, *32*(12), 1283–1294. https://doi.org/10.1016/0010-

938X(91)90048-T

Goñi, S., & Andrade, C. (1990). Synthetic concrete pore solution chemistry and rebar. *Cement and Concrete Research*, *20*(c), 525–539.

Gouda, V. ., Mourad, W. ., & Mikhail, R. S. (1973). Additives to cement pastes: Simultaneous effects on pore structure and corrosion of steel reinforcement. *Journal of Colloid and Interface Science*, *43*(2), 294–302. https://doi.org/10.1016/0021-9797(73)90377-9

Goyal, A., Ganjian, E., Pouya, H. S., & Tyrer, M. (2021). Inhibitor efficiency of migratory corrosion inhibitors to reduce corrosion in reinforced concrete exposed to high chloride environment. *Construction and Building Materials*, *303*(May), 124461. https://doi.org/10.1016/j.conbuildmat.2021.124461

Gu, P., Elliott, S., Hristova, R., Beaudoin, J. J., Brousseau, R., & Baldock, B. (1997). A Study of corrosion inhibitor performance in chloride contaminated concrete by electrochemical impedance spectroscopy. *ACI Materials Journal*, *94*(5), 385–395. https://doi.org/10.14359/323

Guleria, H., Purnima, Tiwari, A. K., & Goyal, S. (2021). Performance of organic and inorganic functional groups as corrosion inhibitors in concrete experiencing extreme corrosive environment. *Indian Concrete Journal*, *95*(4), 39–37.

Herrera Hernández, H., González Díaz, F., Fajardo San Miguel, G. D. J., Velázquez Altamirano, J. C., González Morán, C. O., & Morales Hernández, J. (2019). Electrochemical Impedance Spectroscopy as a Practical Tool for Monitoring the Carbonation Process on Reinforced Concrete Structures. *Arabian Journal for Science and Engineering*, 44(12), 10087–10103. https://doi.org/10.1007/s13369-019-04041-z

Heiyantuduwa, R. (2001). Performance of a penetrating corrosion inhibitor in controlling carbonation induced corrosion in reinforced concrete [University of Cape Town]. https://open.uct.ac.za

Heiyantuduwa, R., Alexander, M. G., & Mackechnie, J. R. (2006). Performance of a Penetrating Corrosion Inhibitor in Concrete Affected by Carbonation-Induced Corrosion. *Journal of Materials in Civil Engineering*, *18*(6), 842–850. https://doi.org/10.1061/(asce)0899-1561(2006)18:6(842)

Hren, M., Bokan Bosiljkov, V., & Legat, A. (2021). Effects of blended cements and carbonation on chloride-induced corrosion propagation. *Cement and Concrete Research*, *145*(August 2020). https://doi.org/10.1016/j.cemconres.2021.106458

Hu, J., Deng, P., Li, X., Zhang, J., & Wang, G. (2018). The vertical Non-uniform corrosion of Reinforced concrete exposed to the marine environments. *Construction and Building Materials*, *183*, 180–188. https://doi.org/10.1016/j.conbuildmat.2018.06.015

Hu, X., & Poon, C. S. (2022). Chloride-related steel corrosion initiation in cement paste prepared with the incorporation of blast-furnace slag. *Cement and Concrete Composites*, *126*(April 2019), 104349. https://doi.org/10.1016/j.cemconcomp.2021.104349

Huang, J., Hu, J., Cai, J., Huang, H., Wei, J., & Yu, Q. (2022). Inhibition Effect of Hydrophobic Functional Organic Corrosion Inhibitor in Reinforced Concrete. *Materials*, *15*(20). https://doi.org/10.3390/ma15207124

Huang, Q., Jiang, Z., Zhang, W., Gu, X., & Dou, X. (2012). Numerical analysis of the effect of coarse aggregate distribution on concrete carbonation. *Construction and Building Materials*, *37*, 27–35. https://doi.org/10.1016/j.conbuildmat.2012.06.074

Hunt, C. M., & Tomes, L. A. (1962). Reaction of hardened portland cement paste with carbon dioxide. *Journal of Research of the National Bureau of Standards Section A: Physics and Chemistry*, *66A*(6), 473. https://doi.org/10.6028/jres.066a.048

Hussain, R. R., Al-Negheimish, A., Alhozaimy, A., & Singh, D. D. N. (2020). Corrosion characteristics of vanadium micro-alloyed steel reinforcement bars exposed in concrete environments and industrially polluted atmosphere. *Cement and Concrete Composites*, *113*(June), 103728. https://doi.org/10.1016/j.cemconcomp.2020.103728

Inam, M. A., Khan, R., Park, D. R., Lee, Y. W., & Yeom, I. T. (2018). Removal of Sb(III) and Sb(V) by ferric chloride coagulation: Implications of Fe solubility. *Water (Switzerland)*, *10*(4). https://doi.org/10.3390/w10040418

IS:1786-2008. (2008). High Strength Deformed Steel Bars and Wires for Concretereinforcement— Specification. *Bureau of Indian Standards, New Delhi*, 1–12.

IS:383. (1970). Specification for Coarse and Fine Aggregates From Natural Sources for

Concrete. *Indian Standards*, 1–24.

IS 456. (2000). Plain Concrete and Reinforced. *Bureau of Indian Standards,New Dehli*, 1–114.

Jamil, H. E., Montemor, M. F., Boulif, R., Shriri, A., & Ferreira, M. G. S. (2003). An electrochemical and analytical approach to the inhibition mechanism of an amino-alcohol-based corrosion inhibitor for reinforced concrete. *Electrochimica Acta*, *48*(23), 3509–3518. https://doi.org/10.1016/S0013-4686(03)00472-9

Jamil, H. E., Shriri, A., Boulif, R., Bastos, C., Montemor, M. F., & Ferreira, M. G. S. (2004). Electrochemical behaviour of amino alcohol-based inhibitors used to control corrosion of reinforcing steel. *Electrochimica Acta*, *49*(17–18), 2753–2760. https://doi.org/10.1016/j.electacta.2004.01.041

Jamil, H. E., Shriri, A., Boulif, R., Montemor, M. F., & Ferreira, M. G. S. (2005). Corrosion behaviour of reinforcing steel exposed to an amino alcohol based corrosion inhibitor. *Cement and Concrete Composites*, *27*(6), 671–678. https://doi.org/10.1016/j.cemconcomp.2004.09.019

Jastrzbski, W., Sitarz, M., Rokita, M., & Bułat, K. (2011). Infrared spectroscopy of different phosphates structures. *Spectrochimica Acta - Part A: Molecular and Biomolecular Spectroscopy*, *79*(4), 722–727. https://doi.org/10.1016/j.saa.2010.08.044

Jayaperumal, D. (2010). Effects of alcohol-based inhibitors on corrosion of mild steel in hydrochloric acid. *Materials Chemistry and Physics*, *119*(3), 478–484. https://doi.org/10.1016/j.matchemphys.2009.09.028

Jung, M. S., Kim, K. B., Lee, S. A., & Ann, K. Y. (2018). Risk of chloride-induced corrosion of steel in SF concrete exposed to a chloride-bearing environment. *Construction and Building Materials*, *166*, 413–422. https://doi.org/10.1016/j.conbuildmat.2018.01.168

Justnes, H., Skocek, J., Østnor, T. A., Engelsen, C. J., & Skjølsvold, O. (2020). Microstructural changes of hydrated cement blended with fly ash upon carbonation. *Cement and Concrete Research*, *137*(August), 106192. https://doi.org/10.1016/j.cemconres.2020.106192

Kannan K, Rajkumar V, D. M. (2012). Inhibitive Effect of Organic Inhibitors in Concrete Containing Quarry Dust As Fine Aggregate. *International Journal of Advances in Engineering*

Sciences, *2*(1), 599–564.

Kasperek, J., Verchere, D., Jacquet, D., & Phillips, N. (1998). Analysis of the corrosion products on galvanized steels by FTIR spectroscopy. *Materials Chemistry and Physics*, *56*(3), 205–213. https://doi.org/10.1016/S0254-0584(98)00167-9

Kaur, K., Goyal, S., Bhattacharje, B., Oh, T., Kim, J., Lee, C., & Park, S. (2017). Electrochemical Impedance Spectroscopy to study the carbonation behavior of concrete treated with corrosion inhibitors. *Journal of Advanced Concrete Technology*, *15*(12), 738–748. https://doi.org/10.3151/jact.15.738

Kaur, K., Goyal, S., Bhattacharjee, B., & Kumar, M. (2016). Efficiency of Migratory-Type Organic Corrosion Inhibitors in Carbonated Environment. *Journal of Advanced Concrete Technology*, *14*(9), 548–558. https://doi.org/10.3151/jact.14.548

Kaur, K., Goyal, S., Bhattacharjee, B., & Kumar, M. (2017). Electrochemical Impedance Spectroscopy to Study the Carbonation Behavior of Concrete Treated with Corrosion Inhibitors. *Journal of Advanced Concrete Technology*, *15*(12), 738–748. https://doi.org/10.3151/jact.15.738

Kondratova, I. L., Montes, P., & Bremner, T. W. (2003). Natural marine exposure results for reinforced concrete slabs with corrosion inhibitors. *Cement and Concrete Composites*, *25*(4-5 SPEC), 483–490. https://doi.org/10.1016/S0958-9465(02)00088-4

Królikowski, A., & Kuziak, J. (2011). Impedance study on calcium nitrite as a penetrating corrosion inhibitor for steel in concrete. *Electrochimica Acta*, *56*(23), 7845–7853. https://doi.org/10.1016/j.electacta.2011.01.069

Kumar, A. V. R., & Balasubramaniam, R. (1998). Corrosion product analysis of corrosion resistant ancient indian iron. *Corrosion Science*, *40*(7), 1169–1178. https://doi.org/10.1016/S0010-938X(98)00024-9

Kuosa, H., Ferreira, R. M., Holt, E., Leivo, M., & Vesikari, E. (2014a). Cement & Concrete Composites Effect of coupled deterioration by freeze – thaw , carbonation and chlorides on concrete service life. *Cement and Concrete Composites*, *47*, 32–40. https://doi.org/10.1016/j.cemconcomp.2013.10.008

Kuosa, H., Ferreira, R. M., Holt, E., Leivo, M., & Vesikari, E. (2014b). Effect of coupled deterioration by freeze-thaw, carbonation and chlorides on concrete service life. *Cement and Concrete Composites*, *47*, 32–40. https://doi.org/10.1016/j.cemconcomp.2013.10.008

Kwon, S. J., Lee, H. S., Karthick, S., Saraswathy, V., & Yang, H. M. (2017). Long-term corrosion performance of blended cement concrete in the marine environment – A real-time study. *Construction and Building Materials*, *154*, 349–360. https://doi.org/10.1016/j.conbuildmat.2017.07.237

Lapiro, I., Mezhov, A., & Kovler, K. (2022). Performance of corrosion inhibitors in reinforced concrete elements under electrical voltage. *Construction and Building Materials*, *342*(PA), 127656. https://doi.org/10.1016/j.conbuildmat.2022.127656

Lee, H.-S., Saraswathy, V., Kwon, S.-J., & Karthick, S. (2018). Corrosion Inhibitors for Reinforced Concrete: A Review. *Corrosion Inhibitors, Principles and Recent Applications*. https://doi.org/10.5772/intechopen.72572

Lee, H. S., Yang, H. M., Singh, J. K., Prasad, S. K., & Yoo, B. (2018). Corrosion mitigation of steel rebars in chloride contaminated concrete pore solution using inhibitor: An electrochemical investigation. *Construction and Building Materials*, *173*, 443–451. https://doi.org/10.1016/j.conbuildmat.2018.04.069

Liu, J. Z., Zhao, D., Cai, J. S., Shi, L., & Liu, J. P. (2016). Aryl aminoalcohols as corrosion inhibitors for carbon steel in chloride-contaminated simulated concrete pore solution. *International Journal of Electrochemical Science*, *11*(2), 1135–1151.

Liu, R., Jiang, L., Xu, J., Xiong, C., & Song, Z. (2014). Influence of carbonation on chloride-induced reinforcement corrosion in simulated concrete pore solutions. *Construction and Building Materials*, *56*, 16–20. https://doi.org/10.1016/j.conbuildmat.2014.01.030

Liu, Y., Song, Z., Wang, W., Jiang, L., Zhang, Y., Guo, M., Song, F., & Xu, N. (2019). Effect of ginger extract as green inhibitor on chloride-induced corrosion of carbon steel in simulated concrete pore solutions. *Journal of Cleaner Production*, *214*, 298–307. https://doi.org/10.1016/j.jclepro.2018.12.299

Luo, H., Su, H., Dong, C., & Li, X. (2017). Passivation and electrochemical behavior of 316L stainless steel in chlorinated simulated concrete pore solution. *Applied Surface Science*, *400*,

38–48. https://doi.org/10.1016/j.apsusc.2016.12.180

Lye, C. Q., Dhir, R. K., & Ghataora, G. S. (2015). Carbonation resistance of fly ash concrete. *Magazine of Concrete Research*, *67*(21), 1150–1178. https://doi.org/10.1680/macr.15.00204

Magdalena Osial, D. W. (2016). Organic substances as corrosion inhibitors for steel in concrete – an overview. *Journal of Building Chemistry*, *May*, 42–53. https://doi.org/10.17461/j.buildchem.2016.107

Mei, K., He, Z., Yi, B., Lin, X., Wang, J., Wang, H., & Liu, J. (2022). Study on electrochemical characteristics of reinforced concrete corrosion under the action of carbonation and chloride. *Case Studies in Construction Materials*, *17*(January), e01351. https://doi.org/10.1016/j.cscm.2022.e01351

Mert, B. D., Yüce, A. O., Kardaş, G., & Yazici, B. (2014). Inhibition effect of 2-amino-4-methylpyridine on mild steel corrosion: Experimental and theoretical investigation. *Corrosion Science*, *85*, 287–295. https://doi.org/10.1016/j.corsci.2014.04.032

Mi, T., Li, Y., Liu, W., Dong, Z., Gong, Q., Min, C., Xing, F., Wang, Y., & Chu, S. H. (2023). The effect of carbonation on chloride redistribution and corrosion of steel reinforcement. *Construction and Building Materials*, *363*(May 2022), 129641. https://doi.org/10.1016/j.conbuildmat.2022.129641

Montemor, M. F., Cunha, M. P., Ferreira, M. G., & Simões, A. M. (2002). Corrosion behaviour of rebars in fly ash mortar exposed to carbon dioxide and chlorides. *Cement and Concrete Composites*, *24*(1), 45–53. https://doi.org/10.1016/S0958-9465(01)00025-7

Montemor, M. F., Simões, A. M. P., & Ferreira, M. G. S. (2003). Chloride-induced corrosion on reinforcing steel: From the fundamentals to the monitoring techniques. *Cement and Concrete Composites*, *25*(4-5 SPEC), 491–502. https://doi.org/10.1016/S0958-9465(02)00089-6

Montemor, M. F., Simões, A. M. P., & Salta, M. M. (2000). Effect of fly ash on concrete reinforcement corrosion studied by EIS. *Cement and Concrete Composites*, *22*(3), 175–185. https://doi.org/10.1016/S0958-9465(00)00003-2

Montes, P., Bremner, T. W., & Lister, D. H. (2004). Influence of calcium nitrite inhibitor and

crack width on corrosion of steel in high performance concrete subjected to a simulated marine environment. *Cement and Concrete Composites*, *26*(3), 243–253. https://doi.org/10.1016/S0958-9465(03)00043-X

Monticelli, C., Frignani, A., Balbo, A., & Zucchi, F. (2011a). Influence of two specific inhibitors on steel corrosion in a synthetic solution simulating a carbonated concrete with chlorides. *Materials and Corrosion*, *62*(2), 178–186. https://doi.org/10.1002/maco.201005764

Monticelli, C., Frignani, A., Balbo, A., & Zucchi, F. (2011b). Influence of two specific inhibitors on steel corrosion in a synthetic solution simulating a carbonated concrete with chlorides. *Materials and Corrosion*, *62*(2), 178–186. https://doi.org/10.1002/maco.201005764

Monticelli, C., Frignani, A., & Trabanelli, G. (2000). *A study on corrosion inhibitors for concrete application*. *30*(January).

Morandeau, A., Thiéry, M., & Dangla, P. (2015). Impact of accelerated carbonation on OPC cement paste blended with fly ash. *Cement and Concrete Research*, *67*, 226–236. https://doi.org/10.1016/j.cemconres.2014.10.003

Morris, W., & Vázquez, M. (2002). A migrating corrosion inhibitor evaluated in concrete containing various contents of admixed chlorides. *Cement and Concrete Research*, *32*(2), 259–267. https://doi.org/10.1016/S0008-8846(01)00669-X

Nahali, H., Dhouibi, L., & Idrissi, H. (2014). Effect of phosphate based inhibitor on the threshold chloride to initiate steel corrosion in saturated hydroxide solution. *Construction and Building Materials*, *50*, 87–94. https://doi.org/10.1016/j.conbuildmat.2013.08.054

Neufeld, A. K., & Cole, I. S. (1997). Using Fourier Transform Infrared Analysis to Detect Corrosion Products on the Surface of Metals Exposed to Atmospheric Conditions. *Corrosion (Houston)*, *53*(10), 788–799. https://doi.org/10.5006/1.3290263

Neville, A. (1995). Chloride attack of reinforced concrete: an overview. *Materials and Structures*, *28*(2), 63–70. https://doi.org/10.1007/BF02473172

Ngala, V. T., & Page, C. L. (1997). EFFECTS OF CARBONATION ON PORE STRUCTURE AND DIFFUSIONAL PROPERTIES OF HYDRATED CEMENT PASTES. *Cement and Concrete Research*, *27*(7), 995–1007. https://doi.org/10.1016/S0008-8846(97)00102-6

Ngala, V. T., Page, C. L., & Page, M. M. (2003). Corrosion inhibitor systems for remedial treatment of reinforced concrete. Part 2: Sodium monofluorophosphate. *Corrosion Science*, *45*(7), 1523–1537. https://doi.org/10.1016/S0010-938X(02)00248-2

Nicolas, R. S., Cyr, M., & Escadeillas, G. (2014). Performance-based approach to durability of concrete containing flash-calcined metakaolin as cement replacement. *Construction and Building Materials*, *55*, 313–322. https://doi.org/10.1016/j.conbuildmat.2014.01.063

Nmai, C. K. (2004). Multi-functional organic corrosion inhibitor. *Cement and Concrete Composites*, *26*(3), 199–207. https://doi.org/10.1016/S0958-9465(03)00039-8

Ormellese, M., Berra, M., Bolzoni, F., & Pastore, T. (2006). Corrosion inhibitors for chlorides induced corrosion in reinforced concrete structures. *Cement and Concrete Research*, *36*(3), 536–547. https://doi.org/10.1016/j.cemconres.2005.11.007

Ormellese, M., Bolzoni, F., Lazzari, L., Brenna, A., & Pedeferri, M. (2011). Organic substances as inhibitors for chloride-induced corrosion in reinforced concrete. *Materials and Corrosion*, *62*(2), 170–177. https://doi.org/10.1002/maco.201005763

Ormellese, M., Lazzari, L., Goidanich, S., Fumagalli, G., & Brenna, A. (2009a). A study of organic substances as inhibitors for chloride-induced corrosion in concrete. *Corrosion Science*, *51*(12), 2959–2968. https://doi.org/10.1016/j.corsci.2009.08.018

Ormellese, M., Lazzari, L., Goidanich, S., Fumagalli, G., & Brenna, A. (2009b). A study of organic substances as inhibitors for chloride-induced corrosion in concrete. *Corrosion Science*, *51*(12), 2959–2968. https://doi.org/10.1016/j.corsci.2009.08.018

Osial, M. (2016). *Organic substances as corrosion inhibitors for steel in concrete – an overview*. *May*. https://doi.org/10.17461/j.buildchem.2016.107

Pacewska, B., & Wilińska, I. (2020). Usage of supplementary cementitious materials: advantages and limitations: Part I. C–S–H, C–A–S–H and other products formed in different binding mixtures. *Journal of Thermal Analysis and Calorimetry*, *142*(1), 371–393. https://doi.org/10.1007/s10973-020-09907-1

Perencatan, K., Keluli, K., Dalam, T., & So, M. L. H. (2014). *SYNTHESIS , CHARACTERIZATION AND CORROSION INHIBITION STUDIES OF o , m , p- DECANOYL*

THIOUREA DERIVATIVES ON MILD STEEL IN 0 . 1 M H 2 SO 4 SOLUTIONS. *18*(1), 21–27.

Pessu, F., Barker, R., & Neville, A. (2020). CO2 Corrosion of Carbon Steel: The Synergy of Chloride Ion Concentration and Temperature on Metal Penetration. In *Corrosion* (Vol. 76, Issue 11). https://doi.org/10.5006/3583

Rakanta, E., Zafeiropoulou, T., & Batis, G. (2013). Corrosion protection of steel with DMEA-based organic inhibitor. *Construction and Building Materials*, *44*, 507–513. https://doi.org/10.1016/j.conbuildmat.2013.03.030

Ramezanianpour, A. A., Ghahari, S. A., & Esmaeili, M. (2014). Effect of combined carbonation and chloride ion ingress by an accelerated test method on microscopic and mechanical properties of concrete. *Construction and Building Materials*, *58*, 138–146. https://doi.org/10.1016/j.conbuildmat.2014.01.102

Ribeiro, D. V., & Abrantes, J. C. C. (2016). Application of electrochemical impedance spectroscopy (EIS) to monitor the corrosion of reinforced concrete: A new approach. *Construction and Building Materials*, *111*(May), 98–104. https://doi.org/10.1016/j.conbuildmat.2016.02.047

Rodrigues, R., Gaboreau, S., Gance, J., Ignatiadis, I., & Betelu, S. (2021). Reinforced concrete structures: A review of corrosion mechanisms and advances in electrical methods for corrosion monitoring. *Construction and Building Materials*, *269*, 121240. https://doi.org/10.1016/j.conbuildmat.2020.121240

Rosenberg, A. M., & Gaidis, J. M. (1979). Mechanism of Nitrite Inhibition of Chloride Attack on Reinforcing Steel in Alkaline Aqueous Environments. *Material Performance*, *18*(11), 45–48. https://doi.org/http://worldcat.org/issn/00941492

Ryu, H. S., Singh, J. K., Yang, H. M., Lee, H. S., & Ismail, M. A. (2016). Evaluation of corrosion resistance properties of N, N′-Dimethyl ethanolamine corrosion inhibitor in saturated Ca(OH)2 solution with different concentrations of chloride ions by electrochemical experiments. *Construction and Building Materials*, *114*, 223–231. https://doi.org/10.1016/j.conbuildmat.2016.03.174

Sancy, M., Gourbeyre, Y., Sutter, E. M. M., & Tribollet, B. (2010). Mechanism of corrosion

of cast iron covered by aged corrosion products: Application of electrochemical impedance spectrometry. *Corrosion Science*, *52*(4), 1222–1227. https://doi.org/10.1016/j.corsci.2009.12.026

Saraswathy, V., & Song, H. W. (2007). Improving the durability of concrete by using inhibitors. *Building and Environment*, *42*(1), 464–472. https://doi.org/10.1016/j.buildenv.2005.08.003

Schweitzer, P. A. (2017). Corrosion inhibitors. In *Corrosion and Corrosion Protection Handbook, Second Edition*. Elsevier. https://doi.org/10.1201/9781315140384

Sharma, N., Sharma, S., Sharma, S. K., & Mehta, R. (2020). Evaluation of corrosion inhibition and self healing capabilities of nanoclay and tung oil microencapsulated epoxy coatings on rebars in concrete. *Construction and Building Materials*, *259*, 120278. https://doi.org/10.1016/j.conbuildmat.2020.120278

Shen, D. (2017). Electrochemical impedance spectroscopy study on corrosion inhibitor for reinforced concrete. *International Journal of Electrochemical Science*, *12*(5), 4183–4192. https://doi.org/10.20964/2017.05.38

Shi, J., Wu, M., & Ming, J. (2022). In-depth insight into the role of molybdate in corrosion resistance of reinforcing steel in chloride-contaminated mortars. *Cement and Concrete Composites*, *132*(June), 104628. https://doi.org/10.1016/j.cemconcomp.2022.104628

Sideris, K. K., & Savva, A. E. (2005). Durability of mixtures containing calcium nitrite based corrosion inhibitor. *Cement and Concrete Composites*, *27*(2), 277–287. https://doi.org/10.1016/j.cemconcomp.2004.02.016

Sieber, I. V., Hildebrand, H., Virtanen, S., & Schmuki, P. (2006). Investigations on the passivity of iron in borate and phosphate buffers, pH 8.4. *Corrosion Science*, *48*(11), 3472–3488. https://doi.org/10.1016/j.corsci.2005.12.008

Sohail, M. G., Kahraman, R., Alnuaimi, N. A., Gencturk, B., Alnahhal, W., Dawood, M., & Belarbi, A. (2020). Electrochemical behavior of mild and corrosion resistant concrete reinforcing steels. *Construction and Building Materials*, *232*, 117205. https://doi.org/10.1016/j.conbuildmat.2019.117205

Song, H. W., & Saraswathy, V. (2007). Corrosion monitoring of reinforced concrete structures - A review. *International Journal of Electrochemical Science*, *2*(1), 1–28.

Söylev, T. A., McNally, C., & Richardson, M. (2007a). Effectiveness of amino alcohol-based surface-applied corrosion inhibitors in chloride-contaminated concrete. *Cement and Concrete Research*, *37*(6), 972–977. https://doi.org/10.1016/j.cemconres.2007.03.010

Söylev, T. A., McNally, C., & Richardson, M. G. (2007b). The effect of a new generation surface-applied organic inhibitor on concrete properties. *Cement and Concrete Composites*, *29*(5), 357–364. https://doi.org/10.1016/j.cemconcomp.2006.12.013

Söylev, T. A., & Richardson, M. G. (2008). Corrosion inhibitors for steel in concrete: State-of-the-art report. *Construction and Building Materials*, *22*(4), 609–622. https://doi.org/10.1016/j.conbuildmat.2006.10.013

Standards Australia Committee, SA HB 84: 2018 *Handbook Guide to Concrete Repair and Protection (2018)*

Stefanoni, M., Angst, U., & Elsener, B. (2018). Corrosion rate of carbon steel in carbonated concrete – A critical review. In *Cement and Concrete Research* (Vol. 103, Issue October 2017, pp. 35–48). Elsevier. https://doi.org/10.1016/j.cemconres.2017.10.007

Talati, J. D., & Joshi, N. H. (1978). Aldehydes as corrosion inhibitors for aluminium-manganese alloys in potassium hydroxide. *Materials and Corrosion*, *29*(7), 461–468. https://doi.org/10.1002/maco.19780290706

Thomas, M. D. A., Hooton, R. D., Scott, A., & Zibara, H. (2012). Cement and Concrete Research The effect of supplementary cementitious materials on chloride binding in hardened cement paste. *Cement and Concrete Research*, *42*(1), 1–7. https://doi.org/10.1016/j.cemconres.2011.01.001

Thuong, T., Thanh, N., Joo, D., & Cuong, T. (2021). Effects of corrosion level and inhibitor on pullout behavior of deformed steel fiber embedded in high performance concrete. *Construction and Building Materials*, *280*, 122449. https://doi.org/10.1016/j.conbuildmat.2021.122449

Tian, Y., Guo, W., Wang, W., Wang, B., Zhang, P., & Zhao, T. (2023). Influence of organic

corrosion inhibitors on steel corrosion in concrete under the coupled action of freeze–thaw cycles and chloride attack. *Construction and Building Materials*, *368*(October 2022), 130385. https://doi.org/10.1016/j.conbuildmat.2023.130385

Tittarelli, F., Mobili, A., Giosuè, C., Belli, A., & Bellezze, T. (2018). Corrosion behaviour of bare and galvanized steel in geopolymer and Ordinary Portland Cement based mortars with the same strength class exposed to chlorides. *Corrosion Science*, *134*(December 2016), 64–77. https://doi.org/10.1016/j.corsci.2018.02.014

Tiwari, A. K., Goyal, S., Luxami, V., Chakraborty, M. K., & Gundlapalli, P. (2021). Evaluation of inhibition efficiency of generic compounds with additional heteroatom in simulated concrete pore solution and migration potential in concrete. *Journal of Building Engineering*, *43*(November 2020), 102490. https://doi.org/10.1016/j.jobe.2021.102490

Trabanelli, G., Monticelli, C., Grassi, V., & Frignani, A. (2005). Electrochemical study on inhibitors of rebar corrosion in carbonated concrete. *Cement and Concrete Research*, *35*(9), 1804–1813. https://doi.org/10.1016/j.cemconres.2004.12.010

Tritthart, J. (2003). Transport of a surface-applied corrosion inhibitor in cement paste and concrete. *Cement and Concrete Research*, *33*(6), 829–834. https://doi.org/10.1016/S0008-8846(02)01067-0

Vedalakshmi, R., & Palaniswamy, N. (2010). Analysis of the electrochemical phenomenon at the rebar-concrete interface using the electrochemical impedance spectroscopic technique. *Magazine of Concrete Research*, *62*(3), 177–189. https://doi.org/10.1680/macr.2010.62.3.177

Vedalakshmi, R., & Thangavel, K. (2011). Reliability of Electrochemical Techniques to Predict the Corrosion Rate of Steel in Concrete Structures. *Arabian Journal for Science and Engineering*, *36*(5), 769–783. https://doi.org/10.1007/s13369-011-0082-4

Verbruggen, H., Terryn, H., & De Graeve, I. (2016). Inhibitor evaluation in different simulated concrete pore solution for the protection of steel rebars. *Construction and Building Materials*, *124*, 887–896. https://doi.org/10.1016/j.conbuildmat.2016.07.115

Verma, C., Ebenso, E. E., & Quraishi, M. A. (2017). Ionic liquids as green and sustainable corrosion inhibitors for metals and alloys: An overview. *Journal of Molecular Liquids*, *233*(2016), 403–414. https://doi.org/10.1016/j.molliq.2017.02.111

Wang, X., Kong, L., Zhao, W., & Liu, Y. (2023a). Chloride transport resistance of alkali-activated concrete exposed to combined chloride, sulfate and carbonation environment. *Construction and Building Materials*, *367*(August 2022), 130353. https://doi.org/10.1016/j.conbuildmat.2023.130353

Wang, X., Kong, L., Zhao, W., & Liu, Y. (2023b). Chloride transport resistance of alkali-activated concrete exposed to combined chloride , sulfate and carbonation environment. *Construction and Building Materials*, *367*(November 2022), 130353. https://doi.org/10.1016/j.conbuildmat.2023.130353

Wang, Y., Nanukuttan, S., Bai, Y., & Basheer, P. A. M. (2017). Influence of combined carbonation and chloride ingress regimes on rate of ingress and redistribution of chlorides in concretes. *Construction and Building Materials*, *140*, 173–183. https://doi.org/10.1016/j.conbuildmat.2017.02.121

Wang, Y., Zuo, Y., & Tang, Y. (2018). Inhibition effect and mechanism of sodium oleate on passivation and pitting corrosion of steel in simulated concrete pore solution. *Construction and Building Materials*, *167*, 197–204. https://doi.org/10.1016/j.conbuildmat.2018.01.170

Weishaar, A., Carpenter, M., Loucks, R., Sakulich, A., & Peterson, A. M. (2018). Evaluation of self-healing epoxy coatings for steel reinforcement. *Construction and Building Materials*, *191*, 125–135. https://doi.org/10.1016/j.conbuildmat.2018.09.197

William Stephen Tait. (1994). *An Introduction to Electrochemical Corrosion Testing for Practicing Engineers and Scientists*. Pair ODocs Publications.

Xu, J., Wei, J., Ma, G., & Tan, Q. (2020). Effect of MgAl-NO2 LDHs inhibitor on steel corrosion in chloride-free and contaminated simulated carbonated concrete pore solutions. *Corrosion Science*, *176*(2), 108940. https://doi.org/10.1016/j.corsci.2020.108940

Xu, Q., Hou, D., Zhang, H., Wang, P., Wang, M., Wu, D., Liu, C., Ding, Z., Zhang, M., Xin, Z., Fu, B., Guan, J., & Zhang, Y. (2022). *Understanding the effect of vitamin B3 , B6 and C as a corrosion inhibitor on the ordinary Portland cement hydration : Experiments and DFT study*. *331*(March). https://doi.org/10.1016/j.conbuildmat.2022.127294

Yadav, M., Gope, L., & Sarkar, T. K. (2016). Synthesized amino acid compounds as eco-friendly corrosion inhibitors for mild steel in hydrochloric acid solution: Electrochemical and

quantum studies. *Research on Chemical Intermediates*, *42*(3), 2641–2660. https://doi.org/10.1007/s11164-015-2172-5

Ye, H., Jin, X., Fu, C., Jin, N., Xu, Y., & Huang, T. (2016). Chloride penetration in concrete exposed to cyclic drying-wetting and carbonation. *Construction and Building Materials*, *112*, 457–463. https://doi.org/10.1016/j.conbuildmat.2016.02.194

Yohai, L., Vázquez, M., & Valcarce, M. B. (2013). Phosphate ions as corrosion inhibitors for reinforcement steel in chloride-rich environments. *Electrochimica Acta*, *102*, 88–96. https://doi.org/10.1016/j.electacta.2013.03.180

Zhang, D., & Shao, Y. (2016). Effect of early carbonation curing on chloride penetration and weathering carbonation in concrete. *Construction and Building Materials*, *123*, 516–526. https://doi.org/10.1016/j.conbuildmat.2016.07.041

Zhang, J., Zhang, L., Xu, B., & Yuan, J. (2023). Influences of Carbonated Recycled Concrete Fines on Cement Hydration. *Buildings*, *13*(4). https://doi.org/10.3390/buildings13040926

Zheng, H., Li, W., Ma, F., & Kong, Q. (2012). The effect of a surface-applied corrosion inhibitor on the durability of concrete. *Construction and Building Materials*, *37*, 36–40. https://doi.org/10.1016/j.conbuildmat.2012.07.007

Zheng, H., Lu, J., Shen, P., Sun, L., Poon, C. S., & Li, W. (2022). Corrosion behavior of carbon steel in chloride-contaminated ultra-high-performance cement pastes. *Cement and Concrete Composites*, *128*(July 2021), 104443. https://doi.org/10.1016/j.cemconcomp.2022.104443

Zhou, X., Yang, H., & Wang, F. (2011). BF4 ionic liquids as effective inhibitor for carbon steel in alkaline chloride solution. *Electrochimica Acta*, *56*(11), 4268–4275. https://doi.org/10.1016/j.electacta.2011.01.081

Zhou, Y., & Zuo, Y. (2015). The inhibitive mechanisms of nitrite and molybdate anions on initiation and propagation of pitting corrosion for mild steel in chloride solution. *Applied Surface Science*, *353*(2), 924–932. https://doi.org/10.1016/j.apsusc.2015.07.037

Zhu, A., Zhang, X., Yang, R., & Wang, C. (2023). The deterioration mechanisms of hardened cement paste exposed to combined action of cyclic wetting–drying, salt attack and carbonation. *Construction and Building Materials*, *366*(October 2022), 130148.

https://doi.org/10.1016/j.conbuildmat.2022.130148

Zomorodian, A., Bagonyi, R., & Al-Tabbaa, A. (2021). The efficiency of eco-friendly corrosion inhibitors in protecting steel reinforcement. *Journal of Building Engineering*, *38*(December 2020), 102171. https://doi.org/10.1016/j.jobe.2021.102171

Annexure I

Table A1. Retention factor (R_f) for ABA applied specimens						
Cement↓	Depth↓	Concentration				
		0.1	0.3	0.5	0.8	1
		15 Days				
OPC	5	0.13	0.27	0.35	0.65	0.69
	10	0.12	0.17	0.28	0.68	0.68
	15	0.25	0.27	0.38	0.66	0.67
PPC	5	0.25	0.27	0.31	0.68	0.65
	10	0.25	0.34	0.31	0.66	0.64
	15	0.25	0.34	0.41	0.67	0.66
		30 Days				
OPC	5	0.15	0.24	0.31	0.67	0.64
	10	0.19	0.14	0.23	0.65	0.67
	15	0.29	0.24	0.33	0.68	0.66
PPC	5	0.11	0.15	0.33	0.68	0.67
	10	0.11	0.15	0.37	0.66	0.66
	15	0.21	0.25	0.34	0.66	0.68
		45 Days				
OPC	5	0.11	0.24	0.27	0.66	0.64
	10	0.17	0.22	0.37	0.67	0.68
	15	0.27	0.32	0.36	0.65	0.66
PPC	5	0.23	0.22	0.37	0.66	0.63
	10	0.19	0.22	0.26	0.64	0.65
	15	0.29	0.27	0.36	0.67	0.66
		60 Days				
OPC	5	0.11	0.29	0.15	0.64	0.65
	10	0.12	0.24	0.31	0.66	0.67
	15	0.17	0.26	0.35	0.67	0.67
PPC	5	0.13	0.22	0.40	0.69	0.62
	10	0.23	0.22	0.42	0.67	0.64
	15	0.13	0.25	0.33	0.67	0.67

Table A2. Retention factor (R_f) for AP applied specimens						
Cement↓	Depth↓	Concentration				
		0.1	0.3	0.5	0.8	1
		15 Days				
OPC	5	0.17	0.27	0.40	0.69	0.71
	10	0.16	0.25	0.42	0.67	0.66
	15	0.27	0.37	0.34	0.67	0.65
PPC	5	0.15	0.25	0.37	0.69	0.63

	10	0.15	0.22	0.24	0.66	0.65
	15	0.17	0.22	0.32	0.67	0.65
		30 Days				
OPC	5	0.23	0.25	0.38	0.67	0.67
	10	0.23	0.35	0.28	0.67	0.65
	15	0.22	0.32	0.38	0.67	0.67
PPC	5	0.11	0.15	0.33	0.68	0.67
	10	0.13	0.19	0.17	0.65	0.67
	15	0.23	0.29	0.47	0.66	0.68
		45 Days				
OPC	5	0.17	0.21	0.37	0.66	0.65
	10	0.27	0.31	0.26	0.69	0.66
	15	0.27	0.38	0.32	0.68	0.67
PPC	5	0.23	0.22	0.37	0.66	0.65
	10	0.18	0.21	0.29	0.66	0.65
	15	0.18	0.31	0.39	0.68	0.67
		60 Days				
OPC	5	0.10	0.15	0.17	0.67	0.68
	10	0.18	0.25	0.11	0.68	0.67
	15	0.28	0.25	0.31	0.68	0.67
PPC	5	0.15	0.13	0.19	0.70	0.68
	10	0.17	0.31	0.29	0.66	0.67
	15	0.25	0.33	0.28	0.67	0.66

Table A3. Retention factor (R_f) for SA applied specimens

Cement↓	Depth↓	Concentration				
		0.1	0.3	0.5	0.8	1
		15 Days				
OPC	5	0.14	0.16	0.33	0.48	0.70
	10	0.24	0.26	0.40	0.42	0.67
	15	0.14	0.26	0.30	0.42	0.69
PPC	5	0.22	0.24	0.30	0.44	0.70
	10	0.12	0.14	0.22	0.42	0.68
	15	0.12	0.24	0.26	0.32	0.68
		30 Days				
OPC	5	0.22	0.24	0.30	0.34	0.64
	10	0.22	0.25	0.30	0.38	0.66
	15	0.27	0.22	0.35	0.37	0.69
PPC	5	0.16	0.26	0.38	0.42	0.69
	10	0.15	0.32	0.37	0.44	0.67
	15	0.15	0.22	0.35	0.41	0.69

		45 Days				
OPC	5	0.14	0.20	0.38	0.44	0.66
	10	0.14	0.25	0.33	0.42	0.67
	15	0.24	0.27	0.38	0.44	0.68
PPC	5	0.08	0.18	0.22	0.38	0.72
	10	0.18	0.22	0.32	0.38	0.70
	15	0.08	0.11	0.22	0.48	0.70
		60 Days				
OPC	5	0.14	0.24	0.16	0.34	0.70
	10	0.14	0.24	0.16	0.44	0.69
	15	0.14	0.22	0.28	0.34	0.69
PPC	5	0.10	0.20	0.32	0.42	0.68
	10	0.17	0.25	0.34	0.42	0.68
	15	0.27	0.25	0.36	0.44	0.70

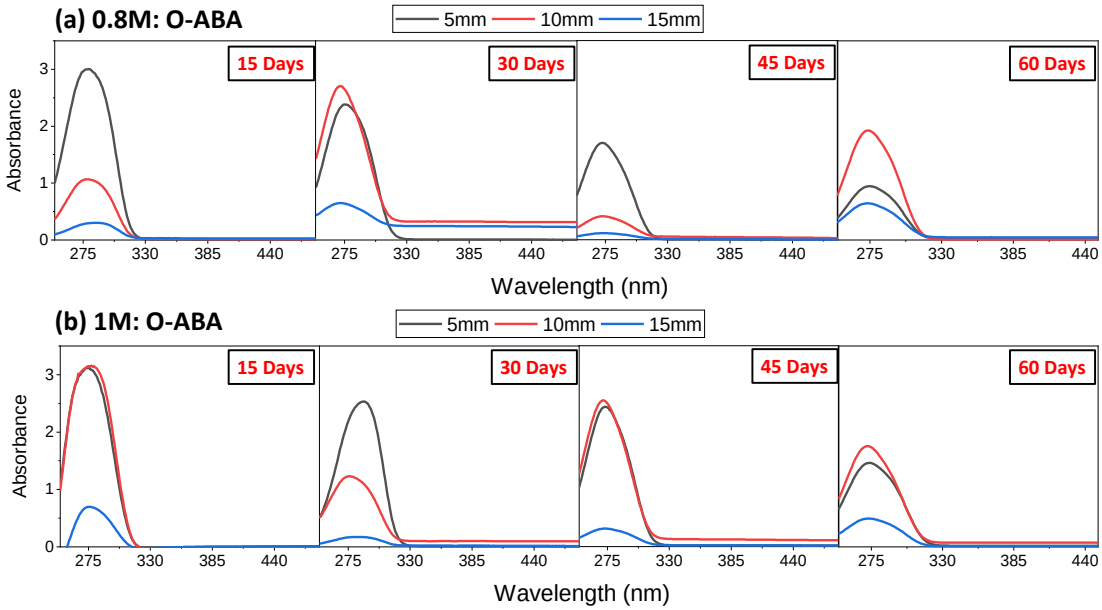

Fig. A1. Absorbance peak of ABA in OPC based specimens at (a) 0.8M; (b) 1M for different duration

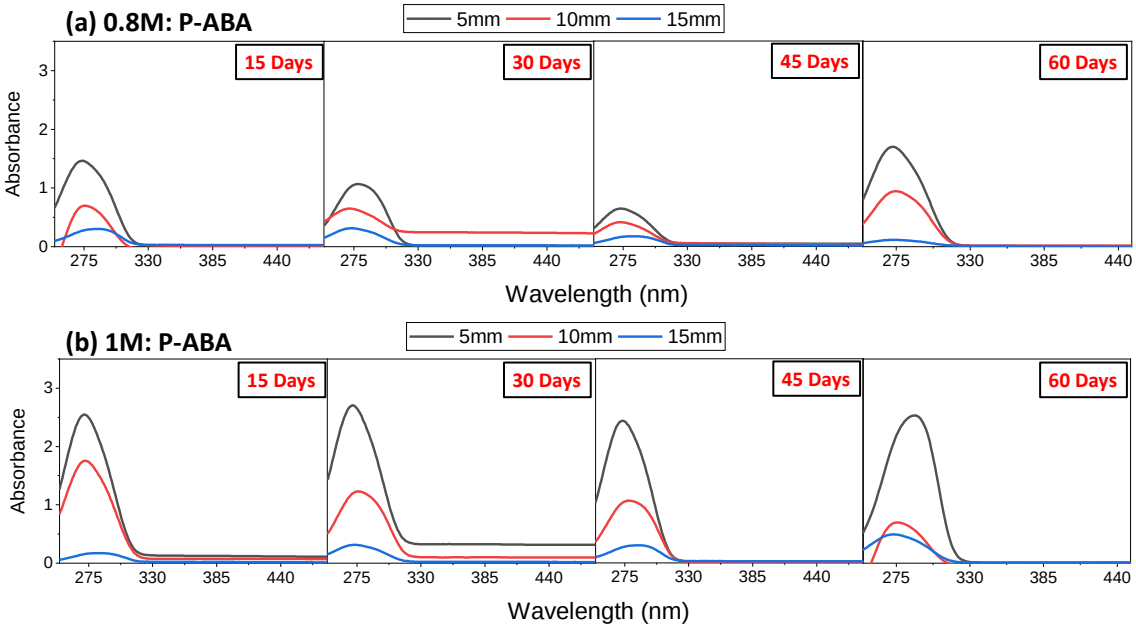

Fig. A2. Absorbance peak of ABA in PPC based specimens at (a) 0.8M; (b) 1M concentration for different duration

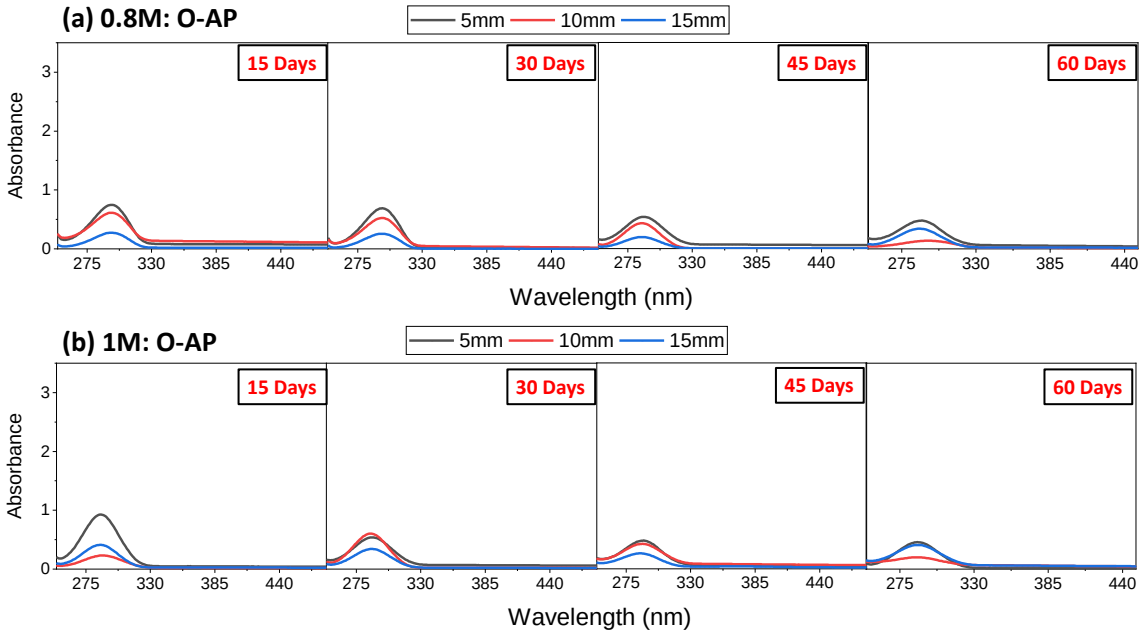

Fig. A3. Absorbance peak of AP in OPC based specimens at (a) 0.8M; (b) 1M for different duration

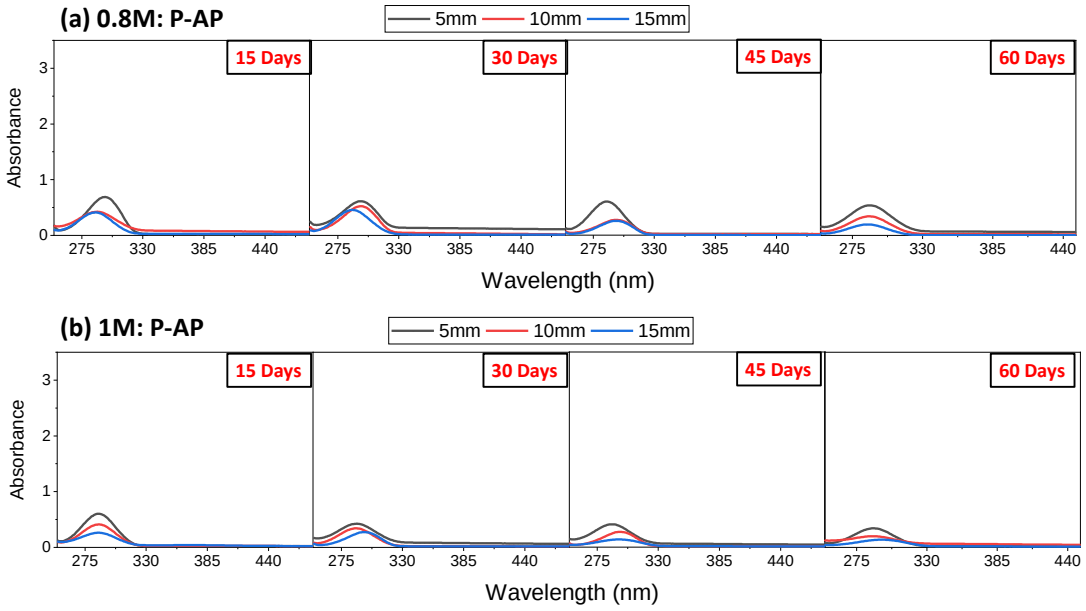

Fig. A4. Absorbance peak of AP in PPC based specimens at (a) 0.8M; (b) 1M for different duration

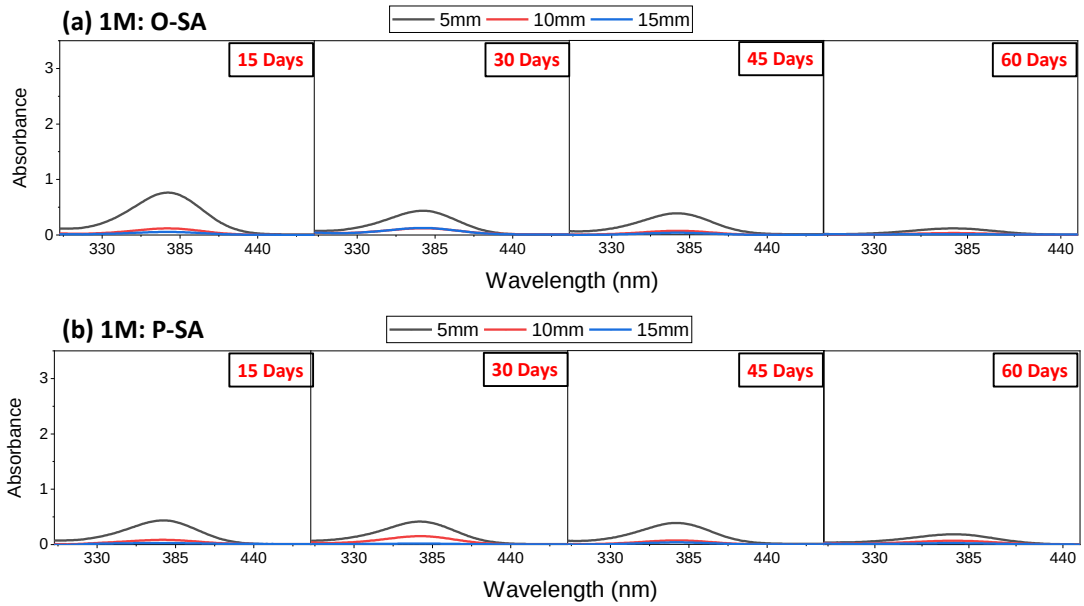

Fig. A5. Absorbance peak of SA after 1M application in (a) OPC based ;(b) PPC based for different duration